ISSN 0021-9673

VOL. 663 NO. 2 MARCH 11, 1994

THIS ISSUE COMPLETES VOL. 663

JOURNAL OF CHROMATOGRAPHY A

INCLUDING ELECTROPHORESIS AND OTHER SEPARATION METHODS

ELSEVIER

JOURNAL OF CHROMATOGRAPHY A

INCLUDING ELECTROPHORESIS AND OTHER SEPARATION METHODS

Scope. The *Journal of Chromatography A* publishes papers on all aspects of **chromatography, electrophoresis** and related methods. Contributions consist mainly of research papers dealing with chromatographic theory, instrumental developments and their applications. In the *Symposium volumes*, which are under separate editorship, proceedings of symposia on chromatography, electrophoresis and related methods are published. *Journal of Chromatography B: Biomedical Applications* —This journal, which is under separate editorship, deals with the following aspects: developments in and applications of chromatographic and electrophoretic techniques related to clinical diagnosis or alterations during medical treatment; screening and profiling of body fluids or tissues related to the analysis of active substances and to metabolic disorders; drug level monitoring and pharmacokinetic studies; clinical toxicology; forensic medicine; veterinary medicine; occupational medicine; results from basic medical research with direct consequences in clinical practice.

Submission of Papers. The preferred medium of submission is on disk with accompanying manuscript (see *Electronic manuscripts* in the Instructions to Authors, which can be obtained from the publisher, Elsevier Science B.V., P.O. Box 330, 1000 AH Amsterdam, Netherlands). Manuscripts (in English: *four* copies are required) should be submitted to: Editorial Office of *Journal of Chromatography A*, P.O. Box 681, 1000 AR Amsterdam, Netherlands, Telefax (+31-20) 5862 304, or to: The Editor of *Journal of Chromatography B: Biomedical Applications*, P.O. Box 681, 1000 AR Amsterdam, Netherlands. Review articles are invited or proposed in writing to the Editors who welcome suggestions for subjects. An outline of the proposed review should first be forwarded to the Editors for preliminary discussion prior to preparation. Submission of an article is understood to imply that the article is original and unpublished and is not being considered for publication elsewhere. For copyright regulations, see below.

Publication information. *Journal of Chromatography A* (ISSN 0021-9673): for 1994 Vols. 652–682 are scheduled for publication. *Journal of Chromatography B: Biomedical Applications* (ISSN 0378-4347): for 1994 Vols. 652–662 are scheduled for publication. Subscription prices for *Journal of Chromatography A*, *Journal of Chromatography B: Biomedical Applications* or a combined subscription are available upon request from the publisher. Subscriptions are accepted on a prepaid basis only and are entered on a calendar year basis. Issues are sent by surface mail except to the following countries where air delivery via SAL is ensured: Argentina, Australia, Brazil, Canada, China, Hong Kong, India, Israel, Japan, Malaysia, Mexico, New Zealand, Pakistan, Singapore, South Africa, South Korea, Taiwan, Thailand, USA. For all other countries airmail rates are available upon request. Claims for missing issues must be made within six months of our publication (mailing) date. Please address all your requests regarding orders and subscription queries to: Elsevier Science B.V., Journal Department, P.O. Box 211, 1000 AE Amsterdam, Netherlands. Tel.: (+31-20) 5803 642; Fax: (+31-20) 5803 598. Customers in the USA and Canada wishing information on this and other Elsevier journals, please contact Journal Information Center, Elsevier Science Inc., 655 Avenue of the Americas, New York, NY 10010, USA, Tel. (+1-212) 633 3750, Telefax (+1-212) 633 3764.

Abstracts/Contents Lists published in Analytical Abstracts, Biochemical Abstracts, Biological Abstracts, Chemical Abstracts, Chemical Titles, Chromatography Abstracts, Current Awareness in Biological Sciences (CABS), Current Contents/Life Sciences, Current Contents/Physical, Chemical & Earth Sciences, Deep-Sea Research/Part B: Oceanographic Literature Review, Excerpta Medica, Index Medicus, Mass Spectrometry Bulletin, PASCAL-CNRS, Referativnyi Zhurnal, Research Alert and Science Citation Index.

US Mailing Notice. *Journal of Chromatography A* (ISSN 0021-9673) is published weekly (total 52 issues) by Elsevier Science B.V., (Sara Burgerhartstraat 25, P.O. Box 211, 1000 AE Amsterdam, Netherlands). Annual subscription price in the USA US$ 4994.00 (US$ price valid in North, Central and South America only) including air speed delivery. Second class postage paid at Jamaica, NY 11431. **USA POSTMASTERS**: Send address changes to *Journal of Chromatography A*, Publications Expediting, Inc., 200 Meacham Avenue, Elmont, NY 11003. Airfreight and mailing in the USA by Publications Expediting.

See inside back cover for Publication Schedule, Information for Authors and information on Advertisements.

0021-9673/94/$07.00

Printed in the Netherlands

VOL. 663, NO. 2 JOURNAL OF CHROMATOGRAPHY A MARCH 11, 1994

CONTENTS

(Abstracts/Contents Lists published in Analytical Abstracts, Biochemical Abstracts, Biological Abstracts, Chemical Abstracts, Chemical Titles, Chromatography Abstracts, Current Awareness in Biological Sciences (CABS), Current Contents/Life Sciences, Current Contents/Physical, Chemical & Earth Sciences, Deep-Sea Research/Part B: Oceanographic Literature Review, Excerpta Medica, Index Medicus, Mass Spectrometry Bulletin, PASCAL-CNRS, Referativnyi Zhurnal, Research Alert and Science Citation Index)

REGULAR PAPERS

Column Liquid Chromatography

Gas Chromatography

Electrophoresis

(Continued overleaf)

Contents (continued)

SHORT COMMUNICATIONS

Column Liquid Chromatography

ELSEVIER

Journal of Chromatography A, 663 (1994) 135–150

JOURNAL OF CHROMATOGRAPHY A

Analysis of unresolved chromatograms by the absorbance ratio and sequential chromatogram ratio techniques coupled with peak suppression

Timothy J. Bahowick, Darren R. Dunphy, Robert E. Synovec*

Department of Chemistry BG-10, University of Washington, Seattle, WA 98195, USA

(First received July 14th, 1992; revised manuscript received July 28th, 1993)

Abstract

The sequential chromatogram ratio (SCR) technique was successively applied or was coupled with the absorbance ratio (AR) technique to facilitate analysis of a peak of interest that was overlapped with two other peaks. First, the AR or SCR technique was used to suppress one undesired peak. This created or elongated a region of pure-component elution for the peak of interest. Then the appropriate ratio technique was applied to this region for qualitative and quantitative analysis. The AR technique allows suppression and qualitative analysis of unknown components via the absorptivity ratio. For the SCR technique, peak identity can be deduced prior to suppression and quantitative analysis. A statistical peak matching procedure that employs user-selected standards is described for the SCR technique, by which components in sequentially injected samples may be identified based on differences in retention time, t_R, or in diffusion coefficient, D_m, which controls peak width. For two similarly retained analytes in sequentially injected samples, having a factor-of-two difference in D_m, the problem of reduced resolution, R_s, with a third peak was investigated by manipulating the data to simulate a reduction in selectivity factor. Below a limit, $R_s = 0.38$, the original two analytes could no longer be qualitatively distinguished. At this same R_s limit, the two-times difference in D_m, for two analytes having essentially zero t_R-based resolution, provided equivalent qualitative discrimination of peaks as a t_R-based resolution of 0.12 for two analytes having equal D_m. The classical problems of inaccurate baseline correction and run-to-run retention variation were examined, and the latter was more limiting for the SCR technique. Still, small t_R shifts were adequately corrected by selecting and aligning a common peak in sequential chromatograms.

1. Introduction

Chromatography necessarily involves an overall compromise between analysis time, resolution of peaks, and instrumental limitations. For application of chromatography to industrial process monitoring [1], the instrumentation should be made simple and reliable, for example by avoiding complicated gradient systems and the increased maintenance and safety concerns associated with high-pressure, high-efficiency analytical HPLC columns and pumps. Further, rapid chromatographic analysis in the high- and superspeed regimes [2] facilitates effective process control. Unfortunately, these desirable characteristics are achieved at the sacrifice of resolution, which increases the likelihood of peak overlap due to bounded peak capacity [3] and

* Corresponding author.

0021-9673/94/$07.00
SSDI 0021-9673(93)E1188-6

inadequate thermodynamic selectivity factors. Even for laboratory applications, especially moderately well defined systems such as routine assays, it is often preferred to use a chemometric technique to extract analytical information from overlapping peaks rather than expend the resources of time and instrument complexity needed to achieve baseline resolution. Therefore, suitable data analysis techniques are continually sought that enable identification and quantification of an analyte or interferent in the case of partial or complete overlap with other peaks.

The most challenging data analysis situation involves the necessity to use single-channel detection, such as refractive index, because minimally, the analyst is merely alerted to the presence of unknown overlapped interferent(s). Quantification of overlapped peaks, including unknowns, requires additional information [4], for example by making assumptions about the chromatographic peak shapes, as is done for simple geometric methods [5] such as perpendicular drop, as well as for non-linear curve-fitting techniques [6]. More powerful data analysis techniques, that do not require peak shape assumptions about unknown components, involve expanding the dimensionality of the data [4]. This is usually achieved using UV–Vis or MS multichannel detection, but was recently done using two sequential conductometric detectors [7]. Two techniques of increasing dimensionality that are simple and work well for analysis of unresolved peaks, including unknown interferents, are the absorbance ratio (AR) technique [8–11] and the sequential chromatogram ratio (SCR) technique [12–14]. Both techniques employ the point-by-point ratio of two baseline-corrected chromatogram data vectors, as obtained from simultaneous dual-wavelength detection of a single sample (AR) and from two single-channel chromatograms obtained by sequential injections of related samples (SCR). Both techniques use the flat, pure-elution region of the ratiogram for peak-purity assessment and peak identification. The AR technique has greater power for unknown identification by means of the absorptivity ratio, but lacks the capability for quantification. For the SCR technique, identification is accomplished by a procedure, described herein, that matches an unknown peak with chromatograms of user-selected candidate standard solutions. Once peak identity is verified in sequential samples, the SCR technique immediately provides quantitative information, the ratio of injected concentrations.

Often, the peak of interest is completely overlapped by more than one other peak and does not possess an adequate pure-elution region within the chromatogram. In such situations, the AR and SCR techniques may be combined in stages, by suppressing the response of an unwanted peak that is overlapped with the peak of interest. The initial stage, suppression, uses a ratio technique with two chromatogram data vectors to calculate a scaling constant that allows the signal contribution of one component, common to both vectors, to be subtracted away. Using the familiar spectral suppression technique [15–17], a component may be suppressed without the need for identification, by virtue of its spectral properties. We will show that a component may similarly be suppressed using two single-channel chromatograms when it is known or can be ascertained from the data that the component is common to both chromatograms. The process of suppression uncovers or elongates a pure-elution region for the desired component. Following suppression, the analysis stage consists of applying the appropriate ratio technique to this pure-elution region to extract qualitative and quantitative information as outlined in the previous paragraph.

In this paper, coupling of the SCR and AR techniques through suppression is applied to a challenging test separation in which the peak to be analyzed is largely overlapped with two other peaks. We begin with successive application of the SCR technique, which requires either advance knowledge of analyte identity or a short list of likely analytes and suspected interferents. In this context, we first digress to evaluate the classical problems of inaccurate baseline correction, common to both techniques but previously unreported for the SCR technique, as well as run-to-run retention time variation, which is

more limiting for the SCR technique. By preselecting a common peak in the chromatograms as a timing standard, run-to-run retention variation can be corrected sufficiently to permit subsequent analysis. After dealing with the classical problems, we demonstrate the peak matching procedure for identification of peaks in sequential chromatograms, subsequent peak suppression, and quantification using the SCR technique. The ability to qualitatively discriminate similarly retained components in sequential chromatograms is enhanced when the components have different diffusion coefficients, D_m, because of the resulting difference in peak width. This result will be established using calculations which compare the sensitivity of differences in D_m and in t_R for distinguishing different components in sequential chromatograms when resolution is below 0.5. The significance is that selectivity due to peak shape differences, which occur among similarly retained analytes having different D_m, is not considered useful for analytical chromatography [18,19]. Recent calculations of higher statistical moments in linear non-ideal chromatography [20,21] suggest otherwise. Note, the data manipulations and plots within this section do not reflect the simple application and interpretation of ratio-based techniques [8–14]. Next, SCR-based suppression of a known analyte followed by AR analysis is demonstrated for obtaining a more confident absorptivity ratio by which to identify an unknown component. Finally, the reverse situation, AR-based suppression followed by SCR analysis, is demonstrated for improved quantification of an identified analyte after conveniently suppressing an unknown peak without requiring identification. Successive application of the AR technique, which has been demonstrated for complete deconvolution of unknown mixtures [22], will not be covered.

2. Theory

A brief review of the AR and SCR techniques is useful to illustrate their mathematical similarity and complimentary nature. Both ratio techniques begin with a detected chromatographic signal, $S^{\lambda 1}(t)$, of an initial sample, S, containing M solutes. Assuming linear, concentration-sensitive absorbance detection and temporarily ignoring noise, the data vector, $S^{\lambda 1}(t)$, is given by

$$S^{\lambda 1}(t) = \sum_{j=1}^{M} \epsilon_{j,1} b C_{j,S} G_j(t) \quad (1)$$

where $\epsilon_{j,1}$ is the absorptivity (molar or specific) at wavelength 1 for analyte j, b is the optical pathlength of the detector, $C_{j,S}$ is the injected concentration of analyte j within sample S, and $G_j(t)$ is the dispersed concentration profile, sensed at the detector, for a unit concentration of solute j injected in a small, constant volume. For all chromatograms, $S^{\lambda 1}(t)$ is the result of digitizing the detected signal at uniform sampling intervals from the point of sample injection, and then applying a suitable algorithm to center the baseline at zero [23]. Use of computer-automated sample injection and data acquisition is necessary for precise timing of events.

Both ratio techniques employ a second chromatogram data vector, defined presently, obtained using the same separation conditions and data acquisition procedures as for $S^{\lambda 1}(t)$. Ideally, each analyte occupies the same time axis region in both data vectors, which have the same number of points. Both ratio techniques involve calculating the point-by-point ratio of the two data vectors, yielding a ratiogram that is plotted *versus* the corresponding time, t, since injection. To increase interpretability and to prevent division by zero, the ratiogram is set to zero in regions where either data vector falls below a specified noise threshold [9,12,13].

The well-known AR technique employs simultaneous dual-wavelength detection of the single injected sample, S. The absorbance ratiogram, $AR(t)$, is defined as the point-by-point ratio of the two chromatogram data vectors corresponding to detection wavelengths 2 and 1 for sample S

$$AR(t) = \frac{S^{\lambda 2}(t)}{S^{\lambda 1}(t)} = \frac{\sum_{j=1}^{M} \epsilon_{j,2} b C_{j,S} G_j(t)}{\sum_{j=1}^{M} \epsilon_{j,1} b C_{j,S} G_j(t)} \quad (2)$$

where the notation emphasizes that the ratios are calculated at corresponding time points, t. Within a pure-elution region of the chromatogram for a particular solute, j, the quantities b, $C_{j,S}$ and $G_j(t)$ are identically equal for the same injected sample, S, detected at both wavelengths. Therefore, $AR(t)$ simplifies, in the absence of significant noise, to a flat, time-invariant form within the pure-elution region

$$AR(t) = AR_j = \frac{\epsilon_{j,2}}{\epsilon_{j,1}} \tag{3}$$

in which AR_j is equal to the ratio of absorptivities for analyte j between the two wavelengths used.

For the SCR technique, the second data vector is obtained from a subsequent chromatogram run, also detected at wavelength 1, for a similar injected sample, U

$$U^{\lambda 1}(t) = \sum_{j=1}^{M} \epsilon_{j,1} b C_{j,U} G_j(t) \tag{4}$$

where the injected concentrations, $C_{j,U}$, may differ from $C_{j,S}$ in Eq. 1. The sequential ratiogram, $R(t)$, is defined as

$$R(t) = \frac{U^{\lambda 1}(t)}{S^{\lambda 1}(t)} = \frac{\sum_{j=1}^{M} \epsilon_{j,1} b C_{j,U} G_j(t)}{\sum_{j=1}^{M} \epsilon_{j,1} b C_{j,S} G_j(t)} \tag{5}$$

Within the pure-elution region for a particular solute, j, the quantities ϵ_j and b are automatically equal, and $G_j(t)$ is ideally equal for sequential chromatograms $S^{\lambda 1}(t)$ and $U^{\lambda 1}(t)$. Therefore, $R(t)$ also simplifies, in the absence of significant noise, to a flat, time-invariant form within the pure-elution region

$$R(t) = R_j = \frac{C_{j,U}}{C_{j,S}} \tag{6}$$

in which R_j is equal to the ratio of injected concentrations for analyte j in the sequential samples, S and U.

For both ratio techniques, objective data analysis beyond visual interpretation requires calculation of the pure elution region ratio values, represented by Eqs. 3 and 6. The two boundaries of the pure-elution region may be located by the threshold process mentioned above or from the first derivative of the ratiogram (Experimental section). The variation in noise magnitude throughout a ratiogram [13,24] may be compensated by using the reciprocal local variance as a weighting factor. Within the pure-j region of a ratiogram, a variance-weighted, least-squares horizontal line is fitted. This procedure yields a weighted-average estimate for AR_j or R_j, as well as a weighted standard deviation, s_w [12,13].

The statistic, s_w, is comprised of two independent variance components that measure the noise-related imprecision of the ratio value and the horizontal flatness of the ratiogram, respectively. This latter component, which quantifies lack-of-fit of the ratio model (Eqs. 3 and 6), gives the s_w statistic several practical uses. Differences in analyte retention time or peak shape between $S^{\lambda 1}(t)$ and $U^{\lambda 1}(t)$ will curve the ratiogram (Eqs. 2 and 5), thus inflating s_w above the minimum value associated with random noise. Therefore, minimization of s_w is a precise method to align a given peak in two sequential chromatograms for elimination of small retention shifts [13]. The s_w statistic may also be used to objectively locate the boundaries between flat pure-elution regions of a ratiogram and curved coelution regions (Experimental section). Also, use of s_w for measuring the flatness of $R(t)$ assists in peak identification, both in confirming the presence of a component in both $S^{\lambda 1}(t)$ and $U^{\lambda 1}(t)$, and in matching an unknown peak with pure-component chromatograms of user selected candidate standard solutions. For this matching procedure, the value of s_w from the sequential ratio of an unknown peak, $U^{\lambda 1}(t)$, with a standard, $S^{\lambda 1}(t)$, should be divided by $\sqrt{1 + R_j^2}$, where this divisor is obtained from propagation of errors [13] and R_j is the weighted-average ratio value. The division adjusts for concentration differences between the unknown and standard solutions. This quotient is then compared to the corresponding quotient calculated from sequential ratiograms of replicate chromatograms for the same standard solution, S. If the quotients match within experimental uncertainty, esti-

mated by performing at least 3 to 5 replicates each, then the evidence for a match is strong. The strength or confidence of the peak match is increased by the existence of peak shape differences among coeluting analytes. This will be demonstrated later.

It is instructive to contrast the information provided by the AR and SCR techniques. For both techniques, observation of a horizontal flat region indicates peak purity and locates the pure-elution region for an analyte. The AR technique possesses greater capability for identification of a completely unknown peak because the absorptivity ratio provides spectral discrimination among solutes. Peaks may also be identified using sequential ratiograms by matching an unknown peak with selected candidate standards, as described above. The SCR technique has the advantage of immediately providing quantitative information once peak identity is established, because for an analyte, j, the quantity $(R_j - 1)$ is the relative concentration change between sequential samples S and U (Eq. 6). In contrast, all concentration information cancels from the pure-elution region of $AR(t)$ (Eq. 3).

A common analysis situation is that the peak of interest is overlapped with one or more peaks and does not possess an adequate pure-elution region. With three independent chromatogram data vectors (defined later by Eqs. 10 and 11), one vector (*i.e.* dimension) may be used to suppress one undesired peak common to all three vectors. The appropriate ratio technique is then applied to analyze the peak of interest within the pure-elution region that was uncovered by suppression. Previous suppression approaches sought to isolate the peak of interest for subsequent height or area analysis [15–17]. By using suppression merely to uncover a pure-elution region, fewer detection wavelengths or samples may be needed.

Suppression involves multiplicative scaling of one data vector by a suppression constant, k_q, so that the signal contribution of the component to be suppressed becomes equal with respect to a second data vector. Subsequent point-by-point subtraction of the two vectors yields a new vector, possessing no contribution from the suppressed component. Assuming linearity of the adsorption isotherm and the detector, the detected signal for a solute to be suppressed, q, is proportionally related, either between dual-wavelength chromatograms for the same injected sample, or between single-wavelength chromatograms for two sequential samples. Therefore, solute q may be suppressed using either dual-wavelength or sequential-chromatogram data as follows. If solute q is completely unknown and unsuspected, it may be suppressed spectrally without requiring identification. Employing dual-wavelength detection, the suppressed chromatogram, $S(t)_{\text{supr}}$, is given as

$$S(t)_{\text{supr}} = S^{\lambda 2}(t) - k_{q,2/1} S^{\lambda 1}(t) \tag{7}$$

Referring to Eq. 3, $k_{q,2/1}$ is equal to the ratio of absorptivities of solute q at wavelengths 2 and 1, and can be calculated from the pure-q region in $AR(t)$. Alternatively, the presence of solute q may be known or suspected in the two sequential samples, S and U. Once the identity of solute q is confirmed, as described earlier, it may be suppressed easily as follows. Using two sequential chromatograms, the suppressed chromatogram, $U(t)_{\text{supr}}$, is given as

$$U(t)_{\text{supr}} = U^{\lambda 1}(t) - k_{q,U/S} S^{\lambda 1}(t) \tag{8}$$

Referring to Eq. 6, $k_{q,U/S}$ is equal to the ratio of concentrations of solute q in samples U and S, and can be calculated from the pure-q region in $R(t)$.

A general limitation of the suppression technique is that it diminishes the S/N ratio for all other peaks in the chromatogram. Because suppression involves subtraction of two chromatograms that each contain noise, the noise level following suppression can increase by a factor of $\sqrt{2}$, assuming a random, independent noise distribution. More importantly, a fraction of the peak for each analyte is removed in the process of suppressing solute q. The percentage signal for a desired solute, j, remaining after suppression of solute q, is given by

$$\text{percentage } j \text{ remaining} = 100(1 - k_q/k_j) \tag{9}$$

For a successful analysis, the S/N ratio for the desired solute, j, must be sufficiently high after suppression. According to Eq. 9, this consideration requires that the suppression constants for solutes q and j be sufficiently different. For a single injected sample detected at two wavelengths, the restriction is

$$k_{j,2/1} = \frac{\epsilon_{j,2}}{\epsilon_{j,1}} \neq \frac{\epsilon_{q,2}}{\epsilon_{q,1}} = k_{q,2/1} \quad (10)$$

and for chromatograms of two sequential samples detected at the same wavelength

$$k_{j,U/S} = \frac{C_{j,U}}{C_{j,S}} \neq \frac{C_{q,U}}{C_{q,S}} = k_{q,U/S} \quad (11)$$

If either Eqs. 10 or 11 is violated, then the desired solute, j, is suppressed along with solute q. This necessitates care in wavelength selection for suppression using the AR technique (Eq. 10), which has been addressed [11,16,25,26]. For suppression using the SCR technique, the analogous cautions and criteria apply to analyte concentrations in sequential samples (Eq. 11). Often, when the peak to be suppressed is known or can be identified, it is potentially more feasible to select or adjust analyte concentrations than to select detection wavelengths. In particular, by employing a pure-component chromatogram of solute q as $S^{\lambda 1}(t)$ (Eq. 8), $k_{j,U/S}$ is theoretically infinite (Eq. 11) and no suppression of solute j occurs (Eq. 9). This advantage was recently demonstrated with high-speed HPLC analysis of high-fructose corn syrup for process monitoring applications [14].

3. Experimental

The chromatographic apparatus employed a Zorbax 150 × 4.6 mm, 5 μm C_{18} column (MacMod, Chadds Ford, PA, USA) and an LC-2600 syringe pump (ISCO, Lincoln, NE, USA). The detector was an ISCO V^4 single-channel UV–Vis absorbance detector, set to 0.02 or 0.05 AU sensitivity, with a flow cell having 5 mm pathlength and 3.5 μl illuminated volume. Dual-wavelength detection was approximated by recording all samples at 250 nm and then at 260 nm. These wavelengths were chosen by the method of absorbance index [25]. Injections were made using a valve (Valco, Houston, TX, USA) equipped with a 5-μl loop and an electric actuator. The eluent was approximately 8% (v/v) water in methanol, flowing at 1 ml/min. Sample mixtures were prepared by volumetric dilution of stock solutions of high-purity chemicals in HPLC-grade methanol. Typical injected concentrations are listed in Table 1.

Automated sample injection and 12-bit res-

Table 1
Solution data and results for ratio-based analysis

	Chlorobenzene	Toluene	Dibutyl phthalate
C_U (mM)	2.09	2.27	0.208
C_S (mM)	2.61	2.27	0.156
W_B (s)[a]	7.0	7.3	9.3
R_{true} [b]	0.80	1.00	1.33
R_{meas} [b,c]	0.797 ± 0.003	1.01 ± 0.01[f]	1.33 ± 0.05
AR_{ref} [d,e]	2.354 ± 0.003	2.39 ± 0.03[f]	0.358 ± 0.001
AR_{meas} [d,c]	2.34 ± 0.04	2.40 ± 0.03[f]	0.37 ± 0.04

All measured ratio values are listed ± one standard deviation (3 trials).
[a] Peak width at base.
[b] $R = (C_U)/(C_S)$ by Eq. 6.
[c] Measured value from pure-elution region in mixture chromatograms.
[d] $AR = (\epsilon_{250\ nm})/(\epsilon_{260\ nm})$ by Eq. 3.
[e] Reference value from pure-component chromatograms.
[f] After suppression of dibutyl phthalate.

olution data acquisition were described previously [13]. The S/N ratio was about 500. The data sampling rate was 54 Hz or 60 Hz, permitting small adjustments for alignment of a selected peak in sequential chromatograms [13]. Data post processing routines were written as MATLAB functions (The Math Works, South Natick, MA, USA). Baseline correction was performed as previously described [23]. The ratiograms were set to zero in regions where the detected signal fell below a noise threshold of about 3–4% of the tallest peak height. This located the pure-elution region boundary in the peak tail for both interferent suppression and analyte analysis (described later). The other "inner" pure-region boundary was located according to the increase in the s_w statistic when the boundary was extended into a coelution region. For the last study, this boundary was located instead where the first derivative of the ratiogram exceeded a threshold value indicative of horizontal (zero) slope [12]. The algorithm details for calculation of the ratio value and s_w were given previously [13]. Data post-processing requires several minutes per trial, although no attempt was made to assemble an all-inclusive, non-interactive package. All reported resolution values were obtained by measuring retention time and width at half height of isolated peaks.

4. Results and discussion

4.1. Suppression and analysis using the SCR technique

This section consists of studies that illustrate analysis of a peak of interest that is overlapped by two other peaks. We begin with the case that only single-channel detection is available, but where available knowledge of sample analytes and interferents permits identification, suppression, and subsequent analysis using the SCR technique. Two overlaid sequential chromatograms are shown in Fig. 1a, as obtained from two different samples, S and U, having analytes in common. The resolutions, R_s, were 1.10 for peaks C (chlorobenzene) and T (toluene), and 0.90 for peaks T and P (dibutyl phthalate). Although the overlap for peak T was not severe, this data will be used to examine the classical problems of ill-defined detector baseline and run-to-run changes in retention time.

The problem of baseline slopes and/or offsets for the AR technique [9,16] is equally relevant to the SCR technique. A sloping baseline correction [23] is most effective when the true baseline can be located before and after the peaks of interest. The SCR technique is also susceptible to difficulties and errors due to small run-to-run retention shifts. An adequate, albeit local retention correction may be achieved by selecting a peak, common to both chromatograms, to serve as a timing standard (TS). Provided that the TS peak is well-resolved ($R_s > 0.8$), it is easy to align the TS peak in both chromatograms, $S(t)$ and $U(t)$, by shifting them so as to minimize the weighted standard deviation, s_w, as calculated from the sequential ratiogram, $R(t)$ (Eq. 5) [13]. For this purpose, both samples in Fig. 1a contained benzene as TS (caution, known carcinogen!), but other similarly retained compounds would suffice. Deferred injection of the TS has also been practiced [27]. The sequential ratiograms in Fig. 1b show that typically occurring, uncorrected run-to-run retention shifts are usually more limiting for the SCR technique than are typical errors in baseline correction. The middle curve, offset downward by 0.35 for clarity, is $R(t)$ as obtained before chromatogram alignment using the TS peak. The retention shift shown, a representative value of only 0.1 s, severely distorted the pure-elution regions of this ratiogram. The top curve in Fig. 1b, for which the TS peak was aligned, shows good retention correction for peaks near the TS peak, as evidenced by the flat pure-elution regions for peaks C and P. In contrast, the bottom curve in Fig. 1b, offset by 0.7, is $R(t)$ as obtained from the aligned chromatograms, but where a large run-to-run error in baseline correction was simulated by first adding the dashed sloping baseline, shown in Fig. 1a, to the later chromatogram, $U(t)$. As expected [9,16], the pure-elution regions of this ratiogram were bowed upward. These baseline correction and chromatogram alignment procedures provided objective and satisfactory corrections for the reported analyses.

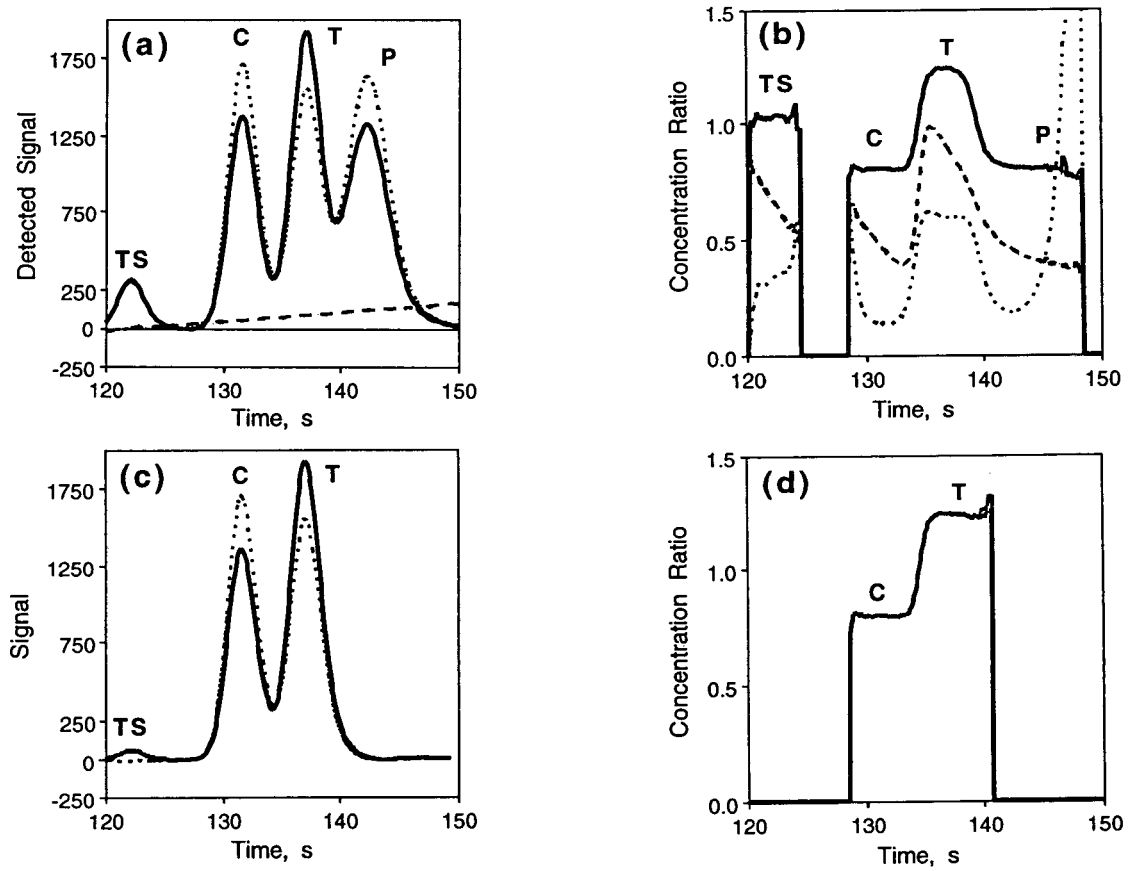

Fig. 1. (a) Overlaid sequential chromatograms of initial (S, dotted) and later (U, solid) samples. Analytes are chlorobenzene (C), toluene (T) and dibutyl phthalate (P), detected at 270 nm. The timing standard peak (TS, benzene) was used to align the chromatograms. The dashed diagonal line is a simulated baseline correction error. (b) Sequential ratiograms, $U(t)/S(t)$, from Fig. 1a after applying a noise threshold. Top curve (solid): proper baseline correction and alignment using the TS was performed prior to ratio; middle curve (dashed, offset downward by 0.35): effect of the typical 0.1-s retention shift that was then corrected (top curve) using the TS peak; bottom curve (dotted, offset by 0.7): effect of adding the sloping baseline error from Fig. 1a to chromatogram $U(t)$. (c) Suppressed chromatograms from Fig. 1a after using a pure-P chromatogram to suppress peak P via SCR. (d) Suppressed sequential ratiogram from Fig. 1c showing extended pure-elution region for analyte T.

Next, the desired analyte, T, was analyzed by first suppressing the overlapping peak, P, to extend the pure-elution region for peak T. A pure-P chromatogram (not shown) was used for suppression, which assumes that peak P was either known in advance or was identified, for example, by peak matching (demonstrated below). Following Eqs. 6 and 8, the suppression constants, $k_{P,U/S}$, were calculated from the pure-P region of sequential ratiograms for both chromatograms, $S(t)$ and $U(t)$, taken with the pure-P chromatogram. For example, the mean and standard deviation suppression constant (four replicates) for the initial solution, S, was 1.022 ± 0.003, which agreed adequately with the expected volumetric value of 1.00. The corresponding sequential chromatograms from Fig. 1a, after suppression of peak P, are shown in Fig. 1c, and $R(t)$ for these suppressed chromatograms is shown in Fig. 1d. After suppression, the pure-T region was extended from 2 to 5 s, about 70% of the baseline peak width. The relative concentration change for peak T was quantified by the weighted-average ratio value, R_j, 1.235 ± 0.002,

which agreed adequately with the expected volumetric value of 1.25. This quantitative result is resistant to errors in the interferent suppression constant. For example, if $R_s = 0.5$ for equal Gaussian peaks, the contribution of the interferent to the analyte peak height is only 13.5%. Residual interferent contribution due to suppression constant error is attenuated accordingly, and the increased residual interferent contribution in the analyte tail receives correspondingly less weight in the algorithm. In summary, suppression of peak P, using a pure-component chromatogram, improved the ability of the SCR technique to verify and then quantify the concentration increase for analyte T.

A second study examines use of single-channel data to qualitatively discriminate and identify two analytes in sequential chromatograms in the case that resolution based on differences in retention time, t_R, is essentially zero, but where significant selectivity exists because of differences in diffusion coefficient, D_m. The same analytes and conditions as in the first study were employed. For brevity, we begin with the sequential ratiogram, $U(t)/S(t)$ (Eq. 5), for two new samples, S and U. In this ratiogram, Fig. 2a, the distorted shape within the pure-T region (135 to 139 s) suggests a new interferent in sample U, rather than an increase in analyte T. The visually flat regions for components TS, C and P in Fig. 2a rule out uncontrolled baseline or timing problems, as studied in Fig. 1b. Similarly to the first study, suppression of overlapping peak(s) facilitates our goal of characterizing the composition change for the middle peak. For this simplified study, analytes C and P did not change concentration between samples S and U, consistent with the two respective flat pure-elution regions at 1.0 in $R(t)$ (Fig. 2a). Therefore, point-by-point subtraction [28] of chromatograms $U(t)$ and $S(t)$ suppresses peaks C and P (Eq. 8, $k_{q,U/S} = 1.0$). More generally, pure-component chromatogram(s) could be used to suppress peaks P and/or C from $U(t)$ and $S(t)$, as demonstrated in Fig. 1c, prior to subtraction. The difference chromatogram, labeled as DIFF in Fig. 2b (solid curve), demonstrates effective suppression of peaks C and P. Also shown in Fig. 2b are two pure-component chromatograms of analyte T (middle curve) and a suspected interferent, X (top curve, benzylbutyl phthalate). For visual clarity, these chromatograms were scaled by factors of 0.3 and 0.6 for components T and X, respectively. The t_R-based resolution of peaks T and X, 0.03, was negligible.

The peak, DIFF, which is the isolated detected response corresponding to the composition change of interest for the middle peak, can be identified by matching the DIFF peak with peaks from sequential chromatograms of standards. After applying the noise threshold [12] to DIFF, $R(t)$ was calculated for the DIFF peak taken in turn with the unscaled chromatograms of components T and X. As shown in Fig. 2c, the bowed, dotted ratiogram is DIFF/T. The flat, solid ratiogram is DIFF/X, thus giving a visual match of the DIFF peak with the interferent, X. If analyte T had changed concentration as well, neither ratiogram in Fig. 2c would have appeared flat, but concentration changes in T only or X only could be excluded. Statistical assessment of ratiogram flatness is demonstrated in the following paragraphs.

Although analytes C and P are suppressed from Fig. 2c, this data may be used to examine use of the SCR technique for identification and quantification of the DIFF peak for the case that peak C is not suppressed and that its resolution with peak T decreases due to a reduction in selectivity factor. Resolution of adjacent peaks is important for both the AR and SCR techniques because it dictates the duration and S/N ratio of the available pure-elution region, which is used for identification, suppression, and quantification. The known pure-component retention times and peak widths were used to relate R_s for peaks C and T with a left-hand boundary of the available pure-T region in both ratiograms (Fig. 2c). For example, when $R_s = 1.10$ for peaks C and T, the right tail of peak C extended to 135.2 s, thus defining the initial left pure-region boundary, labeled α in Fig. 2c. Moving this boundary, α, to the right progressively shortened the pure-T region, as though peak C were artificially moved right toward peak T. For each value of R_s for peaks C and T, the flatness statistic, s_w/

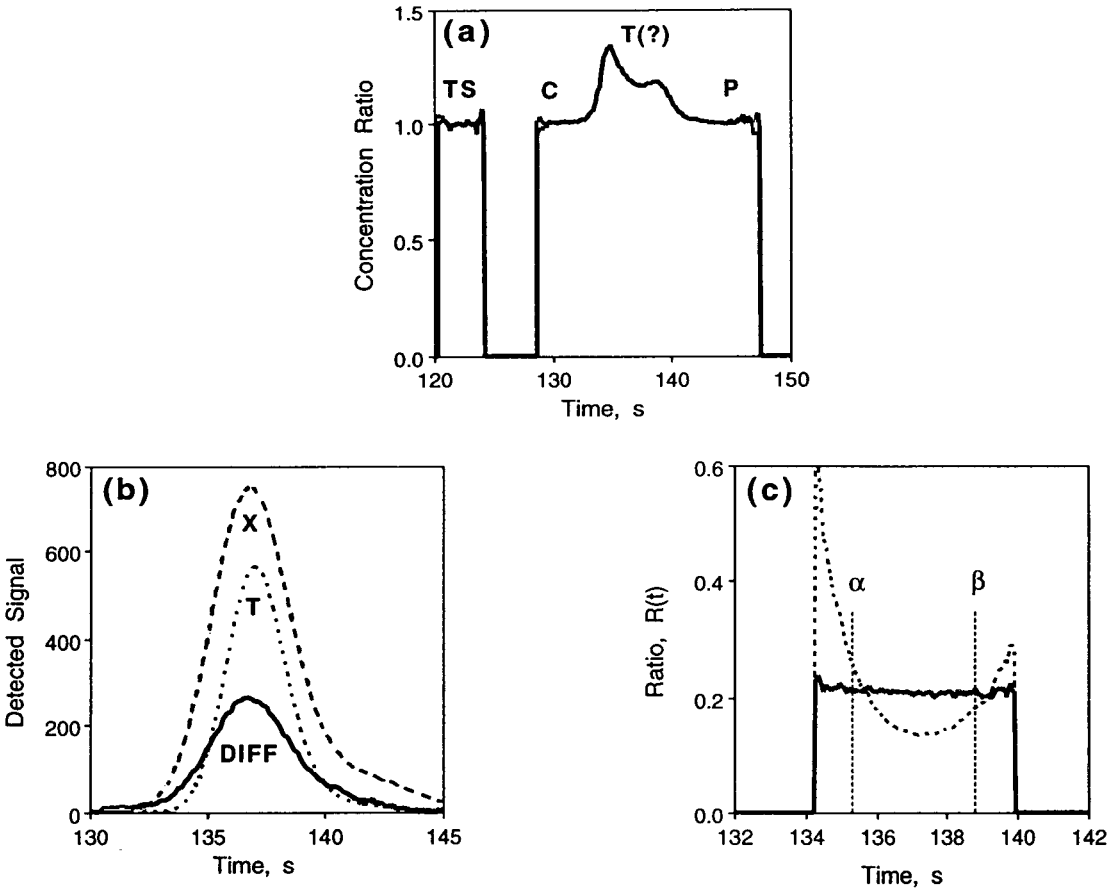

Fig. 2. (a) Sequential ratiogram, $U(t)/S(t)$, corresponding to Fig. 1b (top curve), but for different samples, S and U. The distorted appearance within the pure-T region (135–139 s) suggests a new interferent in $U(t)$. (b) Characterization of composition changes between samples S and U. Bottom curve (solid): point-by-point difference (DIFF) of the original chromatograms (not shown), which for this study suppresses peaks C and P. Also shown are scaled (see text) pure-component chromatograms of analyte T (middle curve, dotted) and a suspected interferent, X (top curve, dashed, benzylbutyl phthalate). Their t_R-based resolution was only 0.03, but the diffusion coefficient, D_m, for analyte T was twice as large. (c) Identification and subsequent quantification of DIFF, from Fig. 2b, via SCR. Solid curve: DIFF/X; dotted curve: DIFF/T. The statistical test of ratiogram flatness matched DIFF with X. Labels α and β are left boundaries of the usable part of the ratiograms for an investigation of reduced R_s of peaks C and T, for which $R_s = 1.10$ (α); 0.38 (β).

$\sqrt{1 + R_j^2}$, and the weighted-average ratio value, R_j, were calculated [13] using the portion of the ratiograms to the right of the boundary (Fig. 2c). These results are shown in Fig. 3a and b as a function of R_s for peaks C and T. In both Fig. 3a and b, the mean values (solid) are enclosed by 95% confidence intervals (dotted) for six replications. The peak identification results in Fig. 3a were that concentration changes for analytes T and X, which lacked significant t_R-based resolution relative to each other, were confidently distinguished by the significant increase in the flatness statistic that occurred for an incorrect peak match. For $R_s = 1.10$ for peaks C and T (α), the flatness statistic for DIFF/X, 0.006 ± 0.004, matched the value for replicate chromatograms of standards, 0.006 ± 0.003, consistent with the visual match of peaks DIFF and X in Fig. 2c. The corresponding value for DIFF/T was significantly larger (Fig. 3a), therefore ex-

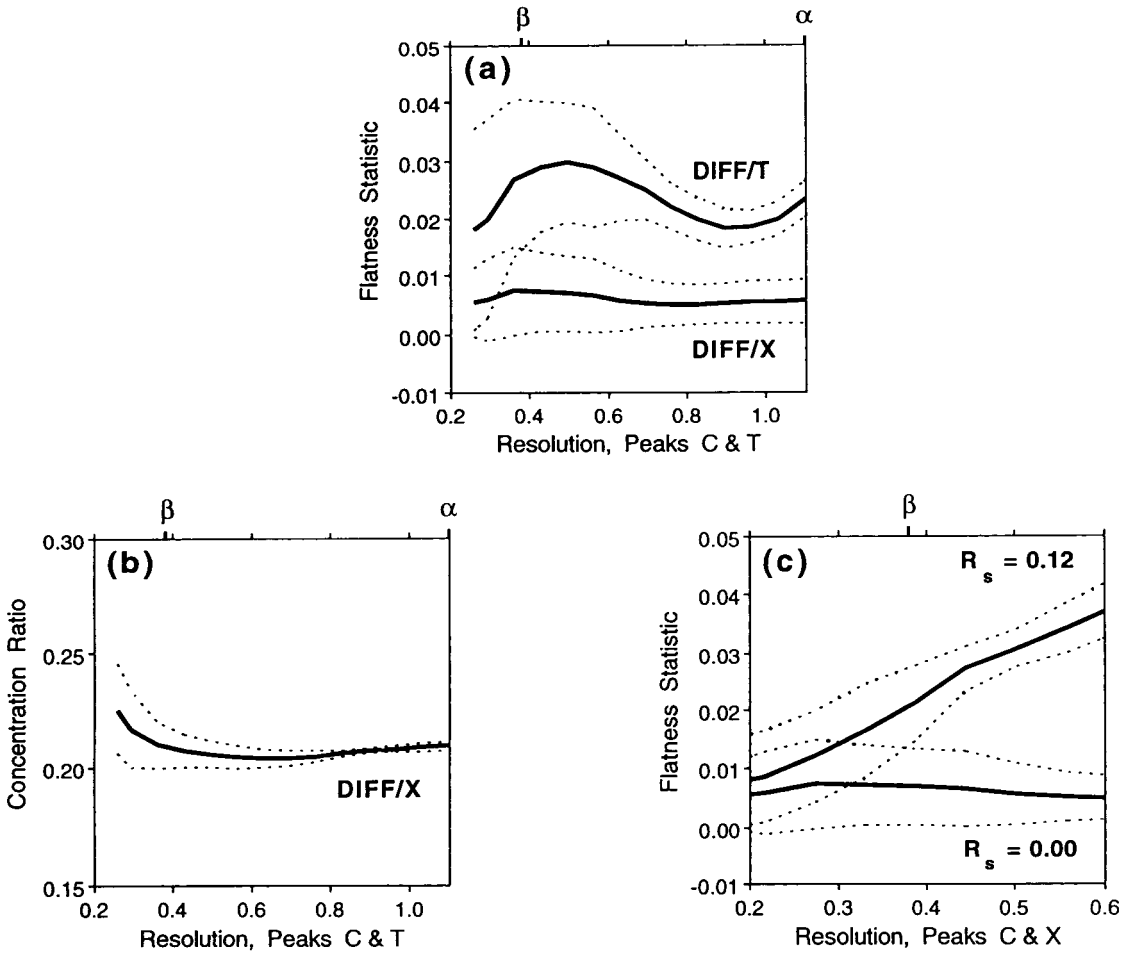

Fig. 3. Identification (a) and quantification (b) of DIFF, using the ratiograms from Fig. 2c, manipulating the data to investigate reduced R_s of peaks C and T. (a) When $R_s < 0.38$ for peaks C and T, the flatness statistic (solid) could not distinguish peaks X and T, because the 95% confidence intervals (dotted, 6 replicates) overlapped. (b) Quantification of DIFF by the weighted-average ratio value as calculated from DIFF/X (Fig. 2c). Good accuracy and precision (expected value 0.20) were maintained down to the R_s limit for identification, 0.38 (labeled β in Figs. 2c and 3). (c) Similar to Fig. 3a, except that the upper line corresponds to peak DIFF shifted to a R_s of 0.12 relative to peak X (Fig. 2b). The lower line is taken from Fig. 3a, where $R_s = 0.0$ for peaks DIFF and X. At the same R_s limit, β, for peaks C and X, the discrimination of the flatness statistic for the two-times difference in D_m for peaks X and T (Fig. 3a, $R_s = 0.03$) was equivalent to that for a t_R-based resolution of 0.12 (Fig. 3c, equal D_m).

cluding analyte T as the sole contribution to the DIFF peak. The ability to qualitatively discriminate peaks T and X became uncertain when R_s for peaks C and T fell below 0.38 (labeled β in Figs. 2c and 3), because the confidence intervals in Fig. 3a overlapped. At this point, β, the usable part of the ratiogram (Fig. 2c) was only one second wide, about 11% of the baseline peak width for X. The quantification results for the addition of interferent, X, are given in Fig. 3b by the ratio of injected concentrations, R_j, calculated over the same diminishing regions of DIFF/X as for Fig 3a. The accuracy and precision of R_j, relative to the expected volumetric value of 0.20, were satisfactory down to the observed R_s limit for identification, 0.38 (β, Fig. 3b). Drouen *et al.* [9] found a similar R_s limit for obtaining accurate absorptivity ratios and confi-

dent peak purity assessments using the AR technique. The limitations at low R_s arose from residual retention imprecision after aligning the TS peak and low S/N ratio in the peak tails, where uncertainty in locating the baseline as well as electronic or hydrodynamic "$1/f$" noise [29] can be relatively significant.

The ability to qualitatively discriminate peaks T and X, for which $R_s = 0.03$, is largely due to the peak width difference, which is a factor of 1.35, based on width at half-height. The upward bow for DIFF/T (Fig. 2c) suggests that peak X is wider than peak T, rather than merely having a small difference in t_R [13]. The larger peak width for X reflects increased band broadening due to slow mass transfer effects [30,31], because component X has a diffusion coefficient, D_m, half as large as for component T [30]. For the two solutes, T and X, having essentially equal capacity factors, k', the mass transfer contribution to peak width varies inversely with $\sqrt{D_m}$ [30,31], thus predicting a factor of 1.4 times larger peak width for component X.

This data may also be used to compare the sensitivity of discriminating peaks in sequential chromatograms for the two cases of differences in t_R and in D_m. By shifting the DIFF peak to the right to artificially create t_R-based resolution with respect to peak X, an exponential shape is produced in $R(t)$ for DIFF/X [13], which significantly increases the flatness statistic. With peaks DIFF and X shifted to a resolution of 0.12, reduced resolution of peaks C and X was investigated, using the same procedure as for Fig. 2c, which involved moving the left pure-region boundary of the ratiograms to the right from point α. The flatness statistic results for DIFF/X ($R_s = 0.12$) are plotted in Fig. 3c *versus* R_s for peaks C and X. For comparison, the results for the null case, DIFF/X ($R_s = 0.0$) from Fig. 3a, are repeated in Fig. 3c. Recall that the limit of resolution in Fig. 3a for peaks C and T, 0.38 (labeled β), referred to discrimination of peaks T and X essentially by their D_m difference. At this same resolution limit, β, for peaks C and X, we see in Fig. 3c that the t_R-based resolution introduced for peaks DIFF and X, 0.12, was just enough to yield a significant increase in the flatness statistic such that the confidence intervals did not overlap. Thus, the discrimination between peaks in sequential chromatograms due to a factor-of-two difference in D_m (Fig. 3a, $R_s = 0.03$) was equivalent to that of a t_R-based resolution of 0.12 (Fig. 3c, equal D_m). Clearly, both properties, t_R and D_m, contribute to the confidence of identification by peak matching. Considering the well-known likelihood of closely-spaced retention times for a complex mixture [3], the "extra" selectivity due to differences in D_m, especially for similarly retained non-homologous analytes or macromolecules, can increase the fraction of peaks in the mixture that are successfully analyzed [3].

4.2. Coupling the AR and SCR techniques through suppression

These studies will demonstrate improved qualitative analysis of an unknown peak via the absorptivity ratio after using sequential chromatograms to suppress a known component. Also, more reliable quantification of concentration changes for an identified component will be demonstrated after performing AR-based suppression of an interferent without requiring its identification. The data consists of chromatograms of two samples, S and U, which have different concentrations. The chromatograms were recorded at two detection wavelengths: 250 nm (Fig. 4a) and 260 nm (Fig. 4b). The resolution between peaks C and T was 1.10; between peaks T and P, 0.63. The left peak, C, served as the internal timing standard for alignment of sequential chromatograms. The absorbance ratiogram, $AR(t)$, for the later solution, U (250 nm/260 nm), and the sequential ratiogram, $R(t)$, for solutions U and S at 250 nm are shown in Fig. 5a and b, respectively. In both Fig. 5a and b, the longer and lighter ratiogram was obtained from the original chromatograms in Fig. 4a and b, whereas the shorter and heavier ratiogram, offset for visual clarity, was obtained after suppression of peak P (described later). For both $AR(t)$ and $R(t)$ (unsuppressed), peaks C and P each had adequate pure-elution regions from which to calculate the absorptivity ratios

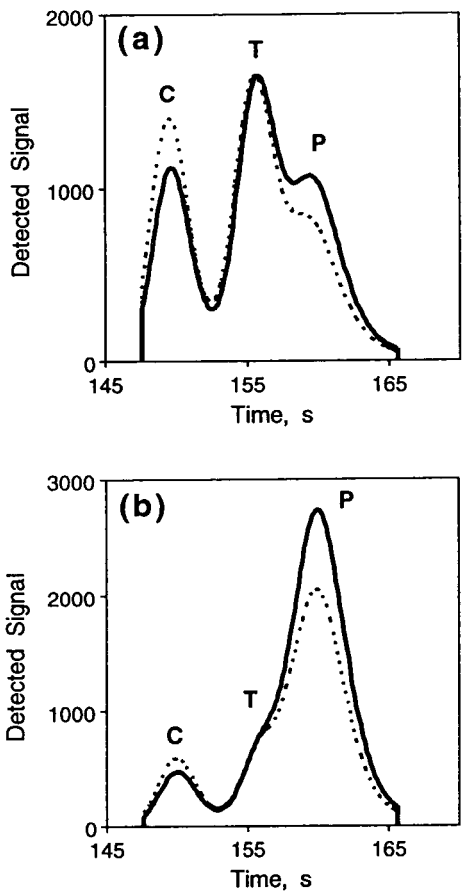

Fig. 4. Overlaid sequential chromatograms of initial (S, dotted) and later (U, solid) samples. Sample compositions are given in Table 1. Detection wavelengths, shown for both samples, were (a) 250 nm and (b) 260 nm. Application of the noise threshold is shown by the peak truncation. Peak C was used as an internal timing standard.

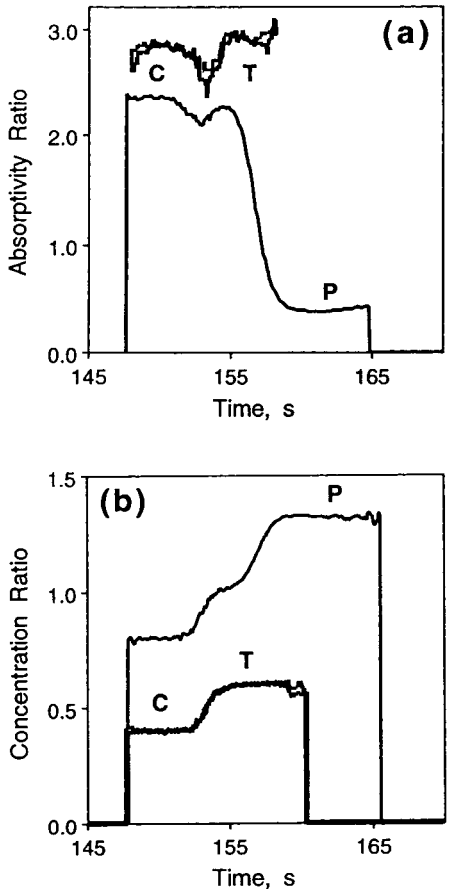

Fig. 5. Two overlaid ratiograms, before (long, light curve) and after (short, heavy curve) suppression of peak P, using only the data from Fig. 4a and b. The extended pure-elution region for peak T after suppression enables analysis of peak T: (a) absorbance ratiograms (250 nm/260 nm) for qualitative analysis, using Eq. 12 for sequential suppression (curve offset upward by 0.5); (b) sequential ratiograms ($U(t)/S(t)$ at 250 nm) for qualitative and quantitative analysis, using Eq. 13 for dual-wavelength suppression (curve offset downward by 0.4).

(Eq. 3) and the ratios of injected concentrations (Eq. 6). These results, collected in Table 1, agreed with the expected values.

Used without suppression, neither ratio technique provided qualitative or quantitative information for the middle peak, T, which lacked an adequate pure-elution region (Fig. 5a and b). By using the four chromatogram data vectors in Fig. 4a and b, any three of which are independent, peak P may be suppressed in order to facilitate analysis of peak T by extending its pure-elution region. This requires fewer runs than the earlier studies, which employed additional chromatograms of pure P for suppression. Analogous to a system of linear equations, suppression of additional peaks, if necessary, would require additional independent detection wavelengths (Eq. 10) or samples (Eq. 11). Sufficient resolution between adjacent peaks, studied in Fig. 3, would also be required for peak identification and subsequent calculation of the suppression constants.

Qualitative analysis of peak T in the dual-

wavelength domain (AR) is preferred when peak T is a true unknown and the absorptivity ratio is desired for identification. However, suppression of peak P using sequential chromatograms (SCR) implies that peak P is known or can be matched in both chromatograms and that its concentration varies independently from that of peak T (Eq. 11). Combining Eqs. 2 and 8, the absorbance ratiogram after suppression of peak P, $AR_{supr}(t)$, is given as

$$AR_{supr}(t) = \frac{U^{250}(t) - k_{P,U/S}S^{250}(t)}{U^{260}(t) - k_{P,U/S}S^{260}(t)} \quad (12)$$

where the suppression constant, $k_{P,U/S}$, (1.33) was calculated from the pure-P region of the unsuppressed sequential ratiogram, Fig. 5b. For $AR_{supr}(t)$ (Eq. 12), shown in Fig. 5a (heavy line, offset upward by 0.5), the pure-T region has been extended from 1 to 3.5 s, about 48% of the baseline peak width. The dip in the signal at 154 s may be attributed to low signal in the valley between peaks C and T, especially for 260 nm (Fig. 4b). The absorptivity ratio for peak T obtained after suppression, 2.40 ± 0.03 (three replicates), agreed with the reference value obtained from chromatograms of pure T, 2.39 ± 0.03.

On the other hand, quantitative analysis of peak T in the sequential-chromatogram domain (SCR) implies that peak T is identified in both samples or that its presence can be confirmed, as demonstrated earlier by peak matching. In this case, suppression of peak P using dual-wavelength data (AR) does not require its identification, only that the absorptivity ratios of peaks P and T differ (Eq. 10). Combining Eqs. 5 and 7, the sequential ratiogram after suppression of peak P, $R_{supr}(t)$, is given as

$$R_{supr}(t) = \frac{U^{250}(t) - k_{P,250/260}U^{260}(t)}{S^{250}(t) - k_{P,250/260}S^{260}(t)} \quad (13)$$

where the suppression constant, $k_{P,250/260}$, (0.37) was calculated from the pure-P region of the unsuppressed absorbance ratiogram (Fig. 5a). For $R_{supr}(t)$ (Eq. 13), shown in Fig. 5b (heavy line, offset downward by 0.4), the pure-T region has been extended to 5.8 s, about 80% of the baseline peak width. The concentration ratio for peak T obtained after suppression, 1.01 ± 0.01, agreed with the expected volumetric value of 1.00.

Note that the precisions of the R and AR values in Table 1 are for a limited data set. For instance, the average percent relative standard deviation (R.S.D.) for R_{meas} is 1.7% with a range of R.S.D. of 0.4 to 3.8%. A previous detailed examination of the precision of the SCR technique [13] revealed that the average R.S.D. was 3% for ten replicate pairs of an analyte peak. Since the SCR technique has the benefit of data averaging when a flat line is fit to a pure-elution region, the SCR technique precision should be limited in much the same way that peak area precision is limited. Comparison of the SCR technique precision level to conventional peak area and height measurements is useful in this regard. A cooperative study comparing the precision of peak height and area measurements in liquid chromatography indicated, as reported in Tables II and VII in ref. 32 as edited data for four test analytes, that the R.S.D. was $2.7\% \pm 1.0\%$ for peak area and $4.2\% \pm 1.1\%$ for electronic peak height measurements [32]. It is reasonable to conclude that the R.S.D. of the R_{meas} values in Table 1, while a bit low at 1.7% on average, are consistent with the precision results of the peak area cooperative study, $2.7\% \pm 1.0\%$ [32], and also with our previously reported precision for the SCR technique, 3% R.S.D. [13]. For the case of resolved chromatographic peaks, peak height and peak area measurements are easier to apply than the SCR technique. The role of the SCR technique is to facilitate analysis of ill-resolved small groups of peaks, possibly simplified by peak suppression, in which the remaining interferents are not known so that only the pure-elution region of the peak of interest is available for analysis, and peak height and peak area measurements are not feasible [12–14].

In comparing the two suppressed ratiograms (Fig. 5a and b), the implication of Eq. 9 is seen from the increased noise and the earlier peak T cut-off in $AR_{supr}(t)$ (Fig. 5a). The percentage

signal for peak T remaining after suppression of peak P, using Eq. 9 with suppression constants from Table 1, was 33% for $AR_{supr}(t)$ and 85% for $R_{supr}(t)$. This distinction reflects the large relative difference in absorptivity ratios for peaks P and T, whereas the concentration ratios were more similar (Table 1). Although the percentage signal for peak T, remaining after dual-wavelength suppression of peak P, was fixed by wavelength selection, the corresponding percentage, remaining after sequential-chromatogram suppression, would be increased if a pure-P chromatogram had been used for suppression.

These studies raise several issues for further work. Diffusion effects are important for qualitative analysis, as studied in Figs. 2c and 3a, and also for quantitative analysis, because diffusion-controlled peak width affects the duration and S/N ratio of the pure-elution region. Because k' and D_m describe somewhat independent thermodynamic and kinetic processes, respectively, the low resolution limits for any chromatographic data analysis technique depend on both analyte properties. Although the simple timing standard concept often works well as demonstrated, run-to-run variations in eluent temperature or flow rate can change peak-to-peak spacing in sequential chromatograms, becoming more severe with increasing distance from the TS peak. The relative importance of these detrimental effects increases with increasing plate count, holding k' constant. High-speed HPLC can reduce both the magnitude and the effect of flow-rate and temperature fluctuations, which are dominated by large low frequency components [29]. We are currently examining the trade-off of analysis time, resolution, and retention precision, as well as the role of solute diffusion rate, for extracting the needed qualitative and quantitative chemical information in the shortest analysis time.

5. Acknowledgements

D.R.D. thanks the National Science Foundation for support under grant No. CHE-900977, a program for undergraduate research experiences. D.J. Woodman is thanked for his work in supervising this program at the University of Washington, Department of Chemistry.

6. References

[1] J.B. Callis, D.L. Illman and B.R. Kowalski, *Anal. Chem.*, 59 (1987) 624A–637A.
[2] C.N. Renn and R.E. Synovec, *Anal. Chem.*, 60 (1988) 200–204.
[3] J.M. Davis and J.C. Giddings, *Anal. Chem.*, 55 (1983) 418–424.
[4] B.R. Kowalski and M.B. Seasholtz, *J. Chemom.*, 5 (1991) 129–145.
[5] A.N. Papas, *Crit. Rev. Anal. Chem.*, 20 (1989) 359–404.
[6] A.H. Anderson, T.C. Gibb and A.B. Littlewood, *J. Chromatogr. Sci.*, 8 (1970) 640–646.
[7] I. Berglund and P.K. Dasgupta, *Anal. Chem.*, 64 (1992) 3007–3012.
[8] A.F. Fell, H.P. Scott, R. Gill and A.C. Moffat, *J. Chromatogr.*, 282 (1983) 123–140.
[9] A.C.J.H. Drouen, H.A.H. Billiet and L. de Galan, *Anal. Chem.*, 56 (1984) 971–978.
[10] P.C. White and T. Catterick, *J. Chromatogr.*, 402 (1987) 135–147.
[11] E.L. Inman, M.D. Lantz and M.M. Strohl, *J. Chromatogr. Sci.*, 28 (1990) 578–583.
[12] R.E. Synovec, E.L. Johnson, T.J. Bahowick and A.W. Sulya, *Anal. Chem.*, 62 (1990) 1597–1603.
[13] T.J. Bahowick and R.E. Synovec, *Anal. Chem.*, 64 (1992) 489–496.
[14] D.R. Dunphy and R.E. Synovec, *Talanta*, 40 (1993) 775–780.
[15] G.T. Carter, R.E. Schiesswohl, H. Burke and R. Yang, *J. Pharm. Sci.*, 71 (1982) 317–321.
[16] P.A. Webb, D. Ball and T. Thornton, *J. Chromatogr. Sci.*, 21 (1983) 447–453.
[17] J.G.D. Marr, P. Horvath, B.J. Clark and A.F. Fell, *Anal. Proc.*, 23 (1986) 254–256.
[18] J.C. Giddings, in H.J. Cortes (Editor), *Multidimensional Chromatography —Techniques and Applications*, Marcel Dekker, New York, 1990, Ch. 1, p. 5.
[19] E.V. Dose and G. Guiochon, *Anal. Chem.*, 62 (1990) 174–181.
[20] M.S. Jeansonne and J.P. Foley, *J. Chromatogr.*, 461 (1989) 149–163.
[21] J.A. Jonsson, *Chromatographia*, 18 (1984) 427–433.
[22] N. Ostojic, *Anal. Chem.*, 46 (1974) 1653–1659.
[23] R.E. Synovec and E.S. Yeung, *Anal. Chem.*, 57 (1985) 2162–2167.
[24] M. Sharaf, G. Arroy and R. Perkins, *J. Chemom.*, 5 (1991) 291–298.
[25] A.F. Poile and R.D. Conlon, *J. Chromatogr.*, 204 (1981) 149–152.

[26] F.V. Warren, Jr., B.A. Bidlingmeyer and M.F. Delaney, *Anal. Chem.*, 59 (1987) 1897–1907.
[27] C.L. Guillemin, *J. Chromatogr.*, 441 (1988) 1–12.
[28] B. Wiese, *J. Pharm. Biomed. Anal.*, 7 (1989) 79–93.
[29] C.N. Renn and R.E. Synovec, *Anal. Chem.*, 60 (1988) 1829–1832.
[30] E.D. Katz and R.P.W. Scott, *J. Chromatogr.*, 270 (1983) 28–50.
[31] F. Erni, *J. Chromatogr.*, 282 (1983) 371–383.
[32] R.E. Pauls, R.W. McCoy, E.R. Ziegel, T. Wolf, G.T. Fritz and D.M. Marmion, *J. Chromatogr. Sci.*, 24 (1986) 273–277.

ELSEVIER

Journal of Chromatography A, 663 (1994) 151–161

JOURNAL OF CHROMATOGRAPHY A

Characterization of adsorbents by high-performance liquid chromatography using aromatic hydrocarbons Porous graphite and its comparison with silica gel, alumina, octadecylsilica and phenylsilica

Josef Kříž*,[a] Eva Adamcová[a] John H. Knox[b], Josef Hora[a]

[a]*Department of Environmental Chemistry, Institute of Chemical Technology, Technická 5, CZ-16628 Prague 6, Czech Republic*
[b]*Wolfson Liquid Chromatography Unit, Department of Chemistry, University of Edinburgh, West Mains Road, Edinburgh EH9 3JJ, UK*

(First received June 17th, 1992; revised manuscript received November 23rd, 1993)

Abstract

The retention characteristics of 52 aromatic hydrocarbons, mostly alkylbenzenes, were measured on porous graphite using methanol as the mobile phase. There is a linear dependence of log k' on the number of carbon atoms, (i) for polymethylbenzenes whose methyl groups are all in *ortho* positions and (ii) for *n*-alkylbenzenes above butylbenzene. As with alumina and silica gel, the *ortho* effect for graphite was also observed, but graphite shows much higher α values (the increase in log k' for addition of a carbon atom) than any of the other packing materials studied. The superior selectivity of graphite is in line with its crystalline structure, consisting of a flat, crystalline array of hexagonally arranged carbon atoms. In terms of optimum eluent and retention graphite behaves like a reversed-phase material, but in terms of selectivity towards isomeric compounds it behaves like the oxide adsorbents silica gel and alumina.

1. Introduction

Previous papers in this series have reported on the structure–retention relationships for a group of aromatic hydrocarbons on a range of stationary phases, *viz.*, silica gel [1], alumina [2], octadecylsilica [3,4] and phenylsilica [5]. In this paper we report data on the retention of the same group of hydrocarbons on porous graphite (previously known as porous graphitic carbon or PGC).

While Kiselev and co-workers pioneered the use of graphites as adsorbents in GC [6] and in LC [7], it was only relatively recently that robust graphites have been available for liquid chromatography. Early work on the use of carbons in liquid chromatography was reviewed by Knox *et al.* [8] and more recent work by Knox and Kaur [9]. In particular Knox *et al.* compared the α values for the addition of a methyl substituent to benzene (0.40–0.45) and of a methylene group to an alkyl chain (0.23–0.26), where the α value is defined as

$$\alpha = \log[k'(n+1)/k'(n)]$$

$k'(n+1)$ and $k'(n)$ being the k' values for

* Corresponding author.

0021-9673/94/$07.00
SSDI 0021-9673(93)E1267-4

hydrocarbons possessing $n+1$ and n carbon atoms, respectively.

The aim of this study was to obtain HPLC data for aromatic hydrocarbons, mostly alkylbenzenes, in order to study the relationship between their molecular structure and their retention behaviour on porous graphite, and to compare this with their behaviour on silica gel, alumina, octadecylsilica and phenylsilica.

2. Experimental

2.1. Apparatus

The HPLC equipment consisted of a Model 8500 liquid chromatograph (Varian, Palo Alto, CA, USA) with a syringe pump and a fixed-wavelength UV detector (254 nm). Peaks were recorded with a Model TZ 4221 double-channel strip-chart recorder (Laboratory Instruments, Prague, Czech Republic). Retention times of peaks were measured with a Model 3390A integrator (Hewlett-Packard, Avondale, PA, USA).

The porous graphite sample was PGC 70B-CL prepared in the Wolfson Liquid Chromatography Unit (WLCU) according to the procedure of Knox *et al.* [10]. An equivalent material is now marketed under the trade name Hypercarb by Shandon Scientific (Runcorn, UK). The porous graphite was packed into a 100×4.7 mm I.D. stainless-steel column using a standard slurry procedure. The packing materials used in the previous work [1–5] were Silasorb silica gel (Lachema, Brno, Czech Republic), Alusorb 160 neutral alumina (Lachema), ODS Hypersil (Shandon Scientific) and phenylsilica (Laboratory Instruments). The silica, phenylsilica and alumina had mean particle sizes of 7.5 μm, the octadecylsilicas had particle sizes of 5 μm and the porous graphite had a nominal particle size of 7 μm.

Retention data were analysed and processed on an HP-85 personal computer (Hewlett-Packard) equipped with a Model 82905B impact printer, a Model 82901M disc drive and a Model 7475A plotter. Lotus 1-2-3 was used to prepare, compute and print tables.

2.2. Chemicals

The eluent throughout was analytical-reagent grade methanol (Lachema) distilled in glass before use. Most of the hydrocarbons were kindly provided by the Institute of Chemical Technology (Prague, Czech Republic); the reminder were purchased from UK chemical suppliers.

2.3. Procedure

On the basis of preliminary chromatographic runs, mixtures containing two to four completely resolved hydrocarbons were prepared in methanol. Injections of between 2 and 10 μl of each mixture were made in triplicate. Column capacity factors, k', were calculated from the retention times measured by the integrator according to

$$k' = (t_R - t_0)/t_0$$

where t_R is the retention time of a solute peak and t_0 is that of the unretained solvent peak; t_0 was taken as the time from injection to the moment when the trace for the solvent disturbance crossed the baseline. The solvent disturbance peak was generated by the 2,2,4-trimethylpentane in which the samples were dissolved. Retention data were reproducible to better than 2% from run to run provided that an entire set of data were obtained over a period of 20 h. The column activity was checked several times during each experiment by injecting a standard mixture of benzene, toluene, *n*-propylbenzene and *n*-butylbenzene.

Table 1 lists the packing materials and the eluents used in this and previous studies in the series.

3. Results and discussion

Table 2 gives the values of the capacity factors for the 52 hydrocarbons eluted by methanol from graphite at 20°C. Each value represents the average of at least three measurements. Most of the compounds examined were alkylbenzenes

Table 1
Packing materials and eluents

Material	Eluent	Ref.
Graphite (PGC 70B-CL)	Methanol	This work
Alumina	Pentane	2
Silica gel	Pentane	1
ODS-silica	Methanol–water[a]	3
Phenylsilica	Methanol–water[b]	5

[a] Proportions 70:30, 80:20 and 90:10 (w/w) were used.
[b] Proportions 50:50, 60:40, 70:30 and 80:20 (w/w) were used.

and had the empirical formula C_nH_{2n-6}, but compounds with the following empirical formulae were also characterized: C_nH_{2n-8} (indane, tetralin, cyclohexylbenzene), C_nH_{2n-10} (indene), C_nH_{2n-12} (naphthalene), C_nH_{2n-14} (biphenyl and acenaphthene) and so on up to C_nH_{2n-22} (*o*-terphenyl).

We examined the following aspects of the structure–retention relationship for the 52 solutes: (i) the general relationship between log k' and the number of carbon atoms in each molecule; (ii) effects of the various structural features on log k', *viz.*, (a) the length of the alkyl chain and the number of alkyl groups, (b) the arrangement of the alkyl groups (the *ortho* effect) and (c) the shape of the alkyl groups; and (iii) differences between various stationary phases, *viz.*, (a) graphite, (b) alumina, (c) silica gel, (d) octadecylsilica bonded phase and (e) phenylsilica bonded phase.

3.1. Relationship between log k' and carbon number

Fig. 1 shows the dependence of log k' on carbon number for the 52-hydrocarbon set using graphite as the packing material and methanol as the eluent. Similar plots have been reported previously [1–3,5] for the other stationary phases listed in Table 1. In general, there is no universal relationship between log k' and carbon number, although there is the expected trend (except for silica gel with pentane as eluent) towards higher retention with the larger carbon numbers. Whenever a further carbon atom is added to a molecule, its k' value is increased (except for silica gel). There are, however, a number of linear or near-linear relationships for specific series of compounds. Examples are shown by the broken line drawn through points for the all-*ortho*-polymethylbenzenes and the full lines drawn through points for *n*-alkylbenzenes (upper) and cyclohexylbenzenes (lower), the dependence for *n*-alkylbenzenes becoming linear only above amylbenzene. To elucidate the effects of the various structural features mentioned above it is necessary to consider more limited sets of data.

3.2. Effects of specific structural changes on retention

Chain length in alkylbenzenes and number of methyl groups in all-ortho-polymethylbenzenes

Figs. 2 and 3 show the dependence of log k' for all-*ortho*-polymethylbenzenes and *n*-alkylbenzenes on carbon number for the five stationary phases listed in Table 1. Broken lines are drawn through points for the *ortho*-polymethylbenzenes and full lines through points for *n*-alkylbenzenes. With graphite (Fig. 2), the retention times of *ortho*-polymethylbenzenes and *n*-alkylbenzenes both increase with increasing number of carbon atoms in the substituent groups. For the *ortho*-polymethyl benzenes the dependence is linear but for the *n*-alkylbenzenes the dependence becomes linear only with amylbenzene and higher homologues. With alumina (Fig. 3) there is a linear increase in log k' for the *ortho*-polymethylbenzenes, but in-

Table 2
Retention data on carbon

No.	Compound	C	H	t_R (min)	k'
1	Benzene	6	6	1.77	0.18
2	Toluene	7	8	2.17	0.45
3	Ethylbenzene	8	10	2.20	0.47
4	*n*-Propylbenzene	9	12	2.50	0.67
5	*n*-Butylbenzene	10	14	3.04	1.03
6	*n*-Amylbenzene	11	16	4.34	1.89
7	*n*-Hexylbenzene	12	18	6.21	3.14
8	*n*-Heptylbenzene	13	20	10.16	5.77
9	*n*-Octylbenzene	14	22	17.02	10.35
10	*n*-Nonylbenzene	15	24	29.94	18.96
11	*n*-Decylbenzene	16	26	52.44	33.96
12	*n*-Tridecylbenzene	19	32	[a]	[a]
13	*o*-Xylene	8	10	3.39	1.26
14	*m*-Xylene	8	10	3.06	1.04
15	*p*-Xylene	8	10	3.33	1.22
16	Isopropylbenzene	9	12	2.03	0.35
17	*o*-Ethyltoluene	9	12	3.64	1.43
18	*p*-Ethyltoluene	9	12	3.12	1.08
19	1,2,3-Trimethylbenzene	9	12	7.22	3.81
20	1,2,4-Trimethylbenzene	9	12	6.41	3.27
21	1,3,5-Trimethylbenzene	9	12	4.96	2.31
22	Isobutylbenzene	10	14	2.45	0.63
23	*sec.*-Butylbenzene	10	14	2.21	0.47
24	*tert.*-Butylbenzene	10	14	2.08	0.39
25	*m*-Cymene	10	14	2.55	0.70
26	*p*-Cymene	10	14	2.51	0.67
27	*o*-Diethylbenzene	10	14	3.62	1.41
28	*m*-Diethylbenzene	10	14	2.98	0.99
29	*p*-Diethylbenzene	10	14	2.96	0.97
30	1,2,3,4-Tetramethylbenzene	10	14	21.36	13.24
31	1,2,3,5-Tetramethylbenzene	10	14	15.08	9.05
32	1,2,4,5-Tetramethylbenzene	10	14	16.17	9.78
33	Pentamethylbenzene	11	16	57.26	37.17
34	4-*tert.*-Butyltoluene	11	16	2.34	0.56
35	Isopentylbenzene	11	16	3.39	1.26
36	*tert.*-Amylbenzene	11	16	2.22	0.48
37	Neopentylbenzene	11	16	2.59	0.73
38	*m*-Diisopropylbenzene	12	18	2.12	0.41
39	*p*-Diisopropylbenzene	12	18	2.42	0.61
40	Hexamethylbenzene	12	18	[a]	[a]
41	1,2,4-Triethylbenzene	12	18	5.72	2.81
42	1,3,5-Triethylbenzene	12	18	4.01	1.67
43	Cyclohexylbenzene	12	16	4.04	1.69
44	*p*-Di-*tert.*-butylbenzene	14	22	2.53	0.69
45	Pentaethylbenzene	16	26	3.57	1.38
46	*p*-Dicyclohexylbenzene	18	26	30.93	19.62
47	Hexaethylbenzene	18	30	2.46	0.64
48	1,3,5-Tri-*tert.*-butylbenzene	18	30	1.94	0.29
49	Indane	9	10	3.45	1.30
50	Indene	9	8	4.85	2.23
51	Tetrahydronaphthalene	10	12	4.43	1.95
52	Naphthalene	10	8	11.70	6.80

Table 2 *(continued)*

No.	Compound	C	H	t_R (min)	k'
53	Phenanthrene	14	10	[a]	[a]
54	Biphenyl	12	10	17.12	10.41
55	Fluorene	13	10	[a]	[a]
56	Acenaphthene	12	10	[a]	[a]
57	*o*-Terphenyl	18	14	28.48	17.99

Mobile phase, methanol; temperature, 20°C. C = No. of carbon atoms in molecule; H = No. of hydrogen atoms; t_R = retention time; k' = capacity factor = $(t_R - t_0)/t_0$; t_0 (retention time of an unretained compound) = 1.50.
[a] Data obtained under different conditions.

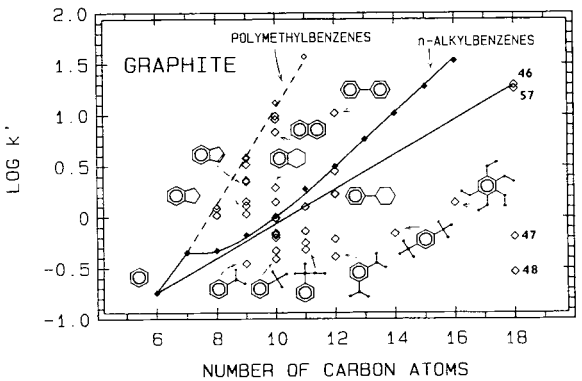

Fig. 1. Dependence of log k' for 52 aromatic hydrocarbons on carbon number. Packing material, graphite; eluent, methanol; temperature, 20°C. Broken line drawn through points for the all-*ortho*-polymethylbenzenes; full lines drawn through points for (top) *n*-alkylbenzenes and (bottom) cyclohexylbenzenes. The names of compounds represented by numbers are listed in Table 2 (46 = *p*-dicyclohexylbenzene; 47 = hexaethylbenzene; 48 = tri-*tert*.-butylbenzene; 57 = *o*-terphenyl).

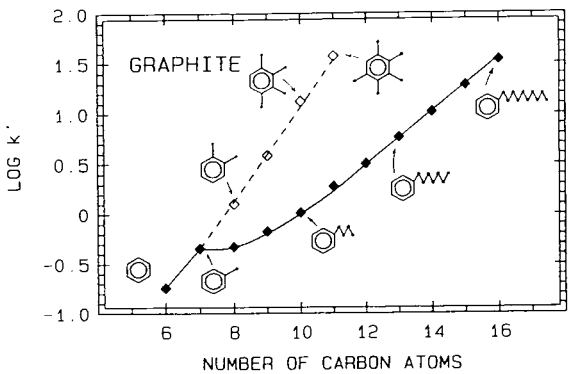

Fig. 2. Dependence of log k' for *ortho*-polymethylbenzenes and *n*-alkylbenzenes on carbon number. Packing material, graphite; eluent, methanol; temperature, 20°C. Broken line drawn through points for the *ortho*-polymethylbenzenes; full line drawn through points for *n*-alkylbenzenes.

creasing the chain length in the *n*-alkylbenzenes gives no change in log k'. With silica gel there is only a slight increase in log k' for the *ortho*-polymethylbenzenes, but a decrease in log k' with increase in chain length for the *n*-alkylbenzenes. Fig. 3 further shows that ODS-silica provides no selectivity between *ortho*-polymethylbenzenes and *n*-alkylbenznes of the same carbon number: for both series there is the same dependence of log k' on carbon number. The increase in log k' with increasing carbon number is similar to that for the alkyl-substitution line with graphite. With phenylsilica there is again little selectivity between the *ortho*-polymethylbenzenes and the *n*-alkylbenzenes, and the dependence of log k' on carbon number is much weaker than with ODS-silica, being similar to that of the *ortho*-polymethylbenzenes on underivatized silica gel.

In general, the position of benzene is anomalous. For graphite the log k' value for benzene lies on the line for the *ortho*-polymethylbenzenes. For alumina and silica gel log k' for benzene lies between the lines for the *ortho*-polymethylbenzenes and *n*-alkylbenzenes. For ODS and phenylsilica gels the point for benzene lie on the lines for both series.

The data in Figs. 2 and 3 may be summarized by listing the α values for methyl substitution at

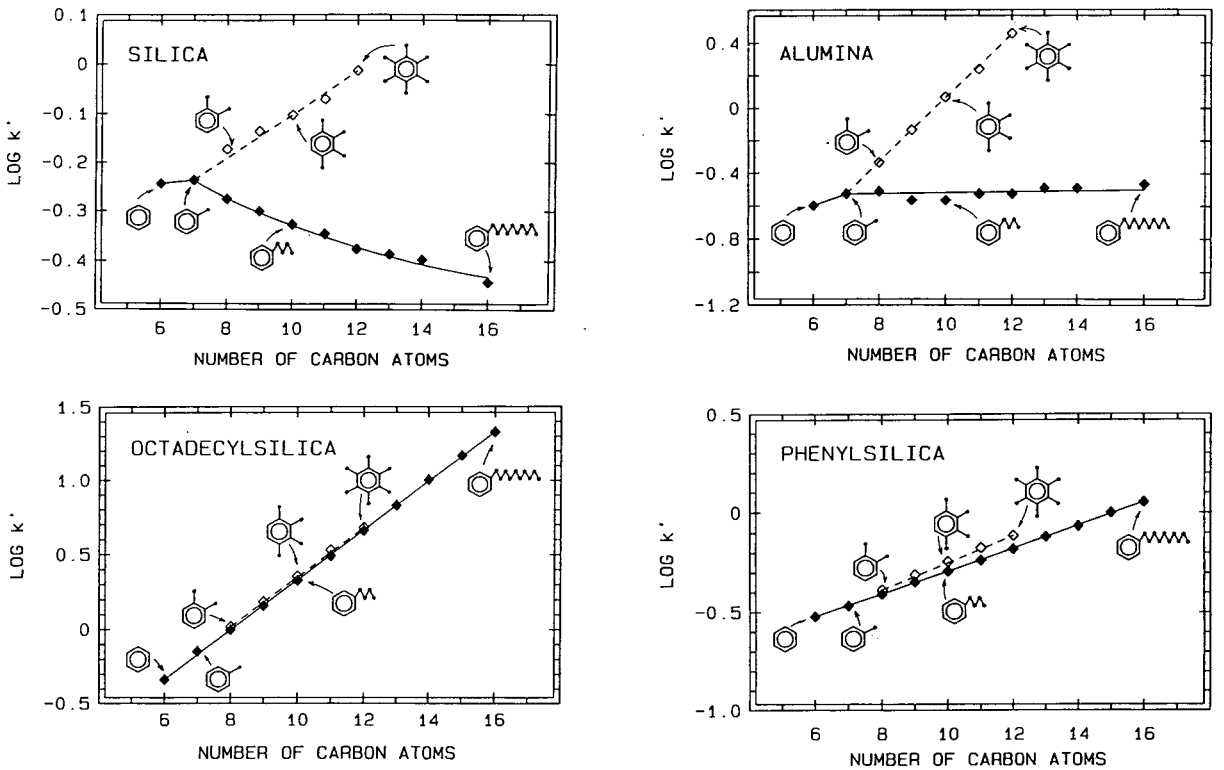

Fig. 3. As Fig. 2, except packing material: silica gel, eluent pentane; alumina, eluent pentane; octadecylsilica, eluent methanol–water (80:20, w/w); and phenylsilica, eluent methanol–water (80:20, w/w).

an *ortho* position and for addition of a methylene group to the alkyl chain in benzene. These values are given in Table 3.

Table 3 shows clearly that graphite is unique in that it provides a very strong dependence of log k' on carbon number, especially for the *ortho*-polymethylenzenes, and at the same time by far the greatest selectivity between methyl substitution at an *ortho* position and methylene addition. The α values agree with those reported by Knox *et al.* [8], namely 0.40–0.45 for methyl substitution and 0.23–0.26 for methylene addition. Alumina shows the next strongest retention and selectivity and silica the least of the three adsorbents. When silica is derivatized with ODS the α values are increased but the selectivity

Table 3
α Values for methylene substitution at an *ortho* position and for addition of a methylene group to the alkyl chain of benzene

Packing	Eluent	Methyl substitution	Methylene addition	Difference
Graphite	Methanol	0.46	0.22[a]	0.24
Alumina	Pentane	0.195	0.00	0.195
Silica gel	Pentane	0.046	−0.014 to −0.03	0.05 to 0.06
ODS-silica	Methanol–water (80:20, w/w)	0.17	0.17	0.00
Phenylsilica	Methanol–water (70:30, w/w)	0.10	0.10	0.00

[a] From C_5 to C_{10} chain. The values for C_8 to C_{10} are 0.25.

shown by the naked adsorbents is lost. Phenylsilica shows slight selectivity but weak retention.

Arrangement of alkyl groups, the ortho effect

The *ortho* effect is an effect observed with alumina and silica gel whereby the retention of substances with substituents in the *ortho* position is greater than that of isomers with substituents in other positions [1,2]. With the ODS- and phenylsilica a reversed *ortho* effect has been observed [3,5].

The effect for graphite is illustrated in Fig. 4, which shows a substitution scheme for generation of all the polymethylbenzenes along with the k' values for each compound and the α values for each substitution. In Fig. 4, each substitution step has been termed *ortho*, *meta* or *para* according to whether the nearest group to the newly added group is *ortho*, *meta* or *para*. When the

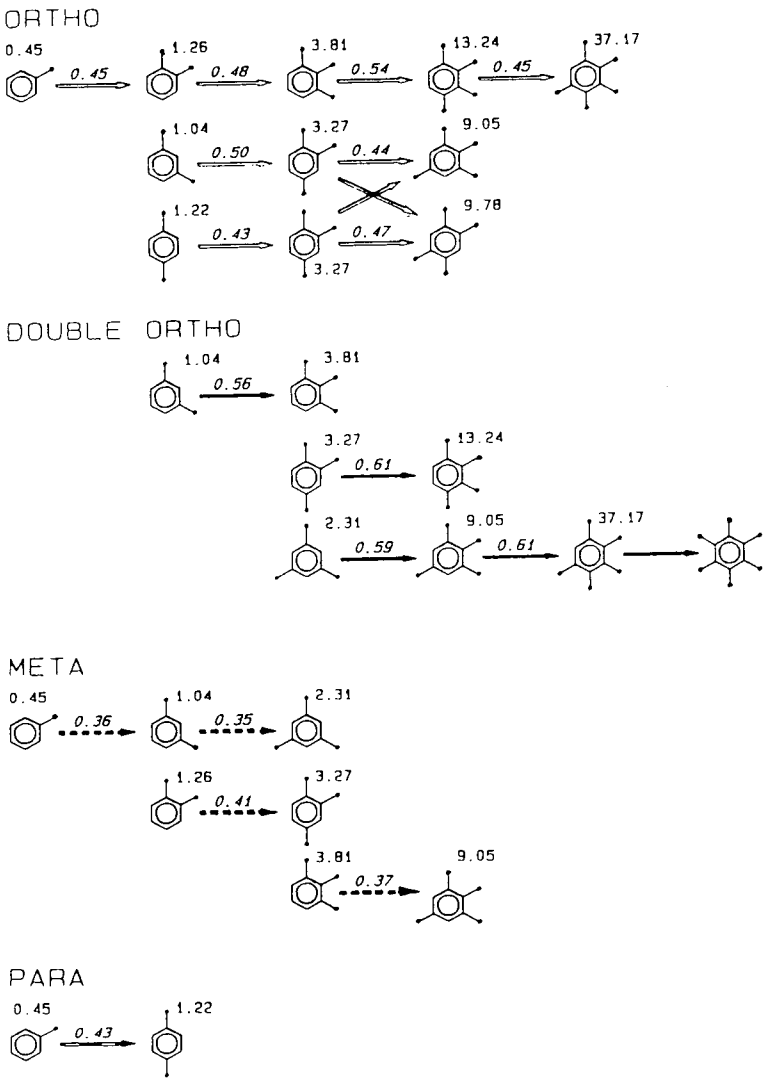

Fig. 4. Substitution scheme for polymethylbenzenes retained by graphite. Numbers on formulae are k' values; numbers above arrows are α values. Elution conditions as in Fig. 2.

new methyl group is inserted between two methyl groups which are *meta* to one another, the new methyl group will be *ortho* to both of the original groups. We have termed this a "double *ortho*" substitution. Fig. 4 shows that on average the α values for different types of substitution are as follows: double *ortho* substitution, $\alpha = 0.59$; *ortho* substitution, $\alpha = 0.47$; *meta* substitution, $\alpha = 0.37$; and *para* substitution, $\alpha = 0.43$.

Although graphite behaves with regard to retention more like a reversed-phase material, it nevertheless shows the same *ortho* effect as the other adsorbents, silica and alumina. In this respect graphite behaves like the classical adsorbents, giving the highest retention for isomeric polymethylbenzenes having the largest number of methyl groups in *ortho* positions.

The data for the five stationary phases are summarized in Table 4. Table 4 shows that all three adsorbents (graphite, alumina and silica gel) show similar trends in that double *ortho* substitution provides the largest α value, *ortho* substitution the next largest followed by *para* substitution and finally *meta* substitution with the lowest α value. Graphite is chiefly distinct from the other adsorbents in having much larger α values for all substitutions and, on the whole, slightly grater selectivity with respect to isomeric polymethylbenzenes (*i.e.*, a wider variation in the bracketed values). With graphite the polymethylbenzenes are eluted as groups of isomers according to carbon number, whereas with the other packing materials there is considerable overlap of groups and with silica complete overlap occur.

Shape of alkyl groups

Branching of the alkyl group generally decreases the retention both in adsorption chromatography and in chromatography on reversed phases. This is clearly illustrated for graphite by the chromatogram of C_9 hydrocarbons shown in Fig. 5, which includes peaks for indane and indene, and by Fig. 6 for C_{10} hydrocarbons, which includes tetrahydronaphthalene.

Fig. 7 shows that, for two-ring hydrocarbons,

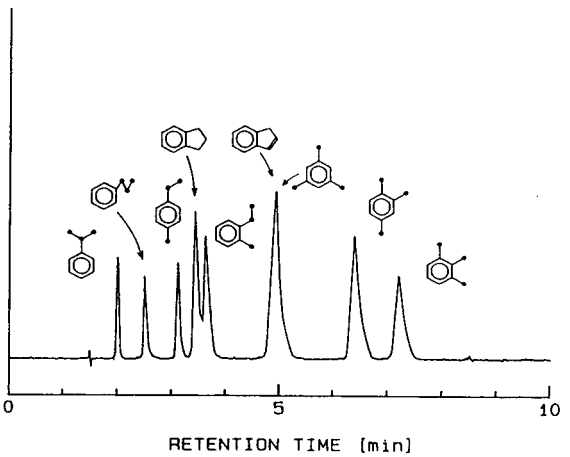

Fig. 5. Chromatogram of selected C_9 hydrocarbons showing selectivity effects. Packing material, graphite; eluent, methanol; temperature, 20°C.

Table 4
α Values for methyl substitution in benzene

Material	Type of substitution			
	Double *ortho*	*ortho*	*meta*	*para*
Graphite	0.59 (+0.12)	*0.47*	0.37 (−0.10)	0.43 (−0.04)
Alumina	0.28 (+0.085)	*0.195*	0.08 (−0.115)	0.09 (−0.105)
Silica gel	0.08 (+0.034)	*0.046*	0.00 (−0.08)	0.01 (−0.07)
ODS-silica[a]	0.15 (−0.02)	*0.17*	0.19 (+0.02)	0.40 (+0.23)
Phenylsilica[b]	0.10 (0.00)	*0.10*	0.09 (−0.01)	0.08 (−0.02)

Values in parentheses are the deviations in α from the values for *ortho* substitution (in italics).
[a] Mobile phase: methanol–water (80:20, w/w).
[b] Mobile phase: methanol–water (70:30, w/w).

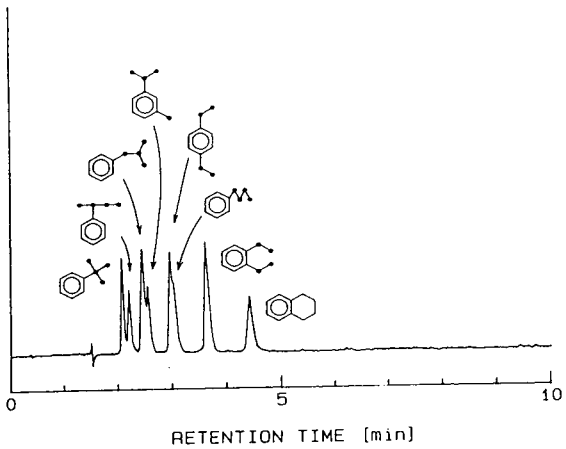

Fig. 6. Chromatogram of selected C_{10} hydrocarbons showing selectivity effects. Conditions as in Fig. 5.

retention on graphite is increased by (a) increased unsaturation, peaks 2 and 5, peaks 3 and 7 and peaks 4 and 6; and (b) an increase in the number of carbon atoms in a ring, peaks 2 and 3.

However, the transition from a isolated-ring system to a condensed-ring system does not produce a consistent effect, as seen by comparing peaks 3 and 4 (cyclohexylbenzene and tetrahydronaphthalene) with peaks 6 and 7 (naphthalene and biphenyl).

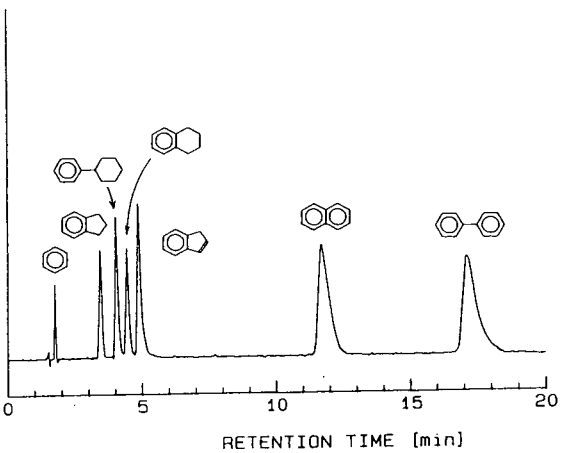

Fig. 7. Chromatogram of selected mixture showing the effect of addition of hydrogen atoms for pairs of compounds with the same carbon numbers: indane–indene; cyclohexylbenzene–biphenyl; tetrahydronaphthalene–naphthalene. Conditions as in Fig. 5.

3.3. Correlation with other stationary phases: the nature of graphite

The original objective in preparing graphites for liquid chromatography was to provide a nearly perfect reversed-phase material that would not suffer from the defects of alkylsilicas such as solubility in eluents, hydrolysis of bonded groups and effects of underivatized silanol groups. In the event, graphite proved to be unique and to show properties both of reversed-phase silica gels and of classical adsorbents.

We may note first that, in order to obtain reasonable elution times for the 52 hydrocarbons used in this and previous studies, it was necessary to use pentane as the eluent for the oxide adsorbents but methanol or methanol–water for graphite and the derivatized silica gels. In this respect graphite must fall into the class of a predominantly reversed-phase material. On the other hand, graphite is clearly an adsorbent, and one with properties that distinguish it from the other adsorbents. It is an extremely strong adsorbent, showing higher α values for addition of a further carbon atom to any molecule than any of the other materials, and it shows much greater selectivity towards isomers. This is thought to be due to its possessing a flat, crystalline surface (a hexagonal array of carbon atoms like a giant aromatic molecule), which can clearly distinguish between molecules that show good and poor fits to the surface. Both alumina and amorphous silica have geometrically heterogeneous surfaces, which will be far from flat at the atomic level and can distinguish molecules only on the basis of specific effects such as dipole and hydrogen-bonding interactions. Likewise, the bonded phases, and particularly ODS-silica, behave more like viscous liquids than adsorbents (especially when in contact with a swelling solvent such as hexane) and therefore show little scope for stereospecific interactions.

Nevertheless, the elution orders of hydrocarbons on graphite are very similar to those on alumina and silica, namely, more aromatic hydrocarbons are more retained, *e.g.*, naphthalene is more retained then tetrahydronaphthalene,

indene more than indane and biphenyl more than cyclohexylbenzene.

In contrast, the elution order of the same groups of compounds on ODS-silica [4] is the reverse, with the alkanes showing the greatest retention. However, as far as the effect of isomerization is concerned, retention decreases with isomerization, cyclization, dehydrogenation, dehydrocyclization and aromatization.

Graphite thus resembles the other adsorbents more than it does ODS-silica with regard to its selectivity for different hydrocarbon types.

The comparison of graphite with other packing materials can also be clarified by plots of log k' on graphite against log k' on the other adsorbents. Fig. 8 shows plots for the *n*-alkylbenzenes and the *ortho*-polymethylbenzenes. There is a marked distinction between graphite and the two oxide adsorbents compared with the relative similarity of the plots for the two bonded silica gels.

4. Conclusions

In terms of retention and the type of eluent required, graphite behaves most like a reversed-phase material. In terms of selectivity towards isomeric compounds, graphite behaves more like oxide adsorbents, such as silica gel and alumina.

Graphite combines good selectivity for species with different carbon numbers with good isomer selectivity within groups. For the polymethylbenzenes this enables essentially all isomers to be separated in groups according to their carbon numbers. This is not possible with either the bare adsorbents or the derivatized silica gels.

The α values for graphite are 0.22–0.25 for

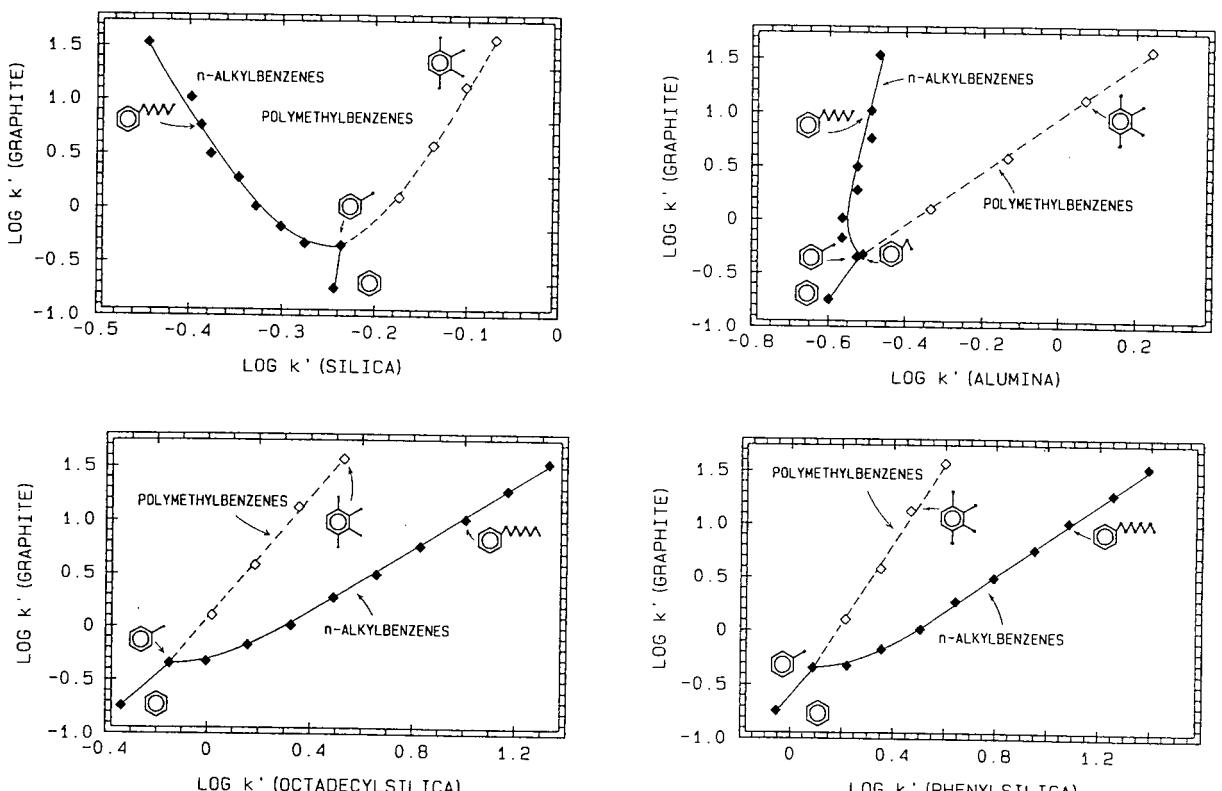

Fig. 8. Correlation of log k' on graphite with log k' on silica gel, alumina, octadecylsilica and phenylsilica. Conditions: for graphite, as in Fig. 1; for silica gel, alumina, octadecylsilica and phenylsilica, as in Fig. 3.

addition of a methylene group to the carbon chain and 0.46 for addition of a methyl group into an *ortho* position to the benzene ring. These are much higher than the corresponding values for the other adsorbents and for the bonded silica gels.

General behavioural patterns found with all the packing materials studied (graphite, silica gel, alumina, octadecylsilica and phenylsilica) are as follows: (a) higher aromatics are more retained than the lower aromatics (number of aromatic rings); (b) compounds with a larger number of methyl groups (*e.g.*, polymethylbenzenes) are more retained; and (c) branching of a substituent alkyl group decreases the retention.

5. References

[1] J. Kříž, L. Vodička, J. Punčochářová and M. Kuraš, *J. Chromatogr.*, 219 (1981) 53.
[2] J. Kříž, J. Punčochářová, L. Vodička and J. Vařeka, *J. Chromatogr.*, 437 (1988) 178.
[3] J.H. Knox, J. Kříž and E. Adamcová, *J. Chromatogr.*, 447 (1988) 13.
[4] J. Kříž, M. Kuraš, L. Vodička and J. Burda, *Ropa Uhlie*, 31 (1989) 645.
[5] J. Kříž, E. Adamcová and L. Obal, in preparation.
[6] A.V. Kiselev and Ya.I. Yashin, *Adsorbtsionnaya Gazovaya i Zhidkostnaya Khromatografya*, Khimiya, Moscow, 1979.
[7] A.V. Kiselev, Yu.S. Nikitin, I.I. Frolov and Ya.I. Yashin *J. Chromatogr.*, 91 (1974) 187.
[8] J.H. Knox, K.K. Unger and H. Mueller, *J. Liq. Chromatogr.*, 6 (S-1) (1983) 1.
[9] J.H. Knox and B. Kaur, in R.A. Hartwick and P.R. Brown (Editors), *High Performance Liquid Chromatography*, Wiley, New York, 1989, pp. 189–222.
[10] J.H. Knox, B. Kaur and G.R. Millward, *J. Chromatogr.*, 352 (1986) 3.

ELSEVIER

Journal of Chromatography A, 663 (1994) 163–174

JOURNAL OF CHROMATOGRAPHY A

Polyvinylpyrrolidone-coated silica packings for chromatography of proteins and peptides

A. Kurganov*[,a,b], Yu. Puchkova[a], V. Davankov[a], F. Eisenbeiss[c]

[a]*Institute of Organo-Element Compounds, Russian Academy of Sciences, Vavilov Str. 28, 117813 Moscow, Russian Federation*

[b]*Institut für Anorganische Chemie und Analytische Chemie, J. Gutenberg Universität, J. Becher Weg 24, 55099 Mainz, Germany*

[c]*R & D Chromatography, E. Merck, Frankfurter Strasse 250, Darmstadt, Germany*

(First received June 28th, 1993; revised manuscript received October 14th, 1993)

Abstract

Polyvinylpyrrolidone (PVP)-coated silica sorbents were synthesized by interaction of a copolymer of vinylmethyldiethoxysilane and vinylpyrrolidone with LiChrospher Si 300 and LiChrospher Si 500 silicas. The coating procedure retains the wide-pore structure of the starting silicas, as was shown by nitrogen adsorption, mercury porosimetry and inverse size-exclusion chromatographic measurements. Good selectivity and separation ability of the synthesized packings toward proteins and peptides were demonstrated in the hydrophobic interaction chromatographic mode of separation. Aromatic compounds undergo a specific interaction with bonded PVP chains which can be used for the preconcentration or selective recovery of polycyclic aromatic hydrocarbons.

1. Introduction

Chromatographic methods are one of the most powerful tools for the separation of complex multi-component mixtures of natural and biologically active substances. Hydrophilic packings are usually used for such separations, as they operate with water-rich eluents compatible with bioactive compounds and prevent denaturation of sensitive bioanalytes. These packings are often polysaccharides (*e.g.*, Sephadex, Sepharose), polyacrylamides (*e.g.*, Separon) or polyalcohols (*e.g.*, TSK-polymer gel, Fractogel). The pressure resistance of these sorbents is generally not sufficient for HPLC separations and many attempts have been made to combine the excellent chemical properties of hydrophilic polymers with the outstanding mechanical stability of silica gel. Many different methods of synthesis of composite materials have been developed and described elsewhere [1,2]. Polyvinylpyrrolidone (PVP)-coated materials are of particular interest for pharmaceutical and medical applications.

The first attempt to synthesize PVP-coated silicas was made by Caude and Rosset [3], who polymerized monomeric vinylpyrrolidone (VP) on the surface of silica modified with vinyltrichlorosilane. A number of protein separations by means of hydrophobic interaction chromatography (HIC) were demonstrated with this packing and a relatively high hydrophobicity of the coating were reported. The concentration of vinyl groups on the surface was obviously too

* Corresponding author. Address for correspondence: Institut für Anorganische Chemie und Analytische Chemie, J. Gutenberg Universität, J. Becher Weg 24, 55099 Mainz, Germany.

0021-9673/94/$07.00
SSDI 0021-9673(93)E1266-3

high, which contributed to the retention of some proteins. In addition, the porosity of the starting silica was substantially changed during the polymer bonding procedure.

Ivanov *et al.* [4] suggested modifying γ-aminopropylated silica by a presynthesized copolymer of VP and acryloyl chloride. Only a certain part of the amino groups on the silica surface and chloroanhydride groups of the copolymer took part in the reaction. The unreacted functional groups had to be deactivated, *e.g.*, by reaction with acetyl chloride and ethanolamine, respectively. As a result, a polyfunctional packing with badly reproducible properties was synthesized.

An original method of immobilization was suggested by Köchler [5]. According to his observations, PVP adsorbed on the silica surface could not be removed by extraction, provided that the composite was heated to 200°C. The chemical nature of the irreversible immobilization is not clear, but Köchler proposed an opening of some lactam rings and the formation of chemical bonds with the surface. The synthesized sorbent was successfully used in the analysis of low-molecular-mass compounds by normal- and reversed-phase (RP) chromatography.

An American patent [6] described the synthesis of a PVP-coated packing by the modification of silica with the copolymer of VP and vinyltrichlorosilane. No attempts were made to purify the copolymer and a rough mixture of homo- and copolymers were used. The synthesized packing exhibited a relatively high hydrophobicity owing to the binding of vinyltrichlorosilane and its oligomers to the surface. Nevertheless, the sorbent could be applied to the separation of proteins by means of size-exclusion chromatography (SEC) with appropriate eluents.

In this paper an improved synthetic procedure for coating silica with PVP using isolated and purified VP–vinylsilane copolymer is described. The properties of these packings were studied in the separations of low- and high-molecular-mass analytes. The changes of the porosity of the silica matrix during the binding of the copolymer were studied and are discussed.

2. Experimental

2.1. Materials

A mixture of polycyclic aromatic hydrocarbons (PAHs) was prepared from individual compounds supplied by Merck and Aldrich.

The proteins used were ribonuclease A, lactate dehydrogenase, catalase, ferritin, ovalbumin, cytochrome *c*, insulin, myoglobin, lysozyme, thyroglobulin, human serum albumin, conalbumin, β-lactoglobulin, chymotrypsinogen A, trypsin and calf thymus and were supplied by Merck and Serva. The peptides were angiotensin I (human, Asp–Arg–Val–Tyr–Ile–His–Pro–Phe–His–Leu), oxytocin (Cys–Tyr–Ile–Glu–Asn–Cys–Pro–Leu–NH_2), neurotensin (pGlu–Leu–Tyr–Glu–Asn–Lys–Pro–Arg–Arg–Pro–Tyr–Ile–Leu) and somastatin (Gly–Cys–Lys–Asn–Phe–Phe–Trp–Lys–Thr–Phe–Thr–Ser–Cys) and were purchased from Sigma.

All solvents were of LiChrosolv grade from Merck and used as received.

2.2. Synthesis of copolymer

The copolymerization of vinylpyrrolidone and methylvinyldiethoxysilane was carried out in sealed ampoules under a nitrogen atmosphere. A solution of monomers and initiator in toluene was placed in an ampoule, frozen, evacuated, filled with nitrogen and then frozen out. This operation was repeated twice before sealing the ampoule. Polymerization was then performed for 7 h at 100°C. The concentration of monomers was 40% (w/w) in a ratio of 1:1. Dicumyl peroxide was used as the initiator at a concentration of 1% (w/w) with respect to the monomers. After the polymerization, the ampoule was cooled and the solution of homo- and copolymers was dropped into diethyl ether. The precipitated copolymer was filtered off and reprecipitated. The purified copolymer was dried under vacuum at 50°C. The molecular mass, determinated by means of ultracentrifugation (Model M-20 ultracentrifuge, Radelkis, Szeged, Hungary), was found to be 6500. The ratio of vinylpyrrolidone to vinylsilane monomer units in

the copolymer was 8:1, as determined by elemental analysis. The high sensitivity of the copolymer to the presence of water in solvents is worth noting. Traces of water cause cross-linking of the copolymer, which may lose its solubility in any solvent after reprecipitation.

2.3. Coating procedure

The initial silica was dried by azeotropic distillation of water with toluene. The solution of the copolymer in toluene was dropped into a suspension of silica in toluene boiling under reflux. A 0.25-g amount of copolymer was taken for modification of 1 g of LiChrospher Si 300 silica and 0.15 g for modification of 1 g of LiChrospher Si 500 silica. The suspension was boiled under reflux for an additional 5 h and the hot suspension was then filtered through a porous glass frit. The coated silica was washed thoroughly with two portions of hot toluene and dried under vacuum at 50°C. End-capping was carried out with hexamethyldisilazane according to standard procedure described elsewhere [7]. The elemental analysis data for the synthesized packings are presented in Table 1.

2.4. Physical measurements

Nitrogen adsorption isotherms were measured with an ASAP-2400 system (Micromeritics). The pore-size distribution and the specific pore volume were calculated from the adsorption isotherms by using standard mathematical software provided with the ASAP-2400 and are given in Table 1.

Mercury porosimetric measurements were performed with a Model 2000 porosimeter (Carlo Erba). The mean pore diameters and pore volumes of the packings determined from these measurements are given in Table 1.

The mean thickness of the polymeric layer was calculated according to the equation

$$d\ (\mathrm{nm}) = 10^3 m/\rho S(1-m)$$

where m is the polymer content in the composite (g/g), ρ is the density of the polymer (1.0 g/cm^3), S is the specific surface area of the native silica (m^2/g) and $1-m$ is the silica content in the composite (g/g).

2.5. Chromatography

The columns were packed by the slurry technique with a 4% (w/w) suspension of sorbent in tetrahydrofuran–tetrachloromethane (1:1) and methanol as the displacement liquid. The pressure during the packing procedure was increased to 350 bar with a Shandon packing device.

The chromatographic system used was an L-6200 intelligent low-pressure gradient pump, an L-4200 variable-wavelength UV detector and a D-2500 integrator (all from Merck). Sample injection was performed with a Rheodyne Model 7125 injection valve equipped with a 20-μl injection loop.

The polystyrene standards used in the inverse SEC experiments were of M_r in the range 3 340 000–580 with a polydispersity of 1.04–1.10 from Merck, Polymer Laboratories and Polymer Standard Service. In low-molecular mass range, benzene ($M_r = 78$), toluene ($M_r = 92$) and 2,3-diphenylbutane ($M_r = 162$) were used as markers (all from Merck). The pore-size distribution was calculated from SEC data according to the method described by Knox and Ritche [8]. The values of the pore volume and specific surface area were determined per millilitre of packing in the column. In order to recalculate these values to a per gram of packing basis, it was assumed that the density of a packing is a linear function of its composition:

$$\rho_{\mathrm{comp.}} = \rho_{\mathrm{silica}} m'_{\mathrm{silica}} + \rho_{\mathrm{polymer}} m'_{\mathrm{polymer}}$$

where ρ is the density of the composite, silica or polymer and m' is the mass of polymer or silica in the composite.

3. Results and discussion

3.1. Physical and chemical properties of PVP-coated packings

Properties of the starting silicas and synthesized coated sorbents are given in Table 1. The

Table 1
Physico-chemical properties of synthesized packings

Silica	Elemental analysis (%)			Polymer content (mg/g)	Thickness of polymer layer (Å)	Coating density μmol/m^2	Low-temperature nitrogen adsorption[a]			Mercury porosimetry[a]			Inverse SEC[a]		
	C	H	N				V (ml/g)	D^b (Å)	S (m^2/g)	V (ml/g)	D (Å)	S^b (m^2/g)	V (ml/g)	D (Å)	S^b (m^2/g)
LiChrospher Si 300, native	–	–	–	–	–	–	2.00	320	250	1.80	380	170	2.10	480	175
LiChrospher Si 300, coated with PVP	13.1	2.7	2.4	200	10	14.0	1.33	407	130	1.21	320	151	2.30	476	195
LiChrospher Si 300, coated and end-capped	12.8	2.7	2.1	200	10	14.0	–	–	–	–	–	–	–	–	–
LiChrospher Si 500, native	–	–	–	–	–	–	0.80	550	45	1.00	500	80	1.05	470	90
LiChrospher Si 500, coated with PVP	5.8	0.9	1.1	89.5	22	13.5	0.64	463	55	0.82	500	65	1.42	442	79
LiChrospher Si 500, coated and end-capped	5.9	0.9	1.0	89.5	22	13.5	–	–	–	–	–	–	–	–	–

[a] V = specific pore volume; S = specific surface area; D = pore diameter.
[b] Calculated according to $V/S = D/4$.

polymer content of the composites was calculated from carbon elemental analysis. It was found to be of about 200 mg of PVP per gram of composite based on LiChrospher Si 300 and of about 90 mg per gram of composite based on LiChrospher Si 500. These values correlated with the specific surface area of the modified silicas. The coating density calculated as micromoles of monomer units per square metre of modified surface is approximately the same for both packings (Table 1), amounting to about 14 μmol/m^2, which is much higher than is typical for silanazed silicas [7]. The end-capping of the coated silicas did not cause any significant increase in the composite carbon content (Table 1) and provided good shielding of the silica surface by the polymer.

The low-temperature nitrogen adsorption measurements revealed that the specific surface area of LiChrospher Si 300 decreased by about 35% after modification. In contrast, a small increase in the specific surface area was observed for LiChrospher Si 500 coated with copolymer (Table 1). Both initial silicas demonstrated a wide pore-size distribution, extending towards small pores for LiChrospher Si 300 but towards large pores for LiChrospher Si 500 (Fig. 1). This pore-size distribution was not significantly changed after the modification (Fig. 1) and it seems to be an indication that a relatively thin polymeric layer was deposited on the pore surface (Table 1). Probably the smallest pores of diameter ≤30 Å, which could not be evaluated by means of the common nitrogen adsorption technique, were partly blocked during the modification by PVP and this caused the large de-

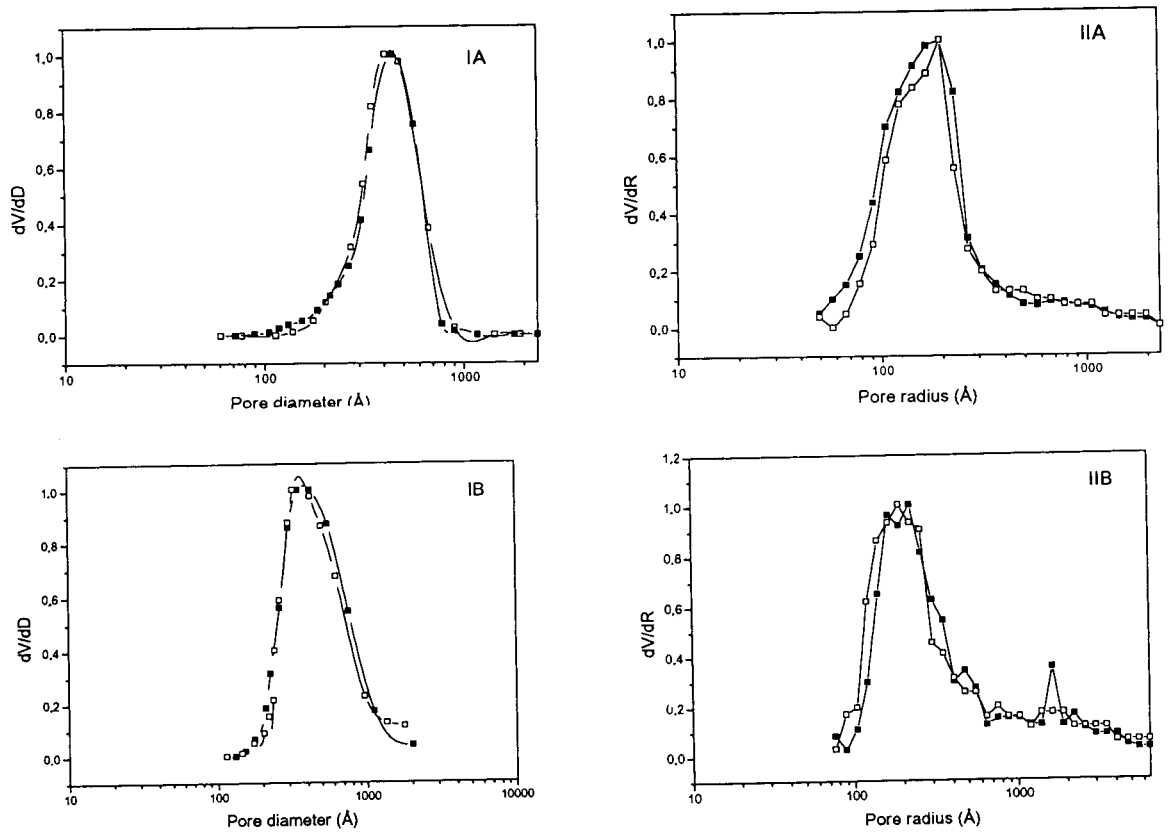

Fig. 1. Pore-size distribution of the (□) native and (■) PVP-coated silicas (A) LiChrospher Si 300 and (B) LiChrospher Si 500 from (I) nitrogen adsorption and (II) mercury porosimetry measurements.

crease in the specific surface area of LiChrospher Si 300 after modification. The same reason can explain the increase in the mean pore diameter of the modified LiChrospher Si 300. For the packing based on LiChrospher Si 500 the contribution of small pores seems to be insignificant, as indicated by the much lower value of its specific surface area. The pore volume of the packings is mainly connected with large pores and it was changed on coating LiChrospher Si 300 to a smaller extent (about 17%) than the surface area. For LiChrospher Si 500 the pore volume decrease was about 10%.

The specific pore volumes of packings based on 300 Å silica determined by means of mercury porosimetry were slightly lower than those measured by nitrogen adsorption, but slightly higher values were found for native and PVP-coated LiChrospher Si 500 packings. These differences could be expected, owing to the different limitations of these two methods. The changes in the porosity of native silicas after modification with the copolymer determined by mercury porosimetry were less pronounced than those found by nitrogen adsorption measurements.

In SEC with polystyrenes as test molecules, both modified and native silicas demonstrated a wide range of molecular mass discrimination (Fig. 2), as could be expected from the wide pore-size distribution determined by nitrogen adsorption or mercury porosimetry. The calibration graphs for PVP-coated packings are slightly lower than those for native silicas (Fig. 2), indicating some decrease in the mean pore diameters of the packings after modification (Table 1). The shape of the calibration graphs was not significantly changed after modification and therefore the pore-size distribution also was not much changed. This agrees with the results obtained by mercury porosimetry and nitrogen adsorption measurements (Fig. 1). The pore diameters and the specific surface areas measured by means of inverse SEC agreed fairly well with the values determined by other methods, but the pore volumes of the modified packings differed by a factor of almost two (Table 1). This major difference can arise because of the difficulties in the discrimination between the inter- and intraparticle volumes in the SEC calibration graphs, as was described by Stegeman *et al.* [9].

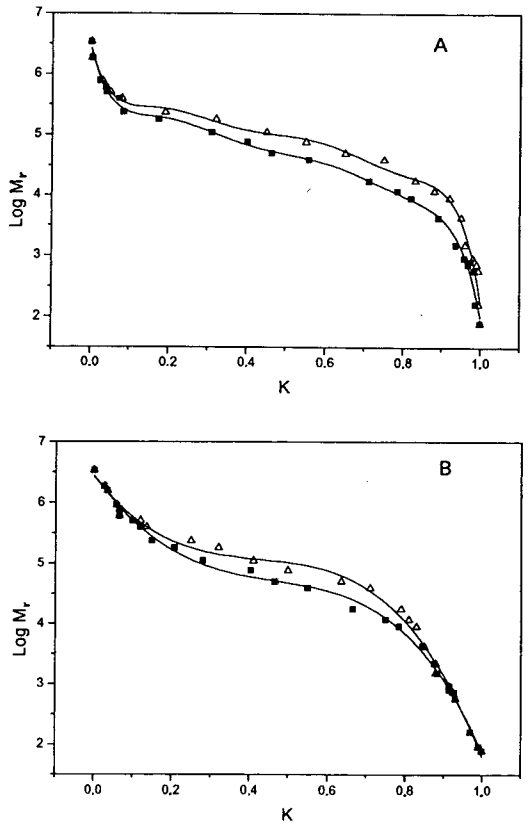

Fig. 2. SEC calibration graph for polystyrene standards on the (△) native and (▲) PVP-coated silicas (A) LiChrospher Si 300 and (B) LiChrospher Si 500. Eluent, tetrahydrofuran; flow-rate, 0.5 ml/min; column, 250 × 4 mm I.D.

3.2. Chromatographic separations on synthesized packings

Normal- and reversed-phase separations of aromatic hydrocarbons

Silica-based packings with covalently bonded pyrrolidone groups can be explored in both normal- and reversed-phase modes of chromatography depending on the eluent used [10]. To prove that PVP-coated packings can be applied to the same modes of separations, some mixtures of aromatic compounds were investigated. One of these mixtures was composed of benzene and

nitrobenzene. For alkyl/aryl stationary phases one assumes that in normal-phase chromatography nitrobenzene elutes before benzene on packings with a low contribution to the retention from silanol surface groups. For polar stationary phases such as PVP-coated silica, an additional contribution to the retention can arise from specific interactions between aromatic analytes and polar groups of modifying layer. The selectivity and retention data for benzene–nitrobenzene separations on the synthesized packings are given in Table 2. The same parameters for the unmodified silica LiChrospher Si 300 and the octadecyl RP packing Superspher-100 RP-18 are also presented in Table 2 for comparison. Benzene was found to be eluted before nitrobenzene on all the sorbents studied. The smallest retention of nitrobenzene was observed on PVP-coated LiChrospher Si 300, and the highest retention, with a broad and tailing peak (the number of theoretical plates was less than 1000), was observed on PVP-coated LiChrospher Si 500. The retention was even higher than that on native silica LiChrospher Si 300 and probably arises owing to specific interactions between the nitro and amide groups because benzene gave a sharp and symmetrical peak (the height equivalent to a theoretical plate was between 3.0 and 3.5 d_p) with all the sorbents studied.

A specific mechanism of interaction between aromatic compounds and pyrrolidone moieties of the modifying layer can be easily demonstrated from a normal-phase separation of PAHs on the synthesized packings (Fig. 3). When pure *n*-pentane was used as the eluent, the copolymer-coated silicas demonstrated higher retentions of PAHs than the unmodified silica or Superspher-100 RP-18. On the column packed with coated LiChrospher Si 500 under given conditions only the first five components could be eluted in a reasonable time of about 1 h and therefore the separation is not shown in Fig. 3. The mechanism of the stronger retention of PAHs on this sorbent is not clear.

Table 2
Capacity factors and selectivity of separation of benzene–nitrobenzene mixture on synthesized sorbents

	k'		α
	Benzene	Nitrobenzene	
LiChrospher Si 300, native	0.09	1.83	20.33
LiChrospher Si 300, coated with PVP	0.15	0.82	6.13
LiChrospher Si 500, coated with PVP	0.25	3.21	12.84
Superspher-100 RP-18	0.20	1.45	7.25

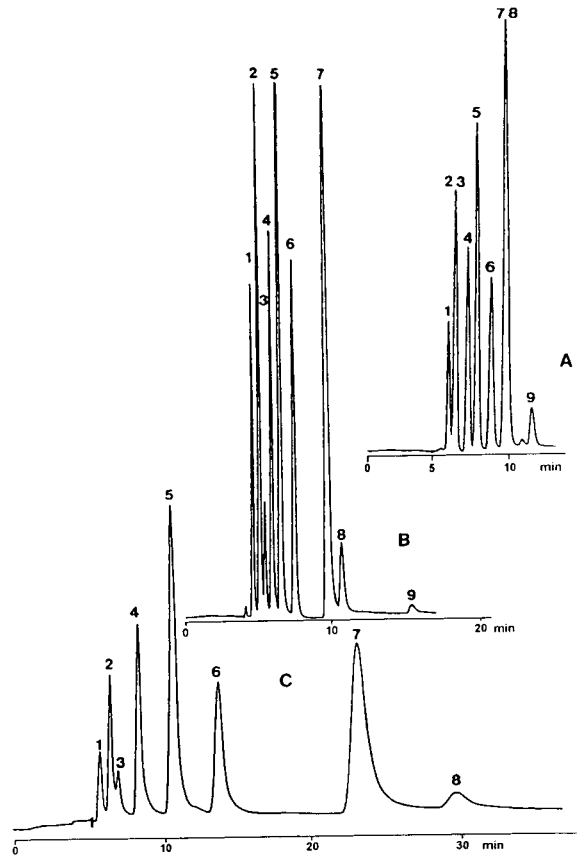

Fig. 3. Normal-phase chromatographic separation of PAH mixture on (A) PVP-coated silica LiChrospher Si 300, (B) unmodified silica LiChrospher Si 300 and (C) RP-silica Superspher-100 RP-18. Eluent, *n*-pentane; flow-rate, 0.5 ml/min; column, 250 × 4 mm I.D. Solutes: 1 = benzene; 2 = naphthalene; 3 = fluorene; 4 = anthracene; 5 = pyrene; 6 = benz[*a*]anthracene; 7 = perylene; 8 = benzo[*a*]pyrene; 9 = coronene.

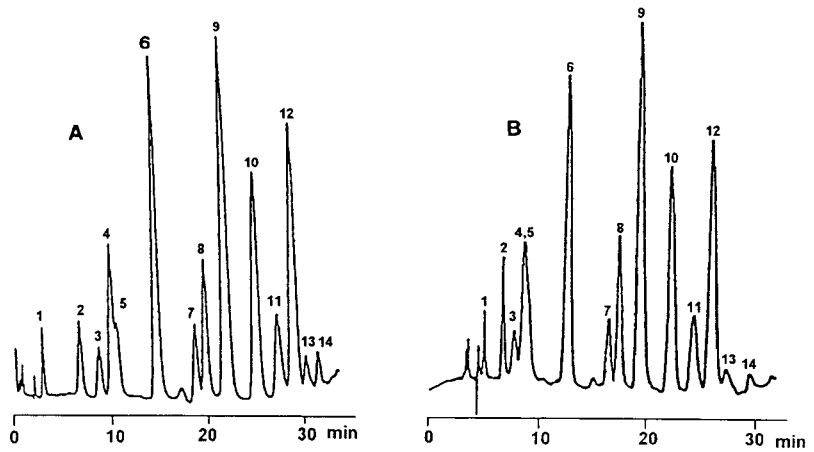

Fig. 4. RP separation of PAH mixture on (A) PVP-coated silica LiChrospher Si 300 and (B) LiChrospher Si 500. Gradient elution: 0–5 min 20% acetonitrile in water; 5–25 min from 20 to 45% acetonitrile in water; 25–30 min from 45 to 100% acetonitrile in water. Flow-rate, 1 ml/min; column, 250 × 4 mm I.D. Solutes: 1 = benzene; 2 = naphthalene; 3 = acenaphthylene; 4 = fluorene; 5 = acenaphthene; 6 = anthracene; 7 = fluoranthene; 8 = pyrene; 9 = chrysene; 10 = benzo[*b*]fluoranthene; 11 = perylene; 12 = indenopyrene; 13 = benzoperylene; 14 = coronene.

In the RP mode of separation, there was no difference between the two PVP-coated sorbents (Fig. 4). The elution order of PAHs and their retentions are roughly the same for both packings, with the retentions being much shorter than those observed with Superspher-100 RP-18. There was a linear correlation between the k' values on the PVP-coated packings and on Superspher-100 RP-18. Hence one can propose similar retention mechanisms with these packings in RP chromatography.

From the above experimental data, one can conclude that the specific interaction between PVP and aromatic compounds in aprotic eluents is probably due to a specific association between the amide groups of PVP and the π-electron system of the benzene rings. Solvation of amide fragments by protic solvents destroys this association. The PVP-coated sorbents with polar eluents demonstrate behaviour typical of weakly hydrophobic packings.

Separation of proteins and peptides

The separation of proteins on the synthesized packings with pure water as eluent was not fully consistent with the SEC mechanism because of the noticeable adsorption of some analytes. Addition of sodium chloride to the eluent at a concentration of 0.2 *M* decreased this adsorption to a minimum. Fig. 5 shows the calibration graphs for proteins with PVP-coated packings under given conditions. For the packing with pore diameter 500 Å, the retention volumes correlate well with the logarithms of molecular mass for almost all the proteins tested (Fig. 5A). For the 300 Å packing, the largest proteins, thyroglobulin and ferritin, deviated from a straight-line correlation (Fig. 5B), eluting with smaller volumes than could be expected from the calibration graph. The basic proteins lysozyme and chymotrypsinogen A do not fit the correlation line. Nevertheless, they could be completely eluted from the columns with this simple eluent.

The SEC of proteins implies mainly a hydrophilic character of the synthesized packings. The weak ion-exchange interactions, still occurring through the thickness of the modified layer, can be effectively suppressed by adding a low concentration of salt to the eluent. A hydrodynamic mechanism of separation [11] probably contributed to the separation of large proteins also. This effect was more pronounced for the packing with 300 Å pores, as its particle size was smaller (Table 1), and for large proteins, such as calf thymus (Fig. 6), the molecular mass of which of *ca.* $1.5 \cdot 10^6$ is too high for separation according

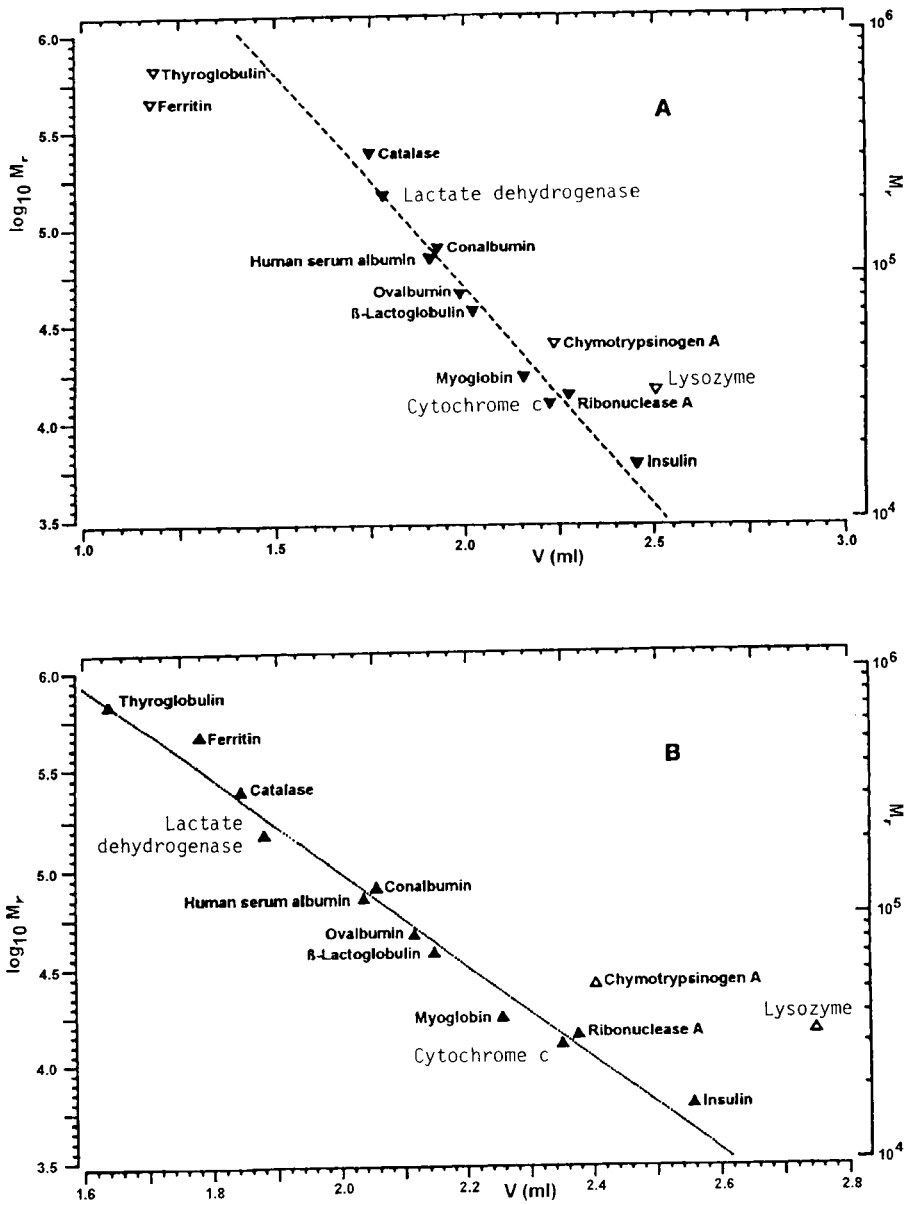

Fig. 5. Calibration graph for the retention of proteins on (A) PVP-coated silica LiChrospher Si 300 and (B) LiChrospher Si 500. Eluent, 0.2 *M* NaCl in 0.05 *M* phosphate buffer (pH 6.97); flow-rate, 0.1 ml/min; column, 250 × 4 mm I.D.

to the SEC mechanism on the synthesized packings.

With further increase in the salt concentration in the eluent, proteins will be retained again by the PVP-coated packings according to the hydrophobic interaction mechanism and they can be eluted with a decreasing salt gradient [12]. Separations of test protein mixtures by means of HIC are shown in Figs. 7 and 8. A salt concentration as high as 2.8 *M* ammonium sulphate has to be used to retain most proteins at the beginning. Nevertheless, cytochrome *c* was still weakly

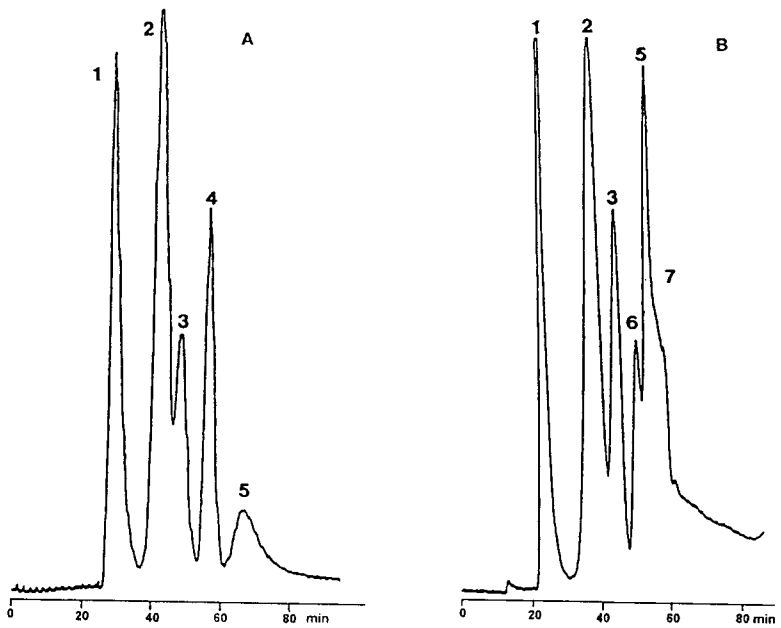

Fig. 6. SEC separation of protein mixture on (A) PVP-coated silica LiChrospher Si 300 and (B) LiChrospher Si 500. Conditions as in Fig. 5. Solutes: 1 = calf thymus; 2 = ferritin; 3 = ovalbumin; 4 = lysozyme; 5 = insulin; 6 = cytochrome *c*; 7 = sodium azide.

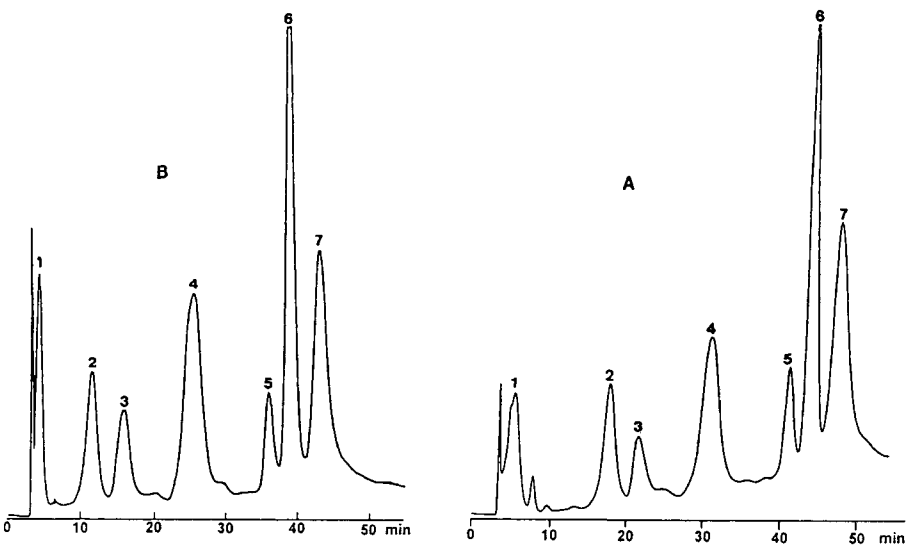

Fig. 7. HIC separation of protein mixture on (A) PVP-coated silica LiChrospher Si 500 and (B) LiChrospher Si 300. Gradient elution: 0–5 min 100% A; 5–65 min 0–100% B; A = 2.8 *M* ammonium sulphate in B and B = 0.05 *M* phosphate buffer (pH 6.97). Flow-rate, 0.5 ml/min; column, 250 × 4 mm I.D. Solutes: 1 = cytochrome *c*; 2 = myoglobin; 3 = β-lactoglobulin; 4 = ovalbumin; 5 = impurity in chymotrypsinogen; 6 = chymotrypsinogen; 7 = ferritin.

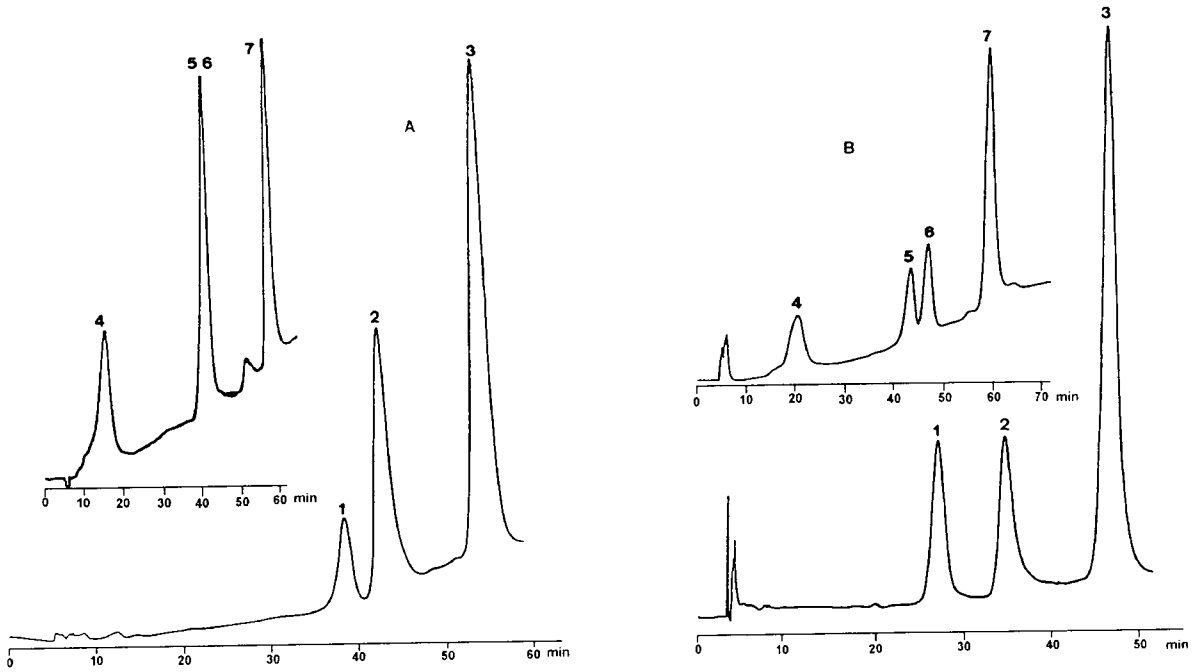

Fig. 8. HIC separation of protein or peptide mixture on (A) PVP-coated silica LiChrospher Si 300 and (B) LiChrospher Si 500. Conditions as in Fig. 7. Solutes: 1 = ribonuclease A; 2 = lactate dehydrogenase; 3 = catalase; 4 = angiotensin; 5 = neurotensin; 6 = oxytocin; 7 = somastatin.

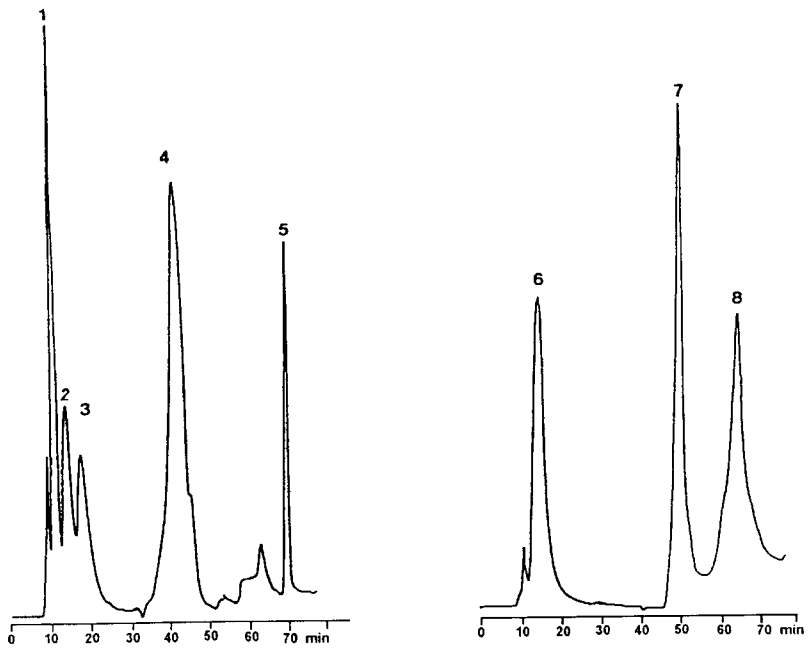

Fig. 9. RP separation of protein mixture on the PVP-coated silica LiChrospher Si 500. Gradient elution: 0–17 min 100% A; 17–47 min 0–50% B; 47–52 min 50% B; A = water–0.1% TFA, B = acetonitrile–0.1% TFA. Flow-rate 0.3 ml/min; column 250 × 4 mm I.D. Sample: 1 = ribonuclease A; 2 = β-lactoglobulin; 3 = trypsin; 4 = cytochrome *c*; 5 = myoglobin; 6 = ovalbumin; 7 = bovine serum albumin; 8 = ferritin.

retained and eluted from the column before the gradient. The elution order of proteins did not correlate with either their hydrophobicities or their molecular masses and there is a combination of different additional contributions, *e.g.*, from ion exchange and size exclusion. Probably the contribution of a size-exclusion mechanism was mainly responsible for the better separation of the pair neurotensin–oxytocin on the PVP-coated packing based on LiChrospher Si 300 (Fig. 8), as compared with the separation on the packing based on LiChrospher Si 500. However, overall there was only a minor difference between the PVP-coated packings in the HIC of proteins and comparable separations of a seven-component mixture of proteins were achieved on both packings in a similar time (Fig. 7).

An attempt to separate of proteins according to the RP mode of chromatography on the synthesized packings clearly demonstrated their hydrophilic character (Fig. 9). Ribonuclease A, β-lactoglobulin, trypsin inhibitor and even the hydrophobic ovalbumin were eluted from the column without a gradient with water containing 0.1% of trifluoroacetic acid as eluent. The elution order observed did not correlate with the hydrophobicity of the solutes, their retention being mainly controlled by other interactions. As is typical for the application of the hydrophilic packings in the RP mode of separation [13], a relatively low efficiency was observed for most of the investigated proteins. In addition, the samples were unstable under the given conditions and additional peaks emerged on the chromatograms of samples that had been standing for 1–2 h. Probably denaturation of some proteins took place during this period [13]. In any case, the synthesized hydrophilic PVP-coated packings do not meet the requirements for RP separations. The latter can be carried out with higher efficiency, *e.g.*, on hydrophobic polystyrene-coated silicas [14].

4. Conclusions

A significant result of the present investigation is that PVP-coated silica packings can be successfully used in various modes of liquid chromatography by exposing to the solute polar, H-bonding and/or apolar fragments of the bonded polymeric chains. Each chain of the copolymer is bonded by multiple covalent bonds to the silica surface. The segments between the two neighbouring links could be expected to retain sufficient flexibility, allowing the polymer to rearrange its conformation in accordance with the nature and properties of the mobile phase. This adaptation of the polymer film to the mobile phase would imply a certain change in the chemical nature of the polymer-coated column packing. In any case, the PVP chains bonded on the surface of porous silica open up new possibilities for chromatographic separations of proteins and peptides by involving a combination of possible interactions to the retention of the solutes.

5. References

[1] M. Hanson and K. Unger, *Trends Anal. Chem.*, 11 (1992) 368.
[2] A. Ivanov, V. Saburov and V. Zubov, *Adv. Polym. Sci.*, 104 (1991) 136.
[3] M. Caude and R. Rosset, *J. Chromatogr. Sci.*, 15 (1977) 405.
[4] A. Ivanov, L. Zhigis, E. Chekhovskich, P. Reshetov and V. Zubov, *Bioorg. Khim.*, 11 (1985) 405.
[5] J. Köchler, *Chromatographia*, 21 (1986) 573.
[6] F. Meiller, C. Bonnebat and M. Deleuil, *US Pat.*, 3 984 349 (1976).
[7] K. Unger, *Porous Silica* (*Journal of Chromatography Library*, Vol. 16), Elsevier, Amsterdam, 1979.
[8] J.H. Knox and H.J. Ritche, *J. Chromatogr.*, 387 (1987) 66.
[9] G. Stegeman, J.C. Kraak and H. Poppe, *J. Chromatogr.*, 550 (1991) 721.
[10] T. Morey, S. Siggia, P. Uden and R. Crowley, *Anal. Chem.*, 52 (1980) 885.
[11] J.C. Kraak, R. Oostervink, H. Poppe, U. Esser and K. Unger, *Chromatographia*, 27 (1989) 585.
[12] K.-O. Eriksson, in J.-C. Janson and L. Ryden (Editors), *Protein Purification Principles, High Resolution Methods, and Application*, VCH, New York, 1989.
[13] M. Hanson, K. Unger, C.T. Mant and R.S. Hodges, *J. Chromatogr.*, 599 (1992) 65.
[14] V. Davankov, A. Kurganov and K. Unger, *J. Chromatogr.*, 500 (1990) 519.

ELSEVIER

Journal of Chromatography A, 663 (1994) 175–186

JOURNAL OF CHROMATOGRAPHY A

Chromatography of human immunoglobulin G on immobilized Drimarene Rubine R/K-5BL
Study of mild, efficient elution procedures

Sylvie Cochet, M'Hammed Hasnaoui, Martine Debbia, Yolande Kroviarski, Patrick Lambin, Jean Pierre Cartron, Olivier Bertrand*

INSERM U 76 and INTS, 6 Rue Alexandre Cabanel, 75739 Paris, France

(First received September 20th, 1993; revised manuscript received November 22nd, 1993)

Abstract

A range of substances were screened to find eluents for human immunoglobulin G (IgG) which are retained with a strong affinity by immobilized Drimarene Rubine R/K-5BL. The strong affinity of IgG for the dye is partly due to the presence of copper in the dye. This was suggested by the effect of substances able to make coordination bonds with metals that elute the IgG and also the effect of metal stripping from the immobilized dye. Several mobile phase conditions were found that allowed desorption of retained IgG on immobilized Drimarene Rubine R/K-5BL without using a protein denaturant. A procedure was also devised for separating IgG_2 from other IgG subclasses using chromatography on immobilized Rubine R/K-5BL and column development with an AMP gradient.

1. Introduction

Immobilized dyes have been widely used as chromatographic supports for purifying a variety of proteins, mostly enzymes [1]. Plasma proteins have been also separated by immobilized dye chromatography. Immobilized Cibacron Blue F3GA has been used to purify human serum albumin on an industrial scale [2,3], and Remazol Yellow GGL has been used for the very large-scale purification of transthyretrin [4]. Many publications have described the purification of diverse plasma proteins at least on a laboratory scale [5–12]. Immunoglobulins have been purified and fractionated on immobilized Remazol yellow GGL [13] and on DEAE-Cibacron Blue [14]. Berg and Scouten [15] screened 65 immobilized dyes for their affinity for immunoglobulins and identified two dyes, Drimarene Blue K-R and Rubine R/K-5BL, that had a high affinity for immunoglobulins. Their affinities were so high that no satisfactory procedure was found for eluting proteins that allowed the recovery of immunoglobulins in a native state.

This paper describes the systematic screening of conditions needed to elute immunoglobulins from an immobilized Rubine R/K-5BL column. It was possible to elute immunoglobulins in good yield with mild eluents. This immobilized dye

* Corresponding author.

0021-9673/94/$07.00
SSDI 0021-9673(93)E1248-X

was also used to separate immunoglobulin G (IgG) subclasses.

2. Experimental

2.1. Materials

Drimarene Rubine R/K-5BL was a gift from Sandoz Chimie (Rueil Malmaison, France). Sepharose CL-4B was obtained from Pharmacia (Uppsala, Sweden). Placental immunoglobulins were a gift from Pasteur Merieux Serum et Vaccins (Marcy L'Etoile, France). All other chemicals were purchased form Sigma (St. Louis, MO, USA), Merck (Darmstadt, Germany) or Bio-Rad (Richmond, CA, USA).

2.2. Dye immobilization [1]

Sepharose CL-4B was rinsed extensively with water and immersed in 0.2 *M* NaOH containing 2% (w/v) NaCl. The gel was transferred into a vessel containing reactive dye (20 mg/ml gel) (the dye was used as obtained from the manufacturer), then, 0.2 *M* NaOH containing 2% (w/v) NaCl was added so that final reaction volume was twice the gel volume. The gel suspension was tumbled at 60°C for 1 h, then rinsed with 10 volumes of 0.2 *M* NaOH followed by 50% dimethyl sulphoxide in water until the washings were clear. The gel was finally rinsed with water and stored as a suspension in 100 m*M* NaCl containing 0.02% sodium azide.

Dye substitution was measured as follows [1]. Immobilized dye was hydrolysed in 50% acetic acid at 110°C until the gel was completely dissolved and the absorbance was then measured at 531 nm. The substitution level was expressed as milligrams of dye per millilitre of support, using the reactive dye, as obtained from the manufacturer, as a standard.

2.3. Preparation and characterization of immunoglobulins used for screening eluents

We used immunoglobulins prepared from human placenta, subsequently called placental IgGs. The human placental immunoglobulins were manufactured for intravenous administration and hence were treated with dilute plasmin [16]. They were characterized by sodium dodecyl sulphate–polyacrylamide gel electrophoresis (SDS-PAGE) under both reducing and non-reducing conditions followed by Western blotting. Blots were revealed using rabbit antibodies directed against Fab and Fc fragments of immunoglobulins. IgG subclasses were assayed by enzyme-linked immunosorbent assay (ELISA) [17].

In order to obtain, when needed, IgG free of degradation products (subsequently called gel-filtered IgG), placental IgGs (150 mg of IgG in 20 ml of equilibration buffer) were chromatographed on an Ultrogel AcA-54 column (70 cm × 5 cm I.D.) equilibrated in 5 m*M* sodium acetate buffer (pH 6.0) containing 0.1 *M* NaCl operated at a flow-rate of 105 ml/h.

Placental or gel-filtered IgGs were passed through a Sephadex G-25 column equilibrated in buffer A [10 m*M* KOH adjusted to pH 6.0 with solid 2-(N-morpholino)ethanesulphonic acid (MES)] prior to their use for screening eluents.

2.4. Preparation of metal-stripped immobilized dye

Metal was removed from immobilized Rubine R/K-5BL by pumping through the column 0.1 *M* EDTA dissolved in buffer B (10 m*M* KOH adjusted to pH 6.0 with solid MES containing 2 *M* NaCl). The copper content of the EDTA eluate was assayed spectrophotometrically at 632 nm.

2.5. Eluent screening

A column (2.6 cm × 1.1 cm I.D.) of immobilized dye was equilibrated in buffer A at a flow-rate of 20 ml/h. Untreated or metal-stripped immobilized dye was used as required. Two types of experiments were performed, as follows.

(i) A 6-mg amount of placental IgGs dissolved in buffer A was loaded on the immobilized dye column. The column was then developed in

sequence with 20 ml of buffer A, 20 ml of buffer B, 20 ml of buffer B′ (buffer B containing one of the eluents tested), 20 ml of buffer B again and finally with 20 ml of buffer C (buffer B containing 6 *M* urea). Protein-containing fractions eluted with buffers A , B and C and finally with buffer B′ (if the buffer itself did not adsorb at 280 nm) were separately pooled and the absorbance at 280 nm of each pool was evaluated.

(ii) A 6-mg amount of gel-filtered IgGs dissolved in buffer A was loaded on the column. The column was then developed with 20 ml of buffer A′ (buffer A containing one of the putative eluents), 20 ml of buffer A and finally 20 ml of buffer C. The absorbances of pools, made similarly as above, were measured.

The procedures used to calculate the amounts of proteins eluted by buffer B′ and A′ (when these buffers contained UV-absorbing substances) are described in Section 3.

2.6. Separation of IgG subclasses

Gel-filtered IgGs (6 mg dissolved in buffer A) were loaded on an immobilized Rubine R/K-5BL column (2.6 cm × 1.1 cm I.D.) equilibrated in buffer A. The flow-rate was 20 ml/h. After sample loading, the column was rinsed with 20 ml of buffer A and developed with 10 ml of buffer A containing 10 m*M* AMP and then with a linear 90 min gradient from 10 to 100 m*M* AMP (in buffer A). The column was then rinsed with 100 m*M* AMP in buffer A and finally with buffer C. Each fraction (2 ml) was assayed for IgG_2 and for total IgG by ELISA.

2.7. Other techniques

SDS-PAGE [18] was carried out on a Novex (San Diego, CA, USA) apparatus. Protein was assayed by measuring the absorbance at 280 nm or by the Bradford assay [19]. The p*K* values of imidazole and imidazole derivatives were measured using a Tacussel (Villeurbanne, France) TT 60 automatic titrator.

3. Results and discussion

3.1. Characterization of immunoglobulin preparations used as starting material

Placental IgGs had been treated with dilute plasmin to remove aggregates [16], and there was some cleavage of IgGs analogous to that produced by papain generating Fab and Fc fragments (Fig. 1). Western blotting of a non-reduced gel confirmed that fragments with apparent molecular masses of 46 000 and 54 000 reacted with the Fab- and Fc-specific anti-IgG. These degradation fragments will be referred to as Fab and Fc fragments. The band migrating with an apparent molecular mass of 30 000 on the non-reduced gel was identified as a degradation product of Fc origin.

A Coomassie Brilliant Blue-stained smear centred at an apparent molecular mass of 150 000 was also seen on the non-reduced gel. A similar pattern has been already described by others and assumed to be due to proteolytic degradation of IgGs [16]. Gel-filtered IgGs were essentially free of Fab and Fc fragments (Fig. 1) but had some M_r 150 000 smear on the non-reduced gel.

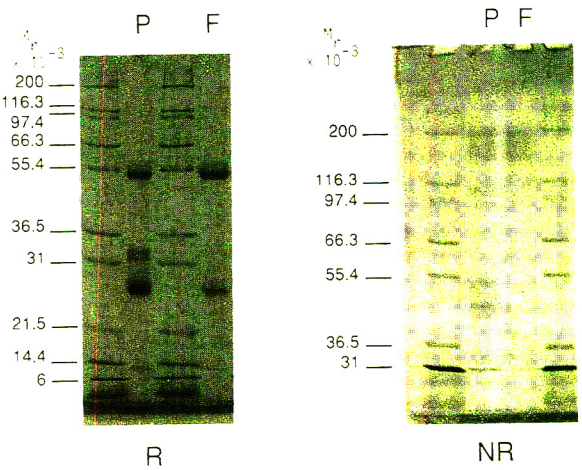

Fig. 1. SDS-PAGE of placental and gel-filtered IgGs. Placental and gel-filtered IgGs were loaded in lanes P and F. Molecular mass standards were loaded in the other lanes. Electrophoreses were run under reducing conditions (R) and non-reducing conditions (NR) on 12.5% and 8% gels.

3.2. Characterization of immobilized dye

Dye substitution was 4.3 mg of dye per millilitre of gel. The copper eluted with EDTA from an aliquot of gel (not used for chromatography) was 7.4 μmol per millilitre of gel.

3.3. Identification of molecular species eluted from Rubine column by buffers A, B and C

The elution pattern of placental IgGs with buffers A, B and C is shown at the top of Fig. 2. SDS-PAGE (Fig. 3) and Western blots (not shown) demonstrated that Fab was the only species eluted from the column during sample loading and washing with buffer A. Fab was also eluted by buffer B. The urea-containing buffer C eluted IgGs and the Fc fragment. These results agree well with the data of Berg and Scouten [15]. Gel-filtered IgGs were eluted only with buffer C (not shown).

3.4. Studies with metallized dye: screening of a range of potential eluting species and insight into the molecular mechanism underlying metallized dye affinity for proteins

It has been known since the very early days of immobilized dye chromatography that an enzyme retained on a dye column can often be eluted by adding a natural ligand for the enzyme to the mobile phase [20,21]. It has also been shown that enzymes retained by a dye could be eluted with substances unrelated to one of their natural ligands. For example, chymotrypsinogen can be eluted from an immobilized dye with cytidine monophosphate [22]. Fragments of natural ligands can be more efficient than natural ligands [23]. This leads to the conclusion [23] that "every substance which in some way mimics a dye (*i.e.*, which associates a high density of charged groups with hydrophobic parts) has the potential to elute a protein from a dye column". In keeping with this background, we tried to discover useful substances allowing immunoglobulins to be eluted in a native state from the Rubine column.

Numerical results representative of the eluting power of the various potential eluents dissolved in buffer B were obtained as follows: proteins present in the peak eluted by infusion of buffer C, following buffer B′ infusion onto the column were evaluated by measuring absorbance at 280 nm: the peak eluted by buffer C after the column had been developed with only buffer A and B was fairly constant and corresponded to 43.2% of total loaded protein; if buffer B′ contained a substance that eluted proteins from the column, peak eluted by buffer C was lower (see Fig. 2, centre and bottom). The eluting power of the substance dissolved in buffer B′ was then evaluated from the ratio.

$$\frac{43.2 - \text{protein eluted by buffer C)}}{43.2} \cdot 100$$

Obviously, in each instance of an absorbing and eluting buffer B′ the effective presence of IgGs in the buffer B′-eluted fractions was checked by SDS-PAGE, ELISA and/or Bradford protein assay. When the test substance in buffer B′ did not absorb at 280 nm the proportion of proteins eluted could be evaluated either through direct absorbance measurement of fractions eluted with buffer B′ or through absorbance measurement of fractions eluted with buffer C and calculation as indicated above. The results obtained with the two methods were in satisfactory agreement.

Numerical results for the experiments in which tested substances were dissolved in buffer A were obtained similarly.

Eluting power of phosphate and phosphorylated compounds, nucleosides and nucleobases

Phosphate is known to be a potential eluent of proteins from immobilized dyes [24], but 0.1 *M* phosphate did not elute IgGs from immobilized Rubinol R/K-5BL. Inositol hexaphosphate (IHP), an inexpensive phosphoryl compound that has been used to elute, with a satisfactory selectivity, proteins from a dye column [25], had no effect (0.1 *M* in buffer B) (Fig. 4, top).

AMP and cyclic AMP, 10 m*M* in buffer B,

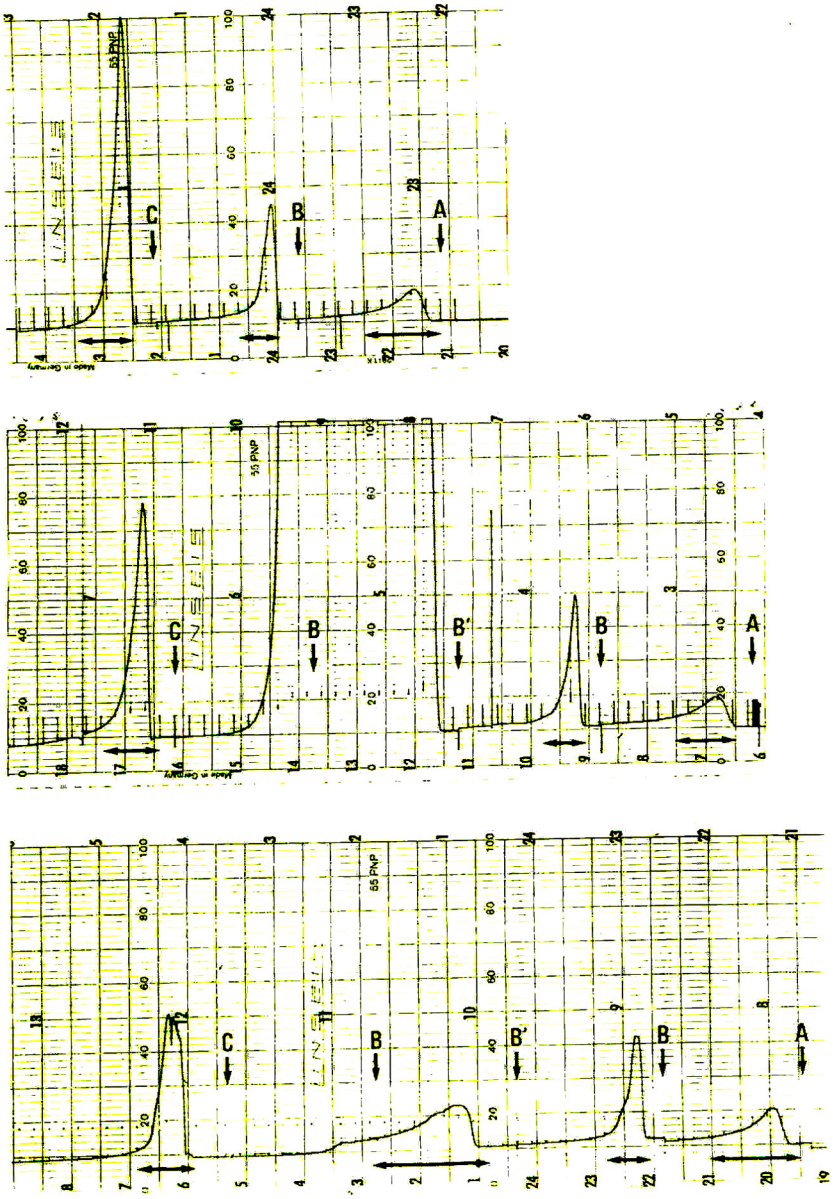

Fig. 2. Chromatography of placental IgGs on immobilized Rubine R/K-5BL. Top, elution with buffers A, B and C; centre, buffer B′ contained 10 m*M* ADP; bottom, buffer B′ contained 0.5 m*M* imidazole. Vertical arrows indicate buffer changes. The column was 2.6 cm × 1.1 cm I.D. and the flow-rate was 20 ml/h. Fractions were pooled as indicated by the double horizontal arrows and protein content was evaluated by absorbance measurements.

eluted some IgGs from the dye column and at 100 m*M* eluted all the IgGs. Adenosine and adenine (10 m*M*) eluted slightly more IgGs than did AMP or cyclic AMP. NAD and CMP (10 m*M* concentration in buffer B) eluted a significant proportion of IgGs (Fig. 4, top).

The eluting power of AMP and adenosine dissolved in buffer A was also evaluated (see Fig.

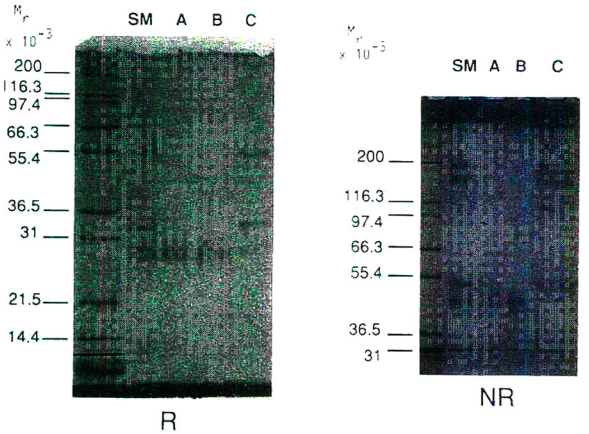

Fig. 3. SDS-PAGE analysis of the chromatogram shown in Fig. 2 (top). An aliquot of starting material for the chromatography (placental IgGs) was loaded in lane SM. Aliquots of the three peaks eluted from the column during sample loading, during buffer B application and during development with buffer C were loaded into lanes A, B and C, respectively. The left lanes of the gels were loaded with molecular mass standards. R and NR indicate reduced and non-reduced conditions, respectively.

4, bottom): 10 m*M* AMP eluted about 20% and 100 m*M* AMP 67% of retained proteins whereas adenosine at the same concentrations had no effect.

Eluting power of amino acids, amino acid derivatives and imidazole compounds

Amino acids were tested because some of them (tryptophan, phenylalanine and tyrosine) are aromatic and bear charges. Some, such as histidine, tryptophan and phenylalanine, have been used in immobilized form to purify immunoglobulins [26–28].

Tryptophan and phenylalanine (0.1 *M*) eluted some, but not all, of the IgGs (Fig. 5). Phenylalanine ethyl ester and N-acetylphenylalanine were both more efficient than the parent amino acids. Glycine had no effect (0.1 *M* concentration in buffer B') while glycinamide eluted some of the IgGs. Histidine (0.1 *M*) eluted IgGs quantitatively. The dramatic effect of histidine is clearly due to the imidazole group, as imidazole at 10 m*M* removed all proteins from the Rubine R/K-5BL column. Imidazole and imidazole derivatives were clearly better eluters if the imidazole nitrogen was unprotonated: (i) imidazole is more efficient at pH 9 than at pH 6.0 (see Fig. 5); the p*K* of imidazole is 6.71, but it is well known that immobilized dyes often show a weaker affinity for proteins at alkaline pH; the p*K* values of substituted imidazoles were measured and found to be 7.13 for methylimidazole and 8.63 for nitroimidazole; it is

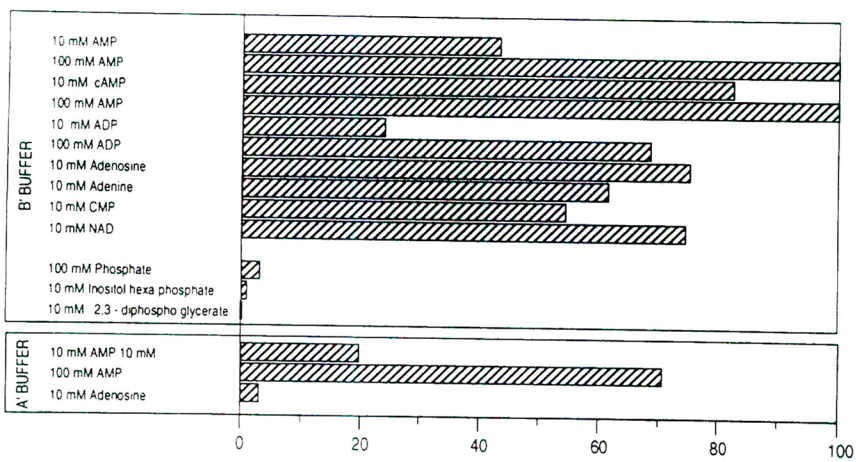

Fig. 4. Amounts of proteins eluted from the metallized Rubine R/K-5BL column with nucleotides, nucleosides nucleobases and some phosphorylated compounds. Numerical values (%) were determined as indicated in the text. Top, test substances were dissolved in buffer B; bottom, test substances were dissolved in buffer A.

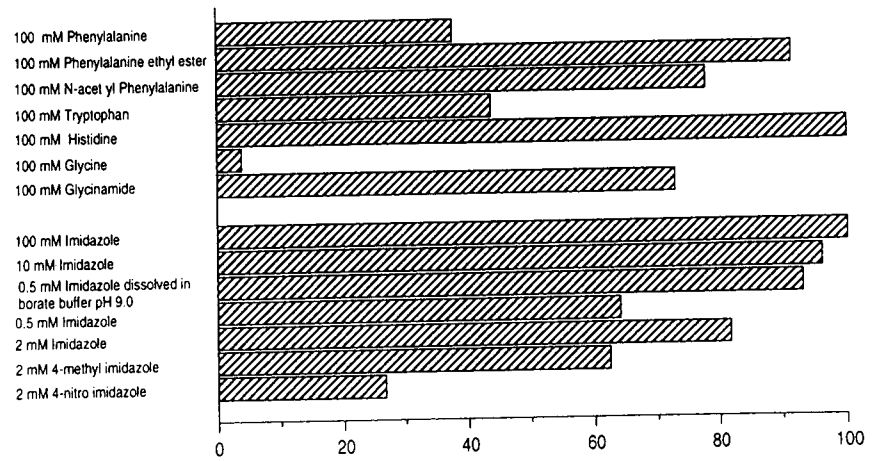

Fig. 5. Amounts of proteins eluted from the metallized Rubine R/K-5BL column by amino acids, derivatives thereof or imidazole compounds. Results shown were obtained by dissolving the tested substances in buffer B. Numerical values (%) were determined as indicated in the text.

obvious that one can rank the eluting power of imidazole and substituted imidazole in order of the nitrogen pK: compounds with higher pK have greater eluting power.

Eluting power of amines and miscellaneous mobile phase conditions

NH_4Cl (100 mM in buffer B) did not elute IgG and Fc fragments retained on the column. Neither diaminohexane nor benzylamine (100 mM) eluted significant amounts of IgGs, but pyridine (10 mM) eluted all the bound IgGs.

Glucosamine (0.1 M) in buffer B eluted more than half of the retained IgGs, but 0.1 M N-acetylglucosamine was much less effective (Fig. 6).

Increasing the pH of mobile phase to 9.0 or lowering it to 5.4 alone eluted only a small fraction of the retained proteins.

Effect of EDTA

The precise structure of Rubine R/K-5BL is not available but it is known to be a copper-containing azo dye [15]. We therefore evaluated the eluting power of EDTA. EDTA eluted a small fraction of the IgGs plus a large amount of copper (corresponding to 5.5 μmol of copper per millilitre of gel). Urea-containing buffer C applied thereafter to the column eluted the remaining retained IgG. The IgG bound to the column may protect the copper from chelation by EDTA because the EDTA eluted only a very small fraction of the bound IgGs and EDTA treatment of the column *after* elution of IgGs removed the copper left on the column after the first EDTA treatment (the amount of copper eluted by the second treatment with EDTA was 1.5 μmol per millilitre of gel). When the column that had been treated twice with EDTA was loaded with another aliquot of the IgG test mixture, most of the absorbance was eluted with buffer B and essentially none with buffer C.

Hence copper plays an important role in the affinity of the immobilized dye for the IgGs. Nevertheless, immobilized Rubine R/K-5BL is not simply some sort of an immobilized metal affinity chromatographic (IMAC) support [29]: lowering the mobile phase pH does not elute retained proteins; raising the ionic strength induces some desorption of retained proteins, as part of the Fab fragment present in placental IgGs and retained on the column is efficiently eluted (see Fig. 2, top), whereas IMAC is normally performed at high ionic strength and EDTA efficiently elutes proteins retained on IMAC supports together with the metal.

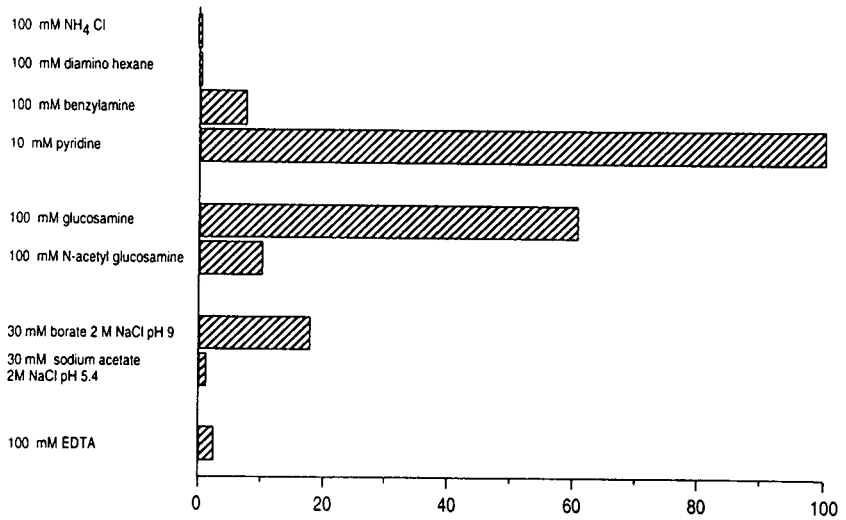

Fig. 6. Amounts of proteins eluted from the metallized Rubine R/K-5BL column by amino-containing substances, miscellaneous additives and mobile phase compositions. Results shown were obtained by dissolving the tested substances in buffer B. Numerical values (%) were determined as indicated in the text.

The copper in azo dyes is often anchored to the organic backbone of the dye by at least three coordination bonds, leaving at best only one bond free to interact with solvent or solutes [30]. The substances that elute significant amounts of IgGs from the metallized immobilized dye (*e.g.*, imidazole or pyridine) can form coordination bonds with metals. Molecules that form bidentate complexes with metals, such EDTA, and unsubstituted amino acids, are not better eluters than substances containing atoms bearing a lone pair of electrons (see results obtained with phenylalanine and its derivatives, with glycine and glycinamide).

Copper in the dye is an important element contributing to the affinity of the dye for the IgGs. Nevertheless, copper does not seem to be the only factor in the affinity of the immobilized dye for the IgGs. The IgGs were retained on the column by probably both coordinative bonding with copper and by electrostatic and/or hydrophobic interactions similar to those usually encountered in immobilized dye chromatography; thus imidazole dissolved in buffer A (a low ionic strength buffer) eluted poorly IgGs from a metallized immobilized dye column (only 2% of the absorbance was eluted with 2 m*M* imidazole dissolved in buffer A). Other experiments were performed to evaluate the eluting power of several substances with a demetallized dye.

3.5. Studies with demetallized dye and design of new elution mixtures for metallized dye

IgGs were quantitatively eluted from the demetallized dye column by raising the ionic strength, as is common with immobilized dyes (Fig. 7); this is usually considered to indicate the importance of electrostatic interactions between proteins and dye.

Imidazole (in buffer A) eluted only a small proportion of IgGs from demetallized dye. Phosphate (0.1 *M*) which was completely unable to elute IgG from metallized dye eluted more than 65% of the bound IgG from a demetallized dye. IHP (10 m*M*) did not elute significant amounts of IgGs from metallized dye but it eluted nearly 65% of the retained IgGs from the demetallized dye; 25 m*M* IHP eluted 100% of the bound IgGs. It was found that 10 m*M* AMP, cyclic AMP and NAD were all less effective than IHP at removing IgGs from demetallized dye; 100 m*M* AMP in buffer A eluted about 80% of the

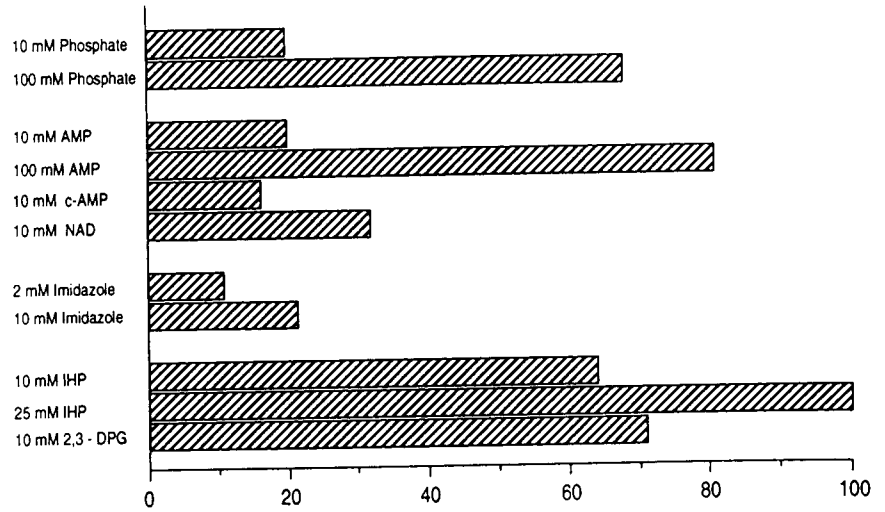

Fig. 7. Amounts of proteins eluted from the metal-stripped Rubine R/K-5BL column by various mobile phase additives (dissolved in buffer A). Numerical values (%) were determined as indicated in the text.

retained proteins from the demetallized dye, as did 100 m*M* AMP in buffer A from a metallized Rubine R/K-5BL column (see above).

We therefore believe that the affinity of Rubine R/K-5BL for IgG is mediated partly by electrostatic (and possibly hydrophobic) interactions, such as those commonly used to explain affinity of dyes for proteins, and partly by coordination to immobilized metal.

Substances such as AMP can probably compete with both types of interactions, as 0.1 *M* AMP also elutes IgGs from an immobilized metallized Rubine R/K-5BL column when dissolved in a low ionic strength buffer (see Fig. 4, bottom). In contrast, other substances probably interfere only with the metal participation in dye bonding to protein (*e.g.*, imidazole), or with the electrostatic components of the interaction (*e.g.*, IHP). We therefore tested new elution mixtures containing substances able to interfere with either component of the Rubine–proteins interactions. The aim was to obtain a non-UV-absorbing, inexpensive eluent that was more efficient than AMP. Buffer A containing 25 m*M* IHP and 10 m*M* imidazole eluted all the IgGs from immobilized (normally metallized) Rubine R/K-5BL. This result is remarkable when it is recalled that at the beginning of this work only urea-containing buffers were known to be able to elute IgGs.

3.6. Use of immobilized Rubine to purify IgGs and separate IgG subclasses

Immobilized Rubine R/K-5BL was not very useful for purifying IgGs from human plasma. Albumin and other proteins were bound to the support along with the IgGs and no eluent has yet been found to elute IgGs with sufficient selectivity to provide a one-step purification procedure (data not shown). In contrast, the dye is promising for separating IgG subclasses. Because the interaction of proteins with metals often involves histidine residues and IgG_2 has one histidine less than IgG_1 (the most abundant IgG subclass) in the constant regions of the γ chain [31], we attempted to separate IgG_2 from the bulk of IgGs on a Rubine R/K-5BL column. There is a need, for therapeutic purposes, for efficient techniques for preparing IgG_2-enriched IgG fractions. An immobilized Rubine R/K-5BL column was loaded with gel-filtered IgGs and developed with a gradient up to 100 m*M* AMP. There are some separation of IgG_2 (Fig. 8). These preliminary results are encouraging. Some

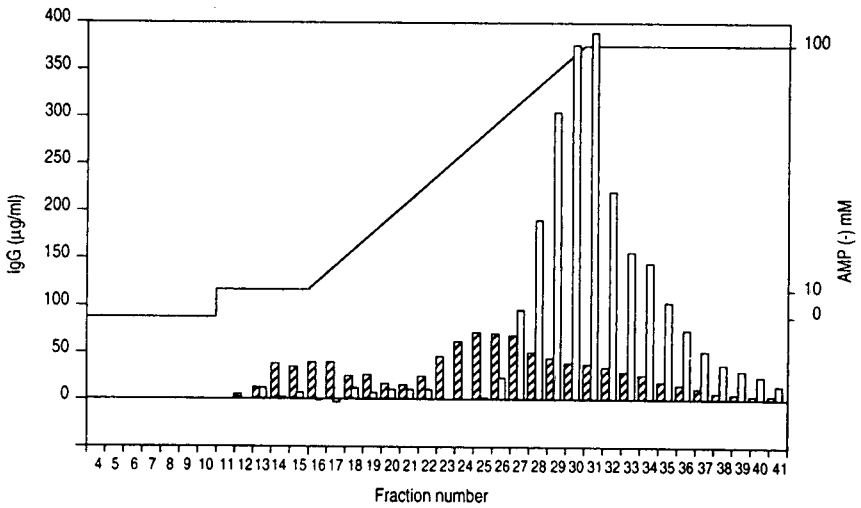

Fig. 8. Separation of IgG_2 from the other subclasses by chromatography on immobilized metallized Rubine R/K-5BL. The column (2.6 cm × 1.1 cm I.D.) was equilibrated and rinsed, after sample loading, with buffer A, then developed with a gradient of AMP dissolved in buffer A (the continuous line shows the gradient profile). The histogram shows the concentrations of IgG_2 (hatched bars) and of IgG of the other subclasses (empty bars) in the collected fractions.

other eluting agents, or mixtures of agents, could well be more efficient and cheaper than AMP.

4. General comments and conclusions

This report is not the first to emphasize the important role of metals in dye–protein interactions. Several papers have shown the dramatic effect of adding metals to mobile phases to promote the binding of proteins to dyes, at least for defined dye–protein pairs [32–35]. A ternary complex between protein, dye and metal seems to be formed in some instances that decreases significantly the dissociation constant of the protein and dye [32]. In other instances the metal could be bound to the dye (through coordination bonds with the azo bridge and sulphonate groups on the dye) [34,35] and this metal-loaded dye may display a greater affinity for the protein of interest. It was suggested that the interaction of metals "with functional groups appended to the dye chromophore stabilizes a particular conformation of the dye which is especially acceptable to the complementary protein" [35].

Proteins could be eluted from immobilized dyes with chelating agents, but all agents are not equally effective (in fact, some of them have little effect [34]). An enzyme retained on a column via a metal-mediated interaction could be eluted with two successive buffers [35]: the first, containing EDTA, presumably interfered with the component of dye–protein interaction due to the metal, and the second (a buffer with higher ionic strength and pH), pumped to the column immediately after the former eluent, presumably interfered with the usual, mostly ionic, component of the dye–protein interactions. This strategy is similar to that which we use to elute IgGs: the eluting mobile phase contained one solute directed against coordination bonds with metals (imidazole) and the other directed against classical dye–protein interactions (inositol hexaphosphate).

In the papers referred to above, the metal was deliberately added to the dye–protein pair. Metals can already be present in the reactive dye as received from the manufacturer: metallization of dyes is used in the dyes and pigments industry to improve light and wet fastness or to produce specific shades [30]. The role of metals in metallized dye–protein interactions have been evaluated by affinity partitioning, chromatography

and spectroscopy [36–39]. It was demonstrated that stripping metal from dyed polyethylene glycol can lead to loss of specificity of the partitioning (partitioning of lactate dehydrogenase) or the selectivity of partitioning can be greater with a metallized dye than after metal stripping (partitioning of glucose-6-phosphate dehydrogenase) [39]. The role of one histidine residue at the active site of alcohol dehydrogenase is crucial for binding of this enzyme to a copper-containing dye [36].

In conclusion, this paper has demonstrated that the systematic screening of eluents can be fruitful: while only denaturing agents were known to elute IgGs from immobilized Rubine R/K-5BL [15], systematic screening allowed the discovery of substances that allowed IgGs to be eluted efficiently in a native state. This screening used, as stated above, aromatic and charged substances, and phosphorylated sugars were also found (in this work and previously [25]) to be potentially useful eluents. Substances able to form coordination bonds with metals have been screened and should probably be systematically tried when a dye structure is unknown. Mixtures of eluents (each being able to compete with one kind of dye–protein interaction) can be very effective, as demonstrated here. Our results and previous work [36–39] demonstrate that interactions of proteins with metals contribute significantly to the affinity of proteins for metallized dyes. Metal stripping can modulate the interactions of proteins with a given immobilized dye. One can guess on the basis of published work [34,35] that changing the metal of a metallized dye could probably alter its properties in interacting with proteins. Rubine R/K-5BL, which is known as a useful reagent for purifying Fab [15], is also suitable for the IgG_2 enrichment of IgG preparations.

5. Acknowledgements

We thank Mr. Menuet (Sandoz Chimie) for the dye used in this study and Dr. M.C. Bonnet (Pasteur Merieux Serum et Vaccins) for the placental IgGs. This work was supported by a CEE grant (EU 384). The authors thank Dr. E. Boschetti (SEPRACOR IBF) for his interest and constructive suggestions. Y.K. is supported by the Association Claude Bernard.

6. References

[1] C.R. Lowe and J.C. Pearson, *Methods Enzymol.*, 104 (1984) 97–113.
[2] J. Travis, J. Bowen, D. Tewksbury, D. Johnson and R. Pannell, *Biochem. J.*, 157 (1976) 301.
[3] J. Saint Blancard, J.M. Kirzin, P. Riberson, F. Petit, J. Foucart, P. Girot and E. Boschetti, in T.C.H. Gribnau, J. Visser and R.J.F. Nivard (Editors), *Affinity Chromatography and Related Techniques (Analytical Chemistry Symposia Series*, Vol. 9), Elsevier, Amsterdam, 1982, pp. 305–312.
[4] V. Regnault, C. Rivat, L. Vallar and J.F. Stoltz, *J. Chromatogr.*, 576 (1992) 87–93.
[5] N.D. Harris and P.G.H. Byfield, *Febs Lett.*, 103 (1979) 162–164.
[6] G. Birkenmeier and G. Kopperschlager, in J.F. Stoltz and C. Rivat (Editors), *Biotechnology of Plasma Proteins*, Vol. 175, INSERM, Paris, 1989, pp. 217–228.
[7] E. Gianazza and P. Arnaud, *Biochem. J.*, 203 (1982) 637–641.
[8] K.G. McFarthing, S. Angal and P.D.G. Dean, *Anal. Biochem.*, 122 (1982) 186–193.
[9] G. Birkenmeier, E. Usbeck, L. Saro and G. Kopperschlager, *J. Chromatogr.*, 265 (1983) 27–35.
[10] K. Use, M. Himmel, G. Birkenmeier, M. Bohla and G. Kopperschlager, *Clin. Chim. Acta*, 133 (1983) 335–340.
[11] A.E. Hanahan, L. Miribel and P. Arnaud, *J. Chromatogr.*, 397 (1987) 197–206.
[12] L. Miribel and P. Arnaud, *J. Biochem. Biophys. Methods*, 14 (1987) 291–302.
[13] P.G.H. Byfield, in J.F. Stoltz and C. Rivat (Editors), *Biotechnology of Plasma Proteins*, Vol. 175, INSERM, Paris, 1989, pp. 185–189.
[14] R.C.M. Simmen, F.J. Michel A.E. Fliss, L.C. Smith and M.F. Ventura Fliss, *Endocrinology*, 130 (1992) 1957–1965.
[15] A. Berg and W.H. Scouten, *Bioseparation*, 1 (1990) 23–31.
[16] F. Skavril, L. Theilka, M. Probst, A. Morell and S. Barandun, *Vox Sang.*, 30 (1976) 334–348.
[17] P. Lambin, A. Gervais, M. Levy, E. Defendini, M. Dubarry, P. Rouger, P. Lebon and E. Schuller, *J. Neuroimmunol.*, 35 (1991) 179–189.
[18] U.K. Laemmli, *Nature (London)*, 227 (1970) 680.
[19] M.A. Bradford, *Anal. Biochem.*, 72 (1976) 248–259.
[20] G. Kopperslager, W. Dietzel, R. Preyer, S. Liebe and E. Hofmann, *Eur. J. Biochem.*, 22 (1971) 40.
[21] R.K. Scopes, *Anal. Biochem.*, 165 (1987) 235–246.

[22] Y.L. Kong Sing, E. Algiman, Y. Kroviarski, D. Dhermy and O. Bertrand, *J. Chromatogr.*, 558 (1991) 43–54.
[23] Y. Kroviarski, S. Cochet, C. Vadon, A. Truskolaski, P. Boivin and O. Bertrand, *J. Chromatogr.*, 449 (1988) 413–422.
[24] R.K. Scopes, *Anal. Biochem.*, 136 (1984) 525–529.
[25] S. El Ouggouti, O. Bournier, P. Boivin, O. Bertrand and D. Dhermy, *Protein Expression Purif.*, 3 (1992) 488–496.
[26] M. Kim, K. Saito, S. Furusaki, T. Sugo and I. Ishigaki, *J. Chromatogr.*, 586 (1991) 27–33.
[27] M. Kim, K. Saito, S. Furusaki, T. Sato, T. Sugo and I. Ishigaki, *J. Chromatogr.*, 585 (1991) 45–51.
[28] A. El-Kak and M.A. Vijayalakshmi, *Bioseparation*, 1 (1992) 47–53.
[29] J. Porath, *Protein Expression Purif.*, 3 (1992) 263–281.
[30] H. Zollinger, *Color Chemistry. Syntheses, Properties and Applications of Organic Dyes and Pigments*, VCH, Weinheim, 1987.
[31] D.R. Burton, L. Gregory and R. Jefferis, *Monogr. Allergy*, 19 (1986) 7–35.
[32] Y.D. Clonis, M.J. Goldfinch and C.R. Lowe, *Biochem. J.*, 197 (1981) 203–211.
[33] P. Hughes, R.F. Sherwood and C.R. Lowe, *Biochem. J.*, 205 (1982) 453–456.
[34] P. Hughes, C.R. Lowe and R.F. Sherwood, *Biochim. Biophys. Acta*, 700 (1982) 90–100.
[35] R.F. Sherwood, R.G. Melton, S.M. Auwan and P. Hughes, *Eur. J. Biochem.*, 148 (1985) 447–453.
[36] S.S. Plaksaite, O.F. Sudziuviene, J.H. Pesliakas and A.A. Glemza, *Biokhimiya*, 52 (1987) 73–81.
[37] S.S. Plaksaite, O.F. Sudziuviene, J.H. Pesliakas and A.A. Glemza, *Bioorg. Khim.* 13 (1987) 283–299.
[38] J.H. Pesliakas, V.D. Zutautas and A.A. Glemza, *Chromatographia*, 26 (1988) 85–90.
[39] V. Zutautas, B. Baskeviciute and J.H. Pesliakas, *J. Chromatogr.*, 606 (1992) 55–64.

ELSEVIER

Journal of Chromatography A, 663 (1994) 187–190

JOURNAL OF CHROMATOGRAPHY A

Determination of *cis*- and *trans*-centchroman in its dosage forms by high-performance liquid chromatography☆

A.K. Dwivedi*, K.P. Sirkar, G.R. Bhatt, R.K. Seth, S. Singh, J.P.S. Sarin

Central Drug Research Institute, Lucknow-226 001, India

(First received June 2nd, 1993; revised manuscript received October 20th, 1993)

Abstract

A high-performance liquid chromatographic (HPLC) method was developed and validated for the determination of *cis* and *trans*-centchroman, an oral contraceptive, in bulk drug samples and its dosage forms. After extraction with methanol, separation was accomplished by reversed-phase HPLC on a C_{18} column with acetonitrile–water (80:20) containing 0.4% of tetramethylammonium hydroxide [10% (v/v) aqueous solution] as the mobile phase. The pH was adjusted to 7.6 with 0.1 *M* orthophosphoric acid. The recoveries of *cis*- and *trans*-centchroman were always greater than 95%. The calibration graphs were linear over the range 0.11–4.0 μg for *cis*-centchroman and 0.18–4.0 μg for *trans*-centchroman.

1. Introduction

Centchroman [1], *trans* - 7 - methoxy - 2,2 - dimethyl - 3 - phenyl - 4 - [4 - (2 - pyrrolidinoethoxy)-phenyl]chroman, is a non-steroidal, once-a-week [2] oral contraceptive for females [3,4]. It is also effective against breast cancer [5]. Several methods have been reported for the determination of centchroman in its dosage forms [6] and in human serum [7], but they were unsuccessful in the separation of *cis* and *trans* isomers of centchroman. In this study, an HPLC method was developed to determine the *cis* and *trans* isomers of centchroman in bulk drug samples and in its dosage forms.

2. Experimental

2.1. Reagents and solvents

Pure *cis*- and *trans*-centchroman (**I** and **II**, respectively; Fig. 1) were obtained from Dr. S. Ray, Medicinal Chemistry Division, CDRI. Tetramethylammonium hydroxide (analytical-reagent grade) and acetonitrile (HPLC grade) were procured from Merck (Bombay, India). Triply distilled water from an all-glass apparatus was used as a solvent. All glassware was washed with detergent, rinsed thoroughly with triply distilled water and dried prior to use.

2.2. HPLC apparatus and chromatographic conditions

The HPLC instrument consisted of Micromeritics (Norcross, GA, USA) Model 750

* Corresponding author.

☆ CDRI Communication No. 5115.

0021-9673/94/$07.00

SSDI 0021-9673(93)E1170-5

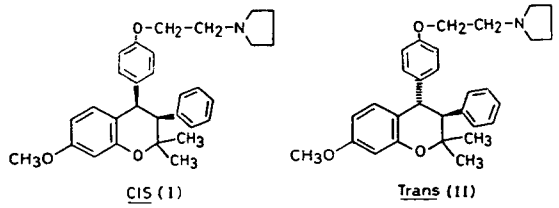

Fig. 1. Structures of *cis*- and *trans*-centchroman.

solvent-delivery system, a Rheodyne (Cotati, CA, USA) Model 7125 injector with a 20-μl loop and a Perkin-Elmer Model 235 diode array detector. Separation was carried out on an ODS Phenomenex (5 μm particle size) column (250 mm × 4.6 mm I.D.). The column effluent was monitored at 280 nm. Chromatograms were recorded on a G.P. 100 printer–plotter. The mobile phase was acetonitrile–water–tetramethylammonium hydroxide [10% (v/v) aqueous solution] (80:20:0.4), adjusted to pH 7.6 with 0.1 *M* orthophosphoric acid. It was filtered and degassed before use. Chromatography was performed at 27 ± 3°C at a flow-rate of 1.5 ml/min.

2.3. Preparation of stock and working standard solutions

Stock standard solutions containing 200 μg/ml of **I** and **II** as hydrochlorides were prepared in the mobile phase. Working standard solutions were prepared in the mobile phase in the range 9–200 μg/ml for **I** and 5.5–200 μg/ml for **II**.

2.4. Extraction

Twenty tablets were weighed and finely powdered. Powder equivalent to 10 mg of centchroman hydrochloride was extracted three times with 5-ml volumes of methanol, the combined extracts were centrifuged and the volume was made up to 25 ml with methanol. A 250-μl volume of this solution was further diluted to 25 ml with mobile phase.

2.5. Accuracy and precision

Known amounts of **I** and **II** were added to the mixed contents of tablets and *cis*- and *trans*-centchroman were determined by interpolation on the corresponding calibration graphs. The accuracy of the method was calculated on the basis of the difference in the mean calculated and added concentrations and the precision was obtained by calculating the inter-day relative standard deviations (R.S.D.s).

3. Results and discussion

3.1. Chromatography

A C_{18} column was used to separate *cis*- and *trans*-centchroman. pH plays an important role in the separation. A decrease in pH results in peak sharpening but with a decrease in the retention time difference between the *trans* and *cis* isomers, leading to merging of the peaks (Fig. 2a and b). Similarly, an increase in pH leads to a better separation of the *cis* and *trans* isomers but with peak broadening (Fig. 2c). Accordingly, pH 7.6 was chosen as higher pH may decrease the column lifetime. Acetonitrile–water–tetramethylammonium hydroxide [10% (v/v) aqueous solution] (80:20:0.4), adjusted up pH 7.6 with 0.1 *M* orthophosphoric acid was found to be the optimum mobile phase for the effective resolution of *cis*- and *trans*-centchroman in bulk drug samples and in formulations.

3.2. Selectivity and specificity

The retention times of **II** and **I** were *ca.* 24.0 and 34.0 min, respectively. No interfering peaks were detected. Based on a signal-to-noise ratio of 3, the detection limits were 0.1 and 0.05 μg for **II** and **I**, respectively. However, the limits of determination were set at 0.18 and 0.11 μg, respectively. The method provided adequate sensitivity for the determination of **I** and **II** in bulk drug substance and dosage forms.

3.3. Linearity and reproducibility

External standardization by peak area was used for the determination of *cis*- and *trans*-centchroman. The calibration graphs were linear

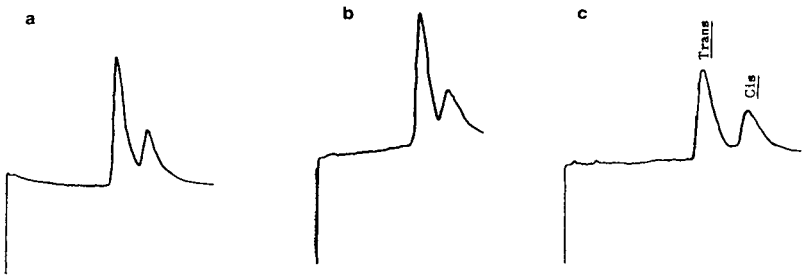

Fig. 2. Separation of *cis*- and *trans*-centchroman at pH (a) 7.4, (b) 7.2 and (c) 7.6.

over the ranges 0.18–4.0 μg for *trans*- and 0.11–4.0 μg for *cis*-centchroman with correlation coefficients (r) of 0.999 and 0.9949, respectively. The calibration equations for **I** and **II** are as follows:

unknown concentration of **I**
= 1.0053 (peak area) − 0.0143

unknown concentration of **II**
= 0.817 (peak area) − 0.0025

The reproducibility and accuracy of the method were determined by intra- and inter-assay variations (Tables 1 and 2).

3.4. Application of method in pharmaceutical analysis

The method was applied to the analysis of bulk drug samples and tablet formulations of centchroman (Table 3). The method is simple and is in use for the analysis of different bulk drug samples and tablet formulations in different manufacturing units and test laboratories. This method has also been proposed for incorporation in the Indian Pharmacopoeia for the determination of centchroman.

Table 1
Precision and accuracy for **II**

Amount taken (μg)	Mean peak area (cm^2)	Bias (%)	R.S.D. (%)
Within-day (n = 3)			
0.16	0.18	0.35	3.2
0.41	0.45	0.58	2.2
0.82	0.66	0	0
1.22	0.96	0	0
1.63	1.40	2.31	2.86
3.3	2.73	0.58	0.37
Day-to-day (n = 3)			
0.16	0.18	0.35	3.2
0.41	0.46	1.15	4.3
0.82	0.66	0	0
1.22	0.93	2.31	4.3
1.63	1.41	2.31	3.0
3.3	2.82	8.7	5.5

Table 2
Precision and accuracy for **I**

Amount taken (μg)	Mean peak area (cm^2)	Bias (%)	R.S.D. (%)
Within-day (n = 3)			
0.11	0.117	0.34	4.93
0.22	0.255	0.87	5.88
0.54	0.563	0.58	1.81
1.08	1.121	3.41	5.29
1.61	1.463	0.75	0.85
2.15	2.20	2.89	2.27
Day-to-day (n = 3)			
0.11	0.123	0.34	4.69
0.22	0.275	0.88	5.94
0.54	0.585	0.76	2.26
1.08	1.28	1.15	1.56
1.61	1.605	6.73	7.26
2.15	2.25	2.89	2.22

Table 3
Determination of centchroman in drug formulations

Sample	Tablets			Bulk drug sample	
	Centchroman content declared (mg)	*trans*-Centchroman found (%)	*cis*-Centchroman found (%)	*trans*-Centchroman found (%)	*cis*-Centchroman found (%)
PHT/ID/2/88	30	99.28	–		
PHT/ID/39/88	30	98.38	–		
PHT/ID/90/88	30	103.13	–		
PHT/ID/129/89	30	100.37	0.02		
PHT/ID/97/92				98.82	–
PHT/ID/97/92 (*cis*-centchroman)				–	98.78
PHT/ID/98/92				98.90	–
PHT/ID/99/92				97.5	0.97
PHT/ID/102/92				98.74	–

4. Acknowledgements

The authors thank Dr. S. Ray, Medicinal Chemistry Division, for providing standard *cis*- and *trans*-centchroman and Dr. Nitya Nand, Former Director, for his encouragement.

5. References

[1] S. Ray, P.K. Grover, V.P. Kamboj, B.S. Setty, A.B. Kar and N. Anand, *J. Med. Chem.*, 19 (1976) 276.

[2] N. Anand, *Proc. Indian Natl. Sci. Acad., Part A*, 49 (1983) 233.

[3] N. Nand and S. Ray, *Indian J. Exp. Biol.*, 15 (1977) 1142.

[4] V.P. Kamboj, presented at the *Joint Symposium Organized by ICMR and WHO, Bangalore, 1985.*

[5] N.C. Mishra, D. Kumar, A.K. Agarwal, B.S. Setty, S.S. Agarwal, S. Ray and V.P. Kamboj, *13th International Congress on Cancer, Seattle, 1982*, Abstract No. 3033.

[6] R.K. Seth, P.L. Kole and J.P.S. Sarin, *Indian J. Pharm. Sci.*, 45, No. 1 (1983) 14.

[7] J. Paliwal, R.C. Gupta, P.K. Grover, O.P. Asthana, J.S. Srivastava and S. Nityanand, *Pharm. Res.*, 6 (1989) 1048.

ELSEVIER

Journal of Chromatography A, 663 (1994) 191–197

JOURNAL OF CHROMATOGRAPHY A

Method to determine resveratrol and pterostilbene in grape berries and wines using high-performance liquid chromatography and highly sensitive fluorimetric detection

R. Pezet*, V. Pont, P. Cuenat

Swiss Federal Agricultural Research Station of Changins, Route de Duillier, CH-1260 Nyon, Switzerland

(First received October 18th, 1993; revised manuscript received December 1st, 1993)

Abstract

Resveratrol and pterostilbene are two hydroxystilbenic phytoalexins synthesized by *Vitaceae*. Produced by leaves and grape berries after biotic or abiotic stress, the determination of their concentration can help to evaluate the disease resistance of different vine varieties. Resveratrol is also found in wines, particularly in red wine. These stilbenes are highly sensitive to light and air oxidation. Extraction must be made under nitrogen and protected from light. HPLC separation of resveratrol and pterostilbene is performed on a reversed phase (C_{18}) with a methanol–formic acid (50 m*M*) gradient. Fluorimetric detection is much more sensitive than UV detection and its specificity allows simple pre-purification of grape berries and direct injection of wines.

1. Introduction

Stilbenes occur naturally in a number of plant families [1]. They can be synthesized by plants after a stress and, in this case, are considered as phytoalexins. Stilbenic phytoalexins have been extensively studied in *Vitaceae* by Langcake and Pryce [2,3]. These authors have described resveratrol (3,5,4′-trihydroxystilbene), pterostilbene (3,5-dimethoxy-4′-hydroxystilbene) and their polymeric forms, the viniferins.

The analysis of resveratrol production by leaves of vitaceae after UV irradiation was considered as a disease resistance index in grape breeding programs [4,5]. More recently resveratrol was identified in wines and considered by Siemann and Creasy [6] as an active ingredient in causing reduction of serum lipids levels in humans. However, this theory is open to discussion in view of the low concentration of resveratrol in wines and the high concentrations of this stilbene necessary to lower lipid levels in the livers of rats with hyperlipemia [7].

Pterostilbene is detected in trace amounts in healthy and immature grape berries [8]. However, its fungitoxicity is much more important than that of resveratrol [9]. Its biosynthesis is not induced by UV irradiation but Langcake *et al.* [2] have detected great amounts of pterostilbene in *Plasmopara viticola* infected leaves of *Vitis vinifera*. This stilbene is probably not synthesized by the same stilbene synthase as resveratrol, as described by Schoeppner and Kindl [10].

Methods to extract and analyse stilbenic phytoalexins in wines and grapes by HPLC have been described by several authors [2,8,11,12]. In

* Corresponding author.

0021-9673/94/$07.00
SSDI 0021-9673(93)E1290-G

most cases, extractions required fastidious manipulations and denaturating vacuum rotary evaporation steps. Detection and quantitative determination of stilbenes were made, until now, by UV detection at 295 to 305 nm [2] or at 280 nm after UV irradiation of the sample [6]. GLC analysis of stilbenic phytoalexins has also been described by several authors [4,12,13]. Both methods are not sufficiently sensitive or reliable enough to detect small natural concentrations of stilbenes, as is generally the case, especially for the highly fungicidal pterostilbene [8].

The use of a fluorimetric detector decreases the threshold of measurable concentrations of stilbenes in the nanomole range and is more specific than UV. This specificity requires only two purification steps for grape berries and a direct injection for wines.

This paper demonstrates the possible denaturating effects of rotary evaporation *in vacuo* (40°C) on resveratrol and pterostilbene and proposes a protective method. It describes a fluorimetric detection method that is more sensitive and specific than UV detection.

2. Experimental

2.1. Chemicals

Pure resveratrol (*trans*-3,5,4′-trihydroxystilbene) and pterostilbene (*trans*-3,5 methoxy-4′-hydroxystilbene) were synthesized in our laboratory as described elsewhere [8,9]. Solvents used for extractions were pro analisi grade and HPLC grade for chromatographic analysis (Romil Chemicals, Shepshed, Loughborough, UK). Mixtures of solvents for HPLC were filtered (Acrodisc LC13 PVDF 0.45 μm, Gelman, Ann Arbor, MI, USA) and degassed under a permanent helium stream.

2.2. HPLC analysis

Automatic injector, pump (tertiary gradient system) and UV detector were from Bruker (LC-51, LC-21C, LC-313). The fluorimetric detector was the SFM 25 Model from Kontron. Chromstar software (Bruker) was used to control injector, pump and UV detector and to analyse data provided by the two detectors through a two-way channel peak integration. Analyses were performed on a reversed-phase column (LiChrospher 100-RP 18, 5 μm, 4.5 × 250 mm, Merck) with the following mobile phase: solvent A: methanol–50 m*M* formic acid (20:80, v/v), solvent B: methanol–50 m*M* formic acid (80:20, v/v) and solvent C: pure methanol. Solvents were delivered according to the following programme: linear gradient from 100% A to 100% B in 25 min; 100% B for 5 min; linear gradient from 100% B to 100% C in 1 min; 100% C for 5 min; linear gradient from 100% C to 100% A in 5 min; 100% A for 5 min.

2.3. Fluorimetric and UV detection

Optima in excitation and emission wavelengths were determined with a Kontron fluorimeter (SFM 25) using suitable solutions of pure resveratrol and pterostilbene in a mixture of methanol–50 m*M* formic acid (80:20, v/v). UV absorption was determined with a UV-160 Shimadzu spectrophotometer using the same stilbene solutions. UV optimum absorbances of resveratrol and pterostilbene are at 305.6 and 306.4 nm, respectively, in methanol–50 m*M* formic acid (80:20, v/v). Maximum excitation wavelength is measured at 330 nm and emission at 374 nm for these two stilbenes. Measured parameters were programmed to detect resveratrol and pterostilbene with the HPLC system described above. Solutions which contained different concentrations of these stilbenes (0.1–100 ng per 10 ml injection volume) were obtained by suitable dilutions of a methanolic solution at 0.1 mg ml^{-1}. Standard calibration curves were established by plotting the area of peaks against different concentrations of resveratrol and pterostilbene. Three replicates were made for each concentration. Standard errors and linear correlation were calculated using the GraFit statistical programm (Erithacus Software, Sigma). The lowest detectable concentration for both resveratrol and pterostilbene was 0.1 ng 10

μl^{-1} with the fluorimeter and 5 ng 10 μl^{-1} with the UV detector (306 nm). Linear correlations were excellent from 0.1–100 ng for fluorimetric detection : correlation coefficient $r = 0.9995$ for resveratrol and $r = 0.9975$ for pterostilbene. According to these results the use of a fluorimetric detector enhances by about 50 times the sensitivity of the analysis. In addition, the specificity of the fluorimetric parameter detection, linked to the chemical structure of the stilbenes, decreases the risk of peak confusion and allows for minimal pre-purification of the samples. In order to compare fluorimetric detection to UV detection, a UV detector was connected on-line and signals were computed by the same procedures. In all manipulations, stilbene solutions were protected from light to avoid *cis*-isomerization, decreasing the sensitivity of the detection.

2.4. Sample preparation

Pure resveratrol and pterostilbene were solubilized in methanol at the concentrations of 3 μg ml^{-1} and 3.5 μg ml^{-1}, respectively. An aliquot of 1 ml was evaporated using rotary evaporation (*in vacuo*, 40°C). The residue was solubilized in 1 ml of methanol. Another aliquot of 1 ml was evaporated under a stream of nitrogen (40°C in a water bath). The dried residue was solubilized in 1 ml of methanol. 10 μl of each methanolic solution were separately injected into the analytical HPLC system.

Downy Mildew infected grape berries (var. Chasselas) were harvested at véraison development stage. Eight berries (10.95 g fresh weight) were crushed in 40 ml of methanol using a mechanical homogenizer (VirTis) at maximum speed (25 000 rpm) for 5 min. The resulting suspension was centrifuged (10 000 g, 20 min). 20% of water was added to the supernatant. This solution was pre-purified by solid-phase extraction (Supelclean LC-18 SPE Tubes, 3 ml) in adsorbing impurities on the phase. The eluate was collected, the column was washed with 5 ml of methanol–water (8:2, v/v) and the resulting eluate added to the first one. Eluates were evaporated under a nitrogen stream while the solution was maintained at 40°C in a water bath. The resulting water solution was extracted with diethyl ether three times. The ether fraction was dried with Na_2SO_4, filtered through paper and evaporated to until dry under a nitrogen stream at 40°C as described below. The dried residue was solubilized in 5 ml of methanol and 10 μl of this solution were injected into the HPLC analytical system. Co-chromatographic analysis was performed by adding 20 μl of a 5 μg ml^{-1} stilbene standard solution (resveratrol and pterostilbene) to 200 μl of methanolic grape berry sample solution. 10 μl of this solution was injected.

To evaluate the efficiency of this extraction procedure, 5 ml of a resveratrol and pterostilbene methanolic solution at 5 μg ml^{-1}, obtained by suitable dilution of a stock solution (0.1 mg ml^{-1}), was treated as described for grape berry extraction. 10 μl of this solution was analyzed before the extraction procedure as a check and after the extraction procedure. Three replicates were made and the standard deviation was calculated.

Wine analyses were performed by injecting 5–50 μl of filtered (0.45 μm, Gelman) wine without any purification. Pure resveratrol and pterostilbene were added to samples of wine for co-chromatographic analysis. All extraction procedures were protected from light.

Grape berry and wine analysis were performed using the fluorimetric detector only. Concentrations of resveratrol and pterostilbene in samples were measured using the external standard method. Response factors (amount of standard/peak area) were calculated with data from the standard calibration curve.

3. Results and discussion

Langcake and Pryce [13] described the spectral properties of resveratrol and measured two λ_{max} at 306 nm and 318.7 nm. These values are in complete accordance with our measurements. These authors have observed that under long wavelength UV light (366 nm) stilbenes shown a bright blue fluorescence. Their fluorimetric analysis of the fluorescent compounds extracted from UV-irradiated leaves give an excitation wavelength at 330 nm and an emission wavelength at

374 nm. These values correspond to those described in this paper for resveratrol and pterostilbene.

Stilbenes are unstable in light and sensitive to oxidation in normal air when deposited on thin-layer plates [1]. This sensitivity is probably at the origin of their denaturation observed using rotary evaporation. In this system, when the solvent is evaporated, compounds are uniformly distributed as a thin layer on the wall of the flask and particularly exposed to air oxidation when vacuum is suddenly broken. All solvent evaporation steps must absolutely be done under nitrogen and protected from light.

HPLC analysis of these stilbenes treated by this method show only one peak for each (Fig. 1, peaks 1 and 2). Retention times for resveratrol is 15.6 min and for pterostilbene 26.3 min. Only two negligible minor peaks can be detected (Fig. 1A). The rotary evaporation concentration step (*in vacuo*, max. temp. 40°C and protected from light) induces an important modification of the

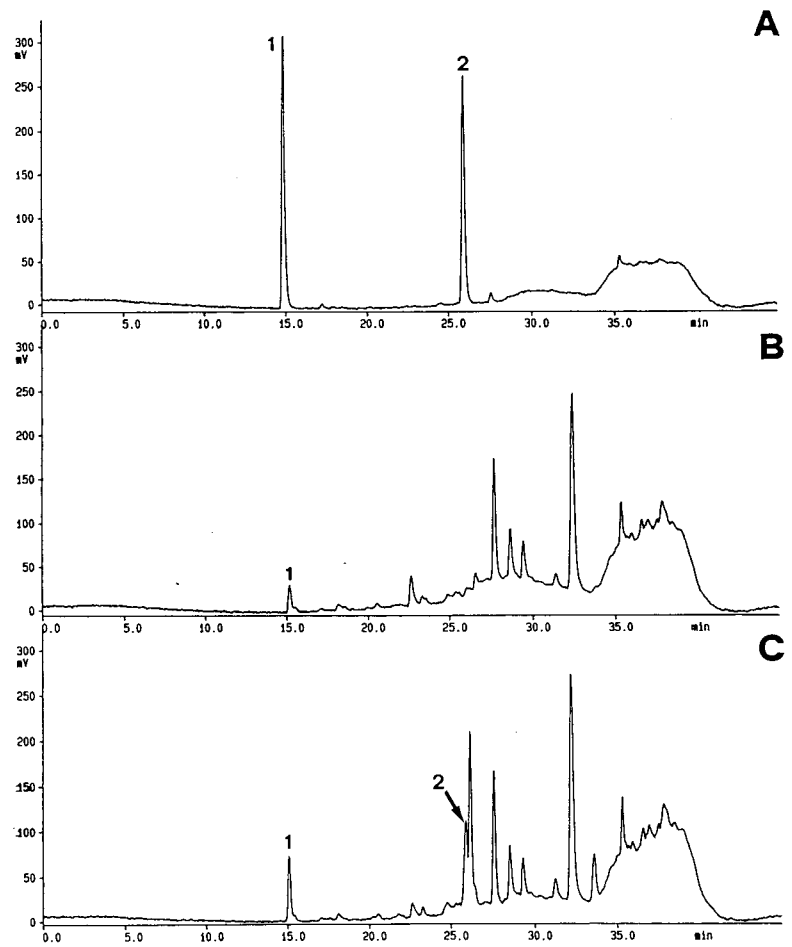

Fig. 1. Demonstration of stilbenes denaturation using rotary evaporation *in vacuo* (40°C). (A) Chromatogram of standard resveratrol (1) (30 ng 10 μl^{-1}; t_R 15.6 min) and pterostilbene (2) (35 ng 10 μl^{-1}; t_R 26.3 min) after concentration of the sample under nitrogen (protective method). Detection: fluorescence, ex. 330 nm, em. 374 nm. (B) Chromatogram of the same concentrations of standard resveratrol (1) after concentration of the sample using rotary evaporation (*in vacuo*; 40°C; protected from light). (C) Chromatogram of the same amounts of standard resveratrol (1) and pterostilbene (2) after concentration using rotary evaporation (*in vacuo*; 40°C; protected from light).

chromatograms. Many secondary peaks appear since major resveratrol and pterostilbene peaks decrease dramatically (Fig. 1B and C). Secondary peaks appear under denaturating extraction conditions for resveratrol at 22.6, 23.3, 27.6, 28.5, 29.3, 31.2, 32.7, and 35.3 min, and four minor peaks between 35.6 and 37.8 min, and for pterostilbene at 26.9 min and 33.6 min. These secondary peaks correspond certainly to oxidation products of these stilbenes as yet not identified.

The recovery concentrations of the extracted standard solutions, determined by HPLC, is 100%. Three replicates give no significant differences between concentration of the check solutions before and after the extraction procedures.

Downy mildew (*Plasmopara viticola*) contaminated grape berries contain 1.21 mg of resveratrol and 35 ng of pterostilbene per gram of fresh weight. Important peaks of other fluorescent compounds appear at retention times situated between those of resveratrol and pterostilbene (Fig. 2A). They were as yet not identified but some of them could correspond to ϵ- and α-viniferine as described elsewhere [2,3]. Co-chromatographic analyses, using standard resveratrol and pterostilbene, are shown in Fig. 2B. Theoretically, 5 ng of each stilbene was added in 10 μl of injected sample. The recovery was 5.6 ng and 5.65 ng, respectively, for resveratrol and pterostilbene.

The specificity of the fluorimetric detection for stilbenes permits direct injection of wines. This procedure avoids any denaturation of the sample. Five swiss wines were analyzed : two white varieties, Chasselas and Chardonnay, and three red varieties: Gamay, Pinot and Gamaret (Gamay × Reichensteiner). In view of the low concentration of resveratrol in white wines, 50 μl of these wines were injected. Due to higher concentrations of resveratrol, only 5 μl of red wines were sufficient to detect this stilbene. Pterostilbene was not detected in wines. Co-chromatographic analyses were realized on a red wine (Gamaret) and a white one (Chasselas). The chromatograms of these wine analyses, with

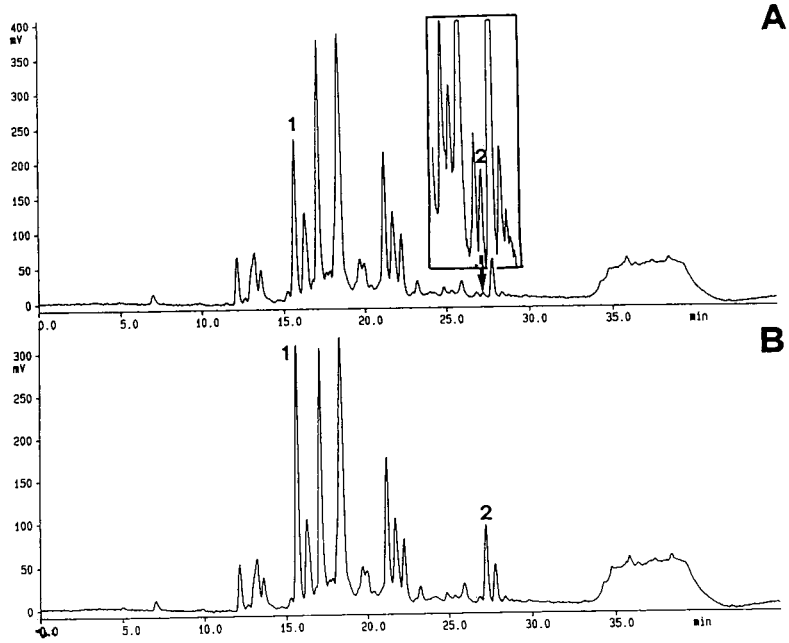

Fig. 2. Chromatograms of Downy Mildew contaminated grape berries (var. Chasselas) extracts using fluorimetric detection (ex. 330 nm, em. 374 nm). (A) Resveratrol: peak 1; pterostilbene: peak 2. In the box: enlarged part of the chromatogram showing the well defined peak of pterostilbene. (B) Co-chromatographic analysis of the same extract after addition of 5 ng each of resveratrol (1) and pterostilbene (2) in 10 μl injected.

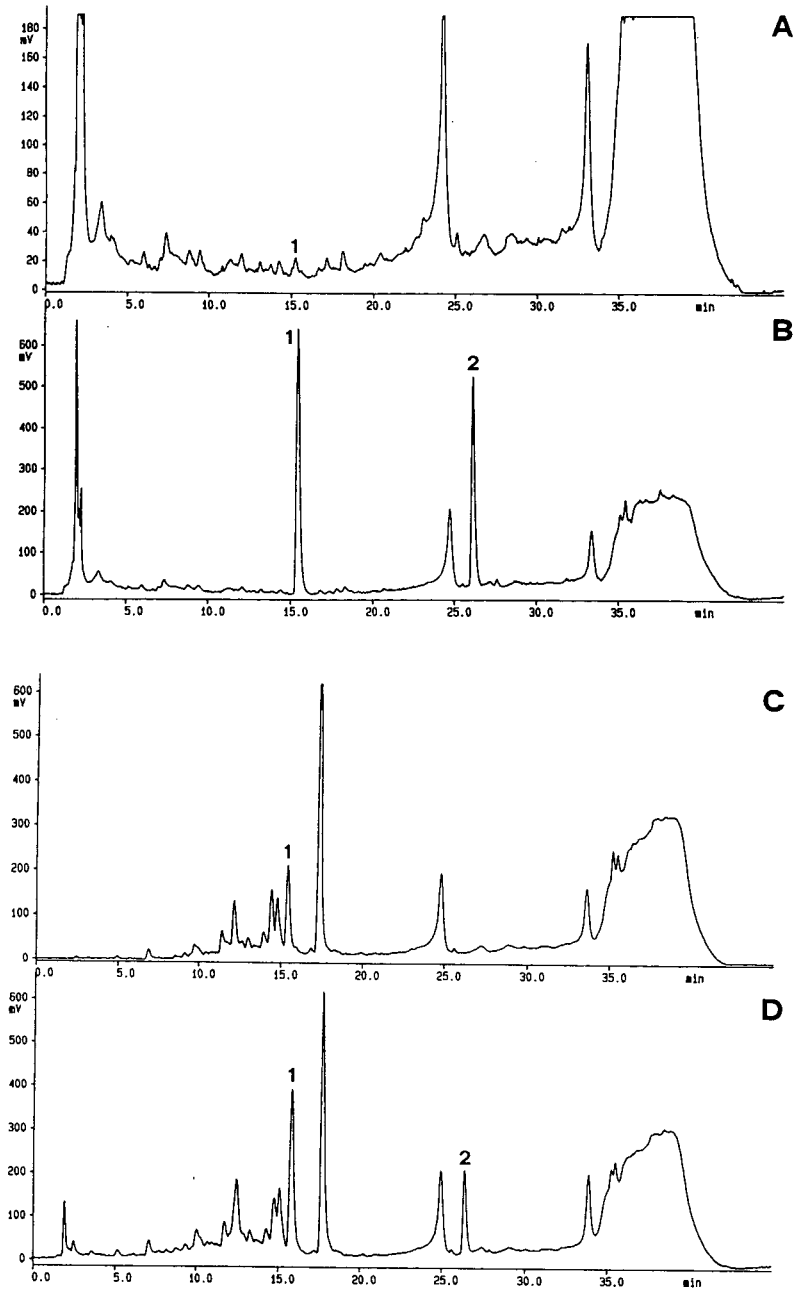

Fig. 3. Chromatograms of wines injected without any purification. Detection: fluorescence, ex. 330 nm, em. 374 nm. (A) and (B) White wine (var. Chasselas) without and with the addition of standard resveratrol (1) and pterostilbene (2), respectively. (C) and (D) Red wine (var. Gamaret) without and with addition of standard resveratrol (1) and pterostilbene (2), respectively.

or without the addition of pure resveratrol and pterostilbene, are shown in Fig. 3A–D. The measured concentrations of resveratrol in the analyzed wines, three replicates drawn from the same bottle for each variety, are presented in Table 1.

Table 1
Amounts of resveratrol in different Swiss wines

Wine variety (1992)		Resveratrol (mmol l^{-1}, mean ± S.D.)
Chardonnay	White	0.14 ± 0.01
Chasselas	White	0.15 ± 0.02
Gamay	Red	6.47 ± 0.54
Pinot	Red	2.95 ± 0.11
Gamaret	Red	2.16 ± 0.25

The use of fluorimetric detection of stilbenes offers much greater sensitivity and selectivity. Many phenolic compounds have a maximum absorbance between 275 to 330 nm while fluorescence parameters are different and specific for each phenolic [14]. This characteristic allows a simple sample preparation and the resulting chromatograms show less unknown peaks, a better resolution and a much greater sensitivity than with UV detection.

4. Acknowledgements

We wish to thank Pr.M. Dewey and Avi Spier (Department of Plant Sciences, University of Oxford) for comments and critically reading the manuscript.

5. References

[1] J.H. Hart, *Ann. Rev. Phytopathol.*, 19 (1981) 437.
[2] P. Langcake, C.A. Cornford and R.J. Pryce, *Phytochemistry*, 18 (1979) 1025.
[3] P. Langcake and R.J. Pryce, *Experientia*, 33, (1977) 151.
[4] M. Barlass, R.M. Miller and T.J. Douglas, *Am. J. Enol. Vitic.*, 38 (1987) 65.
[5] R.M. Pool, L.L. Creasy and A.S. Frackelton, *Vitis*, 20 (1981) 136.
[6] E.H. Siemann and L.L. Creasy, *Am. J. Enol. Vitic.*, 43 (1992) 49.
[7] H. Arichi, Y. Kimura, H. Okuda, K. Baba, M. Kosawa and S. Arichi, *Chem. Pharm. Bull.*, 30 (1982) 1766.
[8] R. Pezet and V. Pont, *Plant Physiol. Biochem. (Paris)*, 26 (1988) 603.
[9] V. Pont and R. Pezet, *J. Phytopathol.*, 130 (1990) 1.
[10] A. Schoeppner and H. Kindl, *FEBS Letters*, 108 (1979) 349.
[11] W. Dercks and L.L. Creasy, *Physiol. Mol. Plant Pathol.*, 34 (1989) 189.
[12] P. Jeandet, R. Bessis and B. Gautheron, *Am. J. Enol. Vitic.*, 42 (1991) 41.
[13] P. Langcake and R.J. Pryce, *Physiol. Plant Pathol.*, 9 (1976) 77.
[14] C.F. Van Sumere, in P.M. Dey and J.B. Harborne (Series editors), *Methods in Plant Biochemistry*, Vol. 1, J.B. Harborne (Editor), Plant Phenolics, Academic Press, London, 1989, Ch. 2, p. 29.

ELSEVIER

Journal of Chromatography A, 663 (1994) 199–210

JOURNAL OF CHROMATOGRAPHY A

Determination of toluenediamine isomers by capillary gas chromatography and chemical ionization mass spectrometry with special reference to the biological monitoring of 2,4- and 2,6-toluene diisocyanate

G. Skarping*, M. Dalene and P. Lind

Department of Occupational and Environmental Medicine, University Hospital, S-221 85 Lund (Sweden)

(First received May 18th, 1993; revised manuscript received September 27th, 1993)

ABSTRACT

The determination of 2,3-, 3,4-, 2,6-, 2,4- and 2,5-toluenediamine (TDA) in hydrolysed human urine and blood plasma was studied by GC–MS. The TDA isomers as their perfluoro-fatty acid anhydride derivatives were investigated. Chemical ionization with ammonia and isobutane as reagent gas and monitoring both positive and negative ions are studied. Negative ion monitoring using ammonia and the TDA pentafluoropropionic anhydride (PFPA) derivatives were chosen owing to the low detection limits and good separations of the isomers studied. The ions monitored were m/z 394 and 374 corresponding to the $(M-20)^-$ and $(M-40)^-$ ions and the $m/z = 397$ and 377 ions of the trideuterium-labelled TDA used as an internal standard. The performance of 2,4-, 2,5- and 2,6-TDA-PFPA in the ion source was studied by varying the ammonia pressure, temperature and electron energy. A 1-ml volume of human urine was added to 1.5 ml of 6 *M* HCl containing 0.5 μg/l of each of the trideuterated 2,6- and 2,4-TDA and the solution was hydrolysed at 100°C overnight. TDA was extracted into 2 ml of toluene by the addition of 5 ml of saturated NaOH solution. Derivatization was performed in toluene by the addition of 10 μl of PFPA. The excesses of the reagent and acid formed were removed by extraction with 1 *M* phosphate buffer solution (pH 7.5). Analyses of 2,6-, 2,4- and 2,5-TDA-spiked human urine (0.2–2.5 μg/l) were performed. The correlation coefficients were 0.999 ($n = 6$). The precision (R.S.D.) for human urine spiked at 1 μg/l was 1.6% for 2,6-TDA, 3,5% for 2,4-TDA and 3.2% for 2,5-TDA ($n = 10$). The detection limit, defined as twice the signal-to-noise ratio, was 1–5 fg injected, corresponding to less than 0.05 μg/l of TDA in human urine or plasma.

INTRODUCTION

The identification and determination of amines and isocyanates in air and biological samples such as urine and blood have been a subject of increasing interest in recent years owing to their environmental and occupational hazards. Kennedy and Brown [1] recently published a review on this topic. Toluene diisocyanate (TDI) is one of the main components in the production of polyurethane polymers. The commercially used TDI is a mixture of 2,4- and 2,6-TDI in the ratio 80:20 or 65:35 (v/v). The two TDI-related aromatic amines 2,4- and 2,6-toluenediamine (TDA) are mainly used as intermediates in TDI, elastomer and dye production [2].

Gas chromatography (GC) with electron-capture or mass spectrometric (MS) detection of amines has been studied in some detail during the last 25 years. Amines normally elute as tailing peaks when analysed as such. Analysis for amines as perfluoro-fatty acid derivatives reduces the adsorption and thereby the peak tailing. These derivatives also show very low detection limits using ECD. MS with chemical ionization

* Corresponding author.

SSDI 0021-9673(93)E1047-4

(CI) monitoring of negative ions also gives low detection limits [3–5].

Several techniques have been used for the determination of aromatic amines in air and biological fluids, including liquid chromatography (LC) and UV [6] and electrochemical detection [7], GC with electron-capture [8] and thermionic specific detection (TSD) [9] and GC–MS using electron impact (EI) and positive ion monitoring [10].

Methods for the determination of low concentrations of TDA in hydrolysed human urine and plasma have been developed [11] at our laboratory. The methods have been used by Brorson *et al.* [12] and Skarping *et al.* [13] for the biological monitoring of exposure to TDI. The main interest has been focused on the 2,4- and 2,6-TDA isomers related to 2,4- and 2,6-TDI. 2,5-TDA, which is a component of hair dyes, is also of interest [14].

Capillary GC methods with thermionic specific detection of 2,4- and 2,6-TDA as acetyl, perfluoro-fatty acid and carbamate ester derivatives have been investigated in our laboratories [11]. In earlier studies, EI and the monitoring of the molecular ion of TDA pentafluoropropionic anhydride derivative (PFPA) using selected-ion monitoring (SIM) were considered [11]. The samples were enriched by a factor of 40 by evaporation of the solvent and the detection limit was *ca.* 8 pg injected, corresponding to a concentration of 0.1 μg/l of TDA in urine. In this paper, a GC–MS method based on monitoring of negative ions formed by CI with ammonia is presented. The determinations of the five isomers 2,3-, 3,4-, 2,6-, 2,4- and 2,5-TDA as their heptafluorobutyric (HFBA), pentafluoropropionic (PFPA) and trifluoroacetic (TFAA) derivatives in hydrolysed human urine and plasma samples are presented. The sixth TDA isomer, 3,5-TDA, was not commercially available and was therefore not included in this study.

EXPERIMENTAL

Apparatus

A VG-Quattro triple quadropole mass spectrometer (Fisons Instruments, VG-Biotech, Altrincham, UK) connected to a Carlo Erba Mega gas chromatograph equipped with an A200S autosampler (Fisons Instruments, Carlo Erba, Milan, Italy) was employed. Injection was performed using splitless injection. The syringe needle was heated in the injector for 10 s before injection (the hot needle technique) and the injector temperature was 290°C. The starting temperature of the column oven was isothermal at 110°C for 1 min, then raised at 15°C/min to 280°C, where it was kept for 2 min. The split-exit valve was kept closed for 1 min after injection. The temperature of the ion source was 230°C and the GC–MS interface temperature was 280°C. The capillary inlet pressure of helium was 0.8 kg/m^2. The solvent delay was set to 2.9 min. After injection, the syringe was cleaned by washing with eight 10-μl volumes of toluene. Before injection the syringe was washed by two 10-μl volumes of the sample.

In most of the quantitative investigations the instrument was used in the CI mode with negative ion monitoring using ammonia as the reagent gas. When determining the TDA-PFPA derivatives the ions monitored were m/z 394 and 374, corresponding to the $(M-20)^-$ (M = molecular ion) and the $(M-40)^-$ ions, and the m/z 397 and 377 ions of the trideuterium-labelled internal standard. The dwell time for each of the ions was 0.2 s and the inter-scan delay was 0.02 s. The pressure in the ion source, in the case of CI with ammonia and negative ion monitoring, was kept at *ca.* $2 \cdot 10^{-4}$ mbar (source readout pressure, not the actual pressure in the ionization cavity). The emission current was 200 mV and the electron energy 60 eV. The tuning of the instrument was optimized and performed using perfluorotributylamine (PFTBA) as a calibrant. The resolution was set by monitoring the fragments at m/z 633 and 634. The valley between the fragments was set to 10% of the peak height of the m/z 634 fragment. Mass spectra were obtained by scanning ions between 50 and 600 u for 0.7 s with an inter-scan delay of 0.1 s.

For the continuous monitoring of TDA derivatives in the MS system, an inlet device was designed at VG-Biotech. A few micrograms of the sample were injected into a heated reservoir kept under vacuum. The reservoir was in contact

with the ion source via a capillary strainless-steel tube of I.D. < 0.1 mm. The inlet device was connected to the MS instrument similarly to the solid sample inlet apparatus. This inlet device makes it possible to optimize the system faster and in much more detail. A Sigma 3E-1 centrifuge (Sigma, Hartz, Germany) was used for phase separation.

Columns

Fused-silica capillary columns with DB-5 chemically bonded stationary phase (J&W Scientific, Folsom, CA, USA) (30 m × 0.25 mm I.D.) with a film thickness of 0.25 μm were used.

Chemicals

The chemicals used were 2,4- and 2,6-TDA from Fluka (Buchs, Switzerland), 2,5-TDA and 3,4-TDA from Janssen (Geel, Belgium) and 2,3-TDA from Aldrich-Europe (Steinheim, Germany). Trifluoroacetic anhydride (TFAA), pentafluoropropionic anhydride (PFPA) and heptafluorobutyric anhydride (HFBA) were obtained from Pierce (Rockford, IL, USA), toluene from Lab-Scan (Dublin, Ireland), HCl, NaOH, perfluorotributylamine (PFTBA) and K_2HPO_4 from Merck (Darmstadt, Germany) and trideuterated 2,6- and 2,4-TDA, 2,6- and 2,4-TDA-PFPA derivatives and 2,6- and 2,4-HFBA derivatives from Syntelec (Lund, Sweden). The synthesis of these derivatives has been described previously [11].

Procedure

Preparation of standard solutions. Standard solutions of the five investigated TDA isomers were prepared by dissolving accurately weighted amounts in 0.1 *M* hydrochloric acid. The solutions were further diluted to appropriate concentrations.

Sampling and storage of biological samples. All urine samples were collected in polyethylene bottles. Urine samples were acidified by addition of 5 ml of 6 *M* HCl per 100 ml of urine. The density, creatinine concentration, pH and total volume of the urine samples were determined. The urine samples were stored in a refrigerator until analysis. Blood was sampled in heparinized tubes (Venoject). Plasma was separated within 8 h and transferred to a new tube. Blood plasma was kept frozen at −20°C until analysis.

Work-up procedure. To a 1-ml urine or plasma sample, 1.5 ml of 6 *M* HCl, containing the trideuterated 2,6- and 2,4-TDA internal standards each at a concentration of 0.5 μg/l, was added and the samples were hydrolysed at 100°C overnight. A 5-ml volume of saturated NaOH and 2 ml of toluene were then added and the mixture was shaken for *ca.* 10 min and then centrifuged at 1500 *g* for 10 min. A 1.5-ml volume of the organic layer was transferred to a new test-tube and 10 μl of the anhydride derivatization reagent were added. The mixture was immediately shaken vigorously for *ca.* 10 min. The excesses of the reagent and acid formed were removed by extraction with 2 ml of 1 *M* phosphate buffer solution (pH 7.5). A 1-ml volume of the toluene layer containing the amide derivative and the internal standard was transferred into an 1.5-ml autosampler vial and was then ready for injection into the GC–MS system.

Internal standard

Trideuterated 2,6- and 2,4-TDA were used as internal standards and were added to the urine samples prior to hydrolysis.

RESULTS AND DISCUSSION

Standards

The identities of the perfluoro-fatty acid amides of the TDAs were confirmed by GC–MS and purities were determined using capillary GC–TSD and GC with flame ionization detection. Elemental analysis of the amide derivatives of HFBA and PFPA gave values differing by less than 0.3% from the calculated values.

The isotopic purities of 2,6- and 2,4-TDA and the trideuterated 2,6- and 2,4-TDA were also checked. When determining 2,6- and 2,4-TDA-PFPA derivatives by GC–SIM using CI with ammonia and negative ion monitoring, the most abundant fragments were m/z $(M-20)^-$ (394). Less than a 0.3% relative abundance was observed for the m/z 397 compared with the m/z 394 fragment. Trideuterated 2,6- and 2,4-TDA-PFPA derivatives were monitored in the same way with the most abundant ions of m/z =

$(M-20)^-$ (397). Less than a 0.3% relative abundance was observed for the m/z 394 compared with the m/z 397 fragment.

Internal standard

All determinations were performed using trideuterated 2,6- and 2,4-TDA as the internal standards. The three hydrogens in the methyl group were exchanged with deuterium. The use of trideuterated 2,6- and 2,4-TDA as internal standards has been discussed previously [11].

TDA and trideuterated TDA show very similar fragmentation patterns. Several fragments [$(M-20)^-$, $(M-40)^-$ and $(M-60)^-$] could be monitored simultaneously.

Work-up procedure

Storage and treatment of samples. Urine samples spiked with 2,6- and 2,4-TDA were found to be stable after acidification. No noticeable degradation of the samples was found after storage for several weeks in the dark at room temperature. Plasma samples were kept frozen until analysis. On analysing the same plasma samples on three different occasions during a 5-week period, no noticeable degradation of the sample was found. In the present study all standards were freshly prepared every other week. The derivatives in toluene solution were found to be stable for several weeks without any noticeable degradation.

Hydrolysis. When performing the work-up procedure with urine samples spiked with the five TDA isomers to a concentration of 20 μg/l, no losses of 2,6-, 2,4- and 2,5-TDA were found. However, more than 70% of the 2,3- and 3,4-TDA isomers were lost. The losses were related to the hydrolysis step and increased with the hydrolysis time. On prolonging the hydrolysis time losses were also seen for 2,4- and 2,6-TDA. A hydrolysis time of *ca.* 240 h gave a 10–20% loss in plasma and a 40% loss in urine. The hydrolyses of pooled humane urine and pooled human plasma from exposed TDI workers were studied under acidic and alkaline conditions. Acidic hydrolysis for 24 h was studied for 4 *M* and 6 *M* HCl at 100°C, 4 *M* and 6 *M* HCl at 110°C and 6 *M* HCl under vacuum with freeze-dried urine at 110°C. Alkaline hydrolysis was studied for 24 h for 5 *M* NaOH at 100 and 110°C. The amounts of both 2,6- and 2,4-TDA released increased by 20–30% with increasing hydrolysis temperature for acid hydrolysis. Hydrolysis under alkaline conditions released about twice as much 2,6- and 2,4-TDA. On varying the hydrolysis time up to 240 h in 4 *M* HCl at 100°C of pooled humane urine and pooled human plasma from exposed workers, the amounts of 2,4- and 2,6-TDA increased with time and no optimum was found. On working up the samples without the hydrolysis step no 2,4- and 2,6-TDA were obtained, within experimental error. For practical reasons and comparison with our earlier studies [12], hydrolysis with 4 *M* HCl at 100°C overnight was chosen and the high sensitivity of the method presented does not necessitate further release of TDA from the biological samples.

The results indicate that the TDAs in plasma and urine are covalently bonded. The bonds seems stronger than peptide bonds. Peptide bonds are expected to break up under acidic hydrolysis. The investigation of the chemical form of TDI/TDA in human urine and plasma is in progress. In a controlled exposure study [12] of human volunteers, 15–19% of 2,4-TDA and 17–23% 2,6-TDA of the estimated dose of the TDI isomers were found in the excreted urine. A linear relationship between urinary excreted amount and the dose was obtained.

Choice of reagent

Several anhydride and chloroformate derivatization reagents were tested. The carbamate ester derivatives formed with TDA after derivatization with chloroformates such as methyl, ethyl and isobutyl chloroformate elute at higher elution temperatures, giving longer elution times than the perfluoro-fatty acid amide derivatives. The carbamate esters are thermolabile and all the carbamate derivatives formed are decomposed in the injector [10]. The cold on-column injection technique is therefore the most suitable injection technique for these kinds of compounds. With the present GC–MS systems available at our laboratory, no automatic on-column injector with an autosampler was available. No thermal decomposition of the perfluoro-fatty TDA

amides was observed. The detection limits achieved for the carbamate esters, using CI and monitoring positive ions, are at least two orders of magnitude higher than those for perfluoro-fatty acid amides when using CI with ammonia and monitoring negative ions. It seems that derivatives giving low detection limits using ECD also give low detection limits using GC–MS with CI with negative ion monitoring [10]. All the tested perfluoro-fatty acid anhydrides gave a *ca.* 100% recovery for the single-phase derivatization. The elution time and temperature varied surprisingly little (less than 10%) with variation in the perfluoro-fatty acid anhydride reagent.

The chromatographic separation achieved for the five TDA isomers studied is almost the same for the three derivatization reagents. The sensitivity when monitoring the $m/z = (M - 20)^-$ fragments is virtually the same for PFPA and HFBA derivatives but 40–200 times less for the TFA derivatives. The sensitivity for the TFA derivatives also varies with the isomer studied and *ca.* ten times higher sensitivities for the 2,3- and 3,4-TDA compared with the 2,6-, 2,4- and 2,5-TDA derivatives are observed. The PFPA derivatization reagent was chosen owing to the 5–10% shorter retention times of the amides formed and because this reagent has been the most frequently used in our earlier studies on the determination of aliphatic and aromatic amines.

Chromatography

TFAA, PFPA and HFBA derivatives of 2,3-, 3,4-, 2,6-, 2,4- and 2,5-TDA were studied. All derivatives showed excellent chromatographic behaviour. Using the DB-5 capillary column, baseline separations of the five TDA amides were obtained with the three derivatization reagents tested. Chromatograms for diluted standards in toluene of the five TDA derivatives are shown in Fig. 1. No interfering peaks were observed in urine from ten unexposed persons when monitoring the $m/z = (M - 20)^-$ fragments. After *ca.* 1000 injections of biological samples the TDA-PFPA peaks started to show some tailing. When about 0.5 m of the capillary column inlet end was cut off, the column performance was restored.

Detection

For the analysis of environmental samples containing traces of aromatic amines, very sensitive determination is necessary. This can be achieved using TSD, ECD and MS detection. Earlier, for air samples, we achieved very sensitive determinations using ECD and TSD. TDI in air was determined below 1 $\mu g/m^3$. The present Swedish Threshold Limit Value (TLV) is 40 $\mu g/m^3$. When monitoring isocyanates in a more complex matrix such as air containing thermal decomposition products, only TSD demonstrated satisfactory selectivity. Initial attempts to analyse biological samples containing TDA using TSD and ECD resulted in chromatograms with an enormous background of peaks giving detection limits several orders of magnitudes higher than required. Using capillary GC–MS very sensitive and selective determinations were possible.

Mass spectrometry

EI and CI with ammonia and isobutane monitoring positive (CI^+) and negative ions (CI^-) were studied. Using EI and determining the TDA-PFPA derivatives the molecular ion (m/z = 414) and the $M - C_2F_5$ ($m/z = 295$) fragment are the most abundant ions, which were selected for quantification. Compared with CI monitoring negative ions, the detection limit was *ca.* 50 times higher. When determining low nanograms per litre concentrations of TDA, interferences relative the matrix were seen. In Table I the mass spectra obtained for the TFAA, PFPA and HFBA derivatives of 2,3-, 3,4-, 2,6-, 2,4- and 2,5-TDA using CI with positive and negative ion monitoring with ammonia and isobutane as the reagent gases are shown.

Chemical ionization with ammonia monitoring positive ions. As can be seen in Table I, positive ions formed with ammonia show simple and easy to interpret spectra and very little fragmentation is seen. The $m/z = (M + 18)^+$ fragment is the most abundant for all the compounds studied.

Chemical ionization with ammonia monitoring negative ions. The negative fragments formed vary with the isomer and derivative studied and a more complicated fragmentation pattern is seen compared with positive ion monitoring. The relative abundance of the molecular ion was less

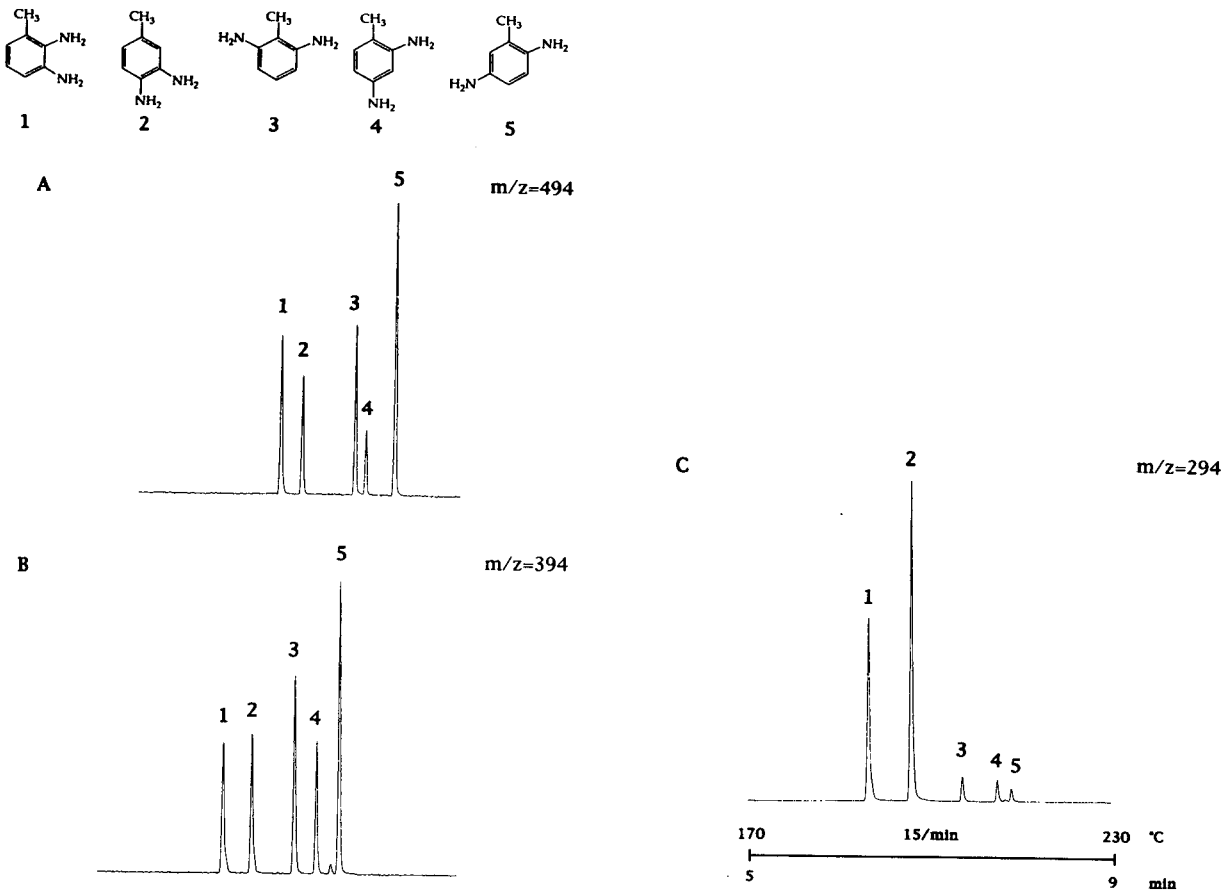

Fig. 1. Selected-ion monitoring of perfluoro-fatty acid amides with TDA in toluene using CI with ammonia and monitoring negative ions of $m/z = (M-20)^-$. (A) TDA-HFBA derivatives (m/z 494). The peaks correspond to 100 fg of TDA. (B) TDA-PFPA derivatives (m/z 394). The peaks correspond to 100 fg of TDA. (C) TDA-TFAA derivatives (m/z 294). The peaks correspond to 1 pg of TDA. Peaks: 1 = 2,3-TDA; 2 = 3,4-TDA; 3 = 2,6-TDA; 4 = 2,4-TDA; 5 = 2,5-TDA. Column, fused silica coated with DB-5 bonded stationary phase (30 m × 0.243 mm I.D.); film thickness, 0.25 μm; inlet pressure of the carrier gas (helium), 0.8 kg/cm^2; splitless injection (1 min) of 1 μl of toluene; temperature programme, isothermal at 110°C (1 min), raised at 15°C/min to 280°C, maintained for 2 min.

than 0.1% and the most abundant fragment was the $m/z = (M-20)^-$ fragment. This fragment probably originates from the molecular ion with the neutral loss of HF. In the spectra of 2,6-TDA-HFBA, further neutral loss ($m/z = M - n \times 20)^-$ of HF may occur (n = 1–4). For 2,6- and 2,4-TDA it is convenient to monitor more than one ion to minimize the influence of interfering compounds. Ammonia as the reagent gas can be used continuously for several weeks, giving reproducible results without the necessity to clean the ion source. Negative ion monitoring with ammonia is by far the most sensitive technique.

Chemical ionization with isobutane monitoring positive ions. CI with positive ion monitoring with isobutane shows, compared with CI^+ with ammonia, simple spectra with very little fragmentation. The $m/z = (M+1)^+$ fragment is the most abundant fragment in all instances. All isomers and derivatives give similar spectra.

Chemical ionization with isobutane monitoring negative ions. On monitoring negative ions formed with isobutane, similar spectra to those with ammonia are obtained. The intensities of the ions formed are lower, resulting in higher detection limits.

Isobutane contaminates the ion source, notice-

TABLE I

MASS SPECTRA OBTAINED FOR TFA-, PFPA- AND HFBA AMIDE DERIVATIVES OF 2,3-, 3,4-, 2,6-, 2,4- AND 2,5-TDA

The injected amount was 10 ng of each TDA isomer. The ion source temperature was 230°C and the capillary inlet pressure of helium was 0.8 kg/m^3. The pressure in the ion source was *ca.* 1×10^{-4} mbar for CI with ammonia and positive ion monitoring and *ca.* 2×10^{-4} mbar for CI with ammonia and negative ion monitoring. The emission current was 200 mV and the electron energy 60 eV. Ions of m/z 50–600 were monitored for under 0.7 s with an inter-scan delay of 0.1 s. Values of m/z and relative abundance (332/100 etc.) are arranged in ascending order. Only fragments with relative abundances >4% are included.

Method	TDA	m/z and relative abundance (%)
CI with ammonia monitoring positive ions of TFAA amides	2,3-TDA	332/100, 201/85, 219/5, 283/5
	2,4-TDA	332/100, 219/15, 236/10, 149/5
	2,5-TDA	332/100, 201/35, 283/5, 219/5
	2,6-TDA	332/100, 236/15, 314/10, 219/5
	3,4-TDA	332/100, 219/10, 236/5
CI with ammonia monitoring negative ions of TFAA amides	2,3-TDA	294/100, 177/85, 279/70, 217/25, 313/5
	2,4-TDA	294/100, 298/30, 274/25, 278/20, 313/15
	2,5-TDA	294/100, 298/65, 313/20, 69/10, 217/8
	2,6-TDA	294/100, 298/45, 313/13
	3,4-TDA	294/100, 217/30, 177/30, 199/15, 314/15
CI with ammonia monitoring positive ions of PFPA amides	2,3-TDA	432/100, 251/20, 148/10
	2,4-TDA	432/100, 286/10, 269/10
	2,5-TDA	432/100, 251/15, 148/10
	2,6-TDA	432/100, 286/10, 414/10
	3,4-TDA	432/100, 269/5, 287/5
CI with ammonia monitoring negative ions of PFPA amides	2,3-TDA	394/100, 379/45, 128/45, 230/45, 275/20, 293/10, 413/5
	2,4-TDA	394/100, 374/100, 128/55, 354/35, 228/10, 248/10, 413/5
	2,5-TDA	394/100, 128/55, 344/15, 248/10, 274/5, 413/5
	2,6-TDA	394/100, 374/55, 128/45, 248/10, 413/5
	3,4-TDA	394/100, 275/70, 128/40, 230/35, 413/5
CI with ammonia monitoring positive ions of HFBA amides	2,3-TDA	532/100, 301/20, 148/10
	2,4-TDA	532/100, 336/5, 319/5
	2,5-TDA	532/100, 301/15, 148/10, 319/5
	2,6-TDA	532/100, 336/10, 514/5
	3,4-TDA	532/100, 319/5, 336/5
CI with ammonia monitoring negative ions of HFBA amides	2,3-TDA	494/100, 325/35, 178/25, 280/25, 479/20, 343/20, 513/5
	2,4-TDA	474/100, 254/80, 494/75, 178/40, 278/10, 513/5
	2,5-TDA	494/100, 178/30, 298/10, 474/10, 324/10, 513/5
	2,6-TDA	494/100, 474/75, 178/30, 454/15, 298.10, 513/5
	3,4-TDA	494/100, 325/90, 178/30, 280/25, 157/10, 146/10, 513/5

able even after 1–2 h of use, and rinsing of the ion source must be performed frequently. Isobutane is therefore not recommended as a reagent gas for automatic "routine" determinations that may take several days to complete.

The positioning of the capillary column outlet in the ion source was critical; moving the column 2–3 mm changed the sensitivity 50-fold. Optimum sensitivity was obtained when the column outlet was only *ca.* 2 mm from the centre of the ion source. At the beginning of the study, changing the ionization mode from CI^- or CI^+ to EI was troublesome, with drifting optimum tuning parameters. Typically, the EI sensitivity was lowered a factor of 10 after using CI for 1–2 weeks. When the same column had been used for several weeks the decrease in EI sensitivity on changing from CI to EI became less. It was also

observed that about 5 mm of the major part of the polyimide polymer coating of the end of the capillary outlet had vanished. By connecting a capillary column after burning off *ca.* 5 mm of the capillary outlet with a micro-flame or a heat gun in order to remove the polyimide layer, switching between CI and EI could be done without any problems. The ion source could be used for weeks without the need for rinsing and with very good repeatability.

Ion source optimization. An inlet device for the continuous introduction of sample molecules into the ion source was tested. Stable conditions (amount of sample introduced into the ion source per unit time) were obtained for more than 10 h. The inlet device makes it possible to optimize the MS conditions in more detail for the compounds under study. Optimum settings for lenses and electron energy and conditions such as reaction gas pressure, temperature and resolution were established. The ion source pressure read out only gives a "good hint" about the real pressure in the source. It was not possible to measure the real pressure inside the source where the chemical reactions take place. In Fig. 2 it can be seen that the pressure giving optimum abundance of the $m/z = (M-20)^-$ (394) fragment was about $1.8 \cdot 10^{-4}$ mbar, which is 40% less than with optimization using PFTBA.

In Fig. 3 the optimum electron energy was *ca.* 80 eV, which is the same as with PFTBA. The temperature of the ion source was varied between 140 and 350°C and standard solutions

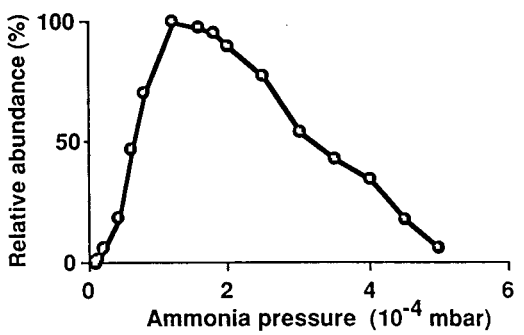

Fig. 2. Variation of the relative abundance of the m/z 394 fragment with source pressure. The ion source pressure readout is an indirect measure which was performed outside the source.

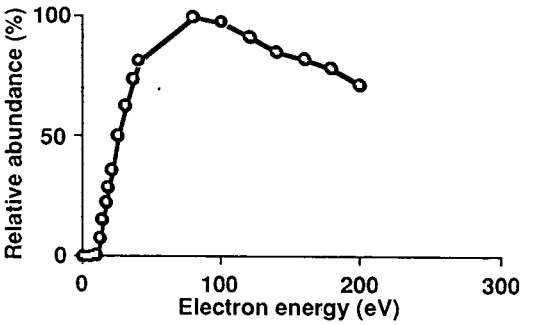

Fig. 3. Variation of the relative abundance of the m/z 394 fragment with electron energy.

containing *ca.* 10 ng/μl of the TFAA, PFPA and HFBA derivatives of 2,3-, 3,4-, 2,6-, 2,4- and 2,5-TDA were repeatedly injected. Mass spectra were obtained and evaluated. The relative abundances of the $m/z = (M - n \times 20)^-$ ($n = 1$–4) fragments *versus* ion source temperature are shown in Fig. 4 for the 2,6- and 2,4-TDA TFAA, PFPA and HFBA derivatives. The typical fragmentation pattern involves increased neutral losses of HF with increase in temperature. The optimum sensitivity was at 140°C, but at this low temperature tailing chromatographic peaks were obtained. It can be seen that 230°C is the optimum temperature for the $m/z = (M-20)^-$ fragment in the PFPA and the HFBA plots. The TFAA plots have an optimum at 250°C.

Quantitative analysis

Recovery. When performing the work-up procedure with urine samples spiked with the five TDA isomers at a concentration of 20 μg/l, for 2,6-, 2,4- and 2,5-TDA the recovery was 100 ± 2% (with a 95% degree of confidence, $n = 5$). However, significant losses, which varied, of >70% of 2,3- and 3,4-TDA was found. It was established that the losses occurred during the hydrolysis of the urine. To apply the present method for the determination of 2,3- and 3,4-TDA in human urine further development is necessary.

Calibration graphs. Human urine were spiked with 2,6-, 2,4- and 2,5-TDA at six different concentrations in the range 0.2–2.5 μg/l and the work-up procedure was then performed. The $m/z = (M-20)^-$ fragments of the TDA and the

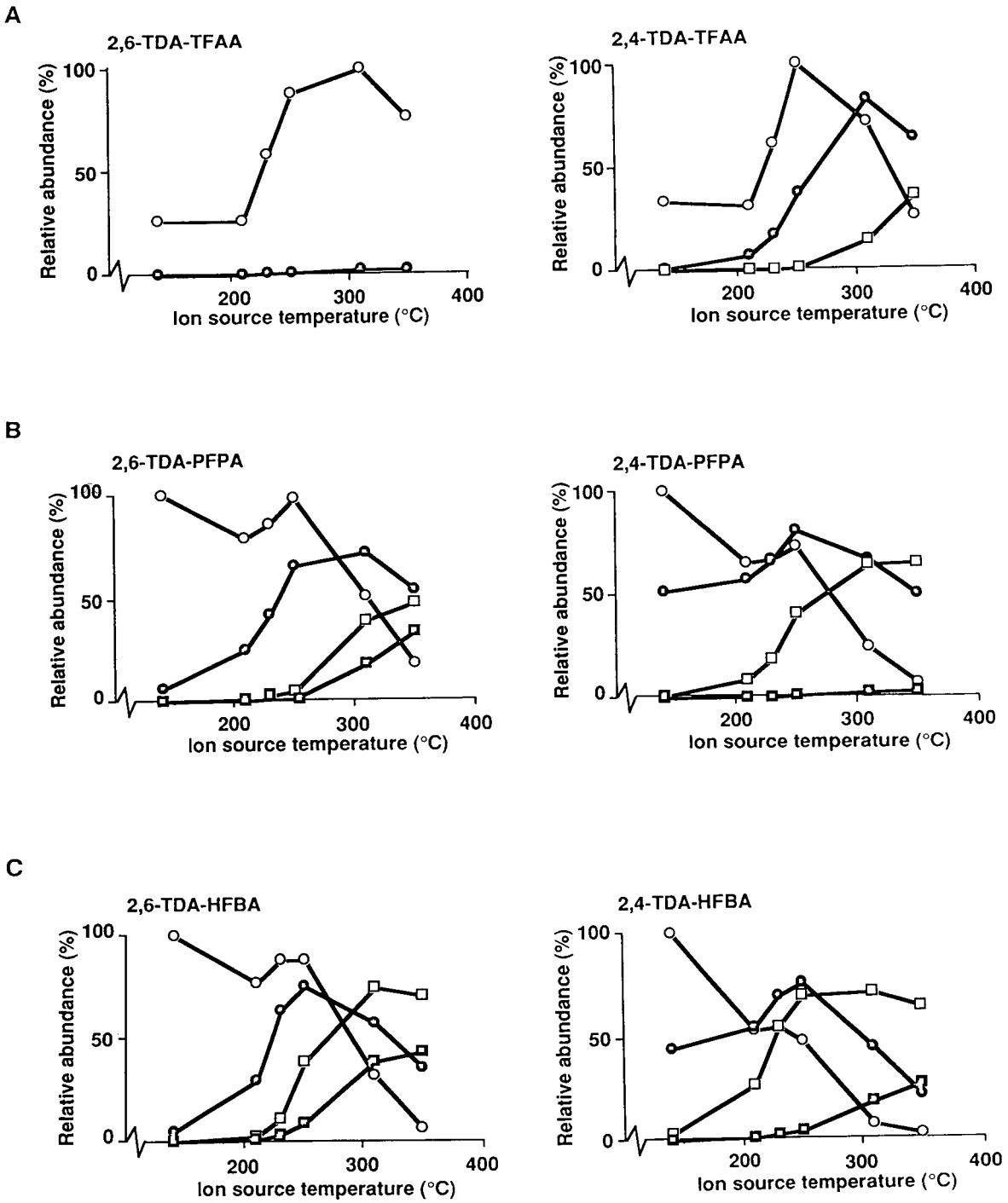

Fig. 4. Variation of the relative abundance of the $m/z = (M - n \times 20)^-$ ($n = 1$–4) fragments with the temperature of the ion source. Amounts of 10 ng of 2,6- and 2,4-TDA derivatized with (A) TFAA, (B) PFPA and (C) HFBA. Mass spectra were obtained by scanning ions between 50 and 600 u for 0.7 s with an inter-scan delay of 0.1 s. Chromatographic conditions as in Fig. 1. ○ = $m/z = (M - 20)^-$; ● = $m/z = (M - 40)^-$; □ = $m/z = (M - 60)^-$; ■ = $m/z = (M - 80)^-$.

internal standards trideuterated 2,6- and 2,4-TDA were monitored. Trideuterated 2,4-TDA was used as the internal standard for the determination of 2,5-TDA. The ratios of the peak area of TDA to that of the internal standards were calculated. For PFPA and HFBA derivatives the slopes of the calibration graphs were *ca.* 2.3 for 2,6-TDA and 2,4-TDA and were *ca.* 4.5 and *ca.* 10, respectively, for 2,5-TDA. TFAA derivatives of 2,6-, 2,4- and 2,5-TDA were studied in the concentration range 2–25 μg/l. Ten times higher concentrations of the internal standards were used. The slopes of the calibration graphs were *ca.* 0.23 for 2,6-TDA and 2,4-TDA and *ca.* 0.14 for 2,5-TDA. Duplicate work-up with duplicate injections were made for each concentration. The linear calibration graphs obtained passed almost through the origin and the correlation coefficients were in the range 0.998–0.999.

Precision. The overall precision for human urine spiked at a concentration of 1 μg/l was found to be 1.6% for 2,6-TDA, 3.5% for 2,4-TDA and 3.2% for 2,5-TDA determined as the PFPA derivatives ($n = 10$).

Detection limit. For the GC–MS system the detection limit, monitoring the $m/z = (M - 20)^-$ fragment, defined as twice the signal-to-noise ratio, is in the range 1–5 fg for the five TDA isomers derivatives with PFPA or HFBA. For the TFAA derivatives the detection limit is 40–200 times higher. The detection limits for biological samples are defined by the matrix. The detection limit defined as the blank plus three standard deviations of the blank was 0.05 μg/l for human urine and plasma. This could be lowered by a factor of 40 if an enrichment step was included.

When processing raw data from the chromatograms in the computer, with the use of a filtering technique, etc., considerably lower detection limits are achievable. In our experience the detection limit when analysing real biological samples can also be improved in the same way, but it is much more difficult to define the conditions.

Application

A male worker in a polyurethane foam factory was exposed to *ca.* 10 μg/m^3 of TDI. The peaks in the chromatogram in Fig. 5 corresponds to a concentration of 2,6-TDA of *ca.* 1 μg/l and of 2,4-TDA of *ca.* 0.7 μg/l in urine. The concentration of TDA in urine varies with time and exposure. The chromatogram in Fig. 6 is for a hydrolysed plasma sample from another TDI worker. The peaks corresponds to a concentration of *ca.* 5.7 μg/l of 2,6- and 0.6 μg/l of 2,4-TDA in plasma. The concentration of TDA in plasma was found to vary by less than 10% from the average and no variations were seen with time (50 h) and exposure. This study has been described in more detail elsewhere [15].

Analytical considerations

The uptake of TDI by oral, dermal and inhalation administration is not known in detail. The metabolism in humans is also unknown. For ethical reasons it is not possible to study the metabolism using ^{14}C-labelled TDI in humans. The high toxicity of TDI results in very low TLVs and therefore only low concentration are found in biological samples from workers. Only during the very infrequent accidents in the industry can high exposure be expected. It has also been suggested that different metabolism may occur at very high exposure compared with exposure under normal working conditions below the TLV levels. The determination of TDA in hydrolysed biological samples described here not only monitors the exposure to TDI but also possibly to TDA or other TDI/TDA related compounds that will release TDA during the hydrolysis. Owing to the carcinogenic properties of 2,4-TDA, this compound is very little used in most countries. The method is well suited for routine determinations of TDA in hydrolysed urine or plasma.

In the work-up procedure, aliphatic and aromatic primary and secondary amines will be derivatized. However, lower extraction recoveries of aliphatic amines from an aqueous phase into toluene have been found owing to the pK_a values of the amines. MDA (4,4′-methylenediphenyldiamine) and HDA (1,6-hexamethylenediamine) can also be determined by the same method by monitoring different mass fragments. Details concerning the determination of these compounds will be presented elsewhere. For the biological monitoring of organic com-

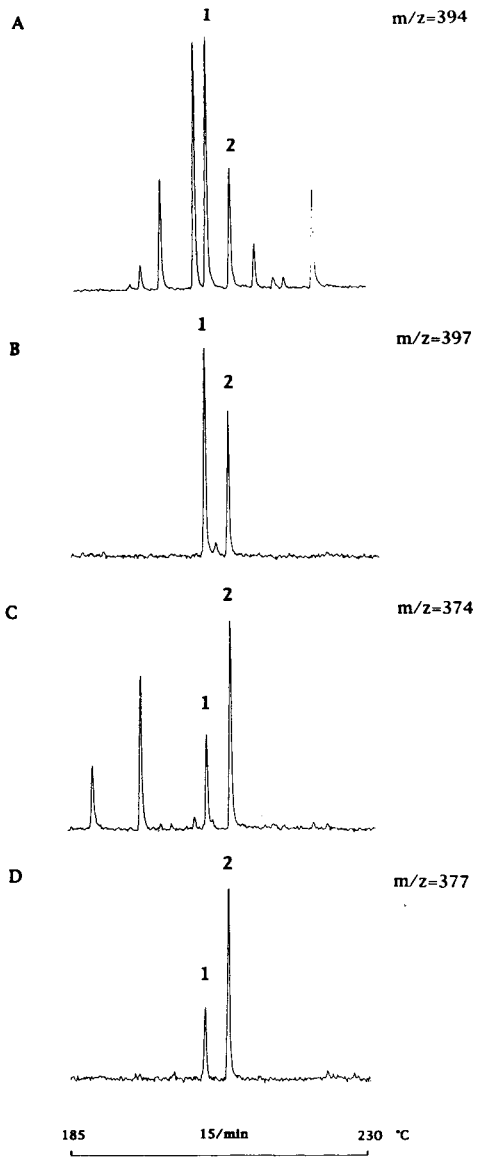

Fig. 5. Chromatograms of a hydrolysed urine sample from a worker exposed to an air concentration of *ca.* 10 $\mu g/m^3$ of 2,4- and 2,6-TDI. SIM using CI with ammonia and negative ion monitoring. (A) $m/z = (M-20)^-$ (394) ion of the TDA-PFPA derivative. (B) $m/z = (M-20)^-$ (397) ion of the trideuterated TDA-PFPA derivative. (C) $m/z = (M-40)^-$ (374) ion of the TDA-PFPA derivative. (D) $m/z = (M-40)^-$ (377) ion of the trideuterated TDA-PFPA derivative. The peaks correspond to a concentration of *ca.* 1 $\mu g/l$ of 2,6- and *ca.* 0.7 $\mu g/l$ of 2,4- in urine. Peaks in (A) and (C): 1 = PFPA derivative of 2,6-TDA; 2 = PFPA derivative of 2,4-TDA. Peaks in (B) and (D): 1 and 2 are the corresponding deuterium-labelled internal standards. Chromatographic conditions as in Fig. 1.

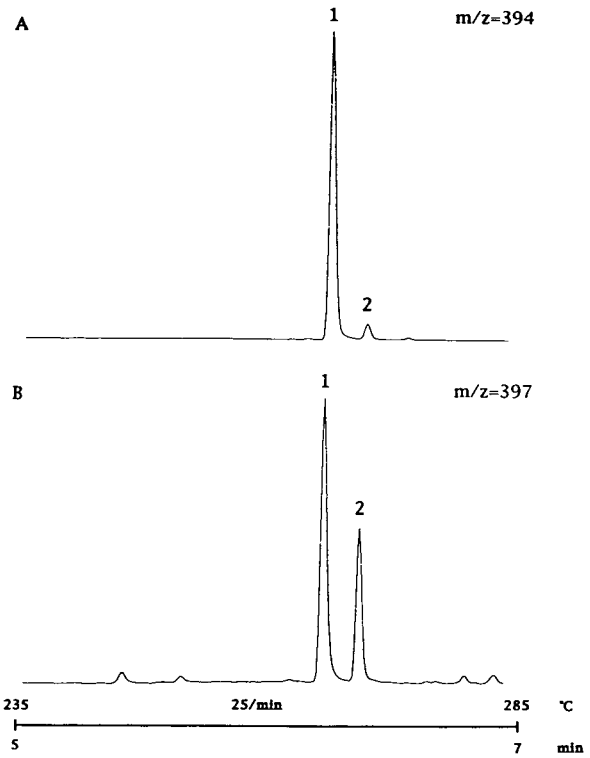

Fig. 6. Chromatograms of a hydrolysed plasma sample from a worker exposed to 2,4- and 2,6-TDI. (A) m/z 394 ion of the TDA-PFPA derivative. (B) $m/z = 397$ ion of the trideuterated TDA-PFPA derivative. The peaks correspond to a concentration of *ca.* 5.7 $\mu g/l$ of 2,6- and *ca.* 0.57 $\mu g/l$ of 2,4- in plasma. Peaks: 1 = 2,6-TDA; 2 = 2,4-TDA. Column: fused silica coated with DB-5 bonded stationary phase (25 m × 0.25 mm I.D.); film thickness, 0.25 μm; temperature programme, isothermal at 110°C (1 min), raised at 25°C/min to 280°C. Other conditions as in Fig. 1.

pounds a proper choice between selectivity and sensitivity must be made. It is possible to monitor exposure to TDI at levels several orders of magnitude below the Swedish TLV by the proposed method. The method cannot differentiate between exposure to TDI or the corresponding amine TDA or related derivatives of TDA. The nature of the TDA-releasing compounds, during hydrolysis, is not known. For the complete speciation of the nature of exposure, further research is necessary. The proposed method was developed for assessing occupational exposure to TDI. Selective and sensitive determinations of TDA isomers in hydrolysed human urine and plasma, at the low $\mu g/l$ level, are possible using GC–SIM. The use of trideu-

terated TDA as internal standard has been demonstrated to give accurate and precise determinations.

ACKNOWLEDGEMENTS

We gratefully acknowledge the Swedish Work Environment Fund (AMFO) and the Medical Faculty, University of Lund, for financial support.

REFERENCES

1 A.L. Kennedy and W.E. Brown, *Isocyanates and Lung Disease: Experimental Approaches to Molecular Mechanisms*, Vol. 7, *Occupational Medicine: State of the Art Reviews*, No. 2, Hanley & Belfus, Philadelphia, 1992, p. 301.
2 World Health Organization, *Environmental Health Criteria 75, Toluene Diisocyanates*, WHO, Geneva, 1987.
3 D.E. Bradway and S. Talaat, *J. Chromatogr. Sci.*, 15 (1977) 322.
4 T.M. Trainor and P. Vouros, *Anal. Chem.*, 59 (1987) 601.
5 H.-B. Lee, *J. Chromatogr.*, 457 (1988) 267.
6 C. Sangö, *J. Liq. Chromatogr.*, 2 (1979) 763.
7 M. Dalene, L. Mathiasson, G. Skarping, C. Sangö and J.F. Sandström, *J. Chromatogr.*, 435 (1988) 469.
8 G. Skarping, C. Sangö and B.E.F. Smith, *J. Chromatogr.*, 208 (1981) 313.
9 G. Skarping, L. Renman and M. Dalene, *J. Chromatogr.*, 270 (1983) 207.
10 G. Skarping, L. Renman, C. Sangö, L. Mathiasson and M. Dalene, *J. Chromatogr.*, 346 (1985) 191.
11 J.F. Sandström, G. Skarping and M. Dalene, *J. Chromatogr.*, 479 (1989) 135.
12 T. Brorson, G. Skarping and C. Sangö, *Int. Arch. Environ. Health*, 63 (1991) 253.
13 G. Skarping, T. Brorson and C. Sangö, *Int. Arch. Environ. Health*, 63 (1991) 83.
14 H. Tokuda, Y. Kimura and S. Takano, *J. Chromatogr.*, 367 (1986) 345.
15 P. Persson, M. Dalene, G. Skarping, M. Adamsson and L. Hagmar, *Br. J. Ind. Med.*, 50 (1993) 1111–1118.

ELSEVIER

Journal of Chromatography A, 663 (1994) 211–218

JOURNAL OF CHROMATOGRAPHY A

Analysis of *Fusarium* mycotoxins by gas chromatography–Fourier transform infrared spectroscopy

J. Christopher Young*[,a], David E. Games[b]

[a] *Plant Research Centre, Agriculture Canada, Ottawa K1A 0C6, Canada*

[b] *Mass Spectrometry Research Unit, Department of Chemistry, University College of Swansea, Singleton Park, Swansea SA2 8PP, Wales, UK*

(First received July 7th, 1993; revised manuscript received December 13th, 1993)

Abstract

The Fourier transform infrared (FTIR) spectra of selected *Fusarium* mycotoxins of various structure types were determined. Absorptions were observed for the following functionalities: hydroxyl at 3625–65 cm^{-1} and 3482 cm^{-1}, the latter being associated with a 7α-hydroxyl adjacent to an 8-carbonyl in *keto* trichothecenes; carbonyl at 1760–6 cm^{-1} for 5-membered rings and at 1695–8 cm^{-1} for those conjugated to a single C=C in a six-membered ring; acetate carbonyl at 1765 cm^{-1} and acetate C–O at 1220–9 cm^{-1}; and C=C at 1680 cm^{-1}. Gas chromatography combined with FTIR and mass spectrometry was applied to the identification of some mycotoxins in a *F. roseum* liquid culture extract.

1. Introduction

Mycotoxins are secondary fungal metabolites formed during the growth of certain fungi when environmental conditions of moisture, temperature and host are suitable. There is considerable interest in the analysis of these compounds because they can occur in food products and are toxic to humans and animals and plants [1]. The *Fusarium* spp. produce an impressive diversity of secondary metabolites (see Fig. 1).

Analysis of mycotoxins typically involves extraction from the sample matrix followed by some preliminary cleanup, chromatographic separation [thin-layer, gas (GC) or high-performance liquid (HPLC)] and detection [2]. Some of the *Fusarium* mycotoxins can be analyzed directly by GC, while others require derivatization. Confirmation of identity usually requires comparison of at least two independent properties, such as chromatographic retention time (or R_F) and a spectrum. One of the most powerful combinations is the coupling of GC with mass spectrometry (MS), which frequently enables direct identification of known compounds and location and partial identification of new compounds. Infrared (IR) spectroscopy has traditionally been restricted to functional group identification in pure samples. However, the recent availability of Fourier transform infrared spectroscopy (FTIR) detectors that can be coupled to GC effluents gives additional dimensions to the analysis of complex mixtures [3–6]. The IR spectra of the individual components of a complex mixture can be recorded as they elute, and, as with MS, such spectra also can be

* Corresponding author.

SSDI 0021-9673(93)E0049-Z

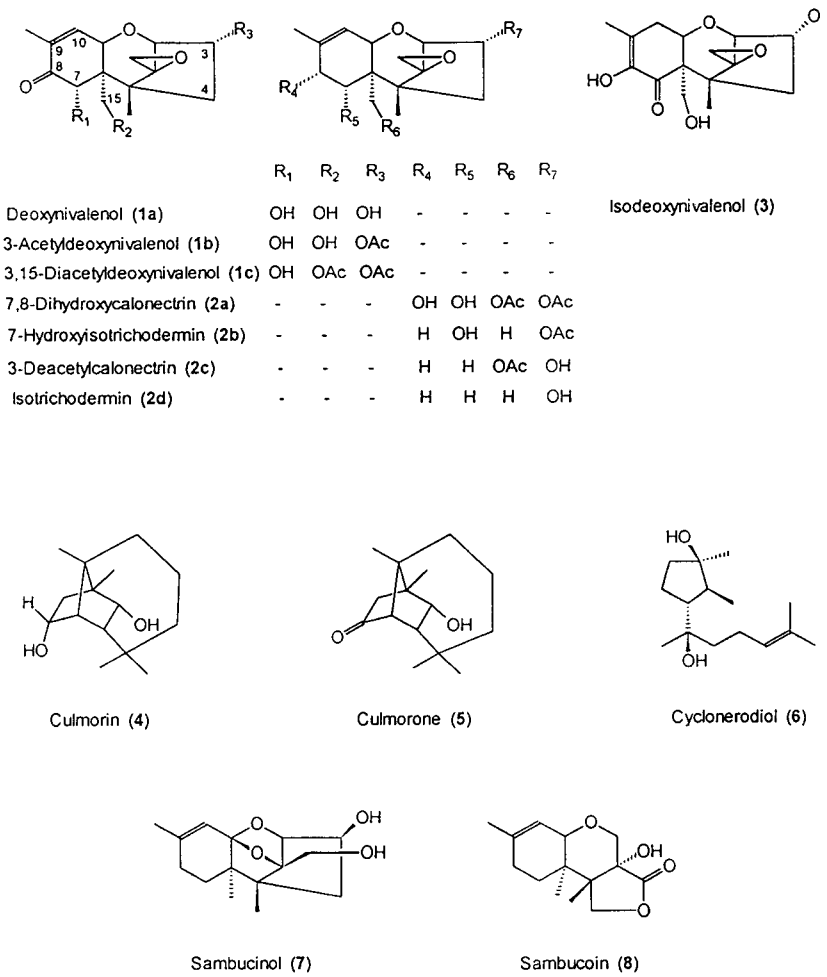

Fig. 1. Structures of some *Fusarium* mycotoxins.

compared with those in IR data bases for confirmation of identity.

This is the first study that reports on the FTIR spectra of *Fusarium* mycotoxins and illustrates the combined application of GC–FTIR and GC–MS to the analysis of a *F. roseum* liquid culture extract.

2. Experimental

2.1. Mycotoxins and reagents

Mycotoxin standards were obtained from liquid cultures of various *Fusarium* spp. (prepared in the Plant Research Centre laboratories, Ottawa, Canada). Purity was established by HPLC and nuclear magnetic resonance analyses. A natural mixture of mycotoxins was obtained from a liquid culture extract of *F. roseum* according to the method of Greenhalgh *et al.* [7]. Standards were dissolved in analytical-reagent grade methanol at a concentration of 1 mg/ml.

2.2. Gas chromatography–Fourier transform infrared (GC–FTIR) analysis

GC–FTIR analyses were conducted on a Hew-

lett-Packard 5890A/GC–5965B/IRD (Hewlett-Packard, Avondale, PA, USA). A J&W Scientific DB5 30 m × 0.25 mm I.D. column with 0.26 μm film (J&W Scientific, Folsom, CA, USA) was used in the splitless mode with a purge delay of 30 s, injector 250°C, and the column was temperature programmed from 100–280°C at 15°C min^{-1}. Transfer lines were at 280°C.

2.3. Gas chromatography–mass spectrometric (GC–MS) analysis

GC–MS analyses were conducted on a Hewlett-Packard 5971A mass selective detector in the electron ionization (EI) mode at 70 eV. A J&W Scientific DB5 30 m × 0.25 mm I.D. column with 0.26 μm film was used in the splitless mode with a purge delay of 30 s, injector 250°C, and the column was temperature programmed from 100–280°C at 15°C min^{-1}.

Identity of components in the *F. roseum* extract was established by comparison of observed FTIR and MS spectra to those in spectral data bases as well as congruence of chromatographic retention times with those of the corresponding standards.

3. Results and discussion

3.1. Fourier transform infrared spectra of standards

Table 1 summarizes the observed FTIR and reported literature value absorption bands for the *Fusarium* mycotoxins examined. Very sharp hydroxyl band absorptions were observed in the 3625–3665 cm^{-1} and 3482 cm^{-1} regions. The absorption at 3482 cm^{-1} was associated with a 7α-hydroxyl adjacent to an 8-carbonyl [*e.g.* in 4-deoxynivalenol (DON) (**1a**)]. This assignment was supported by the observed reduction in and disappearance of the 3665 cm^{-1} absorption band when going from DON to 3-acetylDON (**1b**) and 3,15-diacetylDON (**1c**), respectively. The assignment of the 3482 cm^{-1} band to an α-hydroxyketone in trichothecenes has not been reported before. Bands in this region have been observed, when measured as a film or KBr pellet (see ref. 8, pp. 203, 209, 215), however they tend to be obscured by the general broad hydroxyl absorption. The carbonyls in a five-membered ring appeared at 1760–1767 cm^{-1}, while those conjugated to a single double bond in a six-membered ring appeared at 1695–1698 cm^{-1}. There were two sharp absorption bands associated with acetates: one at 1765 cm^{-1} attributed to the carbonyl and another at 1220–1229 cm^{-1} attributed to the C–O bond. A very strong C=C absorption for *iso*-4-deoxynivalenol (IDON) (**3**) was observed at 1642 cm^{-1} whereas those in sambucinol (**7**) and sambucoin (**8**) at 1680 cm^{-1} were quite weak. The 9,10 double bond absorptions in the trichothecenes studied were generally masked by the overlapping carbonyl absorptions.

Differences in absorption frequencies and band shapes were noted in all cases between those determined by GC–FTIR and those by "classical" methods (*e.g.* in a KBr pellet, as a thin film on NaCl, or in a Nujol mull). GC–FTIR hydroxyl band absorptions were very sharp, compared with the generally very broad absorptions reported by other techniques, and were shifted higher by up to 200 cm^{-1} into the 3625–3665 cm^{-1} region. Carbonyl absorptions were shifted higher by 25 and 10 cm^{-1} for those in a five-membered ring or conjugated to one double bond in a six-membered ring, respectively. In acetates, the carbonyl absorption was shifted higher by about 25 cm^{-1} while that for the C–O absorption was shifted lower by about 10 cm^{-1}. Welti [12] noted that the IR bands associated with stretching and deformation vibrations shift to higher and lower frequencies, respectively, when measured in the vapour state as compared with those obtained in the liquid or solid states.

3.2. Application of GC–FTIR to analysis of a Fusarium extract

One of the advantages of GC–MS is the ability

Table 1
Summary of Fourier transform infrared spectra of selected *Fusarium* mycotoxins

Compound [a]	Absorption maxima (cm^{-1})				Literature
	Hydroxyl	Carbonyl	Acetate	C=C	
3-Acetyl-4-deoxynivalenol (**1b**)	3664, 3482	1695	1767, 1231		
	3465 [b]	*1685*	*1745*		Ref. 8 [c]
Calonectrin (**2d**)			1765, 1232		
			1745, 1240		Ref. 9 [d]
Culmorin (**4**)	3652				
	3340				Ref. 9 [d]
Culmorone (**5**)	3653	1767			
	3420	*1743, 1725*			Ref. 9 [d]
Cyclonerodiol (**6**)	3644				
	3425				Ref. 10 [e]
3-Deacetylcalonectrin (**2c**)	3626		1765, 1227		
4-Deoxynivalenol (**1a**)	3646, 3481	1698			
	3470, 3430,	*1680*			Ref. 8 [c]
iso-4-Deoxynivalenol (**3**)	3588, 3476	1690		1642	
3,15-Diacetyl-4-deoxynivalenol (**1c**)	3482	1698	1767, 1220		
	3455	*1685*	*1745, 1240*		Ref. 9 [d]
7,8-Dihydroxycalonectrin (**2a**)	*3540*		*1735, 1265*		Ref. 9 [c]
			1715, 1252		
7-Hydroxyisotrichodermol (**2b**)	3637				
Sambucinol (**7**)	3660, 3570			1680	
	3350			*1675*	Ref. 11 [c]
Sambucoin (**8**)	3605	1760		1678	
	3380	*1735*		*1760*	Ref. 11 [c]
iso-Trichodermol (**2e**)	3625				

[a] See Fig. 1 for structures.
[b] Literature values in italics.
[c] Determined in KBr pellets.
[d] Determined as thin film on NaCl plates.
[e] Method of determination not reported.

to conduct retrospective selected-ion monitoring of acquired data, which can result in simplification of chromatograms and aid in the identification of individual components. The possibility for computerized comparison of acquired spectra with those in a library for identification purposes also exists. GC–FTIR can offer similar advantages, as illustrated below.

Fig. 2a shows the GC–FTIR total response chromatogram of a *F. roseum* extract. Examination of the FTIR spectrum (Fig. 3a) of the major component A revealed an absorption at 3652 cm^{-1} indicative of the presence of a hydroxyl group. A library search gave an excellent match with the FTIR spectrum of culmorin (**4**). The mass spectrum [13] of this component, obtained by GC–MS using the same column, confirmed the FTIR structural assignment.

The second major component in the GC–FTIR total response chromatogram, peak E, was next examined and its infrared spectrum (Fig. 3e) showed the presence of at least two hydroxyl groups (3644 and 3481 cm^{-1}) and a conjugated carbonyl (1695 cm^{-1}). A library search showed an excellent match with DON (**1a**) and this assignment was confirmed by the mass spectrum [13]. A search of the chromatogram for peaks with particular absorption frequencies was used

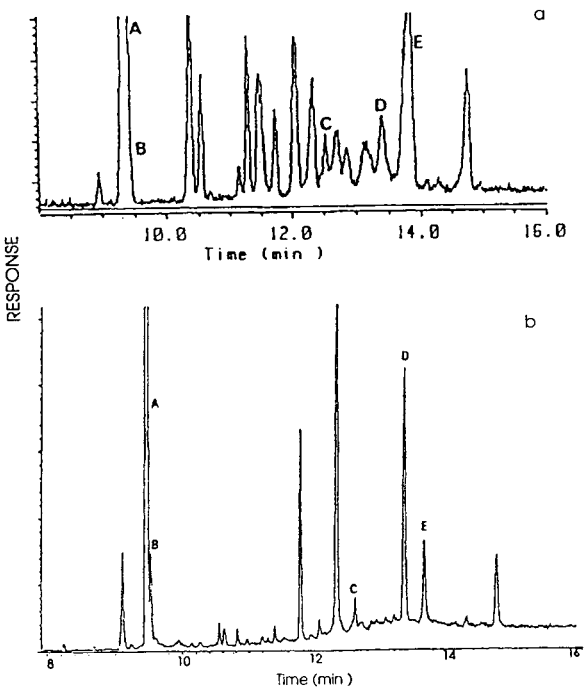

Fig. 2. Gas chromatogram of a *Fusarium roseum* liquid culture extract. Separation by GC on a 30 m × 0.25 mm I.D. DB5 column temperature programmed from 100–280°C at 15°C/min. (a) Detection by Fourier transform infrared spectrocopy; (b) detection by electron ionization mass spectrometry. For peaks A–E, see Fig. 3.

in the exploration for additional components. Fig. 4 shows the results obtained with searching for hydroxyl absorptions. Trace a (3655–3665 cm^{-1}) shows the secondary hydroxyls of culmorin (**4**) at 9.37 min and DON (**1a**) at 13.84 min while in trace b the hydroxyl α to the carbonyl in DON (3465–3485 cm^{-1}) is readily identified as is an additional component (D) at 13.40 min. Component D also showed hydroxyl absorptions at 3588 and 3640 cm^{-1}, a carbonyl absorption at 1690 cm^{-1} and a very strong C=C absorption at 1642 cm^{-1}. A library search of the FTIR spectrum of this component (Fig. 3d) gave an excellent match with IDON (**3**) and its mass spectrum [13] was also consistent with this structural assignment.

Examination of chromatograms for C=O and C=C frequencies (Fig. 5) confirmed the presence of DON (**1a**) (trace b, 1690–1700 cm^{-1}) and IDON (**3**) (trace c, 1635–1650 cm^{-1}). In trace a (1760–1770 cm^{-1}), the presence of a minor component (B) containing a carbonyl was noted at the retention time for culmorin (A). Examination of the GC–MS total ion chromatogram (Fig. 2b) of the extract showed a minor peak eluting shortly after that of culmorin. Retrieval of the FTIR spectrum for this component from the major peak resulted in a spectrum (Fig. 3b), which showed the presence of a hydroxyl group (3652 cm^{-1}) and a carbonyl group (1767 cm^{-1}) and some similarity in the "fingerprint region" (800–1500 cm^{-1}) with that of the spectrum of culmorin (Fig. 3a). Its mass spectrum [13] showed a molecular ion at m/z 236, two mass units less than culmorin. This information suggested that one of the hydroxyl groups in culmorin is changed to a ketone. A library search of the FTIR spectrum gave an excellent match with culmorone (**5**) and the mass spectrum [13] is in agreement with this structural assignment.

Acetylated compounds are common in *Fusarium* species and they have FTIR absorptions in both the C=O (1760–1770 cm^{-1}) and C–O (1218–1235 cm^{-1}) ranges. Study of the chromatograms for these ranges (Fig. 6) showed a component (C) with an elution time of 12.52 min. A library search of its FTIR spectrum (Fig. 3c) gave a good match with 3-deacetylcalonectrin (**2c**) and the mass spectrum [13] was in agreement with this structure.

A comparison of the FTIR and MS chromatograms (Figs. 2a and 2b, respectively), obtained by using the same column, reveals not unexpectedly differences in FTIR and MS response factors for individual components, especially for DON and IDON. Quantitative analyses using these detectors must therefore take individual response factors into consideration. Because FTIR detection is less sensitive than that by MS [14], larger quantities had to be injected, which resulted in a loss of chromatographic resolution *e.g.* for components A and B.

The nature of other components in this extract is currently being investigated and these techniques are being applied to a series of other *Fusarium* extracts enabling identification of a wide range of mycotoxins.

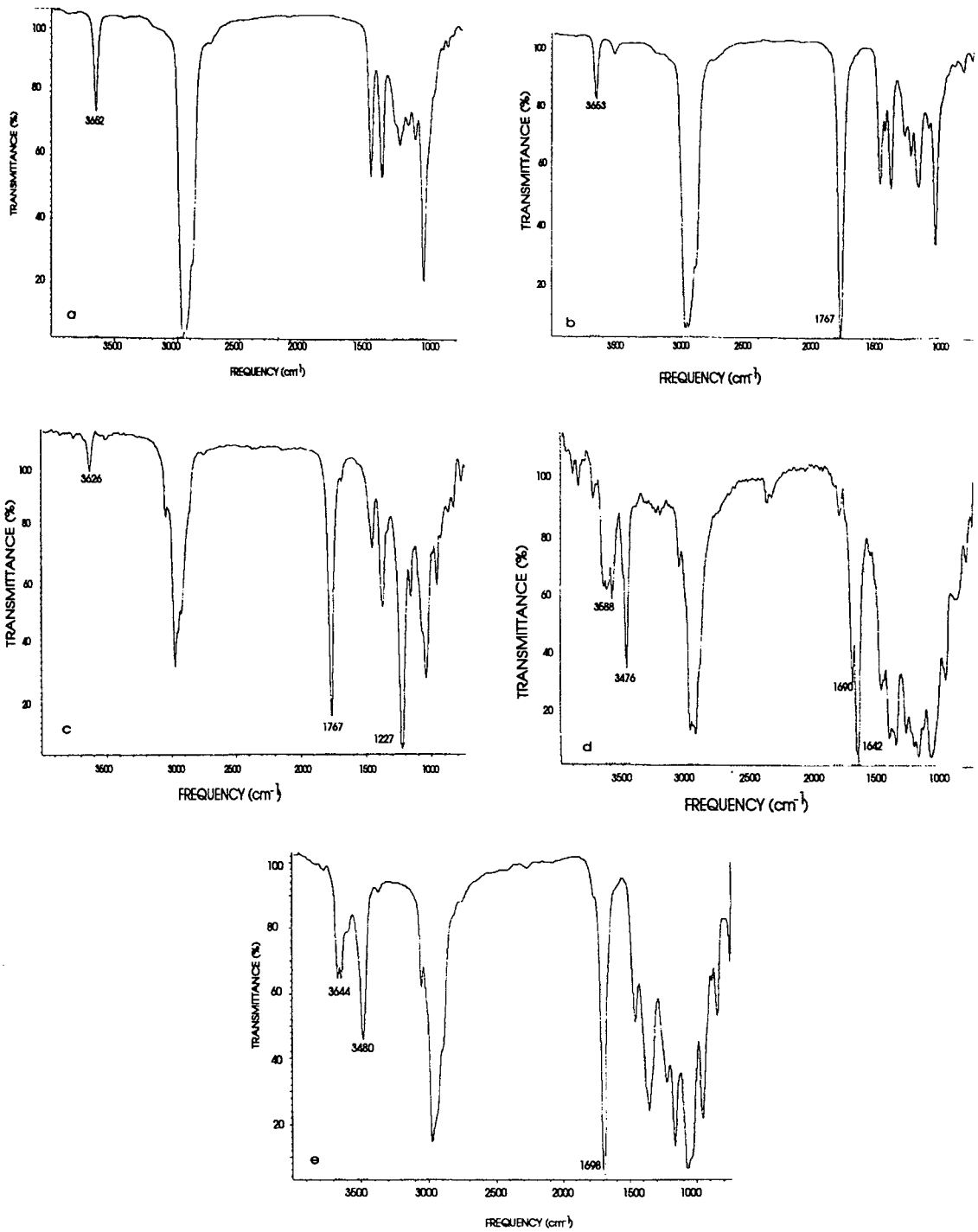

Fig. 3. FTIR spectra (a) of component A, culmorin (**4**); (b) of component B, culmorone (**5**); (c) of component C, 3-deacetylcalonectrin (**2c**); (d) of component D, iso-4-deoxynivalenol (**3**); and (e) of component E, 4-deoxynivalenol (**1a**).

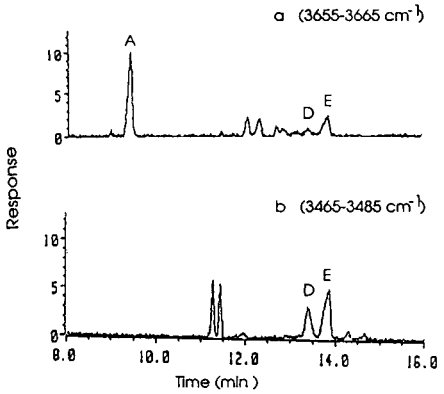

Fig. 4. Gas chromatogram of a *Fusarium roseum* liquid culture extract. Chromatographic conditions as in Fig. 2. Detection by Fourier transform infrared spectroscopy at selected wavelengths characteristic of hydroxyl functionalities: (a) 3655–3665 cm^{-1}; (b) 3465–3485 cm^{-1}.

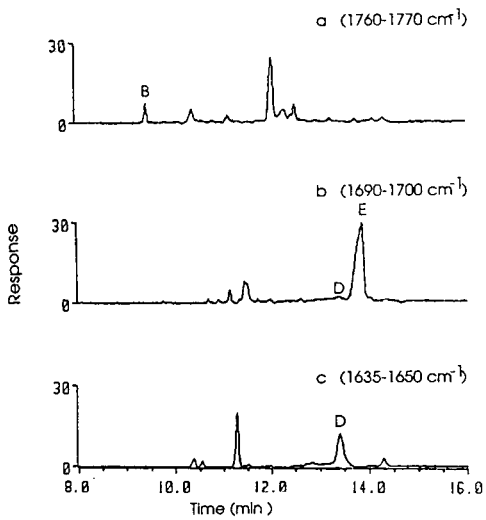

Fig. 5. Gas chromatogram of a *Fusarium roseum* liquid culture extract. Chromatographic conditions as in Fig. 2. Detection by Fourier transform infrared spectroscopy at selected wavelengths characteristic of carbonyl functionalities: (a) 1760–1770 cm^{-1}; (b) 1690–1700 cm^{-1} and double bonds: (c) 1635–1650 cm^{-1}.

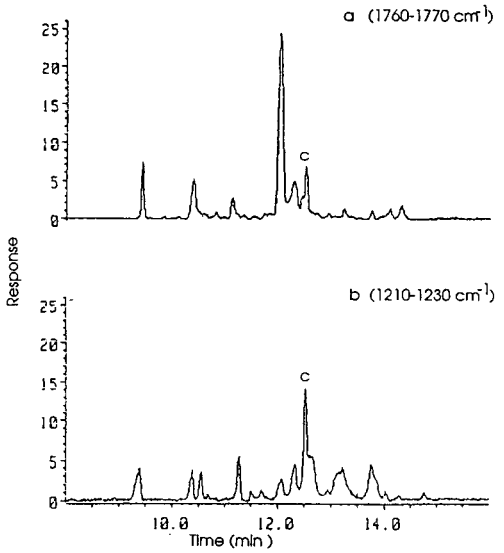

Fig. 6. Gas chromatogram of a *Fusarium roseum* liquid culture extract. Chromatographic conditions as in Fig. 2. Detection by Fourier transform infrared spectroscopy at selected wavelengths characteristic of acetate functionalities: (a) 1760–1770 cm^{-1}; (b) 1210–1230 cm^{-1}.

4. Conclusions

Although GC–FTIR may be a less sensitive technique than GC–MS, it always gives a stable spectrum pattern [14] and thus gives reliable spectra with consistent absorption frequencies useful for characterization of *Fusarium* mycotoxins. The ability to monitor chromatograms at particular frequencies in the IR has proved to be very useful for the location and identification of minor components, particularly those trichothecenes with a 7α-hydroxyl adjacent to an 8-carbonyl as in DON (sharp absorption band at 3482 cm^{-1}) or those with an acetate functionality (two bands at 1765 and 1228 cm^{-1}). The use of GC–FTIR together with GC–MS provides a very powerful combination for the identification of a variety of mycotoxins that represent diverse structure types in fermentation extracts. These combined techniques should also have considerable utility for the identification of such components in food and feed products.

5. Acknowledgements

J.C.Y. wishes to thank D.E.G. for the opportunity to take a sabbatical study leave in the latter's laboratory. The authors thank Dr. J.D. Miller and Mr. W. Adams of the Plant Research

Centre (PRC) of Agriculture Canada for providing *Fusarium roseum* liquid culture extract material and Mr. P. Lafontaine of PRC for some GC–MS analyses. The authors are also grateful to Hewlett-Packard for the provision of the GC–IRD system and to Science and Engineering Research Council for funding for mass spectrometry equipment.

This paper is PRC contribution No. 1512.

6. References

[1] M.E. Savard, R. Greenhalgh and J.W. ApSimon, in Atta-ur-Rahman (Editor), *Studies in Natural Products Chemistry*, Vol. 6, Part D, Elsevier, Amsterdam, New York, 1990, p. 213.

[2] R.J. Cole (Editor), *Modern Methods in the Analysis and Structural Elucidation of Mycotoxins*, Academic Press, Orlando, FL, 1986.

[3] J.R. Ferraro and K. Krishnam (Editors), *Practical Fourier Transform Infrared Spectroscopy: Industrial and Laboratory Chemical Analysis*, Academic Press, San Diego, CA, 1990.

[4] R. White (Editor), *Chromatography/Fourier Transform Infrared Spectroscopy and its Application*, Dekker, New York, 1990.

[5] C. Fijimoto and K. Jinno, *Anal. Chem.*, 64 (1992) 476A.

[6] C.L. Putzig, M.A. Leugers, M.L. McKelvy, G.E. Mitchell, R.A. Nyquist, R.R. Pappenfuss and L. Yurga, *Anal. Chem.*, 64 (1992) 270R.

[7] R. Greenhalgh, R-M. Meier, B.A. Blackwell, J.D. Miller, A. Taylor and J.W. ApSimon, *J. Agric. Food Chem.*, 32 (1984) 1261; *ibid.*, 34 (1986) 115.

[8] R.J. Cole and R.H. Cox, *Handbook of Toxic Fungal Metabolites*, Academic Press, New York, 1981.

[9] R.-M.A. Meier, *M.Sc. Thesis*, Carleton University, Ottawa, ON, Canada, 1985.

[10] Y. Matsuki, M. Kodama and S. Ito, *Tetrahedron Lett.*, (1979) 2901.

[11] P. Mohr, Ch. Tamm, W. Zurcher and M. Zehnder, *Helv. Chim. Acta*, 67 (1984) 406.

[12] D. Welti, *Infrared Vapour Spectra*, Heyden and Son, New York, 1970.

[13] J.C. Young, (1993) unpublished results.

[14] R. Namba, in J.R. Ferraro and K. Krishnan (Editors), *Practical Fourier Transform Infrared Spectroscopy: Industrial and Laboratory Chemical Analysis*, Academic Press, San Diego, CA, 1990, p. 469.

ELSEVIER

Journal of Chromatography A, 663 (1994) 219–227

JOURNAL OF CHROMATOGRAPHY A

Electrophoretic separation of DNA sequencing extension products using low-viscosity entangled polymer networks

Paul D. Grossman

Applied Biosystems (Division of Perkin-Elmer Corporation), 850 Lincoln Center Drive, Foster City, CA 94404, USA

(First received August 5th, 1993; revised manuscript received November 9th, 1993)

Abstract

A low-viscosity (*ca.* 150 cP) polymer solution is used to resolve DNA sequencing fragments up to 580 bases long using the capillary electrophoresis format. Separation performance is compared qualitatively and quantitatively to that of a cross-linked polyacrylamide sequencing slab gel. Both the resolution and length-of-read are essentially equivalent, while the capillary separation is approximately 10 times faster than the slab gel analysis. In addition, separation selectivity and efficiency are examined individually.

1. Introduction

Recently much effort has been directed at the separation of DNA sequencing reaction products by capillary gel electrophoresis [1–6]. The perceived advantages of the capillary format include speed of analysis, increased separation efficiency, on-line real-time detection and automation of sample loading. However, important obstacles to the widespread practical application of this technology still remain: difficulty in capillary gel preparation and instability of the gel matrix during prolonged runs at high voltages [1,2,4,7–9]. The currently reported lifetime of gel-filled capillaries used for DNA sequencing analysis is approximately four injections [10]. Because of the difficulty of gel preparation, this is an unacceptably short lifetime. These problems become particularly serious when one imagines the use of multiple capillary arrays [10] and would almost certainly preclude automation of such systems.

Capillary gel lifetime is limited by three major effects: electroosmosis, bubble formation and capillary inlet fouling with high-molecular-mass sequencing template. Because of the large electroosmotic forces present in microcapillaries [11], the gel can extrude out of the capillary upon application of the electric field, resulting in the formation of a void at the anodic (positive) end of the tube [7]. To counter this effect, gels have been covalently attached to the inside wall of the capillary [1,3,7,12–14]. However, covalent attachment can lead to severe stresses within the gel due to the volume change of the monomer upon polymerization [7,15], leading to the formation of periodic "bubbles", or voids, in the network, causing a devastating loss of separation performance and even loss of electrical continuity along the capillary [4,7,16,17]. This problem has been greatly reduced by using non-cross-linked networks [10,18]. By removing the cross-links, internal stresses within the network can more easily relax, resulting in a "stress-free" network. The use of DNA sequencing mixtures causes additional problems [1–5], further reduc-

0021-9673/94/$07.00
SSDI 0021-9673(93)E1256-Y

ing gel stability. This effect presumably arises from the large amount of high-molecular-mass sequencing template present in the reaction mixture. In fact, to solve this problem, some workers have had to resort to trimming off a portion of the injection end of the capillary subsequent to sample injection [2]. Thus, capillary fouling after repeated injections of DNA sequencing product remains a key obstacle to the extended lifetime, and thus the practical utility, of capillary gels.

Low-viscosity polymer solutions are a recently developed alternative to rigid gels as electrophoretic sieving networks. Because of the flowability of these systems, the separation network can be easily replaced after each run simply by pumping fresh medium into the capillary, eliminating the need for reusability. To date, polymer solutions have been used as sieving networks for the electrophoretic separation of native double-stranded DNA [19–24], chromosomes [25] and micro particles [26]. Furthermore, the theoretical foundation for these systems has been reported [27].

This report describes the application of low-viscosity polymer solutions to the separation of single-stranded DNA sequencing reaction products, and compares the performance of this system to traditional sequencing slab-gel electrophoresis.

2. Experimental

2.1. Capillary electrophoresis apparatus

A length of polyimide-coated fused-silica capillary (Polymicro Technologies, Phoenix, AZ, USA) 55 cm long (40 cm to the detector) with a 50 μm internal diameter connects the anodic reservoir to the electrically grounded cathodic reservoir. A high-voltage power supply capable of producing up to 30 000 V (Gamma High Voltage Research, Ormand Beach, FL, USA) was used to drive the electrophoretic process. On-column fluorescence detection was performed using the optical system described below. Data were collected using a commercial chromatography data system (Model 600 Data Analysis System; Applied Biosystems, Foster City, CA, USA). Samples were introduced into the capillary using electrokinetic injection by applying a voltage of 6 kV for a period of 5 s while the cathodic end of the capillary and the cathodic electrode were immersed in the sample solution. After the sample was introduced into the capillary, the cathodic end of the capillary and the cathodic electrode were placed back into the electrophoresis buffer, and the electrophoresis voltage was applied.

The inside wall of the capillary was coated with a covalently attached layer of non-cross-linked polyacrylamide according to Cobb *et al.* [28]. A 2-mm wide detection window was formed in the capillary prior to coating by burning off the polyimide coating with a hot wire.

2.2. Capillary electrophoresis fluorescence detector

Excitation light from an argon ion laser (488 nm) (Model 221-40MLA; Cyonics, San Jose, CA, USA) was passed through a 0.5 O.D. neutral density filter (FNG 085; Melles Griot, Irvine, CA, USA) and into a set of focusing optics composed of a 64 mm focal length (F.L.), 7 mm diameter positive lens and a 85 mm F.L., 5 mm diameter negative lens, resulting in a 100 μm laser spot size incident onto the capillary. The fluorescence was collected at right angles by a 12 mm F.L. 14 mm diameter aspheric collector lens and passed through a 530 nm RDF bandpass filter (Omega Optical, Brattleboro, VT, USA). Next, the emitted light was passed through a 48 mm L.L. 19 mm diameter aspheric Fabry lens and a 17 mm F.L. 10 mm diameter spherical Fabry lens before imaging on a photomultiplier tube (R928-21; Hamamatsu, San Jose, CA, USA).

2.3. Preparation of linear polyacrylamide

Linear polyacrylamide was synthesized by standard procedures using isopropanol as a chain transfer agent to control the molecular weight of the product. 222 ml of water and 6.55 ml of

isopropanol were added to the reaction vessel, were degassed with helium, and heated to 35°C. A 25-g amount of acrylamide was dissolved in the solution. Next, 1.25 ml of 10% (v/v) N,N,N′,N′-tetramethylethylenediamine (TEMED) in water solution and 1.25 ml of a 10% (w/v) ammonium persulfate in water solution were added. The mixture was allowed to react for 1.5 h.

To remove any unreacted monomer and other small-molecule contaminants, the reaction mixture was dialysed extensively (four changes over two days) against water using a 12 000 to 14 000 molecular mass cut-off dialysis membrane (Spectra/por 2; Spectrum Medical Industries, Los Angéles, CA, USA). This product was then freeze dried to give 18 g of a white solid.

The molecular mass of the polymer was determined by gel permeation chromatography (GPC). Samples and standards were run on a Waters 590 solvent-delivery system (Milford, MA, USA) equipped with two Waters Ultrahydrogel Linear columns connected in series, and a Waters R401 differential refractometer for peak detection. Other conditions: injected sample, 80 μl of a 4 mg/ml stock; flow-rate, 0.6 ml/min; mobile phase, 100 m*M* potassium phosphate, pH 7.0. The weight-average molecular mass, M_w, and the number-average molecular mass, M_n, of the final product were determined to be 339 000 and *ca.* 100 000, respectively. Four standard polyacrylamide standards were used to calibrate the GPC (Polysciences, Warrington, PA, USA). The M_n and the M_w/M_n values of each of the standards were 465 300 and 2.45, 141 000 and 2.6, 44 400 and 1.8, 13 700 and 1.6.

The polymer solution used as the sieving network was prepared by mixing 3.5 ml buffer [220 ml water, 40 ml methanol, 5.6 g Tris titrated to pH 8.00 with 85% (w/w) phosphoric acid in water], and 2.4 g urea, giving a total volume of 5 ml. To this solution was added 0.310 g linear polyacrylamide resulting in a 6.2% (w/v) polymer solution (6.2% T)[a]. The solution was mixed for approximately 3 h and filtered through a 0.45-μm pore size syringe filter (Acrodisc; Gelman Sciences, Ann Arbor, MI, USA). Both electrode reservoirs and the capillary were then filled with the polymer solution. The viscosity of the solution used in these studies was approximately 150 cP at 25°C.

2.4. Preparation of single-color DNA sequencing ladder

A single-color sequencing ladder of fragments terminating at C was prepared by the dideoxy sequencing method using a sequencing kit and accompanying protocols from Applied Biosystems (part No. 401119). An M13mp18 DNA template (m13mp18 (+) strand, 0.1 pmol) was annealed to a fluorescent dye primer [FAM M13 (−21) primer], and primer extension was carried out using *Taq* polymerase, with dideoxycytidine provided as the 3′-terminating base. The resultant mixture was stored as a dried ethanol precipitate in the dark at −20°C.

Shortly before sample was to be loaded into the filled capillary tube, the dried sequencing reaction mixture from above was resuspended in a mixture of 5 m*M* aqueous EDTA (disodium salt) (0.5 μl) and formamide (6 μl). The solution was heated at 95°C for 2 min, and then transferred to an ice bath. The cooled solution was then directly injected onto the capillary.

2.5. Slab-gel system

A fluorescence-based gel scanner was assembled on an optical bench by using components from an Applied Biosystems Model 373 DNA sequencer. The separation distance was 33 cm (40 cm between the electrode reservoirs), the gel thickness was 250 μm and the laser spot size was 73 μm. The gels were run at a constant voltage of 1000 V (25 V/cm). 1 × TBE (see below) buffer was used in both electrode chambers.

The polyacrylamide gels contained 4% total polyacrylamide (4% T) and 5% bisacrylamide (5% T). The gels were prepared by mixing 25 g urea, 1.9 g acrylamide, and 0.1 g bisacrylamide with 5.38 g 10 × TBE (900 m*M* Tris, 900 m*M*

[a] T = (g acrylamide + g N,N′-methylenebisacrylamide)/100 ml solution.

boric acid, 10 m*M* ethylenediaminetetraacetic acid) and water. This solution was then vacuum filtered through a 0.45-μm pore size sterile filter. To the filtered solution was added 35 μl TEMED and 250 μl of a 10% (w/v) solution of ammonium persulfate. The gel was used immediately.

3. Results and discussion

Fig. 1 compares electropherograms obtained using the 6.2% T low-viscosity entangled polymer media in the capillary format to those obtained using a conventional 4% T, 5% C [a] cross-linked polyacrylamide slab gel. Each peak in Fig. 1 corresponds to a C residue in the known M13mp18 sequence. Resolution of fragments differing by a single base is evident out to 585 bases and is comparable between the two systems. However, it should be noted that there are several regions in the electropherogram where single-base resolution is lost (65, 66; 194, 196, 198; 354–356; 397, 399; 541, 543, 544). In the case of the 65, 66 pair, this loss of resolution is seen in both the CE and the slab gel data. These "compression" regions are most likely a result of secondary structure of the DNA and the lower operating temperature (25 *vs.* 30°C) used in the CE analysis, resulting in reduced denaturant efficiency leading to reduced resolving power.

Fig. 2 graphs the reduced mobility against fragment size for the entangled polymer data and for a 3% and a 4% cross-linked polyacrylamide slab gel. (The reduced mobility is defined as the ratio μ/μ_0 where μ is the mobility of the fragment in the sieving network and μ_0 is the free solution mobility derived from a plot of log μ *vs.* fragment size [29]. The reduced mobility is a convenient parameter to use to correlate electrophoretic migration data from different runs because it eliminates the influence on mobility of solvent properties such as viscosity, ionic strength, and denaturants and reflects only differences resulting from the sieving network.) The mobility *vs.* size behavior of the 6.2% polyacrylamide polymer solution system follows that of the 3% gel almost exactly up to about 200 bases, at which point the CE curve flattens out more quickly. This difference between curves probably arises from the influence of biased reptation on the CE data due to the much higher electrical fields used in CE (218 *vs.* 25 V/cm). This deviation becomes apparent at a μ/μ_0 of approximately 1/2, the point at which the migration mechanism transitions from the Ogston regime to the reptation regime [30]. Thus the sieving properties of the entangled polymer solution resemble those of a 3% cross-linked polyacrylamide gel. This is not an unexpected result. Because of the relatively broad molecular mass distribution of the linear polyacrylamide, some fraction of the polymer will be too small to participate in the entangled network [27]. Thus, the effective concentration of the network-forming polyacrylamide will be less than the bulk concentration.

A quantitative measure of separation performance is the resolution. For electrophoretic separations, the resolution, R, can be expressed as [11]

$$R = \frac{1}{4} \cdot \frac{\Delta\mu_{1,2}}{\bar{\mu}_{1,2}} \bar{N}_{1,2}^{1/2} \quad (1)$$

where $\Delta\mu_{1,2}$ is the difference in mobility between species 1 and 2, $\bar{\mu}_{1,2}$ is the average value of the mobility of species 1 and 2, and $\bar{N}_{1,2}$ is the average value of the number of theoretical plates. (The number of theoretical plates, N, is defined as $t^2/\sigma(t)^2$ where t is the migration time and $\sigma^2(t)$ is the variance of the peak in time units. The variance is related to the peak width at 1/2 the maximum peak height by the relation $2.35\sigma = w_{1/2}$.) Fig. 3 shows the resolution per base for a number of nearest-neighbor fragments in each system, where the resolution per base is calculated by dividing Eq. 1 by the difference in fragment size between the two fragments. It is clear from Fig. 3 that by this measure, the separation performance of the 6.2% entangled polymer system is essentially equivalent to that of the 4% cross-linked gel.

[a] C = g N,N'-methylenebisacrylamide/% T.

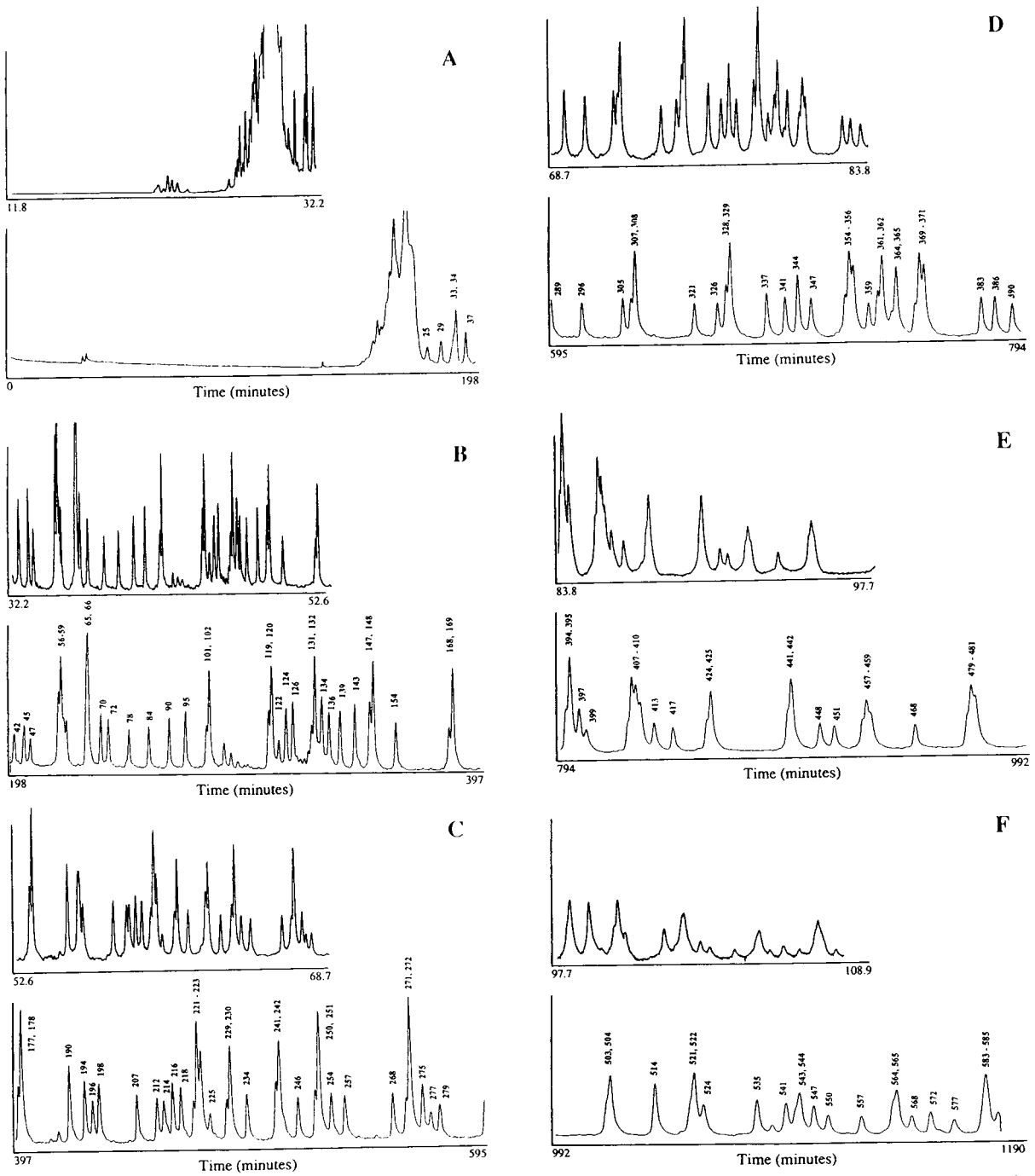

Fig. 1. Comparison of electropherograms showing the separation of C-terminated, fluorescently labeled DNA sequencing reaction products. (Top) Entangled-polymer CE. The polymer concentration was 6.2% T, 0% C linear polyacrylamide, the field strength was 218 V/cm, the current was 7.18 μA, the capillary length from the inlet to the detector window was 40 cm, and the total capillary length was 55 cm. Electrokinetic sample injection was performed at 6 kV for 5 s. (Bottom) 4% T, 5% C cross-linked polyacrylamide slab gel. The field strength was 25 V/cm, the gel length from the top of the gel to the detector window was 33 cm, and the total gel length was 40 cm. The size of each fragment in bases is indicated in the bottom panels.

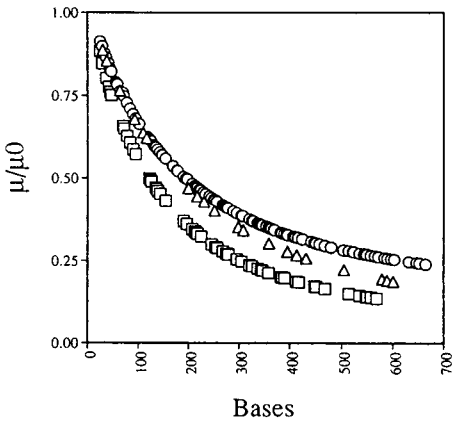

Fig. 2. Reduced electrophoretic mobility, μ/μ_0, as a function of fragment length for the entangled polymer CE system (○), a 3% cross-linked polyacrylamide slab gel (△) and a 4% cross-linked polyacrylamide slab gel (□). (μ_0 = size-independent free solution electrophoretic mobility of the fragments in each system. μ_0 is evaluated by determining the y-intercept of the linear portion of a plot of log μ *vs.* fragment length [29]. The mobilities in the entangled polymer and the 4% polyacrylamide gel system are taken from the electropherograms shown in Fig. 1. The raw data for the 3% polyacrylamide gel are not shown.

An alternative quantitative measure of the performance of a sequencing separation is the length-of-read, LOR. The LOR is defined as the point at which the peak spacing per base equals the half-height peak widths, or

$$\frac{(t_2 - t_1)}{n_2 - n_1} = \overline{w_{1,2}(t)}_{1/2} \qquad (2)$$

where t_2 and t_1 are the migration times of fragments of size n_1 and n_2, respectively, and $\overline{w_{1,2}(t)}$ is the average value of the peak width at 1/2 the maximum peak height in time units. This is a useful parameter because it allows one to compare quantitatively different electrophoresis experiments performed under greatly different conditions using a single parameter. Comparing the value of the LOR for the data in Fig. 1, LOR ≈ 450 bases for the 6.2% polyacrylamide polymer solution CE system, while LOR ≈ 450 bases for the 4% cross-linked polyacrylamide slab-gel system. Thus, it again appears that the overall performance of the 6.2% polyacrylamide polymer solution is quantitatively comparable to that of a traditional 4% cross-linked polyacrylamide slab system.

A more detailed description of the factors controlling the separation performance requires that the influence of peak width and peak spacing on resolution be independently quantified. The term $\Delta\mu_{1,2}/\bar{\mu}_{1,2}$ in Eq. 1 is a measure of the selectivity or peak spacing in a separation and is a measure of the sieving power of the network, while the term $\bar{N}_{1,2}$ in Eq. 1 is a measure of the separation efficiency or peak width and is a measure of the dispersion characteristics of the electrophoresis apparatus.

Fig. 4 shows the selectivity per base as a function of fragment size for the 6.2% polyacrylamide polymer solution CE system and the 4% cross-linked polyacrylamide slab gel. The selectivity per base is calculated by dividing the selectivity term in Eq. 1, $\Delta\mu_{1,2}/\bar{\mu}_{1,2}$, by the difference in size of the two fragments. According to Fig. 4, the selectivity per base for the 6.2% entangled polymer solution system is significantly smaller than that of the 4% polyacrylamide gel over the full spectrum of fragment sizes. The reduced selectivity is probably due to the lower effective polymer concentration in the entangled-polymer solution system re-

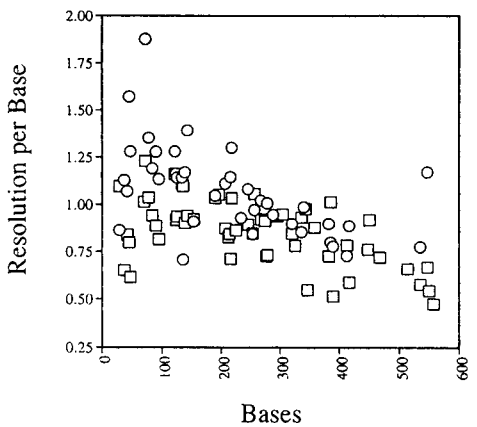

Fig. 3. Plot of resolution per base *vs.* fragment length for the entangled polymer CE system (○) and the cross-linked polyacrylamide slab gel system (□).

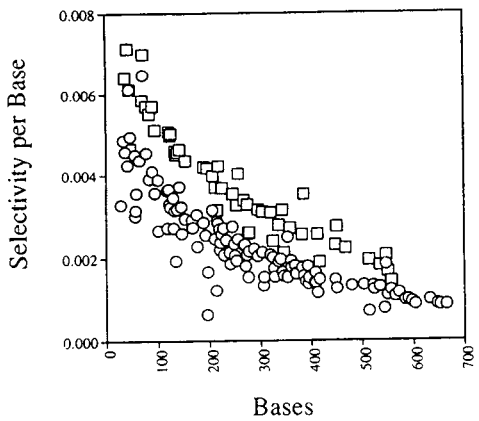

Fig. 4. Selectivity per base as a function of fragment length for the entangled polymer CE system (○) and the 4% cross-linked polyacrylamide slab gel system (□). Mobility data were taken from electropherograms in Fig. 1.

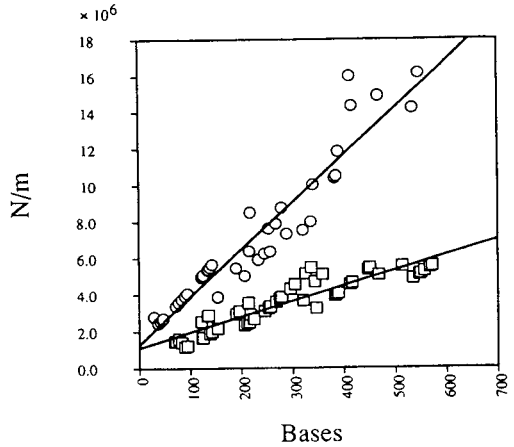

Fig. 5. Number of theoretical plates per meter as a function of fragment length for the entangled polymer CE system (○) and the crosslinked polyacrylamide slab system (□). The lines through each data set results from a linear least squares best fit of the data. Entangled polymer: slope = 25 900, y-intercept = 1 270 000, $r^2 = 0.91$; polyacrylamide gel data, slope = 8370, y-intercept = 1 120 000, $r^2 = 0.84$.

sulting from the molecular weight distribution of the polyacrylamide. Thus, the resolution achieved in Fig. 1 must be due to very sharp peaks, or high efficiency, relative to those obtained in traditional cross-linked polyacrylamide slab-gel electrophoresis.

The next aspect of the resolution to consider is the peak width, or peak efficiency. By dividing N by the separation distance, L, one gets the number of plates per unit separation distance, N/m, a parameter independent of migration distance. Fig. 5 shows a plot of the peak efficiency as a function of fragment length for the 6.2% polyacrylamide polymer solution system and the cross-linked polyacrylamide slab gel system. First, in both the CE and the slab data, it is important to note the linear relationship between N/m and the fragment size. This relationship implies that the time-dependent component of band broadening is due primarily to longitudinal diffusion [29]. This assumption will be exploited in the following analysis.

The next aspect of Fig. 5 to consider is the superior separation efficiency of the CE system. From the ratio of the slopes of the curves in Fig. 5, the efficiency of the CE separation is a factor of 3.1 times higher than the slab system. The superior efficiency of the CE system can be described quantitatively. The ratio of the efficiencies of the two systems is given by the expression

$$\frac{N/\mathrm{m}_{\mathrm{CE}}}{N/\mathrm{m}_{\mathrm{slab}}} = \left(\frac{L_{\mathrm{CE}}}{L_{\mathrm{slab}}}\right) \cdot \left(\frac{\sigma^2_{\mathrm{slab}}}{\sigma^2_{\mathrm{CE}}}\right) \tag{3}$$

Assuming diffusional band broadening,

$$\sigma^2 = 2Dt = \frac{2DL}{v} = \frac{2DL}{\mu E} \tag{4}$$

where D is the longitudinal diffusion coefficient, v is the electrophoretic velocity and E is the electrical field strength. Furthermore, from the Stokes–Einstein relationship and the definition of the electrophoretic mobility,

$$D = \frac{kT}{f} \tag{5}$$

and

$$\mu = \frac{q}{f} \tag{6}$$

where k is Boltzmann's constant, f is the translational friction coefficient, and q is the net charge

of the analyte. Combining Eqs. 4, 5 and 6 results in the expression

$$\sigma^2 = \frac{2LkT}{qE} \tag{7}$$

Therefore, the expected ratio of separation efficiencies of the capillary and the slab systems is

$$\frac{N/m_{CE}}{N/m_{slab}} = \left(\frac{T_{slab}}{T_{CE}}\right) \cdot \left(\frac{q_{CE}}{q_{slab}}\right) \cdot \left(\frac{E_{CE}}{E_{slab}}\right) \tag{8}$$

Each of the parameters in Eq. 8 can be easily determined except the value of q. The evaluation of q is complicated by the fact that the buffer ions used in the two systems are different, resulting in different degrees of charge shielding. However, the value of q for each fragment can be determined from the measured values of σ and μ. Combining Eqs. 5 and 6 results in the expression

$$q = \frac{\mu kT}{D} \tag{9}$$

Furthermore, substituting Eq. 4 into Eq. 9 to eliminate D gives

$$q = \frac{2\mu kTt}{\sigma^2} \tag{10}$$

Therefore, by measuring μ, t and σ for each fragment, a value of q can be determined. Based on measurements of over 30 fragments ranging in size from 100 to 500 bases, the average values for the net electrical charge per base is 0.177 e^- (R.S.D. = 19%) for the slab system and 0.069 e^- (R.S.D = 5.2%) for the CE system. The larger scatter in the slab data is probably due to the changing ionic composition and temperature of a slab gel during a run.

Insertion of the above values for q, and measured values for T_{slab} (30°C) and T_{CE} (25°C) into Eq. 8 results in an expected value of 3.4 for the ratio of efficiencies. Given the uncertainties of the measured parameters, this value agrees well with the measured value of 3.1 determined from Fig. 5.

4. Summary and conclusion

In summary, we have demonstrated that low viscosity entangled polymer solutions used in the capillary electrophoresis format can serve as an alternative sieving matrix for the electrophoretic separation of DNA sequencing fragments. Overall performance is comparable to that of a traditional cross-linked gel in a slab format in terms of both resolution and length of read. Although the separation selectivity of the entangled polymer preparation used here is inferior to that of the cross-linked gel, it is made up for by superior separation efficiency compared to a 0.4 mm thick slab. The enhanced separation efficiency achieved in the CE system agrees with theoretical predictions.

Low-viscosity, flowable media coupled with the capillary electrophoresis format make possible the opportunity for truly continuous and automated electrophoretic analysis of DNA sequencing extension products. By eliminating the time involved in the pouring of gels and automating the sample loading step, this approach will have a substantial impact on the overall throughput of DNA sequencing operations. Coupled with multi-capillary detection schemes [10], this type of medium should provide the basis for very-high-throughput sequencing technologies. In addition, the reproducibility of these systems should be superior to individually prepared gels. Further increases in the speed and resolution of these systems should be possible through optimization of the polymer solutions in terms of reduced solution viscosity, increased separation selectivity and reduced ionic strength.

5. Acknowledgements

The author wishes to thank Sam Woo for invaluable assistance in developing the protocols used to coat the inside surface of the capillary tubes, Charles Connell, George Golda, Steve Hurwitz, Dennis Mead, Mark Oldham and Yefim Raysberg for assisting in the construction of the experimental apparatus, Mitchell Winnik

(University of Toronto) for characterization of the polymer, Steven Menchen for many helpful discussions, and Joel Colburn, Mel Kronick, Bill Efcavitch and Will Bloch for reviewing the manuscript prior to submission.

6. References

[1] H. Drossman, J.A. Luckey, A.J. Kostichka, J. D'Cunha and L.M. Smith, *Anal. Chem.*, 62 (1990) 900.
[2] H. Swerdlow and R. Gesteland, *Nucleic Acids Res.*, 18 (1990) 1415.
[3] A.S. Cohen, D.R. Najarian and B.L. Karger, *J. Chromatogr.*, 516 (1990) 49.
[4] H. Swerdlow, S. Wu, H. Harke and N.J. Dovichi, *J. Chromatogr.*, 516 (1990) 61.
[5] H. Swerdlow, J.Z. Zhang, D.Y. Chen, H.R. Harke, R. Grey, S. Wu, N.J. Dovichi and C. Fuller, *Anal. Chem.*, 63 (1991) 2835.
[6] R.J. Zagursky and R.M. McCormick, *Biotechniques*, 9 (1990) 74.
[7] H.F. Yin, J. Lux and G. Schomburg, *J. High Resolut. Chromatogr.*, 13 (1990) 624.
[8] J.A. Luckey, H. Drossman, A.J. Kostichka, D.A. Mead, J. D'Cunha, T.B. Norris and L.M. Smith, *Nucleic Acids Res.*, 18 (1990) 4417.
[9] Y. Baba and M. Tsuhako, *Trends Anal. Chem.*, 11 (1992) 280.
[10] X.C. Huang, M.A. Quesada and R.A. Mathies, *Anal. Chem.*, 64 (1992) 967.
[11] P.D. Grossman, in P.D. Grossman and J.C. Colburn (Editors), *Capillary Electrophoresis: Theory and Practice*, Academic Press, San Diego, CA, 1992, Ch. 1.
[12] A. Guttman, A.S. Cohen, D.N. Heiger and B.L. Karger, *Anal. Chem.*, 62 (1990) 137.
[13] B.L. Karger and A.S. Cohen, *US Pat.*, 4 865 706 (1989); *US Pat.*, 4 865 707 (1989).
[14] B.J. Radola, *Electrophoresis*, 1 (1980) 43.
[15] P.F. Bente and J. Myerson, *US Pat.*, 4 810 456 (1989).
[16] A. Paulus, E. Gassmann and M.J. Field, *Electrophoresis*, 11 (1990) 702.
[17] A. Paulus and J.I. Ohms, *J. Chromatogr.*, 507 (1990) 113.
[18] A.S. Cohen, S. Carson, A. Belenkii and B.L. Karger, presented at the *4th International Symposium on High Performance Capillary Electrophoresis, Amsterdam, February 9–13, 1992.*
[19] M. Zhu, D.L. Hansen, S. Burd and F. Gannon, *J. Chromatogr.*, 480 (1989) 311.
[20] A.M. Chin and J.C. Colburn, *Am. Biotech. Lab./News Ed.*, 7 (1989) 10A.
[21] H.E. Schwartz, K. Ulfelder, F.J. Sunzeri, M.P. Busch and R.G. Brownlee, *J. Chromatogr.*, 559 (1991) 267.
[22] K.J. Ulfelder, H.E. Schwartz, J.M. Hall and F.J. Sunzeri, *Anal. Biochem.*, 200 (1992) 260.
[23] M. Strege and A. Lagu, *Anal. Chem.*, 63 (1991) 1233.
[24] P. Boček and A. Crambach, *Electrophoresis*, 13 (1992) 31.
[25] T. Guszczynski and A. Crambach, *Biochem. Biophys. Res. Commun.*, 179 (1991) 482.
[26] J.A. Burroughs and A. Crambach, *Biochem. Biophys. Res. Commun.*, 180 (1991) 1070.
[27] P.D. Grossman and D.S. Soane, *Biopolymers*, 31 (1991) 1221.
[28] K.A. Cobb, V. Polnik and M. Novotny, *Anal. Chem.*, 62 (1990) 2478.
[29] P.D. Grossman, S. Menchen and D. Hershey, *Genetic Analysis: Techniques and Applications*, 9 (1992) 9.
[30] G.W. Slater, J. Rousseau, J. Noolandi, C. Trumel and M. Lalande, *Biopolymers*, 27 (1988) 509.

ELSEVIER

Journal of Chromatography A, 663 (1994) 229–237

JOURNAL OF CHROMATOGRAPHY A

Capillary zone electrophoresis of eleven priority phenols with indirect fluorescence detection

Ying-Chieh Chao, Chen-Wen Whang*

Department of Chemistry, Tunghai University, Taichung 40704, Taiwan

(First received September 20th, 1993; revised manuscript received November 30th, 1993)

Abstract

A scheme for the separation and detection of eleven priority phenols using capillary zone electrophoresis (CZE) coupled with laser-induced indirect fluorimetry is described. With a 50 cm × 20 μm I.D. capillary at 9 kV and an electrophoretic buffer of 15 m*M* sodium borate (pH 9.9) containing 1 m*M* fluorescein, complete separation of the eleven compounds can be performed in less than 14 min. Linearity over two orders of magnitude of concentration was generally obtained and limits of detection for the priority phenols were in the ppb (10^{-6}–10^{-7} *M*) range. Quantitative applicability of CZE–indirect fluorimetry was demonstrated by analysing the standard reference material NIST SRM 1584 (priority pollutant phenols in methanol). The method was also applied to the determination of phenols in industrial wastewaters.

1. Introduction

Phenolic compounds are of great environmental concern owing to their high toxicity. The US Environmental Protection Agency (EPA) has listed eleven phenols as organic priority pollutants [1], *viz.*, phenol, 2-nitrophenol (2-NP), 4-nitrophenol (4-NP), 2,4-dinitrophenol (2,4-DNP), 2-chlorophenol (2-CP), 2,4-dichlorophenol (2,4-DCP), 2,4-dimethylphenol (2,4-DMP), 4-chloro-3-methylphenol (4-C-3-MP), 2-methyl-4,6-dinitrophenol (2-M-4,6-DNP), 2,4,6-trichlorophenol (2,4,6-TCP) and pentachlorophenol (PCP). Their concentration level in the environment needs to be constantly monitored.

Both gas chromatography (GC) and high-performance liquid chromatography (HPLC) have been the commonly used techniques for analyses for phenols. In order to enhance the volatility and detectability of phenols, sample derivatization is often necessary prior to GC analysis. In general, GC methods suffer from disadvantages such as lengthy sample preparation time and incomplete recoveries for many phenolic derivatives. Alternatively, HPLC is an advantageous technique and the polarity of phenols and their low vapour pressure, factors that complicate GC analysis, do not have adverse effects on HPLC analysis. HPLC with either isocratic [2,3] or gradient elution [4,5] has been widely used to separate substituted phenols. Ultraviolet (UV) detection is commonly employed as phenols possess strong absorption bands in the UV region. Better sensitivity can be achieved by employing electrochemical detection [2,6].

In the past few years, capillary electrophoresis (CE) has been shown to be a fast, powerful, and efficient separation technique for a variety of

* Corresponding author.

0021-9673/94/$07.00
SSDI 0021-9673(93)E1277-7

compounds [7]. These characteristics are the direct result of the use of a high separation voltage and rapid dissipation of Joule heat in a narrow capillary, typically 25–100 μm I.D. In capillary zone electrophoresis (CZE), a capillary is filled with a buffer solution for the separation of only charged analytes, and neutral substances cannot in principle be separated by conventional CZE. Micellar electrokinetic capillary chromatography (MECC), in which ionic surfactants are added to the CZE buffer at concentrations exceeding the critical micelle concentration (cmc), has extended the enormous power of CZE to the separation of both charged and uncharged solutes [8,9]. The analysis of a series of chlorophenols [8–10] and eleven priority phenols [11] using MECC with UV detection has been demonstrated. An analysis time of *ca.* 45 min was required to separate the eleven priority phenols and the detection levels were in the nanogram range. However, CE with on-column UV detection generally suffers from the disadvantages that the sensitivity is limited by the short optical path length as a result of the use of small I.D. capillaries and the need for chromophoric analyte molecules.

Recently, fluorescence detection, particularly laser-induced fluorimetry, has become popular mainly because of its capability to provide extremely high sensitivity. Detection limits of 10^{-21} mol of fluorescein isothiocyanate-labelled amino acids have been reported [12]. However, a drawback of this detection mode is the need to derivatize most analytes because only a few compounds show native fluorescence. An alternative to derivatizing non-fluorescent substances is the use of indirect detection techniques. The application of indirect fluorimetry in CZE has been reviewed recently [13]. In brief, a non-interacting, fluorescing ion is added to the running buffer to create a constant fluorescence background. When a charged analyte is present, it displaces the fluorescing ion of the same charge due to local charge neutrality, resulting in a decreased background signal even though the analyte does not absorb or fluoresce. Indirect fluorimetry has been applied in CZE for the detection of metal ions [14,15], sugars [16], amino acids [17], peptides [18], nucleotides [19] and DNA restriction fragments [20], and in MECC for the detection of aliphatic alcohols and some phenolic compounds [21].

In this paper, a scheme for the separation and detection of the eleven priority phenols using free solution CZE coupled with indirect fluorescence detection is described. Fluorescein was added to the running buffer as the fluorescing ion and an argon ion laser was used to induce the fluorescence background. Detection limits, linearity and reproducibility were examined. Application of the method to the analysis of priority phenols in industrial wastewaters is also described.

2. Experimental

2.1. Apparatus

The CZE system was assembled in-house. A high-voltage power supply (Model PS/MJ30P0400-11; Glassman High Voltage, Whitehouse Station, NJ, USA) was used to generate the potential across the capillary. Fused-silica capillaries (Polymicro Technologies, Phoenix, AZ, USA) were of 50 cm total length × 20 μm I.D. × 360 μm O.D. Before use, the capillary was washed (pressurized flow) with 0.1 *M* NaOH for 15 min, followed by a 2-min rinse with water and a 2-min flush with the running buffer. The capillary was then equilibrated with the buffer under an electric field of 200 V cm^{-1} for 2 h. Samples were injected by either electromigration or gravity flow injection. Electromigration was used when obtaining migration times for peak identification. Gravity flow injection was used when quantitative measurements of peaks were made.

On-column detection was performed using indirect fluorimetry. A small region of the polymer coating was burned off 5 cm from the cathodic end of the capillary to form a detection window. An argon ion laser (Model ILT-5000; Ion Laser Technology, UT, USA) operating in the light-regulated mode at 10 mW for all lines was used for excitation. The 488-nm beam (about 40% of the total power) was selected with an interference filter (peak wavelength 488 nm,

effective bandwidth 10 nm) (Edmund Scientific, Barrington, NJ, USA). The laser light was focused into the capillary with a 1-cm focal length lens. The capillary was mounted at Brewster's angle to reduce scattered radiation. Background fluorescence emitted from the fluorophore in the CZE buffer was collected with a 10× microscope objective and passed through a 520-nm interference filter (effective bandwidth 10 nm; Edmund Scientific). The fluorescent image was focused on to a silicon photodiode (Model S2281-01; Hamamatsu, Hamamatsu City, Japan) connected with a current amplifier (Model S2719; Hamamatsu). The high background output from the detector was first lowered with a laboratory-built voltage offset circuit, followed by passing through a 1-s *RC* low-pass filter. The data were collected using a Macintosh SE computer connected with a MacLab/4 data acquisition interface (Analog Digital Instruments, NSW, Australia).

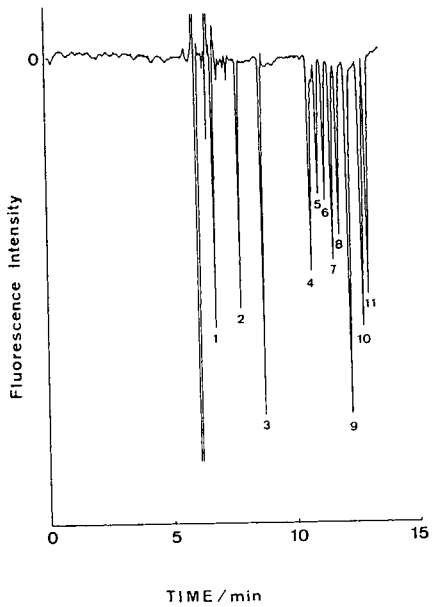

Fig. 1. Electropherogram of the eleven priority phenols with indirect fluorescence detection. Conditions are given in Table 1.

2.2. Chemicals

All phenols were purchased from Supelco (Bellefonte, PA, USA) and used as received. Laser-grade fluorescein was obtained from Eastman Kodak (Rochester, NY, USA). Standard reference material for priority pollutant phenols, SRM 1584, was purchased from the National Institute of Standards and Technology (NIST, Gaithersburg, MD, USA). All other chemicals were of analytical-reagent grade. Distilled water was further purified by passing it through a NANOpure II deionization system (Sybron-Barnstead, Boston, MA, USA). All solutions were filtered through a 0.45-μm pore-size membrane filter before use.

3. Results and discussion

3.1. Separation and detection of the eleven priority phenols

The electropherogram in Fig. 1 shows the separation and detection of the eleven priority phenols using CZE and indirect fluorescence detection. All components of the test mixture are baseline resolved. The large derivative peak at *ca.* 6 min was due to methanol, which was the solvent used for preparing the stock solutions of phenols. Note that all eleven compounds elute within 14 min of injection, which is to be compared to the 25 and 45 min typically needed using HPLC [3] and MECC [11], respectively. The concentrations of the eleven phenols in Fig. 1 are given in Table 1, together with their migration times. The repeatabilities of the migration times for the eleven phenols are good, with relative standard deviations (R.S.D.s) all less than 1%, based on fifteen replicate determinations.

The separation efficiency, represented by the number of theoretical plates, N, was calculated from the peak half-width for each phenol. The peak width and hence the efficiency were found to be governed by both the separation voltage and the duration of injection. With a separation voltage of 9 kV and an electromigration injection time of 2 s, N ranged from 187 000 for phenol to 99 000 for 2,4-DNP (see Table 1).

It is interesting that the elution order of the eleven phenols found in CZE is opposite to that

Table 1
Concentrations, migration times and efficiencies of the eleven phenols in Fig. 1

Peak No.	Compound	Concentration (μg ml^{-1})	Migration time (min)	R.S.D.[a] (%)	N ($\times 10^4$)
1	2,4-DMP	25.2	6.89	0.74	10.6
2	Phenol	0.2	7.94	0.69	18.7
3	4-C-3-MP	0.9	8.89	0.72	11.4
4	PCP	10.8	10.84	0.87	11.9
5	2,4,6-TCP	0.4	11.16	0.87	12.6
6	2,4-DCP	0.4	11.43	0.88	11.1
7	2-M-4,6-DNP	3.6	11.72	0.99	10.3
8	2-CP	0.4	11.98	0.87	12.5
9	2,4-DNP	7.2	12.36	0.90	9.9
10	4-NP	7.2	12.88	0.90	10.8
11	2-NP	10.8	13.09	0.95	11.2

Conditions: column, 50 cm total length (45 cm to the window) × 20 μm I.D.; buffer, 15 mM sodium borate (pH 9.9) containing 1 mM fluorescein; injection, 2 s at 9 kV; electrophoresis, 2.8 μA at 9 kV.
[a] Relative standard deviation of migration times ($n = 15$).

obtained by Ong *et al.* [11] using MECC with a neutral buffer (pH 6.6). For example, 2,4-DMP, phenol and 4-C-3-MP, which are the first three peaks in Fig. 1, were eluted last by MECC, while 4-NP and 2-NP, which are the last in Fig. 1, were eluted first by MECC. This is understandable because the separation mechanisms of CZE and MECC are basically different. The separation in CZE is based on the differences in the electrophoretic mobilities resulting in different velocities of migration of ionic species in the electrophoretic buffer contained in the capillary. Therefore, the separation mechanism in Fig. 1 is mainly based on differences in size and charge of the eleven phenols at a given pH. On the other hand, the main separation mechanism in MECC is based on solute partitioning between the micellar phase and the solution phase. A combination of charge/mass ratios, hydrophobicity and charge interactions at the surface of the micelles combine to affect the separation of the analytes.

In order to improve the efficiency of charge displacement and therefore the sensitivity in indirect fluorescence detection, a buffer with low ionic strength, or preferably a low concentration of fluorescing ion as part of the buffer, has been recommended [13]. However, we found that, in addition to the buffer pH, a relatively high concentration (>10 mM) of borate in the electrophoretic buffer was crucial in the separation of the eleven phenols. With lower borate concentrations, complete separation of the eleven phenols was not possible. This is probably because the electroosmotic velocity is inversely proportional to ionic concentration [22]. Decreasing the buffer concentration induces an increase in electroosmotic velocity, which is generally detrimental to the CZE separation of analytes with similar electrophoretic mobilities. On the other hand, the increase in the concentration of background electrolyte will have an adverse effect on the sensitivity of indirect detection. In principle, a highly sensitive indirect fluorescence signal requires a high transfer ratio (TR, defined as the number of background fluorophore ions displaced by one analyte ion [13]). Unfortunately, borate anions also can be displaced along with fluorescein, which results in a loss of sensitivity. The electrophoretic buffer in Fig. 1 was a solution of 15 mM sodium borate (pH 9.9) containing 1 mM fluorescein as the background fluorophore, which represents a compromise between optimum peak resolution and satisfactory detection sensitivity.

During the investigation of the optimum fluorophore concentration, we also found that the direction of some peaks was affected by both

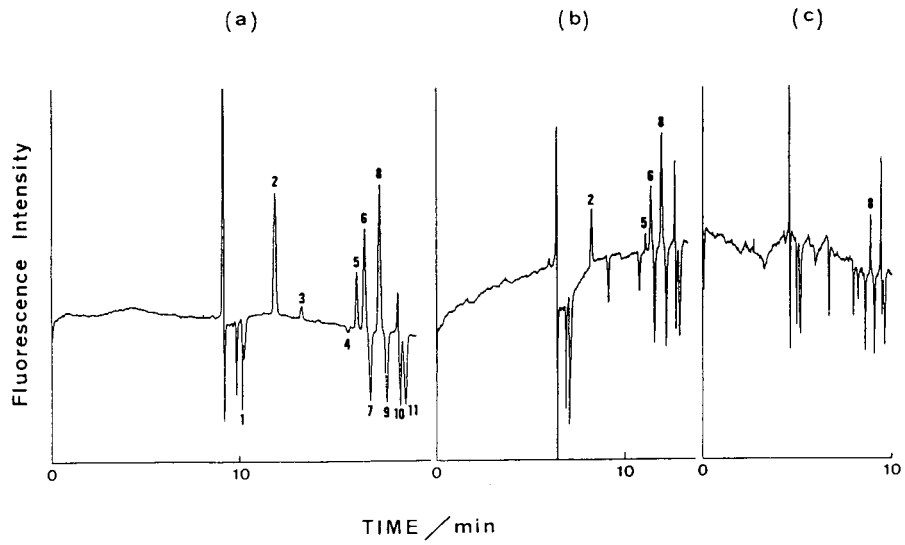

Fig. 2. Electropherograms of phenols obtained under different electric fields with a buffer containing 0.1 m*M* fluorescein: (a) 120; (b) 180; (c) 240 V cm^{-1}. Peak identities and conditions as in Table 1.

electric field and fluorescein concentration. These phenomena are illustrated in Figs. 2 and 3. With a fluorescein concentration of 0.1 m*M* and an electric field of 120 V cm^{-1}, five phenols, *viz.*, phenol, 4-C-3-MP, 2,4,6-TCP, 2,4-DCP and 2-CP, showed positive peaks (Fig. 2a). An increase in field strength caused a gradual reverse of peak position (Fig. 2b), and only the 2-CP

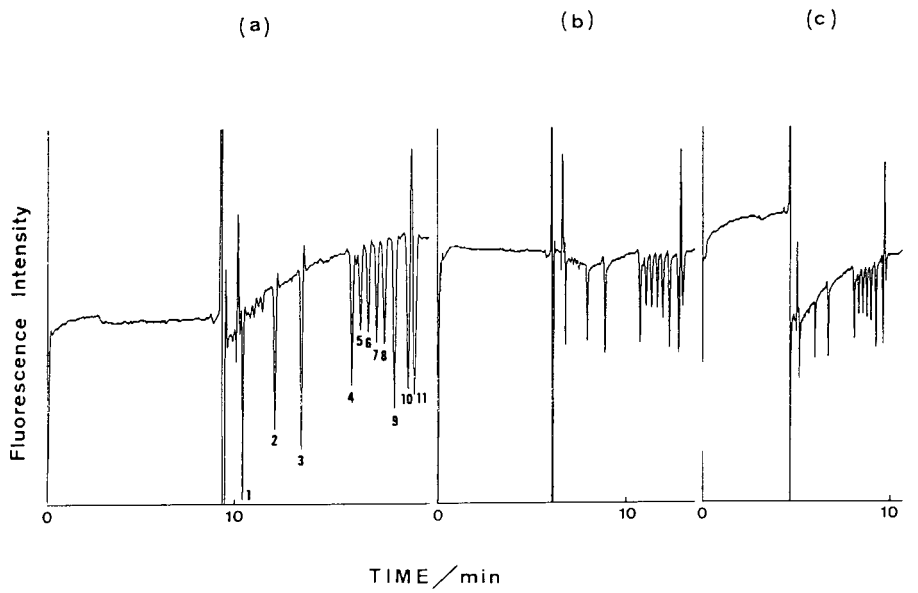

Fig. 3. Electropherograms of phenols obtained under different electric fields with a buffer containing 1 m*M* fluorescein: (a) 120; (b) 180; (c) 240 V cm^{-1}. Peak identities and conditions as in Table 1.

peak was positive-going at a field strength of 240 V cm^{-1} (Fig. 2c). This trend was not observed if the fluorescein concentration was raised to 1 m*M* (Fig. 3). Positive peaks indicate an increase in the concentration of the background fluorophore present at the detector, while negative peaks indicate a decrease. Negative peaks in indirect detection (positive displacement) have positive *TR* values [13], and therefore *TR* values for positive peaks (negative displacement) must carry a minus sign. The negative *TR* values found for those phenols cannot be accounted for by the simple indirect detection theory. Negative *TR* values have also been reported by Williams *et al.* [23] in the indirect absorbance detection of tetraalkylammonium compounds. However, the detailed mechanism behind negative displacement (positive peaks) in indirect detection is not fully understood and further study in this respect is needed.

3.2. Calibration graphs for the eleven priority phenols

A series of solution mixtures containing known amounts of the eleven phenols were prepared using the electrophoretic buffer as the solvent. These standard solutions were used for the construction of calibration graphs. Samples were injected by gravity flow at a 12-cm height for 20 s. The results are summarized in Table 2. Within the concentration range studied, a good linear correlation ($r \geq 0.99$) between peak height and concentration was obtained for each species. The linear dynamic range generally covered more than two orders of magnitude of concentration. The linearity obtained by electromigration injection (2 s at 9 kV) was poorer, covering less than two orders of magnitude of concentration. Similar results were obtained if peak areas were used for regression analysis. From the slopes of the regression lines listed in Table 2, considerably higher sensitivity was obtained for phenol, 4-C-3-MP, 2,4,6-TCP, 2,4-DCP and 2-CP. This is probably due to fluorescence quenching by phenol and chlorophenols (via the external heavy atom effect [24]) on the fluorescein, which further decreases the background fluorescence. Phenols have been shown to have a strong quenching effect on quinine fluorescence [21].

The reproducibility was examined by seven replicate injections of each compound at a concentration corresponding to the lower limit of the calibration line. The R.S.D.s on peak heights

Table 2
Calibration data for the eleven priority phenols

Peak No.	Compound	Linear range ($\mu g\ ml^{-1}$)	Slope (mV ml μg^{-1})	Intercept (mV)	r^a	R.S.D.[b] (%)	LOD[c] ($\mu g\ ml^{-1}$)
1	2,4-DMP	1.61–57.60	2.7	+3.5	0.997	3.2	0.75
2	Phenol	0.01– 3.69	195.8	+14.3	0.986	2.7	0.01
3	4-C-3-MP	0.06– 9.22	64.0	+7.5	0.988	4.3	0.02
4	PCP	0.69–57.60	4.5	+2.9	0.999	3.7	0.48
5	2,4,6-TCP	0.02– 3.69	73.0	+8.2	0.992	6.3	0.02
6	2,4-DCP	0.02– 3.69	67.6	+11.7	0.993	4.3	0.02
7	2-M-4,6-DNP	0.23–57.60	13.9	+3.6	0.999	4.9	0.17
8	2-CP	0.02– 3.69	137.2	+4.0	0.996	4.7	0.02
9	2,4-DNP	0.46–36.00	8.3	+13.1	0.990	5.9	0.15
10	4-NP	0.46–57.60	4.6	+3.3	0.998	5.2	0.38
11	2-NP	0.69–57.60	4.2	+1.4	0.992	2.8	0.33

Gravity flow injection at 12-cm height for 20 s; other conditions as in Table 1.
[a] Correlation coefficients ($n = 7$).
[b] Based on seven measurements with replicate injections of each compound at the concentration corresponding to the lower limit of the calibration line.
[c] Signal-to-noise ratio = 3.

ranged from 2.7% for phenol to 6.3% for 2,4,6-TCP. The R.S.D.s on peak areas were slightly larger (4.7–9.2%), which was probably due to the lower accuracy of the integration data at concentrations near the detection limits. The limits of detection (LOD) listed in Table 2 were calculated based on a ratio of the signal to the background noise level of 3, which range from 0.01 μg ml^{-1} (0.11 μM) for phenol to 0.75 μg ml^{-1} (6.14 μM) for 2,4-DMP. These values are in agreement with the LOD levels achievable with CZE–indirect fluorimetry [13], and are much better than those with UV detection [11]. An electropherogram of the eleven phenols at concentrations close to their respective LODs are given in Fig. 4.

3.3. Applications

In order to validate the method, the concentrations of the eleven phenols were determined in a standard reference material, NIST SRM 1584 (priority pollutant phenols in methanol). For the determination of phenol, 4-C-3-MP, 2,4,6-TCP, 2,4-DCP and 2-CP, which possess a higher detection sensitivity, the sample was diluted 250-fold with the electrophoretic buffer before analysis. For determining the others, the sample was diluted tenfold prior to analysis. Quantification of each compound was performed using the calibration lines constructed simultaneously with the analysis of sample. The results are given in Table 3, along with the certified values for the eleven phenols. The experimental results are in good agreement with the certified values for most phenols, but not phenol, 2,4-DCP and 2-CP. One of the reasons for the larger deviations of these three is probably the larger dilution factor, which amplifies the experimental errors. Nevertheless, the results in Table 3 clearly demonstrate the applicability of CZE–indirect fluorimetry to the determination of phenols.

The method was applied to the determination of priority phenols in two industrial wastewater samples taken from a coke plant, one an untreated wastewater and the other an effluent

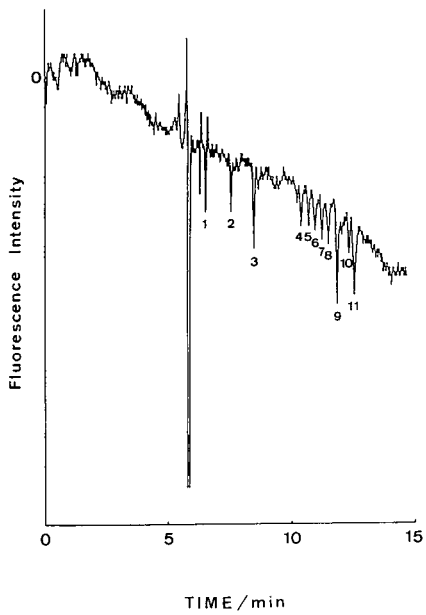

Fig. 4. Electropherogram of the eleven priority phenols at trace levels. Gravity flow injection at a 12-cm height for 20 s; the concentration of each compound corresponds to the lower limit of the respective calibration line in Table 2. Other conditions as in Table 1.

Table 3
Determination of the eleven phenols in NIST SRM 1584 by CZE–indirect fluorimetry

Compound	Concentration (μg ml^{-1})	
	Experimental[a]	Certified
2,4-DMP	51.1 ± 2.9	51.6 ± 0.2
Phenol	33.2 ± 1.4[b]	29.7 ± 0.9
4-C-3-MP	26.8 ± 0.9[b]	27.4 ± 0.9
PCP	16.8 ± 0.9	15.4 ± 1.1
2,4,6-TCP	19.8 ± 0.5[b]	20.4 ± 1.9
2,4-DCP	31.9 ± 0.9[b]	35.6 ± 1.3
2-M-4,6-DNP	23.2 ± 1.0	20.1 ± 0.9
2-CP	73.8 ± 1.0[b]	64.4 ± 1.4
2,4-DNP	23.9 ± 1.2	22.4
4-NP	20.9 ± 2.7	20.7 ± 0.7
2-NP	23.9 ± 2.6	25.2 ± 0.7

Conditions as in Table 2.

[a] Uncertainties are given as 95% confidence intervals about the mean ($n = 5$). Before analysis, sample was diluted tenfold with the electrophoretic buffer.

[b] The sample was diluted 250-fold with the electrophoretic buffer.

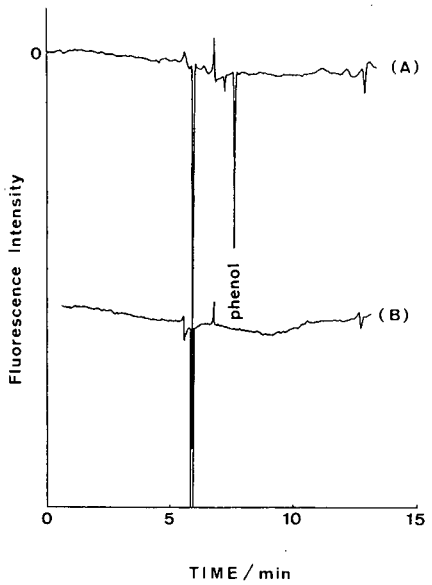

Fig. 5. Electropherograms of (A) an untreated industrial wastewater sample (500-fold dilution) and (B) a treated wastewater sample (tenfold dilution). Conditions as in Table 1.

from the microbiological treatment plant. Both samples were first filtered through a 0.45-μm membrane filter. For the untreated wastewater sample, a 500-fold dilution with the electrophoretic buffer was made before analysis. A typical electropherogram obtained for the untreated wastewater is shown in Fig. 5A. Only phenol could be found in this sample. No interferences from the impurities present in the sample were observed. The concentration of phenol in this untreated wastewater was determined to be 269 ± 8 μg ml^{-1}, based on five replicate analyses. Fig. 5B shows the electropherogram obtained from the treated wastewater sample. This sample was diluted tenfold with the electrophoretic buffer before analysis. No phenol was found in the effluent after microbiological treatment.

4. Conclusions

CZE with laser-induced indirect fluorimetry can provide rapid separation and sensitive detection of the eleven priority phenols. Complete separation of the eleven compounds can be achieved in *ca.* 14 min using an electrophoretic buffer of 15 m*M* sodium borate (pH 9.9) containing 1 m*M* fluorescein. Linearity of the calibration graphs over two orders of magnitude of concentration was generally obtained and the limits of detection were in the ppb (10^{-6}–10^{-7} *M*) range. Quantitative applicability of the CZE–indirect fluorimetry method was demonstrated by analysing the standard reference material NIST SRM 1584. The method was successfully applied to the determination of priority phenols in industrial wastewaters.

5. Acknowledgement

Financial support from the National Science Council of Taiwan is gratefully acknowledged.

6. References

[1] *Sampling and Analysis Procedures for Screening of Industrial Effluents for Priority Pollutants*, US Environmental Protection Agency, Environment Monitoring and Support Laboratory, Cincinnati, OH, 1977.
[2] C.W. Whang, *J. Chin. Chem. Soc. (Taipei)*, 34 (1987) 81.
[3] H.K. Lee, S.F.Y. Li and Y.H. Tay, *J. Chromatogr.*, 438 (1988) 429.
[4] S. Hussain and M. Kifayatulla, *J. Chromatogr.*, 168 (1979) 517.
[5] D.N. Armentrout, J.D. McLean and M.W. Long, *Anal. Chem.*, 51 (1979) 1039.
[6] R.E. Shoup and G.S. Mayer, *Anal. Chem.*, 54 (1982) 1164.
[7] W.G. Kuhr and C.A. Monnig, *Anal. Chem.*, 64 (1992) 389R.
[8] S. Terabe, K. Otsuka, K. Ichikawa, A. Tsuchiya and T. Ando, *Anal. Chem.*, 56 (1984) 111.
[9] S. Terabe, K. Otsuka and T. Ando, *Anal. Chem.*, 57 (1985) 834.
[10] M.G. Khaledi, S.C. Smith and J.K. Strasters, *Anal. Chem.*, 63 (1991) 1820.
[11] C.P. Ong, C.L. Ng, N.C. Chong, H.K. Lee and S.F.Y. Li, *J. Chromatogr.*, 516 (1990) 263.
[12] S. Wu and N.J. Dovichi, *J. Chromatogr.*, 480 (1989) 141.
[13] E.S. Yeung and W.G. Kuhr, *Anal. Chem.*, 63 (1991) 275A.

[14] L. Gross and E.S. Yeung, *Anal. Chem.*, 62 (1990) 427.
[15] L. Gross and E.S. Yeung, *J. Chromatogr.*, 480 (1989) 169.
[16] T. Garner and E.S. Yeung, *J. Chromatogr.*, 515 (1990) 639.
[17] W.G. Kuhr and E.S. Yeung, *Anal. Chem.*, 60 (1988) 1832.
[18] B.L. Hogan and E.S. Yeung, *J. Chromatogr. Sci.*, 28 (1990) 15.
[19] W.G. Kuhr and E.S. Yeung, *Anal. Chem.*, 60 (1988) 2642.
[20] K.C. Chan, C.W. Whang and E.S. Yeung, *J. Liq. Chromatogr.*, 16 (1993) 1941.
[21] L.N. Amankwa and W.G. Kuhr, *Anal. Chem.*, 63 (1991) 1733.
[22] T. Tsuda, K. Nomura and G. Nakagawa, *J. Chromatogr.*, 248 (1982) 241.
[23] S.J. Williams, E.T. Bergström, D.M. Goodall, H. Kawazumi and K.P. Evans, *J. Chromatogr.*, 636 (1993) 39.
[24] J.D. Ingle, Jr., and S.R. Crouch, *Spectrochemical Analysis*, Prentice-Hall, Englewood Cliffs, NJ, 1988, Ch. 12.

ELSEVIER

Journal of Chromatography A, 663 (1994) 239–243

JOURNAL OF CHROMATOGRAPHY A

Separation of aromatic acids by reversed electroosmotic flow capillary electrophoresis

Ying-Mei Liu, Shuenn-Jyi Sheu*

Department of Chemistry, National Taiwan Normal University, Taipei, Taiwan

(First received September 8th, 1993; revised manuscript received November 22nd, 1993)

Abstract

A reversed electroosmotic flow (EOF) capillary electrophoretic method for the separation of eight aromatic acids was developed. A carrier composed of aqueous buffer solution (10 m*M* lauryltrimethylammonium chloride, 8 m*M* sodium borate and 2 m*M* sodium dihydrogenphosphate)–acetonitrile (7:3) was found to be the most suitable electrolyte for this separation. The analysis time (5 min) was shorter than that of standard capillary zone electrophoresis (21 min). The effects of pH, EOF modifier concentration and organic modifier (acetonitrile) concentration of the carrier on the migration behaviour of the solutes were also studied.

1. Introduction

Capillary zone electrophoresis (CZE) is a powerful separation method, generally applicable to the determination of charged components. Jorgenson and Lukacs [1] reported that the electroosmotic flow (EOF) generated in capillary tubes was strong, and its direction was towards the cathode. Although the velocity of the flow could be affected by ionic species, salt concentration and the pH of the carrier, and also the material of construction of the capillary [1–4], its direction was generally the same. In order to obtain a reversed EOF, several methods have been used including the use of coating capillaries [5,6] and adding a cationic detergent to the carrier [7–11]. In reversed EOF and anionic-mode detection, the order of migrating species will be anions, neutral molecules and cations. Therefore, reversed EOF should be advantageous in the separation of anions, especially those derived from carboxylic acids and phenolic compounds. However, no work has been reported on the analysis of aromatic acids using reversed EOF.

In this work, the separations of eight aromatic acids which are common to herbs (Fig. 1) by standard CZE and reversed EOF CZE were examined. In addition, the effects of pH, EOF modifier concentration and organic modifier (acetonitrile) concentration of the carrier on the migration behaviour of the eight aromatic acids were investigated.

2. Experimental

2.1. Apparatus

The elecrophoretic experiments were carried out on a BioFocus 3000 capillary electrophoresis system equipped with a UV detector set at 210 nm and a 60 cm × 75 μm I.D. fused-silica capil-

* Corresponding author.

0021-9673/94/$07.00
SSDI 0021-9673(93)E1269-6

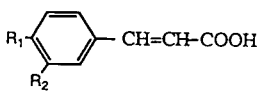

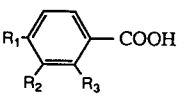

1 , R_1=R_2=H, cinnamic acid

2 , R_1=OH, R_2=OMe, ferulic acid

6 , R_1=R_2=OH, caffeic acid

3 ,  , nicotinic acid

4 , R_1=R_2=R_3=H, benzoic acid

5 , R_1=OH, R_2=R_3=H, p-hydroxybenzoic acid

7 , R_1=R_2=H, R_3=COOH, phthalic acid

8 , R_1=R_3=COOH, R_2=H, trimellitic acid

Fig. 1. Structures of the eight aromatic acids.

lary tube (Polymicro Technologies, Phoenix, AZ, USA) with the detection window placed at 55.4 cm. The conditions were as follows: injection mode, pressure 1 p.s.i. s (1 p.s.i. = 6894.76 Pa); cartridge temperature, 20°C; carousel temperature, 25°C; and applied voltage, +30 kV (constant voltage, positive to negative polarity) for the standard CZE method and −30 kV (constant voltage, negative to positive polarity) for reversed EOF CZE.

2.2. Reagents

Deionized water was provided by a Milli-Q Plus water-purification system (Millipore, Bedford, MA, USA). Lauryltrimethylammonium chloride (LTAC) was obtained from Nacalai Tesque (Kyoto, Japan), sodium borate from Wako (Osaka, Japan) and sodium dihydrogenphosphate from Kanto Chemicals (Kyoto, Japan). Nicotinic acid (**3**), ferulic acid (**2**) and caffeic acid (**6**) were purchased from Sigma (St. Louis, MO, USA) and benzoic acid (**4**), *p*-hydroxybenzoic acid (**5**), *trans*-cinnamic acid (**1**), phthalic acid (**7**) and trimellitic acid (**8**) from Aldrich (Milwaukee, WI, USA). Acetonitrile was of HPLC grade. All other reagents were of analytical-reagent grade and were used as received.

2.3. Standard solution

The standard solution used for electrophoretic experiments was prepared by dissolving the eight standard aromatic acids in water–methanol (1:1, v/v) and the concentration of each compound was 0.1 mg/ml.

3. Results and discussion

3.1. Standard CZE method

It is very common to assay aromatic acids by high-performance liquid chromatography (HPLC) [12,13]. In 1986, Fujiwara and Honda [14] separated cinnamic acid and its analogues by standard CZE: carrier, 0.025 *M* phosphate buffer (pH 9.2); voltage, 7.5 kV; run time, about 25 min. With our system, the best carrier for the eight aromatic acids was a mixture of 70% of borate–phosphate buffer (8 m*M* $Na_2B_4O_7$–2 m*M* NaH_2PO_4, pH 9.63) and 30% of acetonitrile. Fig. 2 shows the separation of eight aromatic acids by the standard CZE method with the following migration times: *trans*-cinnamic acid, 6.5 min; ferulic acid, 6.6 min; nicotinic acid, 7.1 min; benzoic acid, 7.4 min; *p*-hydroxybenzoic acid, 7.7 min; caffeic acid, 9.0 min; phthalic acid, 13.3 min; and trimellitic acid, 19.5 min (plate numbers: 19 000–160 000). The migration time of each compound became longer as the pH value of the buffer was increased, in accordance with the report of Fujiwara and Honda [14]. When the pH of the buffer was below 9.6, **1** and **2** were overlapped, as were **3**, **4** and **5**. As the acetonitrile concentration of the carrier was decreased, the migration times of the solutes became shorter, but **1** and **3** were not separated from **2** and **4**, respectively. Fig. 2 is the

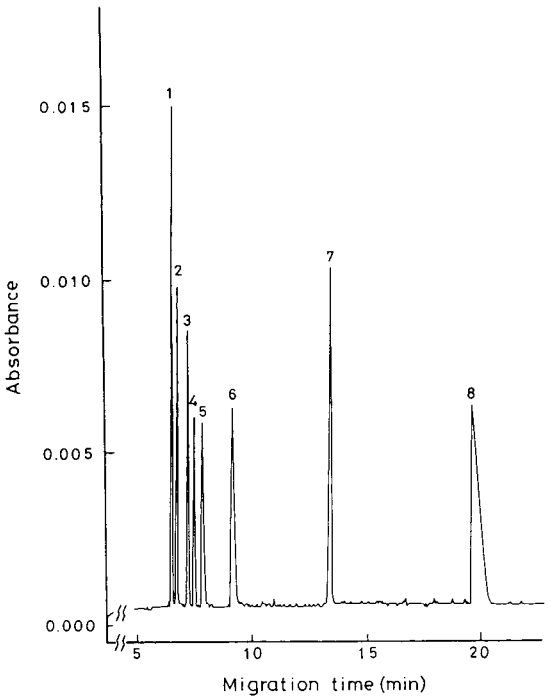

Fig. 2. Capillary electropherogram of the eight aromatic acids separated by standard CZE method: capillary, fused silica (60 cm × 75 μm I.D.); carrier, borate–phosphate buffer (8 m*M* $Na_2B_4O_7$–2 m*M* NaH_2PO_4, pH 9.63)–acetonitrile (7:3); applied voltage, +30 kV; wavelength for detection, 210 nm; injection, 1 p.s.i. s of a water–methanol solution containing 0.1 mg/ml each of the compounds. Peak assignment: 1 = *trans*-cinnamic acid; 2 = ferulic acid; 3 = nicotinic acid; 4 = benzoic acid; 5 = *p*-hydroxybenzoic acid; 6 = caffeic acid; 7 = phthalic acid; 8 = trimellitic acid.

best electropherogram that we could obtain and gives a good resolution for compounds **1–6**. However, for separating more negatively charged components (**7** and **8**), this standard CZE method was not good enough owing to the long migration times and broad peak widths.

3.2. Reversed EOF CZE

All eight aromatic acids were successfully separated in a single run by reversed EOF CZE under suitable conditions. The separation was achieved by optimizing the pH value, EOF modifier concentration and organic modifier (acetonitrile) concentration of the carrier. In reversed EOF with anionic-mode detection, the higher the negative charge the ion the shorter is the migration time.

Several electrolyte systems containing 70% of 10 m*M* EOF modifier (lauryltrimethylammonium chloride) at different pH values ranging from 7.47 to 9.77 (consisting of $Na_2B_4O_7$ and NaH_2PO_4, respective concentrations 2, 8 m*M*; 4, 6 m*M*; 6, 4 m*M*; 8, 2 m*M*; and 10, 0 m*M*) and 30% of acetonitrile were used in order to study the effect of pH on the selectivity of the separation. In Fig. 3, the migration times for the aromatic acids at different pH values are shown. The pH dependence of the migration time of each compound was similar and as the pH increased, the migration time became shorter. However, the migration orders of the compounds with hydroxyl groups (**2**, **5** and **6**) were

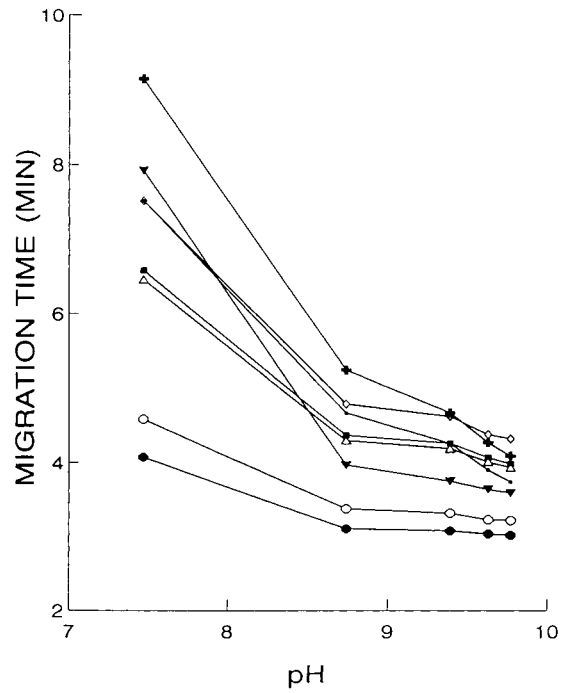

Fig. 3. Effect of pH on migration time. All these experiments were conducted at a voltage of −30 kV across the separating tube filled with 70% of borate–phosphate buffers of different pH values containing 10 m*M* LTAC and 30% of acetonitrile. Other conditions as in Fig. 2. ● = Trimellitic acid; ○ = phthalic acid; ▼ = caffeic acid; ▪ = *p*-hydroxybenzoic acid; △ = benzoic acid; □ = nicotinic acid; + = ferulic acid; ◇ = *trans*-cinnamic acid.

changed as the pH increased. As higher pH, the carboxyl and phenolic hydroxyl groups were dissociated to form the carboxylate–phenolate divalent anions, which exhibited increased mobility. From the results, buffer solutions of pH 9.77 and 9.63 gave the best separations.

Fig. 4 shows the effect of EOF modifier concentration on the selectivity of the separation. The migration time of all the compounds became shorter as the electroosmotic flow increased with increasing EOF modifier concentration. The separation at 5 and 10 m*M* were good enough, but the latter has a shorter analysis time.

Fig. 5 shows the effect of organic modifier concentration on the selectivity of the separation. As the acetonitrile concentration increased, the migration times of all eight compounds became longer. This was because the EOF decreased as the acetonitrile concentration increased. When acetonitrile was not added or was present at a low concentration, many compounds were not separated. At 20% acetonitrile, most peaks were well separated but **3** and **4** overlapped. Analysis at either 30% or 40% acetonitrile could offer good separations but with a shorter run time at 30%. In addition, the response signals of the compounds became larger as the acetonitrile concentration increased.

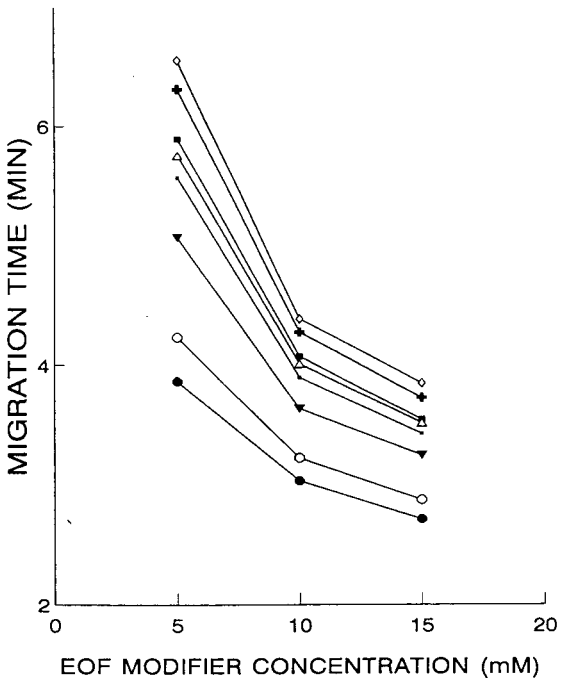

Fig. 4. Effect of EOF modifier concentration on migration time. The carriers were 70% of borate–phosphate buffer (8 m*M* $Na_2B_4O_7$–2 m*M* NaH_2PO_4, pH 9.63) containing 5–15 m*M* LTAC and 30% of acetonitrile. Other conditions and symbols as in Fig. 3.

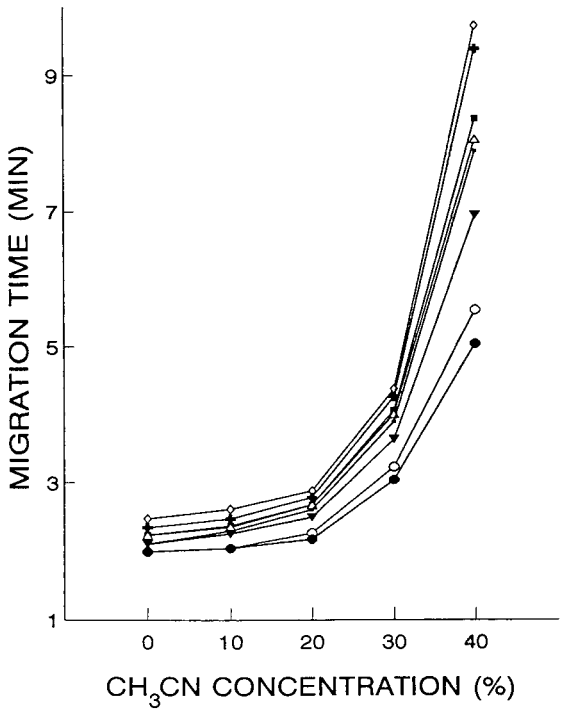

Fig. 5. Effect of acetonitrile concentration on migration time. The carriers were buffer solutions (10 m*M* LTAC–8 m*M* $Na_2B_4O_7$–2 m*M* NaH_2PO_4) mixed with different amounts of acetonitrile. Other conditions and symbols as in Fig. 3.

From the above results, the best resolution was obtained with an electrolyte containing 70% of buffer solution (10 m*M* LTAC, 8 m*M* $Na_2B_4O_7$ and 2 m*M* NaH_2PO_4) and 30% of acetonitrile. Fig. 6 is an electropherogram showing the separation of the eight aromatic acids with the following migration times: trimellitic acid, 3.04 min; phthalic acid, 3.23 min; caffeic acid, 3.64 min; *p*-hydroxybenzoic acid, 3.90 min; benzoic acid, 4.01 min; nicotinic acid, 4.07 min;

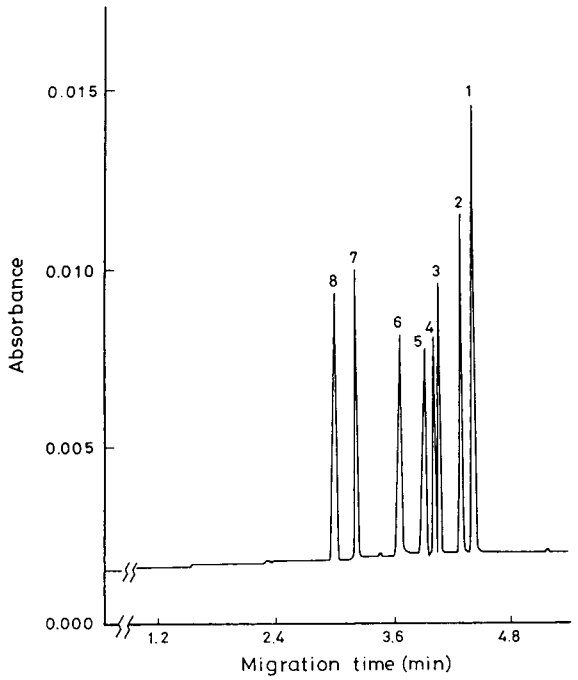

Fig. 6. Capillary electropherogram of the eight aromatic acids separated by reversed EOF CZE. Carrier, buffer solution (10 m*M* LTAC–8 m*M* $Na_2B_4O_7$–2 m*M* NaH_2PO_4)–acetonitrile (7:3); applied voltage, −30 kV; other conditions and peak numbers as in Fig. 2.

ferulic acid, 4.27 min; and *trans*-cinnamic acid, 4.38 min (plate numbers: 46 000–186 000).

In conclusion, by optimizing the pH value, EOF modifier and organic modifier concentration of the carrier, the separation of eight aromatic acids by reversed EOF CZE could be achieved within 5 min with a much smoother baseline. Compared with the standard CZE method, this method is more attractive, especially for those compounds with more than one net negative charge. Application of this technique to natural products and Chinese herb medicines is being studied.

4. Acknowledgement

Financial support from the National Science Council, Republic of China, is gratefully acknowledged.

5. References

[1] J.W. Jorgenson and K.D. Lukacs, *Anal. Chem.*, 53 (1981) 1298.
[2] J.W. Jorgenson and K.D. Lukacs, *J. Chromatogr.*, 218 (1981) 209.
[3] T. Tsuda, K. Nomura and G. Nakagawa, *J. Chromatogr.*, 264 (1983) 385.
[4] T. Tsuda, K. Nomura and G. Nakagawa, *J. Chromatogr.*, 248 (1982) 241.
[5] S. Hjerten, *J. Chromatogr.*, 347 (1985) 191.
[6] J.E. Wiktorowicz and J.C. Colburn, *Electrophoresis*, 11 (1990) 769.
[7] S. Terabe, K. Otsuka, K. Ichikawa, A. Tsuchiya and T. Ando, *Anal. Chem.*, 56 (1984) 111.
[8] X. Huang, J.A. Luckey, M.J. Gordon and R.N. Zare, *Anal. Chem.*, 61 (1989) 766.
[9] B.F. Kenney, *J. Chromatogr.*, 546 (1991) 423.
[10] X. Huang, R.N. Zare, S. Sloss and A.G. Ewing, *Anal. Chem.*, 63 (1991) 189.
[11] M.T. Ackermans, F.M. Everaerts and J.L. Beckers, *J. Chromatogr.*, 606 (1992) 229.
[12] K. Sagara, T. Oshima, T. Yoshida, Y. Tong, G. Zhang and Y. Chen, *J. Chromatogr.*, 409 (1987) 365.
[13] K.C. Wen, C.Y. Huang and F.S. Liu, *J. Chromatogr.*, 593 (1992) 191.
[14] S. Fujiwara and S. Honda, *Anal. Chem.*, 58 (1986) 1811.

ELSEVIER

Journal of Chromatography A, 663 (1994) 245–254

JOURNAL OF CHROMATOGRAPHY A

Study of isotachophoretic separation behaviour of metal cations by means of particle-induced X-ray emission VI. Selective separation of twenty metal cations using tartaric acid as a complexing agent

Takeshi Hirokawa*,[a], Wen Xia[a], Ken-ichiro Nakamura[a], Isamu Tanaka[a], Fumitaka Nishiyama[a], Yoshiyuki Kiso☆,[a], Bohuslav Gaš[b], Jiri Vacík[b]

[a]*Applied Physics and Chemistry, Faculty of Engineering, Hiroshima University, Kagamiyama 1, Higashi-Hiroshima 724, Japan*
[b]*Department of Physical and Macromolecular Chemistry, Faculty of Sciences, Charles University, Albertov 2030, 128 40 Prague 2, Czech Republic*

(Received October 20th, 1993)

Abstract

The selective isotachophoresic (ITP) separation of twenty metal ions that form kinetically labile complexes with tartaric acid was investigated. The leading electrolyte was 20 m*M* ammonia solution buffered by adding acetic acid (pH 4.8) and the concentration of tartaric acid (C_{Tar}) was varied in the range 0–5 m*M*. The terminator was 20 m*M* carnitine hydrochloride solution. Isotachophoretic qualitative indices (R_E) of the metal ions were measured by using a high-frequency contactless conductivity detector. An equimolar test mixture was separated by using a micro-preparative apparatus and the fractions were analysed off-line by particle-induced X-ray emission method (ITP–PIXE). When $C_{Tar} = 1$ m*M*, the separability was good on average. The migration order was Ba^{2+}, (Sr^{2+}, Na^{+}), Ca^{2+}, Mg^{2+}, Mn^{2+}, Fe^{2+}, Co^{2+}, Cd^{2+}, (Ni^{2+}, Li^{+}), Zn^{2+}, La^{2+}, (Ce^{3+}, Pb^{2+}), Y^{3+}, Gd^{3+}, Lu^{3+}, Cu^{2+}, where the ions in parentheses were not separated. $Zr^{IV}O^{2+}$ was not detected. With increase in C_{Tar}, the number of detectable elements decreased owing to the decrease in the effective mobilities of the separands. When $C_{Tar} = 5$ m*M*, the migration order was Na^{+}, Ba^{2+}, Sr^{2+}, Mg^{2+}, Li^{+}, Ca^{2+}, Mn^{2+}, Cd^{2+}, Co^{2+}, Ni^{2+} and Zn^{2+}. A model waste from a nuclear fuel was successfully analysed using the electrolyte system.

1. Introduction

Isotachophoresis (ITP) has been applied to analyses for many kinds of inorganic ions such as metal ions and also organic ions [1]. The separation of metal ions usually utilizes complex-forming equilibria between the metal ions and suitable complexing agents. The separation behaviour of metal ions in such a system depends on the complexing agent selected, its concentration and the pH of the operational electrolyte system [2,3], because these factors directly affect the effective mobilites of metal ions. The appropriate use of complexing agents permits the selective separation of metal ions from a complex mixture.

Gebauer and Boček [4] have reviewed the

* Corresponding author.
☆ Present address: Hijiyama Women's College, Ushita-shinmachi, Hiroshima 732, Japan.

0021-9673/94/$07.00
SSDI 0021-9673(93)E1229-S

utility of complex-forming equilibria in ITP separations and presented a table of complexing reagents and inorganic ions separated by using the reagents. Although various reagents have been used for ITP analysis, only a few systematic approaches have been made to describe the separability of metal cations [5]. This situation is presumably related to the fact that there have been no convenient detection methods with high detectability for metal ions: when similar qualitative indices are obtained for different separands by using universal detectors (*e.g.*, a potential gradient detector), separability assessment of the separands is almost impossible. Even if the same values of the qualitative indices are obtained for separands at the isotachophoretic steady state, suggesting the same effective mobilities, it does not always mean an imperfect separation [6]. That is, the separability of adjacent samples depends on the difference between the separand mobilities in the mixed zone, not on that in the steady-state zones. Although photometric detection may give supplementary qualitative information [7], it is not as useful for metal ions as it is for organic ions.

This is the reason why more discriminating detection methods that the conventional methods are necessary to describe the exact separation behaviour of metal ions. The use of a light-absorbing chelating agent to provide co-counter ions is a possible approach to achieving high detectability for metal ions [8], although selection of the chelating agent causes another problem for samples with complex constituents.

Our approach to the above topic is the analysis of the ITP-separated fractions by particle-induced X-ray emission (PIXE), which is a method with high detectability [9]. In the first paper in this series [10], the separation behaviour of twenty metal ions forming complexes with α-hydroxyisobutyric acid (HIB) was investigated by using ITP–PIXE, demonstrating that PIXE can be a powerful detection method for metal ions.

The aim of this paper is to clarify the separation behaviour of the same twenty metal ions forming cationic ion pairs with tartrate ions, which has been proved useful for recovering precious metals as non-ions from a model nuclear fuel waste solution by using a free-flow ITP apparatus [11]. First, the isotachophoretic qualitative index, R_E [12], of the metal ions was measured by varying the concentration in the leading electrolyte. Next, the ITP separation behaviour of the mixture was investigated by means of ITP–PIXE. Finally, the electrolyte systems used were applied to a model waste to demonstrate the practical utility of the method.

2. Experimental

2.1. Samples

The twenty metal ions treated were Li^+, Na^+, Mg^{2+}, Ca^{2+}, Mn^{2+}, Fe^{2+}, Co^{2+}, Ni^{2+}, Cu^{2+}, Zn^{2+}, Sr^{2+}, Cd^{2+}, $Zr^{IV}O^{2+}$, Ba^{2+}, Pb^{2+}, Y^{3+}, La^{3+}, Ce^{3+}, Gd^{3+} and Lu^{3+}. Stock standard solutions (10 m*M*) were prepared using the chlorides obtained from Tokyo Kasei (Tokyo, Japan). Several test mixtures containing four or five metal cations were prepared from the stock standard solutions for R_E measurement. The sample used for ITP–PIXE analysis contained all of the metal cations, each at a concentration of 0.5 m*M*. The pH of the sample solution was adjusted to 3 by adding a small amount of concentrated hydrochloric acid. Small amounts of cationic dyes [toluidine blue (TB) and astrazon pink (AP)] were co-migrated in order to monitor the migration process and to determine the timing of fractionation.

2.2. Electrolytes system

The leading electrolyte was 20 m*M* aqueous ammonia solution containing tartaric acid (Tar) as the complexing agent at concentrations of 0, 0.5, 1, 1.5, 2, 2.5, 3, 4 and 5 m*M*. The pH of the leading electrolyte (pH_L) was adjusted to 4.8 by adding acetic acid. The above leading electrolytes are abbreviated as WNH_4Ac–Tar (W designates aqueous solution and Ac is acetate) hereafter according to the abbreviations used by Everaerts *et al.* [5]. The leading electrolytes contained 0.05% (w/w) of hydroxypropylcellu-

lose (HPC) (Tokyo Kasei) to suppress electroosmotic flow. The viscosity of the 2% HPC solution was 1000–4000 cP at 20°C. Although the terminating electrolyte used was 20 m*M* carnitine hydrochloride solution, the actual terminator was proton at the isotachophoretic steady state. Table 1 summarizes the operational electrolyte system used.

All the reagents were purchased from Tokyo Kasei. pH measurements were made using a Horiba (Tokyo, Japan) Model F-7 AD digital pH meter.

2.3. Isotachophoretic apparatus used for R_E measurement

The detector used for the measurement of R_E was a high-frequency contactless conductivity detector (HFCCD) [13,14]. The separation unit of the apparatus used was Labeco (Spišská Nová Ves, Slovak Republic) ZKI-001. The separation column consisted of a preseparation capillary (10 cm × 0.5 mm I.D.) and a main capillary (20 cm × 0.25 mm I.D.). The migration current when detecting zones was 50 μA, which was supplied by a high-voltage power supply for a Shimadzu IP-2A. The measurements were made at 25°C in a temperature-controlled room.

The qualitative index R_E is defined as the ratio of the potential gradient [E (V cm^{-1})] of a sample zone (E_S) to that of the leading zone (E_L) [12]. When a conductivity detector is used, it is equal to the ratio of the specific resistances (ρ) of the respective zones. It is also equal to the ratio of the effective mobility ($\bar{m}$) of the leading ion to that of a sample ion in its zone from the equality of the velocities of migrating zones ($v = \bar{m}E$):

$$R_E = E_S/E_L = \rho_S/\rho_L = \bar{m}_L/\bar{m}_S \quad (1)$$

As the output signal of the HFCCD shows a non-linear response to the specific resistance [13,14], the signal obtained was converted into specific resistance using a fourth-order polynomial expression of the output voltage. Na^+ and Li^+ were used as internal standards to correct for the slight drift of the HFCCD signals. The simulated R_E values were 1.495 and 1.963, respectively.

2.4. Preparative isotachophoretic analyser

The micro-preparative analyser used was a capillary type as reported [15]. The separation column consisted of a PTFE precolumn (37 cm × 1 mm I.D.) and a PTFE main column (37 cm × 0.5 mm I.D.). The total volume of the column was 0.32 ml. A typical single run took about 1 h. The migration current was 300 μA for the first 57 min, then it was decreased to 150 μA during detection and fractionation. After monitoring with a potential gradient detector, the separated zones were fractionated dropwise on to Nuclepore filter backings (thickness 5 μm and pore size 0.1 μm) through a platinum capillary. A 15-μm square filter was mounted on a aluminium flame. One drop (*ca.* 5 μl) was one fraction, which contained *ca.* 5 nmol of component. The interval of fractionation was *ca.* 10 s.

2.5. PIXE analysis

The ITP fractions were bombarded by a 2-MeV H^+ beam after drying in a desiccator. The

Table 1
Operational electrolyte system (WNH_4Ac–Tar) used in isotachophoresis

Leading electrolyte	20 m*M* ammonia solution
Complexing agent	Tartaric acid (0, 0.5, 1, 1.5, 2, 2.5, 3, 4 and 5 m*M*)
pH-buffering agent	Acetic acid (40.2, 34.1, 32.5, 30.9, 29.2, 27.6, 26.0, 22.8, 19.5 m*M*)[a]
pH of leading electrolyte	4.8
Additive	0.05% Hydroxypropylcellulose
Terminating electrolyte	20 m*M* Carnitine hydrochloride

[a] Simulated values.

probe beam was generated by using a Van de Graaff accelerator Model AN-2500; (Nisshin High Voltage, Tokyo, Japan). The beam current was 50 nA. A typical single run to acquire an X-ray spectrum of an ITP fraction was *ca.* 200 s. The detector used was a Ge detector (Ortec Model GLP-10180) and the multi-channel pulse-height analyser used was a Laboratory Equipment (Tokyo, Japan) Model AMS-1000. Owing to the limitations of the X-ray detection system used, light elements below atomic number 14 (Si) could not be detected.

3. Results and discussion

3.1. Complex-forming equilibria

The pK_a values of tartaric acid are 3.036 and 4.366 [16]. At $pH_L = 4.8$, *ca.* 80% of tartaric acid exists as divalent ions and the rest as monovalent ions. However, the abundance of divalent tartrate ions in each sample zone decreases at the steady state, because the pH of the zone is lower than pH_L (*e.g.*, pH 4.5) depending on the effective mobility of the sample. The pK_a value of acetic acid is 4.756, and 50% or less of acetic acid exists as acetate ions.

The ion-pair-forming equilibria among metal cations (M^{n+}), tartrate ion ($HTar^-$, Tar^{2-}) and acetate ion (Ac^-) can be written assuming 1:1 ion pairs as

$$\begin{aligned} M^{n+} + HTar^- &\rightleftharpoons MHTar^{(n-1)+} \\ M^{n+} + Tar^{2-} &\rightleftharpoons MTar^{(n-2)+} \\ M^{n+} + Ac^- &\rightleftharpoons MAc^{(n-1)+} \end{aligned} \quad (2)$$

The effective mobility of a metal ion M^{n+} can be expressed as in Eq. 3, where the brackets represent the concentrations of ionic species, m_1, m_2, m_3 and m_4 are the mobilities of M^{n+}, $MHTar^{(n-1)+}$, $MTar^{(n-2)+}$ and $MAc^{(n-1)+}$, respectively, and K_1, K_2 and K_3 are the stability constants of $MHTar^{(n-1)+}$, $MTar^{(n-2)+}$ and $MAc^{(n-1)+}$, respectively.

As the mobility of the ion pairs formed is smaller than that of non-complexing metal ions, Eq. 3 indicates that the effective mobility of metal ions decreases with increase in the concentration of the complexing counter ions.

3.2. R_E values

Fig. 1 shows the R_E values of the metal ions observed for nine leading electrolytes containing 0–5 m*M* tartaric acid. Although the R_E values increased with increase in tartaric acid concentration (C_{Tar}), the increments were different among the metal ions, indicating that the stability constants differed. It seemed that La^{3+}, Ce^{3+}, Gd^{3+}, Y^{3+}, Lu^{3+}, Cu^{2+} and Pb^{2+} had higher stability constants than the others. When C_{Tar} was >1 m*M*, the above ions tended to form a mixed zone even if two components with sufficiently different R_E values were selected. Further, the reproducibility of the R_E values shown in Fig. 1 was not good for these ions. The reason is not clear.

Among the twenty metal ions, the R_E values of $Zr^{IV}O^{2+}$ could not be measured, because the ions did not form a quantitative zone. On the other hand, the R_E values of Fe^{2+} were measurable for all of the operational systems used. However, quantitative analysis was difficult with every system because the zone length corresponding to the same amount injected quickly decreased with increase in C_{Tar}. This is probably due to oxidation of Fe^{2+} to Fe^{3+} and the successive formation of hydroxyl complexes.

The R_E value of the terminating H^+ zone was 5.5 ± 0.5 on average. The reproducibility was not as good as those for the sample ions (usually the error in the observed R_E values is ± 0.1 or less). The corresponding effective mobility was $12.7 \cdot 10^{-5}$ cm^2 V^{-1} s^{-1} according to our simulation. The metal ions with smaller effective mobilities such as ZrO^{2+} did not migrate isotachophoretically, but migrated zone electrophoretically in the terminating zone.

$$\bar{m}_M = \frac{m_1[M^{n+}] + m_2[MHTar^{(n-1)+}] + m_3[MTar^{(n-2)+}] + m_4[MAc^{(n-1)+}]}{[M^{n+}] + [MHTar^{(n-1)+}] + [MTar^{(n-2)+}] + [MAc^{(n-1)+}]} = \frac{m_1 + m_2K_1[HTar^-] + m_3K_2[Tar^{-2}] + m_4K_3[Ac^-]}{1 + K_1[HTar^-] + K_2[Tar^{-2}] + K_3[Ac^-]} \quad (3)$$

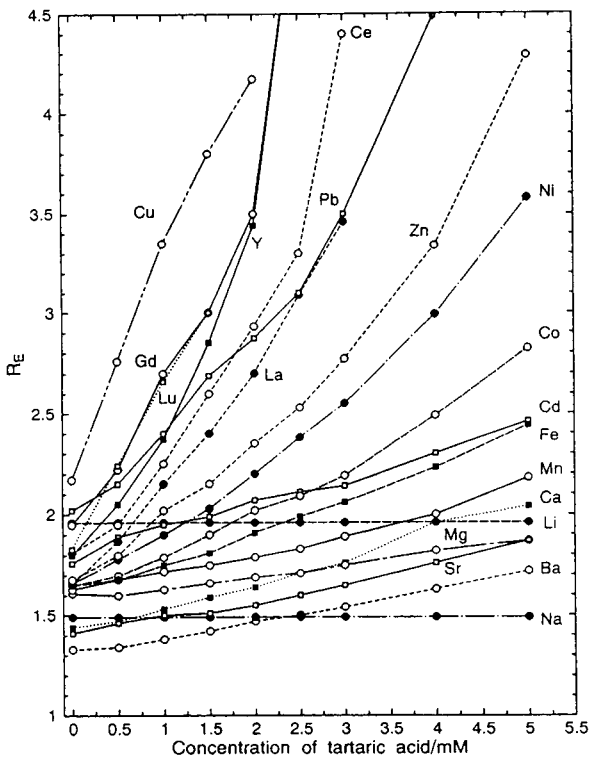

Fig. 1. R_E values of nineteen metal cations observed by using a high-frequency contactless conductivity detector. Operational electrolyte system as in Table 1. Na^+ and Li^+ were the internal standards for R_E measurement.

3.3. Separation behaviour of the twenty metal cations and migration order

Fig. 2 shows isotachopherograms of the mixture of the twenty metal cations obtained by using an HFCCD, where C_{Tar} was varied as (a) 0, (b) 1, (c) 2.5 and (d) 5 m*M*. A 1.2-μl volume of sample mixture containing 0.6 nmol of each metal cation (total 12 nmol) was separated. The quantity of electric charge integrated until the first sample zone was 0.282 C (125 μA · 36 min + 50 μA · 4 min) and the electric charge applied for a unit molar amount was 23.5 mC $nmol^{-1}$.

Fig. 3 shows the analytical results for ITP fractions obtained by PIXE. A 20-μl volume of the sample mixture (10 nmol of each component) was separated and fractionated using three leading electrolyes ($C_{Tar} = 0$, 1 and 2.5 m*M*). The zone passing time of all the sample zones was *ca.* 8 min (migration current = 150 μA). The quantity of electric charge applied was 1.09 C (300 μA · 57 min + 150 μA · 7 min) and the electric charge applied for a unit molar amount was 5.5 mC $nmol^{-1}$. It should be noted that the electric charge per sample amount was different between the above two experiments, and obviously a better separation was expected with HFCCD detection (Fig. 2).

The assignments shown in Fig. 2 were made in comparison with the analytical results obtained by PIXE shown in Fig. 3. As Li, Na and Mg could not be detected with the PIXE detection system used, they were assigned by using a conventional isotachophoretic method using standard samples.

When tartaric acid was not present in the leading electrolyte, as shown in Fig. 2a, the Mn, Co, Ni and Zn zones had the same conductivity, suggesting mixed-zone formation. This conclusion was partly valid judging from the PIXE result shown in Fig. 3a. On the other hand, a similar situation was found for the zones of Ce, Cd and Y in Fig. 2a. However in these instances, they were completely separated, as shown in Fig. 3a.

When a leading electrolyte containing 1 m*M* tartaric acid was used, in general a good separability was obtained, as shown in Figs. 2b and 3b. Although the separations between Cd and Ni and between Ce and Pb were incomplete, a slight amount of additional charge might allow complete separation.

When the concentration of tartaric acid was increased to 2.5 m*M*, the quality of separation become poor again. Obviously, from Figs. 2c and 3c a major mixed zone of Pb, Y, La, Ce and Gd was formed. Mg and Ca of the same step height were separated, as were Cd and Co.

For ZrO^{2+}, no quantitative steps were observed for any of the electrolyte systems examined. It was found from PIXE analysis that the ions migrated just before the terminating zone, presumably forming colloidal particles of

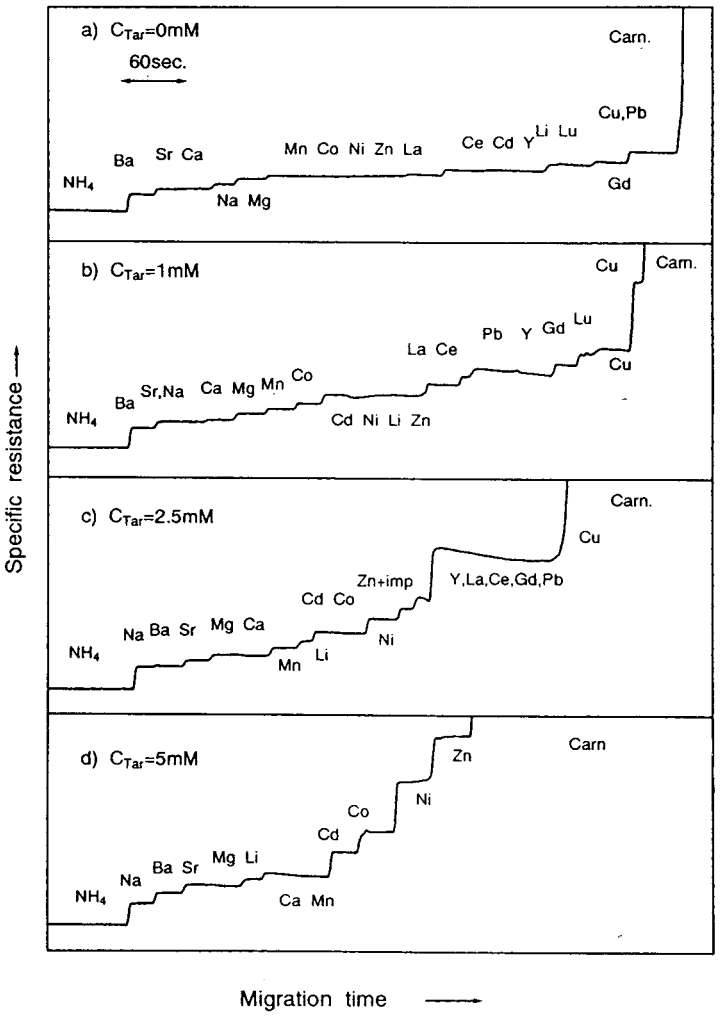

Fig. 2. Observed isotachopherograms of a test mixture containing twenty metal cations. The injected sample amount was 1.2 μl (12 nmol of metal ions). Operational electrolyte systems as in Table 1. Migration current = 150 μA. Quantity of integrated charge = 0.28 C.

the hydroxides. This observation was limited to the operational system without tartaric acid. The addition of tartaric acid so decreased the effective mobility of colloidal particles of ZrO and Fe^{III} that they were not detection as cations.

Fig. 4 summarizes the migration order with the electrolyte systems used. The effective mobilities of Na^+ and Li^+ can be regarded as constant with the electrolyte systems used, because the interaction with tartrate and acetate ions is negligibly small.

With increase in tartaric acid concentration, the number of analysable ionic species gradually decreased. When WNH_4Ac–Tar (5 mM) was used, it decreased to half of that with the WNH_4Ac system. However, a high separability was obtained for the detectable ionic species, as already shown in Fig. 2d. This phenomenon can be utilized for selective separation from the other metal ions. When C_{Tar} is as high as 5 mM, for example, lanthanide ions in a sample can be purged to facilitate the detection of the other

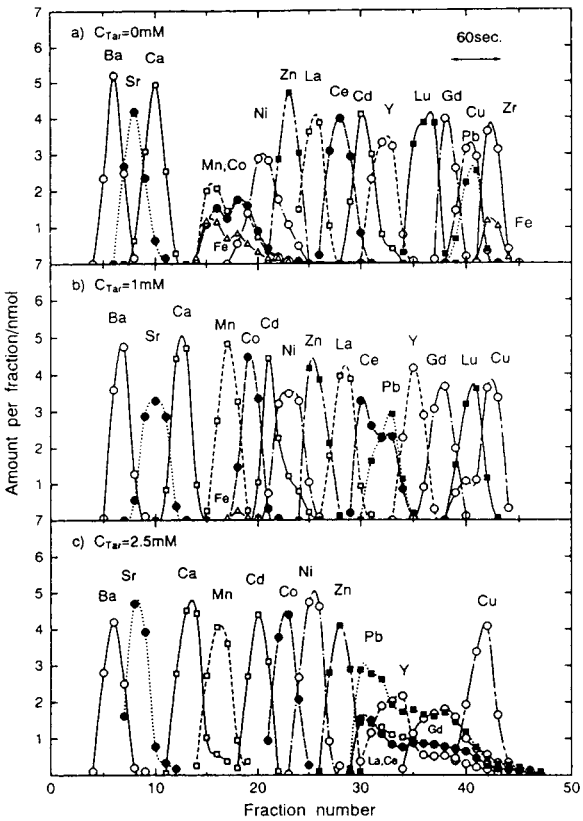

Fig. 3. Analytical results for ITP fractions of a test mixture containing twenty metal cations using PIXE. The injected sample amount was 20 μl (200 nmol of metal ions). Operational electrolyte system as in Table 1. Quantity of integrated charge = 1.1 C.

ions in the sample. Light lanthanide ions can be detected when C_{Tar} is as low as 1 mM.

3.4. Sample recovery

The isotachophoretic recovery of metal cations was evaluated on the basis of PIXE analysis as

$$\text{Recovery (\%)} = \frac{\text{measured amount of element in fractions}}{\text{measured amount of element injected}} \cdot 100 \quad (4)$$

Table 2 shows the percentage recoveries of nine ions, which were selected because no recovery was obtained at C_{Tar} = 5 mM. Although 88% of $Zr^{IV}O^{2+}$ and 90% of Fe^{2+} were recovered using the WNH_4AC system (C_{Tar} = 0), they were not recovered when tartaric acid was present in the leading electrolyte and the amount injected was 10 nmol.

When C_{Tar} = 2.5 mM, an isotachophoretic Lu zone was not detected (Fig. 3c). The 20% recovery of Lu in Table 2 was due to the Lu zone which migrated zone electrophoretically in the terminating zone (fractions 52–60, not shown in Fig. 3c). This suggested that the effective mobility of Lu was slightly smaller than that of the terminating ion when C_{Tar} was 2.5 mM. A similar situation was observed with Y with a 77% recovery.

Table 2
Recoveries (%) of fractionated metal cations evaluated by PIXE

Z	Metal ion	Electrolyte system			
		WNH_4Ac	WNH_4Ac–Tar (1 mM)	WNH_4Ac–Tar (2.5 mM)	WNH_4Ac–Tar (5 mM)
26	Fe^{II}	100[a]	17	n.d.[b]	n.d.
29	Cu	104	102	99	n.d.
39	Y	100	99	77	n.d.
40	$Zr^{IV}O$	88	n.d.	n.d.	n.d.
57	La	101	98	97	n.d.
58	Ce	99	97	101	n.d.
64	Gd	100	96	98	n.d.
71	Lu	102	100	20	n.d.
82	Pb	100	101	100	n.d.

[a] 10% was found as Fe^{III}.
[b] n.d. = Not detected.

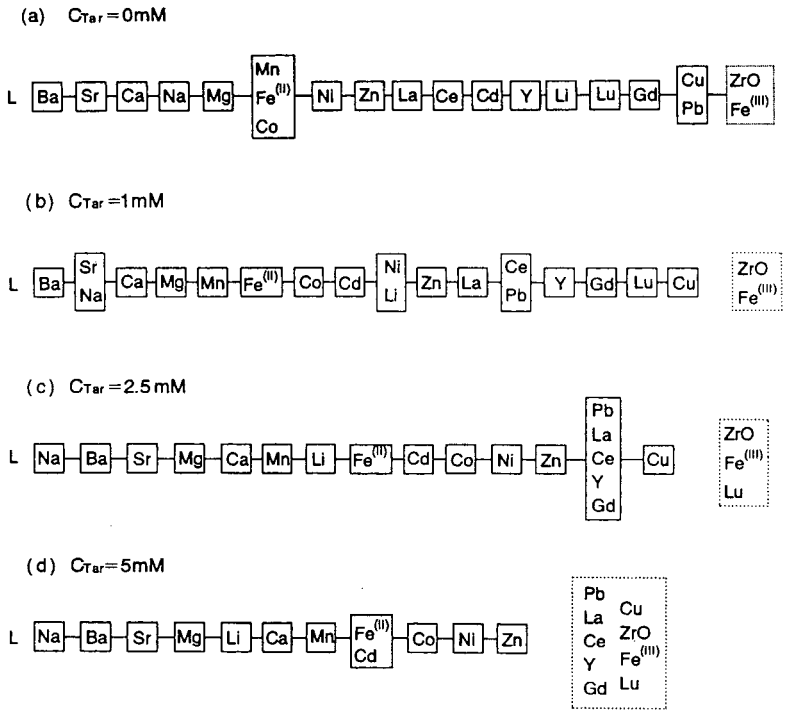

Fig. 4. Migration order of twenty metal cations observed for five operational electrolyte systems. Operational electrolyte system as in Table 1. Metal ions in a different solid box can be separated. Metal ions in a dashed box were not detected before the terminating zone of proton.

Table 3
Sample composition of model waste from nuclear fuel cycle (MW-2)

Z	Element	Concentration (m*M*)	Form[a]	Z	Element	Concentration (m*M*)	Form[a]
11	Na	19.6198	$NaNO_3$	46	Pd	0.1732	$Pd(NO_3)_2$
13	Al	0.00901	Al	47	Ag	0.0068	$AgNO_3$
15	P	0.2538	P	48	Cd	0.0092	$Cd(NO_3)_2$
24	Cr	0.0788	$Cr(NO_3)_3$	50	Sn	0.0066	Sn
25	Mn	0.2622	$Mn(NO_3)_2$	52	Te	0.0714	TeO_2
26	Fe	1.5538	$Fe(NO_3)_3$	55	Cs	0.322	$CsNO_3$
28	Ni	0.1874	$Ni(NO_3)_2$	56	Ba	0.1944	$Ba(NO_3)_2$
34	Se	0.0110	Na_2SeO_3	57	La	0.1642	$La_2(CO_3)_3$
37	Rb	0.0728	$RbNO_3$	58	Ce	1.1780	$Ce(CO_3)_2$
38	Sr	0.175	$Sr(NO_3)_2$	59	Pr	0.1492	Pr_6O_{11}
39	Y	0.1256	Y_2O_3	60	Nd	0.5000	Nd_2O_3
40	Zr	0.722	$ZrO(NO_3)_2$	62	Sm	0.1020	Sm_2O_3
42	Mo	0.612	Na_2MoO_4	63	Eu	0.0160	Eu_2O_3
44	Ru	0.338	$Ru(NO_3)_3$	64	Gd	0.0078	Gd_2O_3
45	Rh	0.06789	$Rh(NO_3)_3$				

[a] Chemicals used for preparation.

3.5. Separation of a nuclear fuel model waste solution

The operational electrolyte systems containing tartaric acid were applied to the analysis of a nuclear fuel model waste, the components of which are several metal cations with different abundances, as shown in Table 3.

Fig. 5 shows isotachopherograms of the model waste obtained by using the HFCCD. A 10-μl volume of sample containing 270 nmol of the components was separated. Fig. 6 shows the analytical results for the ITP fractions obtained by using four leading electrolytes ($C_{Tar} = 0$, 1, 2.5 and 5 mM). A 60-μl volume of sample containing 1.62 μmol of the components was separated. Fractionation was started at the end of the Na^+ zone, which was the matrix component of the model waste treated (Table 3). The quantity of electric charge integrated through the migration process was 1.4 C (300 μA · 65 min + 150 μA · 25 min).

When tartaric acid was not used as a complexing agent, a mixed zone of Ce and Nd was observed, as is obvious from Fig. 6a. Additionally, the separability of Mn, Ni and La was not high. On the other hand, a good separation was achieved on addition of 1 mM tartaric acid to the leading electrolyte (Fig. 6b). The separation behaviour of the model waste with the electrolyte systems used was very similar to that with a leading electrolyte containing α-hydroxy-

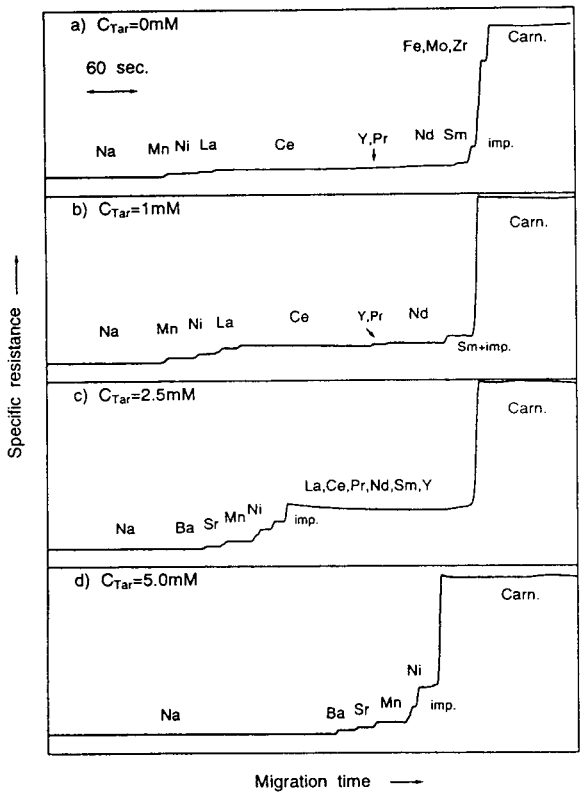

Fig. 5. Observed isotachopherogram of a model waste produced in a nuclear fuel cycle. The injected sample amount was 10-μl (270 nmol of metal ions). Operational electrolyte system as in Table 1. Migration current = 150 μA. Quantity of integrated charge = 0.3 C.

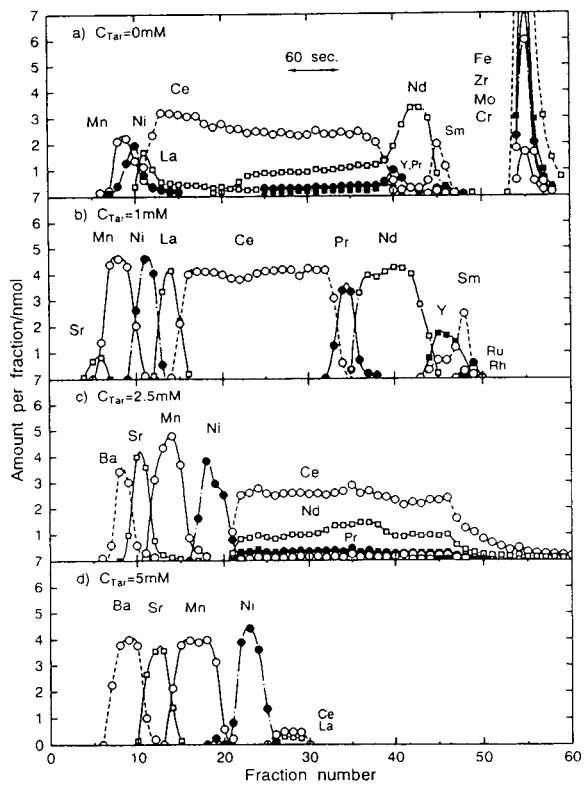

Fig. 6. Analysis results for the cationic fractions of the nuclear fuel model waste obtained by PIXE. The injected sample amount was 60 μl (1.6 μmol of metal ions). Operational electrolyte system as in Table 1. Quantity of integrated charge = 1.4 C.

isobutyric acid [10], except for the migration order of Sm and Y.

With increase in tartaric acid concentration, the separability of lanthanide ions became poor, as shown in Fig. 6c ($C_{Tar} = 2.5$ mM). When C_{Tar} was increased to 5 mM, the lanthanide ions did not migrate isotachophoretically, as expected. This allowed the selective detection of Ba^{2+}, Sr^{2+}, Mn^{2+} and Ni^{2+} contained in the sample. If the number of detectable samples can be decreased in such a way, conventional detection methods using a potential gradient detector and a conductivity detector become very useful.

The other metal ions (not detected as cations) might partly migrate in the terminating zone as cations when the effective mobilities are smaller than that of the terminator. Another part of them might stop around the injection port if non-ionic ion pairs are formed, with the other part migrating as anions towards the cathode if the ion pairs are anions. Such a conversion from cations is important from the viewpoint of preparative applications [11]. It is also important for analytical purposes because cations and anions can be detected simultaneously when dual detection systems are used with a bidirectional electrolyte system [17].

4. References

[1] P. Boček and F. Foret, *J. Chromatogr.*, 313 (1984) 189.
[2] T. Hirokawa and Y. Kiso, *J. Chromatogr.*, 242 (1982) 227.
[3] T. Hirokawa, T. Matsuki, H. Takemi and Y. Kiso, *J. Chromatogr.*, 280 (1983) 233.
[4] G. Gebauer and P. Boček, *Folia Fac. Sci. Nat. Univ. Purikynianae Brun.*, 26 (1985) 37.
[5] F.M. Everaerts, J.L. Beckers and Th.P.E.M. Verheggen, *Isotachophoresis*, Elsevier, Amsterdam, 1976.
[6] F.E.P. Mikkers, F.M. Everaerts and J.A.F. Peek, *J. Chromatogr.*, 168 (1979) 317.
[7] F.M. Everaerts, Th.P.E.M. Verheggen, J.C. Reijenga, G.V.A. Aben, P. Gebauer and P. Boček, *J. Chromatogr.*, 320 (1985) 263.
[8] I. Zelenšky, D. Kaniansky, P. Havasi, Th.P.E.M. Verheggen and F.M. Everaerts, *J. Chromatogr.*, 470 (1989) 155.
[9] S.A.E. Johansson and J.L. Campbell, *PIXE, A Novel Technique for Elemental Analysis*, Wiley, New York, 1988.
[10] T. Hirokawa, J. Hu, S. Eguchi, F. Nishiyama and Y. Kiso, *J. Chromatogr.*, 538 (1991) 413.
[11] T. Hirokawa, T. Ohta, T. Tanaka, K. Nakamura, W. Xia, F. Nishiyama and Y. Kiso, *J. Chromatogr.*, 638 (1993) 215.
[12] T. Hirokawa, M. Nishino, N. Aoki, Y. Kiso, Y. Sawamoto, T. Yagi and J. Akiyama, *J. Chromatogr.*, 271 (1983) D1.
[13] B. Gaš, M. Demjaněnko and J. Vacík, *J. Chromatogr.*, 192 (1980) 253.
[14] J. Vacík, J. Zuska and I. Muselasová, *J. Chromatogr.*, 320 (1985) 233.
[15] T. Hirokawa, J. Hu, K. Umeda, G. Kimura, H. Ikeda, F. Nishiyama and Y. Kiso, *J. Chromatogr.*, 513 (1990) 297.
[16] L.G. Sillen and A.E. Martell (Editors), *Stability Constants of Metal–Ion Complexes* (*Special Publication*, No. 17), Chemical Society, London, 1964.
[17] T. Hirokawa, K. Watanabe, Y. Yokota and Y. Kiso, *J. Chromatogr.*, 633 (1993) 251.

ELSEVIER

Journal of Chromatography A, 663 (1994) 255–258

JOURNAL OF CHROMATOGRAPHY A

Short Communication

Sulphite stabilizer in ion chromatography

Yoshimasa Michigami*, Kazumasa Ueda

Department of Chemistry and Chemical Engineering, Faculty of Technology, Kanazawa University, 2-40 Kodatsuno, Kanazawa 920, Japan

(First received August 20th, 1993; revised manuscript received November 9th, 1993)

Abstract

The stability of sulphite in various stabilizers has been studied in ion chromatography. Sulphate–formaldehyde was the most stable system towards air oxidation. However, its retention was very weak in weak acidic eluent. Sulphite–methanol was also stable for at least 48 h towards air oxidation in the absence of metals such as iron.

1. Introduction

Sulphite is an interesting but difficult to determine anion because it is very unstable and is readily oxidized to sulphate in aqueous solution. The addition of formaldehyde [1–3], acetone, alcohols [1], glycerol [4], triethanolamine [5], etc., to prevent this oxidation has been proposed. Sulphite reacts with formaldehyde and is stabilized as hydroxymethanesulphonate, which is stable towards air oxidation and hydrolysis in slightly acidic solutions [6]. Formaldehyde has been widely used as a sulphite stabilizer.

Ion chromatography [1,3–9] has been reported for the determination of sulphite, including methods with no stabilizer [7] and with formaldehyde as a stabilizer [1,8]. Sulphite standard solution prepared from sodium hydroxymethanesulphonate has also been reported [6,9]. However, it has been found that formaldehyde affected the peak height obtained with an eluent not containing formaldehyde [3]. The efficiency of sulphate stabilizer has also been reported to be in order carbonyls > alcohols = saccharides [1], triethanolamine > EDTA [5] or formaldehyde > glycerol and fructose [3].

Formaldehyde sulphite stabilizer can be determined only in basic solution by ion chromatography, because in basic solution hydroxymethanesulphonate decomposes to give sulphite ion [6], but in neutral or acidic solution it does not decompose and its retention time is very short in ion chromatography with a neutral or acidic eluent.

In this paper, the stability of sulphite with various stabilizers was examined with respect to storage period and temperature and the effect of foreign ions (especially metal ions which act as a catalyst of the oxidation). In ion chromatography with 1 mmol l^{-1} phthalate (pH 6.0) as eluent, hydrogensulphite and hydroxymethanesulphonate ions, in the presence of formaldehyde as a stabilizer, are present and hydroxymethanesulphonate elutes very near to the solvent front. The degree of oxidation of sulphite (or conversion into sulphate) was calculated from

* Corresponding author.

SSDI 0021-9673(93)E1204-D

the determination of sulphite and of sulphate (formed from the oxidation of sulphite).

2. Experimental

The ion chromatographic equipment consisted of a pump (CCPD; Tosoh), a variable-wavelength ultraviolet detector (UV-8000; Tosoh) monitoring at 255 nm, an injector (Rheodyne) with a 100-μl sample loop, a column oven (CO-8000; Tosoh) maintained at 35°C and a pen recoder (YEW Type 3066; Yokogawa).

All chemicals were of analytical-reagent grade and deionized, distilled water, further filtered through a 0.45-μm membrane filter, was used throughout. Standard sulphite solution was prepared from sodium sulphite and 5% (v/v) of various stabilizers. The stabilizers were used as received. Standard sulphate solution was prepared from sodium sulphate. The eluent was 1 mmol l^{-1} phthalate, adjusted to pH 6.0 with dilute sodium hydroxide solution and filtered through a 0.45-μm membrane filter before use.

Separation columns were prepared from 50 × 4.6 mm I.D. columns packed with ODS resin (Capcell Pack C18, AG120, particle size 5 μm; Shiseido) and then coated with cetyltrimethylammonium bromide (CTAB). The ion-exchange capacity of the coated column was about 0.15 mequiv. per column for phthalate ion. Both sulphite and sulphate were determined and the conversion to sulphate from sulphite was calculated.

3. Results and discussion

Methanol, formalin (37% aqueous formaldehyde solution), glycerol, acetone, ethanol and triethanolamine were tested as sulphite stabilizers. The conversions to sulphate from sulphite are given in Table 1 and a typical chromatogram is shown in Fig. 1. It was found that 20% of sulphite was converted into sulphate after 6 h and 100% after about 48 h in aqueous sulphite solution with no stabilizer. A 5% concentration of formalin (about 2% as formaldehyde) was allowed to be present in sulphite (in practice, present as hydroxymethanesulphonate) for more

Table 1
Effect of stabilizers on the conversion of sulphite into sulphate

Stabilizer		Conversion into sulphate (%)					
Compound	Concentration (%)[a]	6 h	24 h	48 h	3 days	7 days	14 days
None	–	20.0	65	80	–	100	–
	– (a)	–	–	5.0	–	52	90
	– (b)	–	–	25.0	–	32.0	50
Methanol	1.0	<0.1	<0.1	<0.5	1.1	2.8	10.3
	5.0	<0.1	<0.5	–	<0.5	2.0	4.0
	5.0 (a)	–	<0.1	<0.5	–	<0.5	<0.5
	5.0 (b)	–	–	<0.5	–	<0.5	<0.5
	5.0 (c)	–	30	40	–	–	100
	10.0	<0.1	<0.1	<0.1	–	5.7	–
Formalin	5.0	<0.1	<0.1	<0.1	<0.1	<0.1	<0.1
	5.0 (a)	–	<0.1	<0.1	–	<0.1	<0.5
	5.0 (b)	–	<0.5	1.0	–	–	1.0
Glycerol	5.0	–	7.8	–	17.0	48	50
Acetone	5.0	<0.5	<0.5	–	0.7	0.7	0.7
Ethanol	5.0	<0.5	2.7	–	7.7	15.0	15.5
Triethanolamine	5.0	<0.1	1.5	–	–	3.0	3.0

[a] Storage temperature: (a) 4°C; (b) 50°C; (c) in a freezer; all others, room temperature.

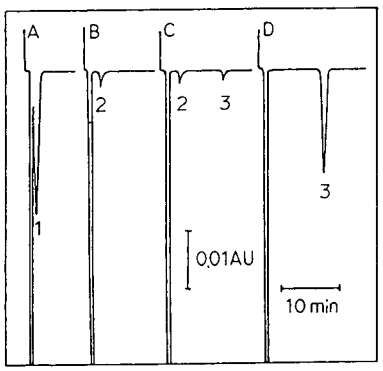

Fig. 1. Chromatogram of sulphite and sulphate with formalin and methanol as stabilizers. Sulphite 10 μg ml^{-1} in (A) 1% formalin, (B) 1% methanol, (C) aqueous solutions; (D) sulphate 10 μg ml^{-1} in aqueous solution. Eluent, 1 mmol l^{-1} phthalate (pH 6.0); flow-rate, 1 ml min^{-1}; detection wavelength, 255 nm. Peaks: 1 = hydroxymethanesulphonate; 2 = sulphite; 3 = sulphate.

than 2 weeks at room temperature. However, the retention time of hydroxymethanesulphonate was shortened (to 2 min) and this peak was overlapped by many other peaks (*e.g.*, chloride, formate) and was very near the solvent front in this chromatographic system. Sulphite was almost completely stable in 1–10% methanol solution for at least 48 h. Glycerol and ethanol as stabilizers were undesirable. Although acetone stabilized sulphite, the stability of acetone–sulphite was weaker than that of formalin–sulphite. Sulphite in triethanolamine was not detected owing to the interference of the large triethanolamine peak in this chromatographic system. Therefore, only sulphate converted from sulphite was determined. The retention times of sulphite in methanol, ethanol and glycerol were almost the same as that of sulphite (3.5 min) in

Table 2
Effect of foreign ions on the conversion of sulphite into sulphate

Ion	Added (μg)	Conversion into sulphate (%)			
		Methanol	Formalin	Glycerol	Acetone
Cl^- as NaCl	1000	<0.1	<0.1	<0.5	<0.5
NO_3^- as $NaNO_3$	1000	<0.1	<0.1	<0.5	<0.5
NO_2^- as $NaNO_2$	1000	<0.1	<0.1	<0.5	<0.5
Br^- as NaBr	1000	<0.1	<0.1	<0.5	<0.5
$HCOO^-$ as HCOONa	1000	<0.1	<0.5	<0.5	<0.5
Fe(III) as $FeCl_3$	1000	95	1.0	93	100.0
	1	1.0	–	<0.5	<0.5
	1000[a]	<0.1	<0.5	<0.5	<0.5
Mn(II) as $MnCl_2$	1000	100	1.5	88	15.1
	10	2.0	–	25.1	5.4
	1000[a]	<0.1	<0.5	<0.5	<0.5
Cu(II) as $CuCl_2$	1000	50	<0.1	38.8	10.8
	10	60	–	–	–
	1	56	–	–	–
	1000[a]	<0.1	<0.5	<0.5	<0.5
Zn(II) as $ZnCl_2$	1000	<1.0	<0.5	<0.5	<0.5
Ai(III) as $AlCl_3$	1000	<0.5	<0.5	5.4	7.1
Mo(VI) as Na_2MoO_4	1000	3.0	–	–	–
Si(IV) as Na_2SiO_3	1000	30.0	<0.5	<0.5	<0.5
	100	1.0	–	–	–

Sulphite concentration: 25 μg ml^{-1} in 5% solution of each stabilizer.
[a] After cation-exchange resin column.

aqueous solution. Sulphite with these stabilizers may be present as almost same species as in aqueous solution. In eluents of high pH, sulphite with formalin as stabilizer may also be present as sulphite ion and the separation of sulphite from the solvent front can be improved.

Whereas sulphite was liable to be converted into sulphate in methanol solution as stabilizer at high temperature (50°C), formalin stabilized sulphite at this temperature. However, both methanol and formalin prevented the conversion of sulphite into sulphate at low temperature (4°C) for at least 1 week and more than 1 week, respectively. With storage of sulphite–methanol in a freezer, greater stability of sulphite was observed.

The effect of the addition of typical anions and cations to sulphite solution in the presence of stabilizers was examined with respect to the conversion to sulphite after about 2 h. The results obtained are given in Table 2. Iron, manganese and copper cations accelerate the conversion from sulphite into sulphate in the presence of all the stabilizers except formalin. However, no conversion in the presence (1 mg) of zinc, aluminium and molybdenum cations and ascorbate, chloride, nitrate, nitrite and formate anions was observed in the presence of any of the stabilizers studied. When a sample solution containing iron, manganese or copper was passed through a cation-exchange resin column (Na^+ form), no conversion was observed. Formalin as stabilizer prevented the conversion of sulphite into sulphate in the presence of iron, manganese or copper.

Sulphite–formaldehyde in the most stable system towards air oxidation and cations such as iron, as shown in Tables 1 and 2. However, formaldehyde is toxic and the retention of sulphite(–formaldehyde) was very weak with neutral and acidic eluents. Sulphite–methanol is stable for at least 48 h, but a sample should be passed through a cation-exchange resin for the determination of sulphite in environmental and biological fluids containing many cations (iron, copper, etc.) because sulphite with methanol as stabilizer was easily converted into sulphate in the presence of cations such as iron.

4. References

[1] M. Lindgren, A. Cedergren and J. Lindberg, *Anal. Chim. Acta*, 141 (1982) 279.
[2] M. Weidenauer, P. Hoffmann and K.H. Lieser, *Fresenius' J. Anal. Chem.*, 342 (1992) 333.
[3] L. Campanella, M. Majone and R. Pocci, *Talanta*, 37 (1990) 201.
[4] K. Fujimura and M. Tsuchiya, *Bunseki Kagaku*, 37 (1988) 59.
[5] S. Tanaka, K. Yamanaka, S. Sato and Y. Hashimoto, *Bunseki Kagaku*, 35 (1986) 465.
[6] L.D. Hansen, B.E. Richter, D.K. Rolins, J.D. Lamb and D.J. Eatough, *Anal. Chem.*, 51 (1979) 633.
[7] M. Nagase, *Bunseki Kagaku*, 37 (1988) 30.
[8] T.S. Stevens, V.T. Turkelson and W.R. Albe, *Anal. Chem.*, 49 (1977) 1176.
[9] T. Sundén, M. Lindgren, A. Cedergren and D.D. Siemer, *Anal. Chem.*, 55 (1983) 2.

ELSEVIER

Journal of Chromatography A, 663 (1994) 259–263

JOURNAL OF CHROMATOGRAPHY A

Short Communication

Quantitation of gentamicin sulfate in injectable solutions by capillary electrophoresis☆

Cheryl L. Flurer*, Karen A. Wolnik

National Forensic Chemistry Center, US Food and Drug Administration, 1141 Central Parkway, Cincinnati, OH 45202, USA

(First received October 18th, 1993; revised manuscript received December 20th, 1993)

Abstract

The results presented in this communication establish the use of capillary electrophoresis as a tool in the analysis of injectable solutions containing the antibiotic complex gentamicin sulfate. The utilization of a borate buffer leads to the separation of the individual components and their visualization by direct UV detection. This rapid and straightforward procedure yields qualitative and quantitative information simultaneously, and could be utilized as an alternative to the multiple assays required by current US Pharmacopeia protocols.

1. Introduction

Gentamicin is an aminoglycoside antibiotic complex produced by *Micromonospora purpurea*, *M. echinospora*, or variants thereof [1] and is used as an antibacterial agent in humans and animals. Each of the three major components, C_1, C_{1a} and C_2, is comprised of the aminocyclitol 2-deoxystreptamine and two additional amino sugars, as shown in Fig. 1. Other minor components such as gentamicins C_{2a} and C_{2b} may be produced as well [2].

Current US Pharmacopeia (USP) methods for gentamicin sulfate require separate tests for identification and quantitation [3]. The composition of the bulk drug is determined by its derivatization with *o*-phthalaldehyde and the separation of the three major components and

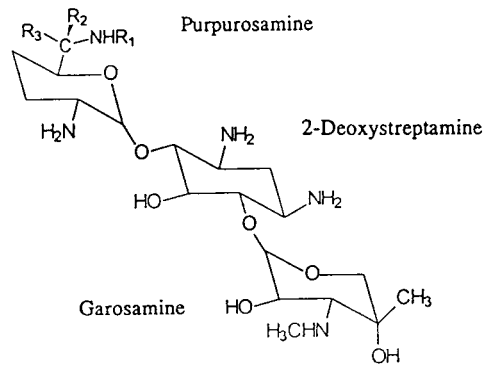

Gentamicin	R_1	R_2	R_3	MW
C_1	CH_3	H	CH_3	477
C_{1a}	H	H	H	449
C_2	H	CH_3	H	463
C_{2a}	H	H	CH_3	463
C_{2b}	CH_3	H	H	463

Fig. 1. Structures of components of gentamicin sulfate.

* Corresponding author.

☆ Presented in part at the *5th International Symposium on High Performance Capillary Electrophoresis, Orlando, FL, January 25–28, 1993* as a last-minute poster.

SSDI 0021-9673(93)E0062-Y

C_{2a} by high-performance liquid chromatography (HPLC). Gentamicin contained in creams, ointments and injectables is identified by the appearance of three bands using thin-layer chromatography (TLC). Quantitation in all matrices is accomplished by performing a microbial assay, which requires either 2–4 h (turbidimetric method) or 16–18 h (cylinder-plate method) for analysis, in addition to the 24-h incubation period for the preparation of the inoculum.

Suspect injectable solutions were received at the National Forensic Chemistry Center (NFCC) and required the identification of gentamicin sulfate and its subsequent quantitation. Microbial assays cannot be performed at the NFCC, so an alternative analytical procedure was desired. In addition to the USP HPLC method, on-line HPLC–thermospray mass spectrometry [4] has been utilized to resolve, identify and quantitate the components. Gentamicin sulfate has been studied by capillary electrophoresis (CE) using an indirect detection method at low pH, but without the resolution of the individual components [5]. Previous work concerning carbohydrate complexation of underivatized mono- and oligosaccharides with borate buffers [6,7] suggested the use of direct UV detection for the analysis of gentamicin sulfate in a straightforward and rapid manner. The CE method presented in this communication does not require sample derivatization, yields qualitative and quantitative information simultaneously, and needs only 10 min per analysis.

2. Experimental

2.1. Reagents

Sodium tetraborate decahydrate (borate) was purchased from Aldrich (Milwaukee, WI, USA), and the reference standard gentamicin sulfate was obtained from US Pharmacopeial Convention (Rockville, MD, USA). Distilled deionized water (DDW) was produced in the laboratory using a Milli-Q water purification system (Millipore, Milford, MA, USA). Buffer solutions were filtered through 0.2-μm nylon 66 filters (Alltech, Deerfield, IL, USA).

2.2. Methods

Sample preparation

Approximately 20 mg total mass of USP reference standard gentamicin sulfate were placed in a vial and dried for at least 3 h at 110°C as directed [3]. This standard was dissolved in 2.00 ml DDW to prepare a gentamicin sulfate stock solution, and was diluted as required. Based on the current USP lot (I-1) in which 1 mg standard is equivalent to 0.682 mg gentamicin base, a 2.00 mg/ml gentamicin sulfate working solution contains 1.36 mg gentamicin base/ml. Aliquots of the injectable solutions were diluted with DDW so that the amount of gentamicin base contained in the final working solution was approximately 2.0 mg base/ml. All solutions were stored at 4°C.

Capillary electrophoresis

An ISCO Model 3140 capillary electropherograph (ISCO, Lincoln, NE, USA) was used for all electrophoretic separations. An uncoated, 70 cm length (45 cm to detector) × 50 μm I.D. fused-silica capillary (ISCO) was installed.

Separations occurred in a 0.150 *M* borate buffer, pH 9.4 at +15 kV and 34°C. Direct detection was accomplished at 195 nm. The capillary was rinsed with borate buffer for 180 s at the start of every analysis. Samples were introduced into the capillary by vacuum injection at 25.0 kPa · s. Each analysis required 600 s, and data were collected at a rate of 10 points/s. Peak areas were normalized with respect to their migration times [8].

Gentamicin identification was accomplished by comparing the retention times of the peaks seen in the sample to those of the three peaks visualized with the USP Standard. Sample quantitation utilized total peak area as a single point comparison to the total peak area generated by the USP Standard.

3. Results and discussion

Fig. 2 is a typical electropherogram obtained from the USP Standard working solution. As a confirmation of the presence of gentamicin base,

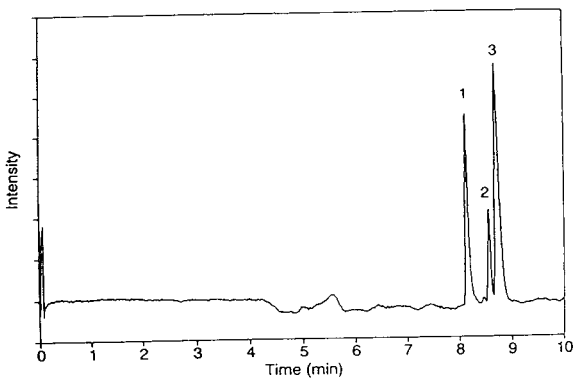

Fig. 2. CE analysis of 1.51 mg gentamicin base/ml from USP reference standard gentamicin sulfate. Separation conditions are given in the Experimental section. Peaks 1, 2 and 3 are discussed in Table 1, and are identified as components C_1, C_{1a}, and $C_2 + C_{2a}$, respectively.

the migration times of the components in the unknown samples are compared to those in the USP Standard. The presumed component migration order is C_1 (peak 1), C_{1a} (peak 2), and C_2 and C_{2a} co-migrating (peak 3). Under the present buffer conditions, it is unlikely that these latter two components would be resolved (see Fig. 1), so co-migration is expected. The unknown solutions exhibit similar electrophoretic behavior, which is verified by the average values for migration times obtained for each peak, found in Table 1. The "control" sample indicated in Table 1 is a manufacturer's declared 100 mg gentamicin base/ml veterinary solution. The three "unknown" samples are injectable solutions that originated with the same source; "unknown 1" and "unknown 2" were collected on the same day, and "unknown 3" was collected three days later. The relative standard deviations (R.S.D.s) of migration times seen with all solutions are less than 0.5%, and demonstrate reproducibility that is comparable to that obtained with HPLC. The migration data in Table 1 indicate that gentamicin is present in all three unknown injectables.

Table 1
Migration data for gentamicin sulfate

	Migration time (min)[a]		
	Peak 1	Peak 2	Peak 3
USP Standard[b]	8.07 ± 0.03 (0.37%)	8.50 ± 0.03 (0.35%)	8.63 ± 0.03 (0.35%)
Control	8.08	8.51	8.64
Unknown 1	8.04	8.46	8.60
Unknown 2	8.06	8.48	8.62
Unknown 3	8.12	8.54	8.68

[a] $n = 4$ unless otherwise noted.
[b] $n = 8$; value in parentheses is relative standard deviation.

Total peak area responses were used for quantitation of gentamicin base in the control and unknown samples by a simple ratio:

$$\frac{\text{mg base/ml USP Standard}}{\text{total peak area USP Standard}} = \frac{\text{mg base/ml sample}}{\text{total peak area sample}}$$

The resulting calculated concentrations for the control and the three unknowns are given in Table 2. For example, when the dilution factor is taken into account, the quantity of gentamicin base in the control injectable solution is 98.8 mg/ml, and is within USP guidelines of 90–125% for acceptable concentration ranges [3]. The values obtained for the three unknown samples using the CE method are in excellent agreement with the results of the microbial assay, with peak area R.S.D.s between 2.1 and 3.6%. The concentration ranges possible, based on standard deviations of the USP Standard and sample solutions, encompass the values obtained with the microbial assay. Based on the amount of gentamicin base present (Table 2), the data indicate that unknowns 1 and 2 were prepared in a similar manner, and unknown 3 was prepared separately.

The data in Table 3 indicate the reproducibility of the method when the buffer and/or capillary are changed. The decrease in the concentration of the control in system 2 is probably due to the age of the USP Standard solution. The same standard was used in systems 1 and 2; a fresh standard solution was prepared and utilized in systems 3 and 4. It is also unclear whether the USP reference standard gentamicin sulfate must be dried beforehand as directed [3]; the USP Standard used in systems 1 and 2 was *not* dried, as opposed to the USP Standard in systems 3 and 4.

Table 2
Determination of gentamicin base in injectable solutions

	Dilution	Gentamicin base concentration (mg/ml)		
		CE[a]	Range[b]	Microbial assay (mg/ml)[c]
USP Standard[d]	–	1.51 (2.56%)	–	–
Control[e]	1:50	98.8 (3.09%)	93.4–104	–
Unknown 1	1:100	114 (2.12%)	108–119	116
Unknown 2	1:100	108 (2.69%)	102–114	111
Unknown 3	1:100	93.6 (3.58%)	88.0–99.5	90.2

[a] $n = 4$ unless otherwise noted; values in parentheses are relative standard deviations.
[b] Values represent concentration range based on standard deviations of USP Standard and sample.
[c] Assays performed by Denver District Office.
[d] $n = 8$; (2.22 mg USP Standard/ml)(0.682 mg gentamicin base/mg USP Standard) = 1.51 mg gentamicin base/ml.
[e] Label declaration 100 mg gentamicin base/ml veterinary solution.

4. Conclusions

The method described in this communication establishes the use of CE in the analysis of gentamicin sulfate in injectable solutions. This method is much simpler and more rapid than the TLC procedure for identification and the microbial assay for quantitation. Because it yields

Table 3
Reproducibility of method

	Date of preparation	Gentamicin base concentration in control (mg/ml)
System 1[a]		98.8
Capillary	October 27th, 1992	
Borate buffer	November 2nd, 1992	
System 2[b]		92.0
Capillary	October 27th, 1992	
Borate buffer	December 15th, 1992	
System 3[c]		99.4
Capillary	December 21st, 1992	
Borate buffer	December 15th, 1992	
System 4[c]		104 (day 1)
Capillary	December 21st, 1992	102 (day 2)
Borate buffer	December 23rd, 1992	103 (day 6)

[a] $n = 8$ for USP Standard; $n = 4$ for control.
[b] $n = 10$ for both solutions.
[c] $n = 6$ for both solutions.

qualitative and quantitative information in one experiment, this CE procedure greatly reduces the amount of time required for routine analyses. The utilization of total peak area for quantitation of gentamicin base in injectable solutions leads to values that are in excellent agreement with those obtained via the accepted USP microbial assay, and demonstrates reproducibility over different capillary/buffer combinations. At this time, means of verifying the presumed migration order are being explored. Preliminary results obtained with bulk gentamicin sulfate samples [9] indicate that component percentage composition can be used for same-source verification. Because pre-column derivatization is not necessary, this method does not discriminate among components based on the presence or absence of primary amine groups, unlike the USP HPLC procedure [10], and therefore is more representative of the true composition of the sample.

5. Acknowledgement

Special thanks to Karen Kreuzer and her staff (US Food and Drug Administration, Denver District Office) for performing the microbial assays.

6. References

[1] S. Budavari (Editor), *The Merck Index*, Merck & Co., Rahway, NJ, 11th ed., 1989, pp. 686–687.
[2] B.E. Rosenkrantz, J.R. Greco, J.G. Hoogerheide and E.M. Oden, in K. Florey (Editor), *Analytical Profiles of Drug Substances*, Vol. 9, Academic Press, New York, 1980, pp. 295–340.
[3] *The United States Pharmacopeia*, United States Pharmacopeial Convention, Rockville, MD, 22nd revision, 1989, pp. 603, 604, 1488–1493; *Supplement 5*, pp. 2620–2621.
[4] T.A. Getek, M.L. Vestal and T.G. Alexander, *J. Chromatogr.*, 554 (1991) 191.
[5] M.T. Ackermans, F.M. Everaerts and J.L. Beckers, *J. Chromatogr.*, 606 (1992) 229.
[6] S. Hoffstetter-Kuhn, A. Paulus, E. Gassmann and H.M. Widmer, *Anal. Chem.*, 63 (1991) 1541.
[7] A.M. Arentoft, S. Michaelsen and H. Sørensen, *J. Chromatogr. A*, 652 (1993) 517.
[8] K.D. Altria, *J. Chromatogr.*, 634 (1993) 323.
[9] C.L. Flurer, presented at the *5th International Symposium on High Performance Capillary Electrophoresis, Orlando, FL, January 25–28, 1993*, poster.
[10] P.J. Claes, R. Busson and H. Vanderhaeghe, *J. Chromatogr.*, 298 (1984) 445.

ELSEVIER

Journal of Chromatography A, 663 (1994) 264–266

JOURNAL OF CHROMATOGRAPHY A

Short Communication

Chiral separations on cellulose in electrophoresis

T.K.X. Huynh, L. Ossicini*, C. Polcaro

Istituto di Cromatografia del CNR, Casella Postale 10, 00016 Monterotondo Scalo (Rome), Italy

(First received September 14th, 1993; revised manuscript received November 24th, 1993)

Abstract

Chiral separations are possible in zone electrophoresis if a chiral support such as microcrystalline cellulose is used as the support. This was shown by separating DL-methyltryptophans by electrophoresis on microcrystalline cellulose with 0.05 *M* Na_2HPO_4 or 0.05 *M* $(NH_4)_2SO_4$ (pH range 2–12) as electrolyte. The separations were best at intermediate pH and with electrolyte concentrations not higher than 0.05 *M*.

1. Introduction

In adsorption chromatography on cellulose it became evident that cellulose can produce separations of enantiomers under suitable conditions [1–3]. Such chiral behaviour can vary considerably depending on whether the cellulose is "native" or "microcrystalline" [4]. There is an extensive literature on paper electrophoresis, which in the "high-voltage" mode can produce separations comparable to those now obtained in capillary zone electrophoresis [5]. Although numerous asymmetric compounds have been examined electrophoretically, there has been no mention, to our knowledge, of chiral separations due to the cellulose support.

Chiral separations in paper electrophoresis have been reported [6] using optically active ion-pairing counter ions in the electrolyte. In this paper, some experiments are described to show that under suitable conditions chiral separations can be achieved by paper electrophoresis that are due to the chiral properties of the cellulose used as the support.

* Corresponding author.

2. Experimental

A Camag (Muttenz, Switzerland) high-voltage paper electrophoresis apparatus was used. From work on adsorption chromatography on cellulose it was evident that only microcrystalline cellulose was likely to give separation effects with short migration distances. The only microcrystalline cellulose available was in the form of Merck 5577 20-cm long thin layers (Merck, Darmstadt, Germany). As the electrophoresis chamber is designed for 40-cm long paper strips, the thin layers were connected to the electrolyte vessels with Whatman 3MM paper (Whatman, Maidstone, UK) holding the same electrolyte. The spots were detected with 1% ninhydrin in acetone.

3. Results and discussion

Preliminary results showed that separations occurred and these improved if the electrolyte was not more concentrated than 0.05 *M* and when run for 60 min at 2500 V.

Figs. 1 and 2 show electropherograms of DL-

0021-9673/94/$07.00
SSDI 0021-9673(93)E0044-U

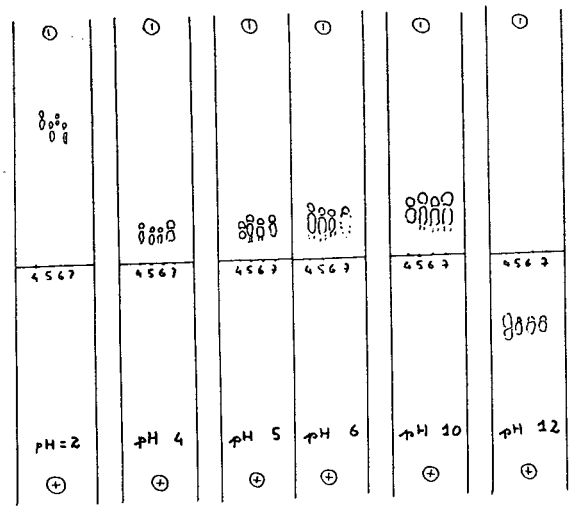

Fig. 1. Thin-layer electrophoresis of DL-methyltryptophans on Merck 5577 microcrystalline cellulose in a Camag electrophoresis apparatus operated at 2500 V for 60 min. Electrolyte, 0.05 *M* Na_2HPO_4 at pH 2, 4, 5, 6, 10 and 12 (from left to right). The samples (from left to right) are DL-4-methyltryptophan, DL-5-methyltryptophan, DL-6-methyltryptophan and DL-7-methyltryptophan. Note that "baseline" separations occur for DL-4-methyltryptophan from pH 4 to 10.

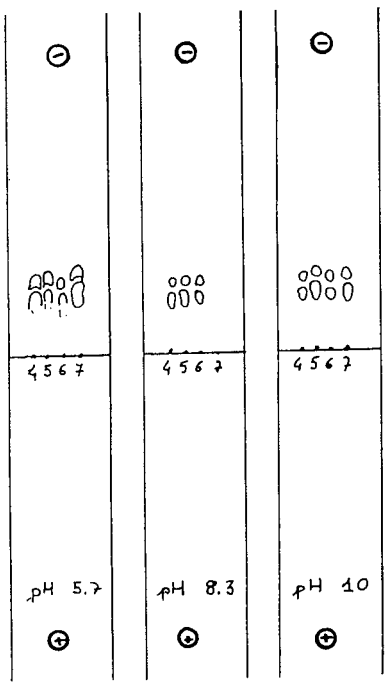

Fig. 2. As Fig. 1, except that 0.05 *M* $(NH_4)_2SO_4$ was used as the electrolyte at pH 5.7, 8.3 and 10 (from left to right). Note that all four methyltryptophans yield baseline separations of their enantiomers.

methyltryptophans at different pH values in 0.05 *M* Na_2HPO_4 and in 0.05 *M* $(NH_4)_2SO_4$. The separations are better in the intermediate pH range when the electrophoretic movement is small, *i.e.*, when much of the tryptophan is in a non-ionized form. This agrees with the results found in TLC on cellulose, where the best separations are obtained in the neutral range. Various cations were tried in the electrolyte and Li^+, Na^+, K^+ and Mg^{2+} yielded essentially the same results (Fig. 3). The anion of the electrolyte also has little effect on the separation; sulphate, chloride and acetate yielded the same results as phosphate buffers (Figs. 4 and 5). The separations could be due to a displacement by electroosmotic flow and differential adsorption on cellulose or to electrophoretic movement and differential adsorption, or both.

It was shown, however, that complete separations are possible in favourable circumstances and they must be considered as a possibility in electrophoretic work with cellulose as a stabilizing medium.

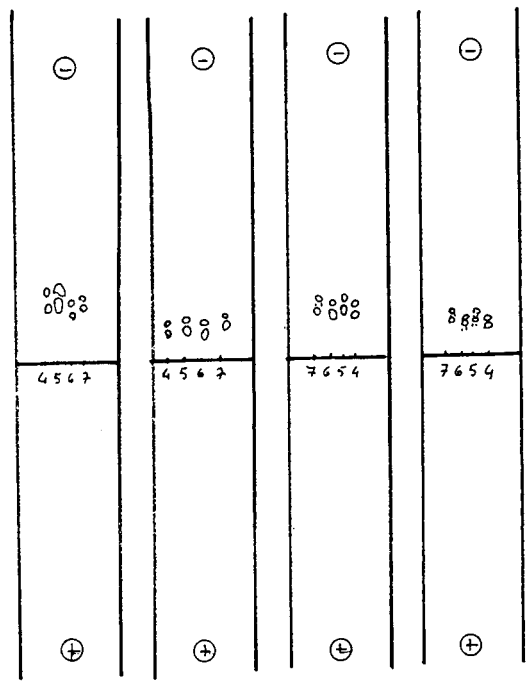

Fig. 3. As Fig. 1, using unbuffered 0.05 *M* LiCl, NaCl, KCl and $MgCl_2$ (from left to right) as electrolytes. All four methyltryptophans examined yield baseline separations.

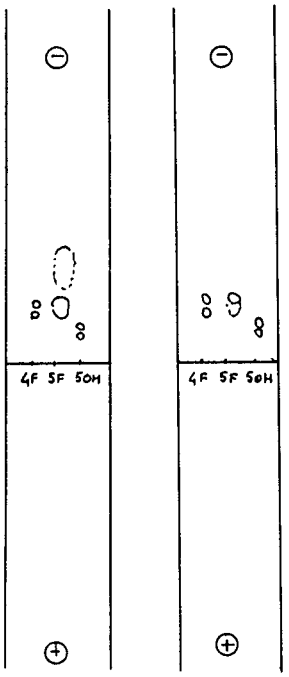

Fig. 4. As Fig. 1 with (left) 0.05 *M* $(NH_4)_2SO_4$ and (right) 0.05 *M* NaCl as electrolytes. The compounds examined were DL-4-fluorotryptophan, DL-5-fluorotryptophan and DL-5-hydroxytryptophan; only DL-4-fluorotryptophan yields a complete separation.

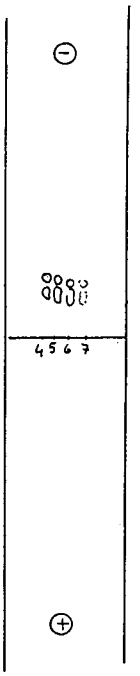

Fig. 5. As Fig. 1, with 0.05 *M* sodium acetate at pH 5 as electrolyte. Samples (from left to right): DL-4-methyltryptophan, DL-5-methyltryptophan, DL-6-methyltryptophan and DL-7-methyltryptophan.

4. References

[1] C.E. Dalgliesh, *Biochem. J.*, 64 (1956) 483.
[2] R. Weichert, *Acta Chem. Scand.*, 8 (1954) 1542.
[3] A.O. Kuhn, M. Lederer and M. Sinibaldi, *J. Chromatogr.*, 469 (1989) 253.
[4] M. Lederer, *J. Chromatogr.*, 604 (1992) 55.
[5] R. Clotten and A. Clotten, *Hochspannungselektrophorese*, Georg. Thieme, Stuttgart, 1962.
[6] L. Ossicini and C. Celli, *J. Chromatogr.*, 115 (1975) 655.

Author Index

PUBLICATION SCHEDULE FOR THE 1994 SUBSCRIPTION

Journal of Chromatography A and *Journal of Chromatography B: Biomedical Applications*

MONTH	O 1993	N 1993	D 1993	J	F	M	A	
Journal of Chromatography A	652/1 652/2 653/1	653/2 654/1 654/2 655/1	655/2 656/1 + 2 657/1 657/2	658/1 658/2 659/1 659/2	660/1 + 2 661/1 + 2 662/1 662/2	663/1 663/2 664/1	664/2 665/1 665/2 666/1 + 2 667/1	The publication schedule for further issues will be published later.
Bibliography Section						681/1		
Journal of Chromatography B: Biomedical Applications				652/1	652/2 653/1	653/2 654/1	654/2 655/1	

INFORMATION FOR AUTHORS

(Detailed *Instructions to Authors* were published in *J. Chromatogr. A*, Vol. 657, pp. 463–469. A free reprint can be obtained by application to the publisher, Elsevier Science B.V., P.O. Box 330, 1000 AH Amsterdam, Netherlands.)

Types of Contributions. The following types of papers are published: Regular research papers (full-length papers), Review articles, Short Communications and Discussions. Short Communications are usually descriptions of short investigations, or they can report minor technical improvements of previously published procedures; they reflect the same quality of research as full-length papers, but should preferably not exceed five printed pages. Discussions (one or two pages) should explain, amplify, correct or otherwise comment substantively upon an article recently published in the journal. For Review articles, see inside front cover under Submission of Papers.

Submission. Every paper must be accompanied by a letter from the senior author, stating that he/she is submitting the paper for publication in the *Journal of Chromatography A* or *B*.

Manuscripts. Manuscripts should be typed in **double spacing** on consecutively numbered pages of uniform size. The manuscript should be preceded by a sheet of manuscript paper carrying the title of the paper and the name and full postal address of the person to whom the proofs are to be sent. As a rule, papers should be divided into sections, headed by a caption (*e.g.*, Abstract, Introduction, Experimental, Results, Discussion, etc.). All illustrations, photographs, tables, etc., should be on separate sheets.

Abstract. All articles should have an abstract of 50–100 words which clearly and briefly indicates what is new, different and significant. No references should be given.

Introduction. Every paper must have a concise introduction mentioning what has been done before on the topic described, and stating clearly what is new in the paper now submitted.

Experimental conditions should preferably be given on a *separate* sheet, headed "Conditions". These conditions will, if appropriate, be printed in a block, directly following the heading "Experimental".

Illustrations. The figures should be submitted in a form suitable for reproduction, drawn in Indian ink on drawing or tracing paper. Each illustration should have a caption, all the *captions* being typed (with double spacing) together on a *separate sheet*. If structures are given in the text, the original drawings should be provided. Coloured illustrations are reproduced at the author's expense, the cost being determined by the number of pages and by the number of colours needed. The written permission of the author and publisher must be obtained for the use of any figure already published. Its source must be indicated in the legend.

References. References should be numbered in the order in which they are cited in the text, and listed in numerical sequence on a separate sheet at the end of the article. Please check a recent issue for the layout of the reference list. Abbreviations for the titles of journals should follow the system used by *Chemical Abstracts*. Articles not yet published should be given as "in press" (journal should be specified), "submitted for publication" (journal should be specified), "in preparation" or "personal communication".

Vols. 1–651 of the *Journal of Chromatography*; *Journal of Chromatography, Biomedical Applications* and *Journal of Chromatography, Symposium Volumes* should be cited as *J. Chromatogr.* From Vol. 652 on, *Journal of Chromatography A* (incl. Symposium Volumes) should be cited as *J. Chromatogr. A* and *Journal of Chromatography B: Biomedical Applications* as *J. Chromatogr. B.*

Dispatch. Before sending the manuscript to the Editor please check that the envelope contains four copies of the paper complete with references, captions and figures. One of the sets of figures must be the originals suitable for direct reproduction. Please also ensure that permission to publish has been obtained from your institute.

Proofs. One set of proofs will be sent to the author to be carefully checked for printer's errors. Corrections must be restricted to instances in which the proof is at variance with the manuscript.

Reprints. Fifty reprints will be supplied free of charge. Additional reprints can be ordered by the authors. An order form containing price quotations will be sent to the authors together with the proofs of their article.

Ovomucoid Bonded Column for Direct Chiral Separation

ULTRON ES-OVM

Narrow-Bore Column (2.0 I.D. x 150 mm) for Trace Analyses
Analytical Column (4.6 I.D. , 6.0 I.D. x 150 mm) for Regular Analyses
Semi-Preparative Column (20.0 I.D. x 250 mm) for Preparative Separation

Analysis of Trace FLURBIPROFEN in Metabolite with NARROW-BORE COLUMN

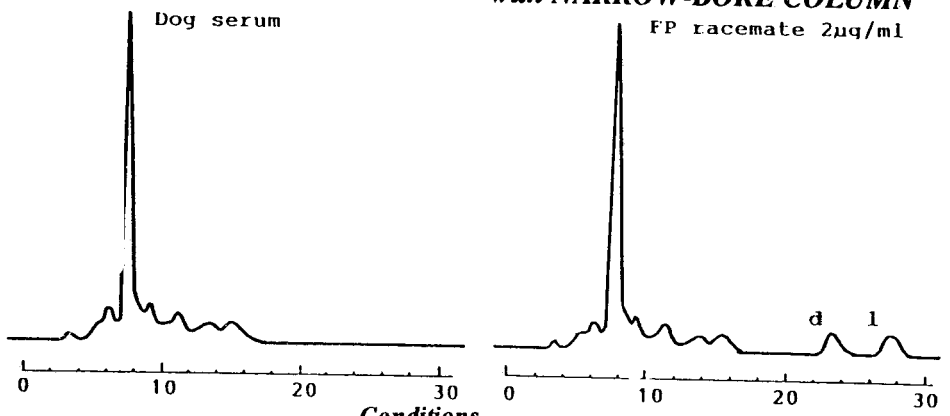

Conditions

Column: ULTRON ES-OVM(2.0I.D. x 150mm)
Mobile Phase: 20mMPhosphate Buffer(pH=3.0)/CH3CN =100/15
Flow Rate: 0.1ml/min
Temperature: 25°C
Injection: 5μl
Detection: UV- 247nm(0.05AUFS)

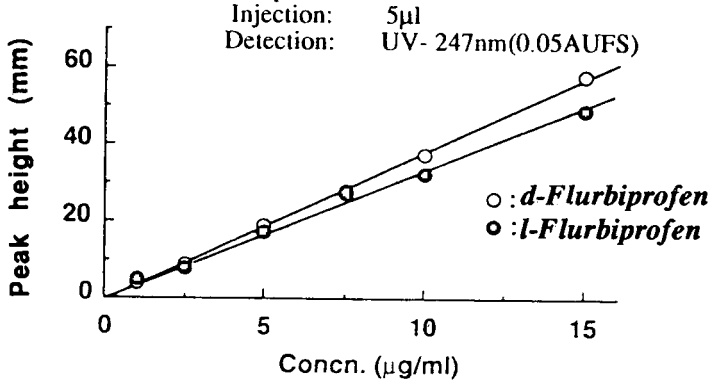

Calibration Curve for Each Enantiomer of Flurbiprofen

SHINWA CHEMICAL INDUSTRIES, LTD.

50 Kagekatsu-cho, Fushimi-ku, Kyoto 612, JAPAN
Phone:+81-75-621-2360 Fax:+81-75-602-2660

In the United States and Europe, please contact:

Rockland Technologies, Inc.

538 First State Boulevard, Newport, DE 19804, U.S.A.
Phone: 302-633-5880 Fax: 302-633-5893

This product is licenced by Eisai Co., Ltd.